

**Supramolecular photochemistry of new ruthenium(II) oligopyridine
complexes: From design to light conversion.**

INAUGURALDISSERTATION

zur

Erlangung der Würde eines Doktors der Philosophie

Vorgelegt der

Philosophisch-Naturwissenschaftlichen Fakultät

der

Universität Basel

von

AMAR BOUDEBOUS

aus Belfort, Frankreich

Basel, 2006

Geehmigt von der Philosophisch-Naturwissenschaftlichen Fakultät auf Antrag von

Prof. Dr. E. C. Constable

Prof . Dr. H. J. Wirz

Basel, den 24. 01. 2007

Prof. Dr. H-P. Hauri

Dekan

Acknowledgements

I would like to thank Prof. Dr. Ed Constable for giving me the opportunity to join his research group, for guiding and supporting my work.

I thank Prof. Dr. Jakob Wirz for agreeing to act as co-referee.

I thank Prof. Dr. Catherine Housecroft for agreeing to act as chairman of the thesis committee.

I would like to thank the Constable-Housecroft group members, and the scientific and technical members of the Department of Chemistry of the University of Basel. Markus Neuburger and Dr. Silvia Schaffner are acknowledge for the crystal structure elucidations

I would like to thank also Dr. Hassen Boudebous, Prof. Dr. Jakob Wirz for the laser flash photolysis measurements and for the interesting discussions.

I would like to thank Dr. Francesco Barigelletti, and Dr. Cristiana Sabatini ans ISOF staff for supporting photophysical measurments.

I thank my family for their constant encouragement.

I would like also to thank the Swiss National Science Foundation and the University of Basel for their financial support.

Table of Contents

Chapter I: Introduction to supramolecular photochemistry	11
I. Supramolecular photochemistry.....	12
Introduction.....	12
Supramolecular species.....	13
Photochemical and photophysical process.....	15
[Ru(bpy) ₃] ²⁺	21
Cage-type systems.....	23
Host-Guest systems.....	24
II. Supramolecular systems using Ru(II)-polypyridine complexes.....	26
Molecular machines.....	26
Covalently-linked molecular components.....	40
Dendrimers.....	42
Metallosupramolecular chemistry.....	45
References.....	49
Chapter II: Synthesis of ruthenium (II) complexes of 4,4'-bis(phenyl)-2,2'-bipyridine ligands	55
I. Introduction.....	56
II. Synthesis of 4,4'-bis(4-methoxyphenyl)-2,2'-bipyridine 7 , and 4,4'-bis(3,5-dimethoxyphenyl)-2,2'-bipyridine 10	57
The synthetic strategy.....	57
The Suzuki-Miyaura cross coupling.....	58
Synthesis of 4,4'-dibromo-2,2'-bipyridine.....	59
Synthesis of 4,4'-bis-(4-methoxyphenyl)-2,2'-bipyridine 7	60
Synthesis of 4,4'-bis(3,5-dimethoxyphenyl)-2,2'-bipyridine 10	61
Synthesis of 4,4'-bis-(1-naphtyl)-2,2'-bipyridine 13	66
III. Synthesis of [Ru(bpy) ₂ (7)] [PF ₆] ₂ and [Ru(bpy) ₂ (10)] [PF ₆] ₂	67
Synthesis of [Ru(bpy) ₂ (7)] [PF ₆] ₂ 15	67
Synthesis of [Ru(bpy) ₂ (10)] [PF ₆] ₂ 17	68
IV. Synthesis of [Ru(bpy)(10) ₂] [PF ₆] ₂ 19 and [Ru(10) ₃] [PF ₆] ₂	73
Synthesis of [Ru(bpy)(10) ₂] [PF ₆] ₂ 19	73

Synthesis of [Ru(10) ₃] [PF ₆] ₂ 20	77
IV. Conclusion and perspectives.....	79
V. Experimental section.....	80
VI. References.....	87

Chapter III: Synthesis of ruthenium (II) complexes of 4'-phenylsubstitued-2,2':6',2''-terpyridine complexes.....88

I. Introduction.....	89
II. Synthesis of 4-substitued-2,2':6',2''-terpyridine ruthenium(II) complexes.....	89
1) Synthesis of 4-bromo-2,2':6',2''-terpyridine 25	90
2) Synthesis of 4-phenyl-substitued-2,2':6',2''-terpyridine.....	90
3) Synthesis of ruthenium(II) 4-phenyl-substitued-2,2':6',2''-terpyridine complexes.....	92
III. Synthesis of ruthenium(II) shaped 3,5-dioxyphenyl spaced metallostars.....	93
1) Synthesis of Dendron A 45	93
2) Synthesis of Dendron B 46	102
3) Synthesis of Dendron C and D.....	108
4) Conclusion.....	112
IV. Experimental procedures.....	114
V. References.....	121

Chapter IV: Photophysical and electrochemical investigations of the 4-methoxy and 3,5-dimethoxyphenyl substituted ruthenium(II) oligopyridine complexes.....122

I. Introduction.....	123
II. Theoretical aspects of the metal-to-ligand charge tranfert (MLCT).....	124
1). The photoinduced meta-to-ligand charge transfert.....	124
III. Photophysical properties of products 15, 17, 19, 20, 39 and 45	126
IV. Electrochemical potentials of complexes 20, 39 and 45	137
V. References.....	138

Chapter V: Synthesis and photochemical investigation of 4,4'-bis(3,5-dimethoxyphenyl)-6,6'-dimethyl-2,2'-bipyridine copper(I) and ruthenium(II) complexes.....139

I. Introduction.....	140
II. Synthesis of 4,4'-bis(3,5-dimethoxyphenyl)-6,6'-dimethyl-2,2'-bipyridine copper(I) complex 59	140

III. Synthesis of [Ru(bpy) ₂ (58)]PF ₆ complex 60	145
IV. Photophysical and electrochemical properties of complexes 59, 60	148
1) Steady-state absorption and emission spectrums of 59, 60	148
2) Kinetic investigations of emission of 59 and 60	151
3) Electrochemistry of complex 59	153
V. Conclusion.....	153
VI. Experimental section.....	155
VII. References.....	157
Chapter VI: From pyrene to polymetallic dyads	158
I. Introduction.....	159
II. Wire type polyads.....	159
III. The pyrene excimer theory.....	161
1) What are excimer and exciplexes?	161
2) Example of excimers : pyrene.....	161
IV. Synthesis of 1-pyrenyl Ru , Os and Ir complexes.....	163
V. Photophysical and electrochemical properties of the 4-pyrenyl-2,2':6', 2''-terpyridine complexes.....	173
1) UV/Vis steady-state absorption spectroscopy of 61, 62, 63, 64, 65, 66, 67	173
2) Emission spectrum.....	175
3) Electrochemical investigations.....	181
VI. Conclusion.....	182
VII. Experimental section.....	183
VIII. References.....	188
Chapter VII: Synthesis of narrow band gap spacers using non-classical π-electron ring systems	189
I. Introduction.....	190
II. Organic π -conjugated systems.....	191
III. Synthesis of 4,7-diethynyltrimethylsilylbenzo[c][1,2,5]thiadiazole 75	193
IV. Synthesis of 6,13-pentacene derivates.....	198
1) Synthesis of 6,13-diethynyltriisopropylpentacene 81	199
V. Conclusion.....	201
VI. Experimental section.....	202

VII. References.....	206
Annexes: Crystallographic data, data collection and refinement parameters of compounds 4 , 9 , 59 , 61 , 72 , 73 , 74 and 80	208

Symbols and Abbreviations

Alox	aluminiumoxide
AM1	Austin model 1
Asol	MeCN: KNO ₃ ^(sat) : H ₂ O 7:1:0.5 (v/v)
biq	2,2'-biquinoline
bpy	2,2'-bipyridyl
<i>n</i> -BuLi	<i>n</i> -butyllithium (1.6 M in Hexane)
B(OH) ₂	borate
B(OMe) ₃	trimethylborate
COSY	correlated spectroscopy
cyclam	1,4,8,11-tetraazacyclotetradecane
tpy	2,2':6',2''-terpyridine
DABCO	1,4-diazabicyclo[2.2.2]octane
DBE	1,2-dibromoethane
DEA	diethylamine
DME	1,2-dimethoxyethane
DMF	N,N-dimethylformamide
DMSO	dimethylsulfoxide
dpp	2,3-bis(2-pyridyl)pyrazine
<i>d</i>	doublet
<i>dd</i>	doublet of doublet
EI	electron impact
ES	electron spray
EtOH	ethanol
Et	ethyl
FAB	fast atom bombardement
fs	femtosecond
hν	light
HOMO	Highest occupied molecular orbital
IC	internal conversion
IR	infrared
ISC	intersystem crossing
LFP	laser flash photolysis
LUMO	lowest unoccupied molecular orbital
Me	methyl
MeCN	acetonitrile
MeOH	methanol
MHz	megahertz
MLCT	metal-to-ligand charge transfer
<i>m</i>	middle-strong
<i>m</i>	multiplet
M	molecular peak
ms	millisecond
MS	mass spectroscopy
<i>m/z</i>	mass/charge
NEM	N-ethylmorpholine
NMR	nuclear magnetic resonance spectroscopy
NOESY	nuclear overhauser effect spectroscopy
ns	nanosecond

ORTEP	Oak Ridge thermal ellipsoid plot
Ph	phenyl
<i>i</i> -Pr	<i>iso</i> -propyl
PM3	parametric method number 3
R _f	retention factor
s	strong
<i>s</i>	singlet
SiO ₂	silica gel (230-400 mesh, 0.04-0.063 mm)
t	triplet
TEA	triethylamine
TFA	2,2,2-trifluoroacetic acid
THF	tetrahydrofuran
TLC	thin layer chromatography
TMS	trimethylsilyl
TMSA	trimethylsilylacetylene
TIPS	triisopropylsilyl
TIPSA	triisopropylsilylacetylene
UV	ultra-violet
w	weak
XNOR	logical equality logic gate
XOR	exclusive disjunction logic gate
ZINDO	Zerner intermediate neglect differential overlap
₁	singlet
₃	triplet
μW	micro-waves

Summary:

This work shows the design of new ruthenium (II) oligopyridine complexes and their photophysical and electrochemical properties.

Chapter I highlights some recent developments of those topics in chemistry and especially in supramolecular systems.

Chapter II describes the synthesis via Suzuki-coupling of the in the 4-methoxyphenyl, 3,5-dimethoxy and 1-naphthyl substitution of 4,4' position of 2,2'-bipyridine. The corresponding Ru(II) complexes have been prepared.

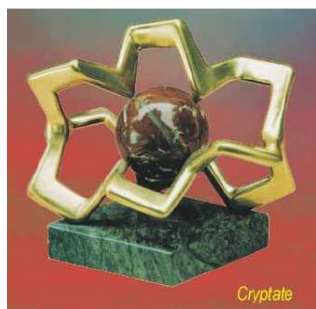
Chapter III deals with the synthesis of new starshaped X and Y metallodendrimers, the synthesis of 4'-substituted tpy ligands their complexation with Ru(II), and the synthesis of polynuclear supramolecular assemblies.

Chapter IV concerns the photophysical and electrochemical properties of some chapter II and III complexes Ru(II), determination of luminescence lifetimes and quantum yields.

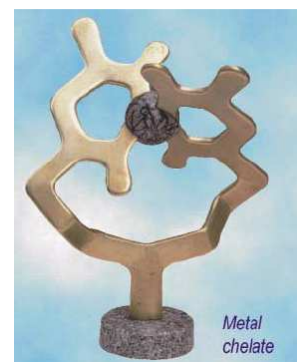
Chapter V describes the synthesis of 6,6'-dimethyl-4,4'-(3,5-dimethoxyphenyl)-2,2'-bipyridine ligand, its complexation with Cu(I) and Ru(II) and their photophysical and electrochemical properties.

Chapter VI shows the synthesis of 1-pyrenyl substituted tpy ligand and its complexation with Ru(II), Os(II) and Ir(III) as potent donors and acceptors for the formation of polyads.

Chapter VII concerns the synthesis of narrow band gap spacer with non-classical π electron ring spacer. The synthesis of 4,7-trimethylsilylacetylenyl-3,1,2-benzothiadiazole and 6,13 derivate of pentacene as potent new spacers for polymetallic rod-like systems.



Chapter I : Introduction to supramolecular photochemistry



I. Supramolecular photochemistry.

1.) Introduction.

Photochemistry is a natural phenomenon, which began at the origin of the universe and the world and also a modern science which describes the interaction between light and matter in several main science domains, such as chemistry, physics and biology. Photochemistry plays a fundamental role in life (photosynthesis, vision, phototaxis, etc...) and also in technology (image reproduction, photocatalysis, photodegradation, etc...). The last 30 years of photochemistry have shown the fundamental role played in experiment and theoretical investigations. From determination of molecular mechanisms to photocatalysis and electronic information of complex devices, studying photochemistry is now indispensable. The photochemical and photophysical processes of thousands of organic and organometallic, coordination compounds complexes have been studied and elucidated, and now confirmed with the help of theoretical tools to explain the structural, energetic and dynamic properties of the molecules in their most important excited state. The major part of photochemical investigations were focused on molecular species with simple processes (molecular photochemistry).



Fig I-1- A cloud illuminated by sunlight example of photochemical reaction.

The combination of atoms leads to molecules and the combination of molecular components leads to supramolecular species. Current chemical research shows us that photons and energy information can be used in supramolecular species. The interest in the chemistry of the interaction of supramolecular species with light is great because it allows several types of

properties not previously observed. In the last few year supramolecular photochemistry^[1,2] has taken an important part in chemistry. Photochemistry and supramolecular photochemistry are interdisciplinary areas.

In this introduction we will show the meaning of supramolecular chemistry and also define some fundamental concepts of photochemistry, and the host-guest theory and explain some recent investigations oligopyridine chemistry .

2. Supramolecular species

The definition of a supramolecular species, is somewhat arbitrary and the word may have different meanings depending on the area in which it is applied. The difference between a supramolecular specie and a large molecule is the possibility to divide the system into individual molecules which can exist individually^[2].

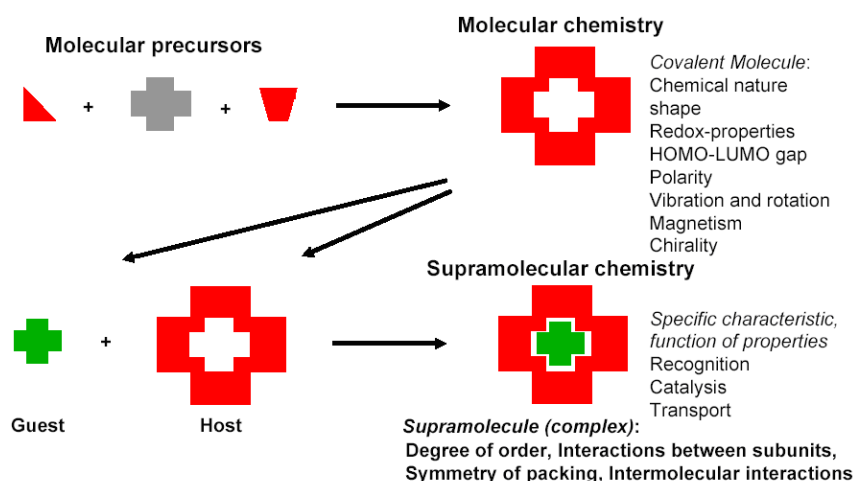


Fig I-2 Supramolecular chemistry concept

According to this definition^[2], the systems where the individual parts or molecules are held together by intermolecular forces (*Fig I-2*) or individual molecules are interlocked can be defined as supramolecular species. The molecules bind together by coordination or covalent bonds. Macrocyclic complexes (*Fig I-3*) where metal ions and ligands conserve their chemical properties, and systems made of covalently-linked but differentiable subunits can also be called supramolecular species.

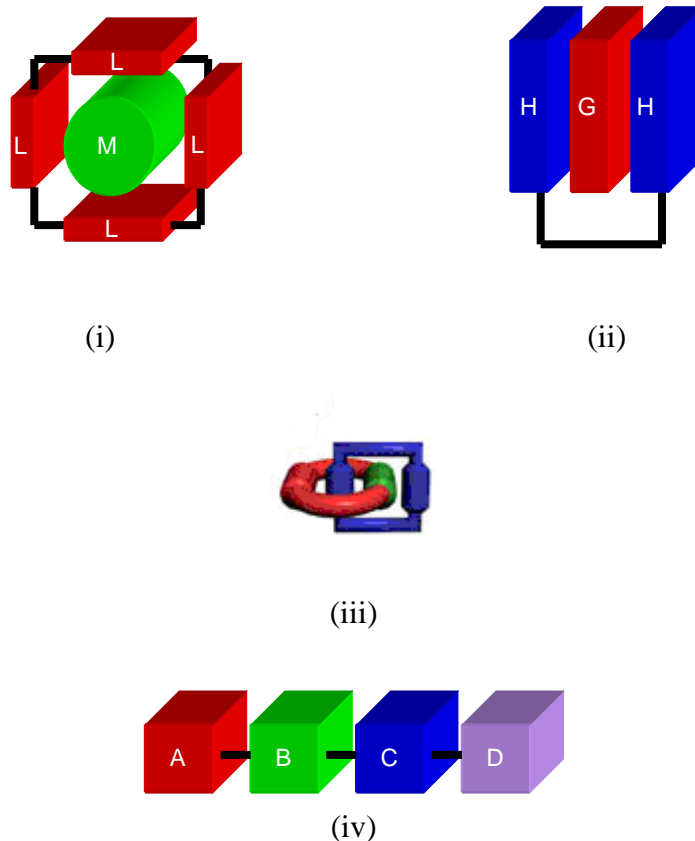


Fig I-3- Schematic representation of four types of molecular and supramolecular species: (i) cage-type systems, (ii) host-guest systems, (iii) catenanes, (iv) covalently linked molecular components^[7].

The difference between large molecules and supramolecular species is based on the interactions between independent molecular parts. When the interaction energy between subunits is small compared to other relevant energy parameters, the system can be defined as a supramolecular species. As shown in (*Fig I-4*), light excitation of a supramolecular species A-B (where – means any type of bond binding together the part A and B of the system) leads to excited states localised on A or B, or causes an electron transfer from A to B (or vice versa). When the excited states are completely delocalized on the molecule the species is called a large molecule^[7].

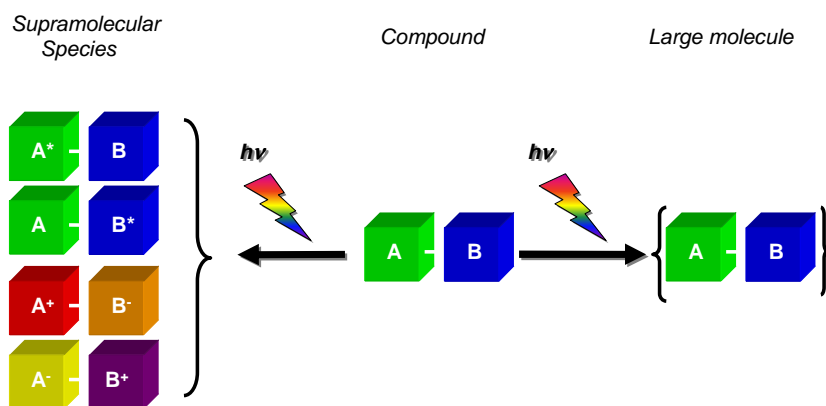


Fig I-4- Light excitation of a supramolecular species^[7].

Oxidation and reduction processes in a supramolecular species can be understood in terms of oxidation and reduction of independent components A and B (Fig I-5), while oxidation and reduction of a large molecule show a total delocalization of the electron in the molecule.

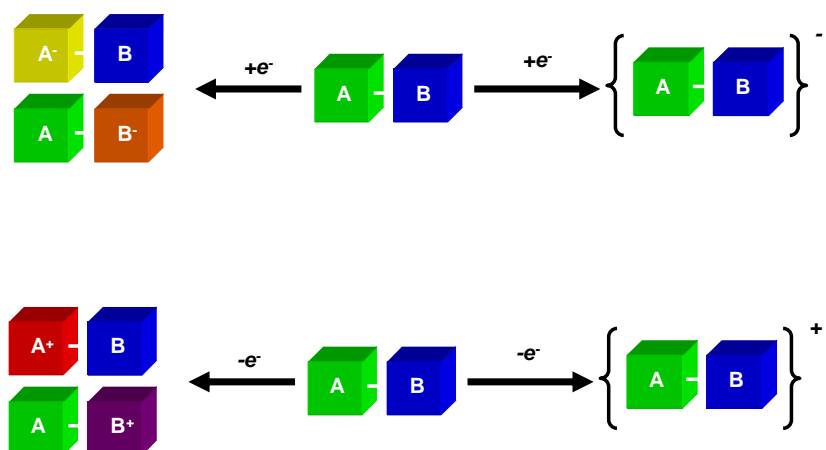


Fig I-5-Oxidation and reduction of A-B species^[7].

3. Photochemical and photophysical processes

The fundamental reaction in a photochemical or photophysical process is the absorption of a photon by a molecule. The excited state which is formed is at a high energy level, unstable

with respect to return to the lowest energy level (ground-state) by several possible deactivation processes.



The excited state deactivation processes can be explained by a simple scheme (*Fig I-6*) (1) dissociation of the original molecule and formation of products (photochemical reaction), (2) emission of light (radiative deactivation, also called luminescence), (3) dissipation of excess energy into heat (non-radiative deactivation), (4) interaction with other species in solution (quenching processes).

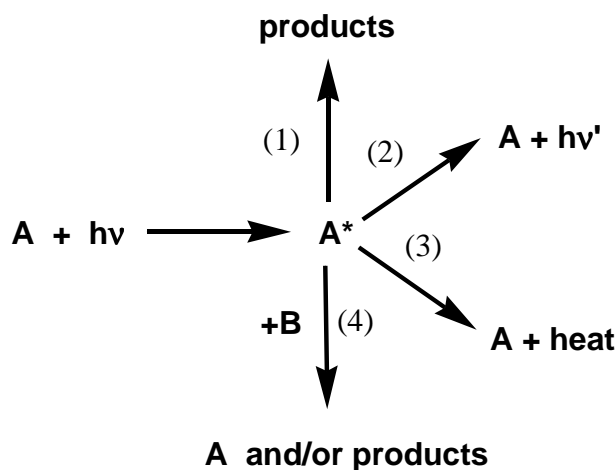


Fig I-6- Light excitation of a molecule and deactivation of the electronically excited state

Electronic spectroscopy shows that the probability of light absorption (corresponding to the intensity of the light absorption band) is related to the quantum chemical characteristics of the states involved and particularly to their spin quantum number. Transitions from the ground states to excited states with the same multiplicity value are allowed and give rise to intense bands, whereas transitions to excited states of different multiplicity are forbidden and only have low intensity if observed at all in the absorption spectra. The majority of molecules are in the ground singlet state and the lowest excited state is often a triplet that cannot be directly populated by light absorption but can be obtained after relaxation of higher singlet excited states. We can summarise the relationship of the states involved in the photochemical process in a Perrin-Jablonski diagram (*Fig I-7*); the deactivation by chemical reaction is not

represented to simplify it. Emission of light (luminescence) is called fluorescence f or phosphorescence p and depends

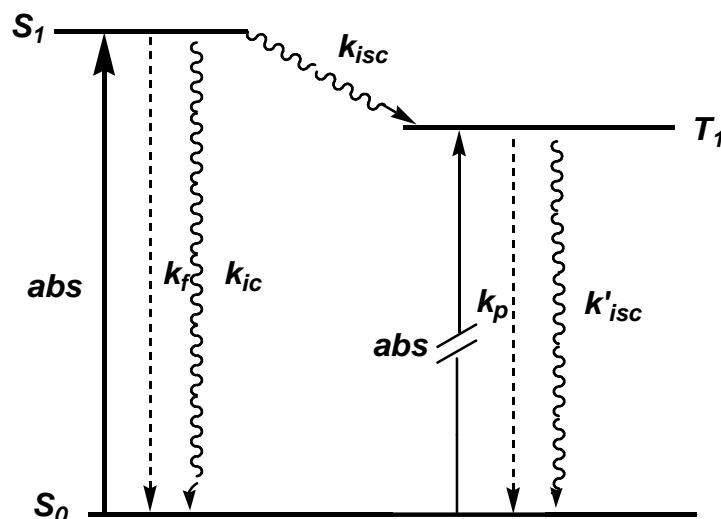


Fig I-7- Perrin-Jablonski diagram, with energy levels for a simple molecular species. S_0 , S_1 , and T_1 are the singlet ground state, singlet excited state, and triplet excited state respectively; k_f , k_{ic} , k_{isc} , k_p and k'_{isc} are the rate constants for fluorescence, internal conversion $S_1 \Rightarrow T_1$ intersystem crossing, phosphorescence, and $T_1 \Rightarrow S_0$ intersystem crossing, respectively.

On the multiplicity of the excited and ground states. The radiationless deactivation is called internal conversion (ic) when it occurs between the same spin state and intersystem crossing when it occurs between states with different spin. Fluorescence and internal conversion are spin-allowed transitions, whereas phosphorescence and intersystem crossing are spin-forbidden steps.

The intramolecular decay step is characterized by its own rate constant (Fig I-7) k_i , and each excited state is characterized by its lifetime, given by the formula:

$$\tau = \frac{1}{\sum_i k_i}$$

Where k_i is the first order rate constant for a unimolecular process that causes the relaxation of the corresponding excited state^[3]. The quantum yield of each process, Φ , is the ratio between the number of moles of species (photons or molecules) produced and the number of

moles of photons that have been absorbed. For example with the help of the *Fig-I-7* , the phosphorescence emission quantum yield Φ_p can be expressed by the following equation:

$$\Phi_p = \eta_{isc} k_p \tau_{T1}$$

With η_{isc} the efficiency of population of the emitting excited state from the state populated by light absorption.

$$\eta_{isc} = \frac{k_{isc}}{k_{isc} + k_f + k_{ic}}$$

And τ_{T1} is the lifetime of the emitting excited state

$$\tau_{T1} = \frac{1}{k_p + k'_{isc}}$$

When the intramolecular deactivation steps are not too fast or when the lifetime of the excited state enough long is, the molecules have a chance to encounter another molecule (*Fig I-8*). In this case the interaction which can occur is specific and the process is called bimolecular process. Experimental kinetic investigations, show that excited states with a lifetime longer than 1 ns may have a good chance to encounter another dissolved molecule.

The excited states that satisfy this condition are the lowest spin-allowed and spin-forbidden excited states for organic molecules, and the lowest spin-forbidden excited state for coordination compounds^[7].

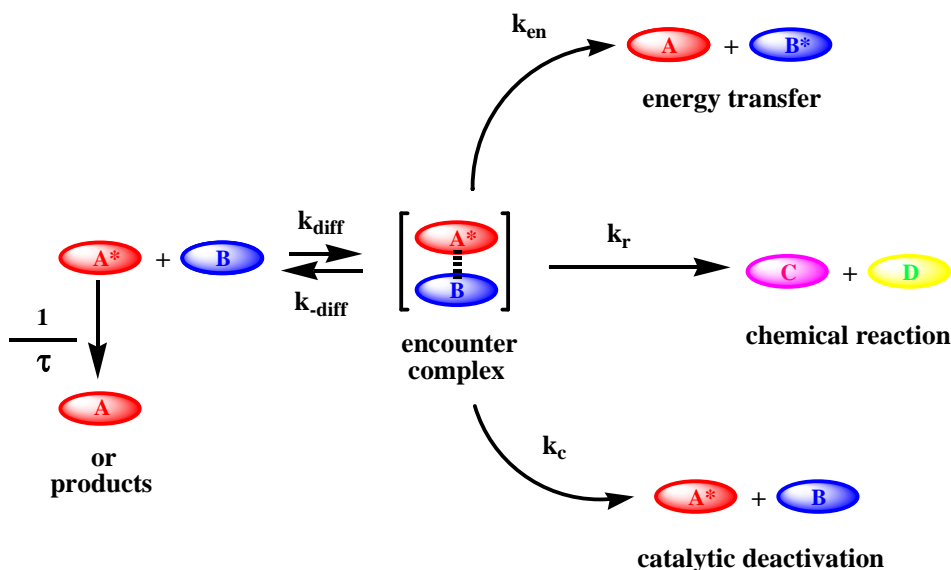
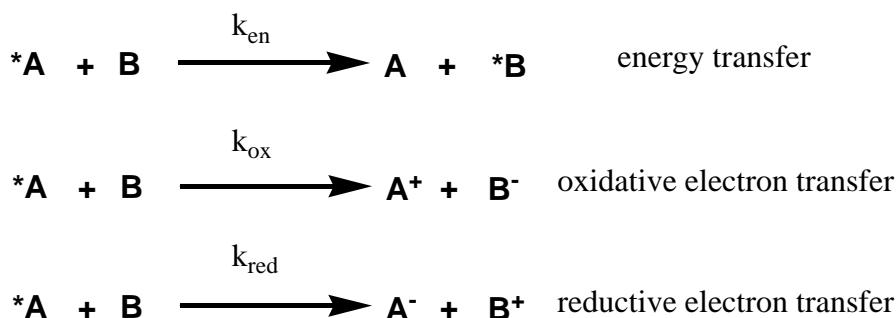


Fig I-8- Schematic representation of bimolecular processes that may take place following an encounter between an excited state and another chemical species^[4].

The most important bimolecular processes are energy transfer^[4,5] and electron transfer^[4,5], this latter process corresponding to the oxidation or reduction of the excited state :



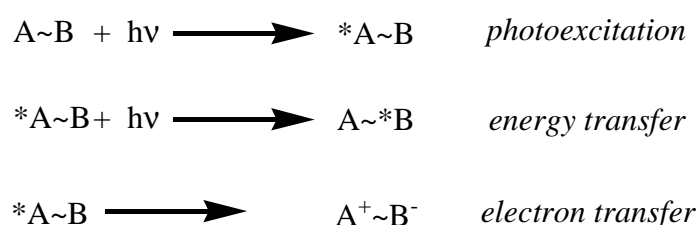
The thermodynamic ability of an excited state to undergo an energy transfer process is related to its zero-zero spectroscopy. For the electron transfer process the thermodynamic parameters are given by the oxidation and the reduction potentials of the ${}^*A/A^+$ and ${}^*A/A^-$ couples. A first approximation allows us to calculate the redox potentials for the excited state couples from the potentials of the ground state couples and the one-electron potential corresponding to the zero-zero excitation energy:

$$E(A^+/*A) = E(A^+/A) - E^{0-0}$$

$$E(*A/A^-) = E(A/A^-) + E^{0-0}$$

Kinetic parameters (intrinsic barrier and electronic transmission coefficient) can also play an important role in energy and electron transfer processes^[7].

Photoinduced energy transfer and electron transfer processes can also take place between components of supramolecular species^[8]:



In supramolecular species composed of several molecular components, successive energy or electron transfer steps may lead to energy migration or charge separation over long distances. Another interesting event that can take place upon light excitation of a supramolecular species is the so called optical electron transfer process, which leads to the direct formation of an intercomponent charge-transfer state.



Both photoinduced electron transfer and optical electron transfer may be followed by a thermal back electron transfer process:

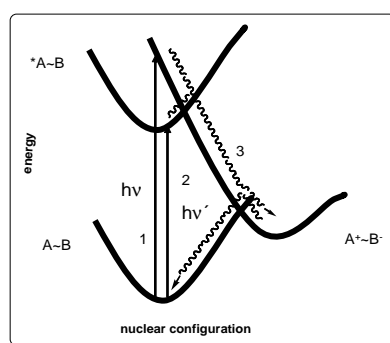


Fig I-9- Optical (1), photoinduced (2,3), and thermal back electron transfer processes in supramolecular species^[7].

The relationships between optical, photoinduced, and back electron transfer processes in a supramolecular species are schematized in (*Fig I- 9*). Several examples of energy and electron transfer processes in supramolecular species have been discussed in a number of book and review articles^[1,2,6-13].

4. $[\text{Ru}(\text{bpy})_3]^{2+}$.

In the end of 1960's Crosby^[14,15] et al measured the spectroscopic properties of a bipyridine-type based metal complex series and detected the luminescence of $[\text{Ru}(\text{bpy})_3]^{2+}$, from its lowest triplet metal-to-ligand charge transfer excited-state, ³MLCT. In 1970 $[\text{Ru}(\text{bpy})_3]^{2+}$ was mentioned as a luminescent but not a photoreactive compound. In 1972, Gafney and Adamson^[16] discovered the reductive electron-transfer quenching of the ³MLCT excited-state of $[\text{Ru}(\text{bpy})_3]^{2+}$ by $[\text{Co}(\text{NH}_3)_5\text{Cl}]^{2+}$:



This discovery had a strong impact on the photochemical community, because in that period excited-state electron-transfer reactions were not common, even in the more mature field of organic photochemistry. Several research groups^[17-19] became immediately interested in the use of $*[\text{Ru}(\text{bpy})_3]^{2+}$ as a reactant and in few years it was clear that this complex shows a unique combination of chemical stability, redox properties, excited-state reactivity, and excited state lifetime. In 1975 Balzani^[20] reported experimental studies of water photosplitting by using $[\text{Ru}(\text{bpy})_3]^{2+}$ complexes as photosensitizer and photocatalyst. Since then, interest in the study of photochemical properties of bipyridine-type Ru(II) complexes has increased exponentially. In a special issue on the state-of-the art in inorganic photochemistry, published by the Journal of Chemical Education in 1983, an article^[21] was dedicated to ruthenium polypyridyl compounds and several other articles about their use in energy^[22] and electron^[23] transfer process. In the middle 1980s most of the properties of $[\text{Ru}(\text{bpy})_3]^{2+}$ were fully characterized (*Fig I-10*)^[24].

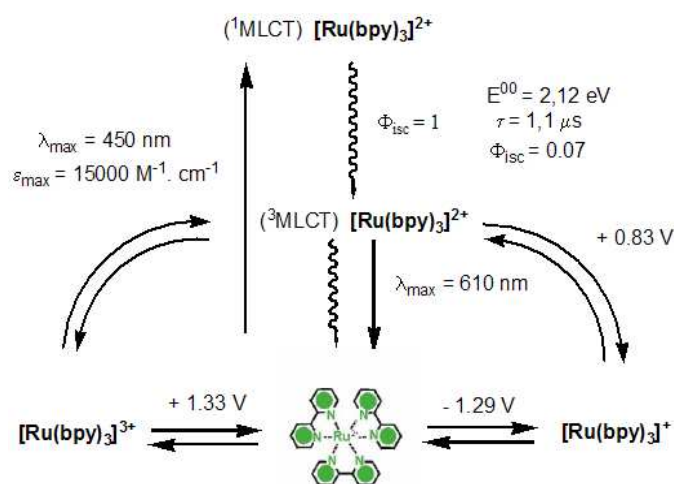


Fig I-10 Schematic representation of some important properties of $[\text{Ru}(\text{bpy})_3]^{2+}$ in deaerated CH_3CN solution at 298 K. The potential values are referred to SCE.

By choosing the right counter-ion, $[\text{Ru}(\text{bpy})_3]^{2+}$ salts can be dissolved in several solvents, from dichloromethane to water. The complex is thermodynamically stable and kinetically inert and shows very intense ligand-centered absorption bands in the UV spectral region and a broad and intense MLCT band in the visible region with a maximum at 450 nm. Its lowest excited state, $^3\text{MLCT}$ is relatively long-lived (1.1 μs in deaerated acetonitrile solution at 298 K, 5 μs in rigid matrix at 77 K), and exhibits an intense emission at 605 nm ($\phi = 0.07$ in deaerated acetonitrile at 298 K). $[\text{Ru}(\text{bpy})_3]^{2+}$ has also very interesting electrochemical properties^[25,26]. It shows a metal-centered (MC) oxidation process in acetonitrile and six distinct ligand-centered reduction processes in DMF at 219 K^[27]. In its $^3\text{MLCT}$ excited-state, $[\text{Ru}(\text{bpy})_3]^{2+}$ is also a good reductant and good oxidant (*Fig I-10*). Several thousands of Ru-polypyridine complexes have been synthesized and characterized and it has been found that the redox and excited-state properties can be tuned by changing the ligand or ligand substituents^[22,23]. In the following years it became clear that Ru(II)-bipyridine-type complexes are very useful building blocks for the construction of supramolecular species capable of exhibiting particular photochemical and electrochemical properties^[1,28] and since the middle 1990s a variety of molecular devices and machines comprising a Ru-bpy complex as photoactive component have been constructed^[29,30].

5. Cage-type systems

Definition

Systems made of a metal ion enclosed in a macrocyclic ligand or encapsulated by a cage-type ligand may often be considered as supramolecular species ^[1,11]. In this introduction, we showed examples of metal complexes where the presence of cage type ligands modifies the photochemical and photophysical properties.

Photo-cleavable cages.

For several types of applications, it would be necessary to have cages that can be opened and/or closed by light excitation. Two different approaches to this problem have been reported.

It is well known that the 2.1.1, 2.2.1, and 2,2,2 polyoxadiazamacrobicyclic cryptands, prepared long ago by Lehn et Sauvage^[31,32] exhibit a high selectivity towards particular alkali metal ions due to the different cavity sizes. Photocleavage of one of the cryptand strand would cause a substantial fluorescence decrease, with a consequent release of the metal cation into the solution. To obtain this result, Lehn, et al ^[33] have introduced the photocleavable 2-nitrobenzyl ether into one of the bridges of the cryptand (*Fig I-11*). In principle, these compounds could be used to create light controlled jumps or pulses of cation concentrations, that would be quite useful for physiological investigations. Photocleavable chelating ligands for alkaline-earth cations have also been described^[34,35].

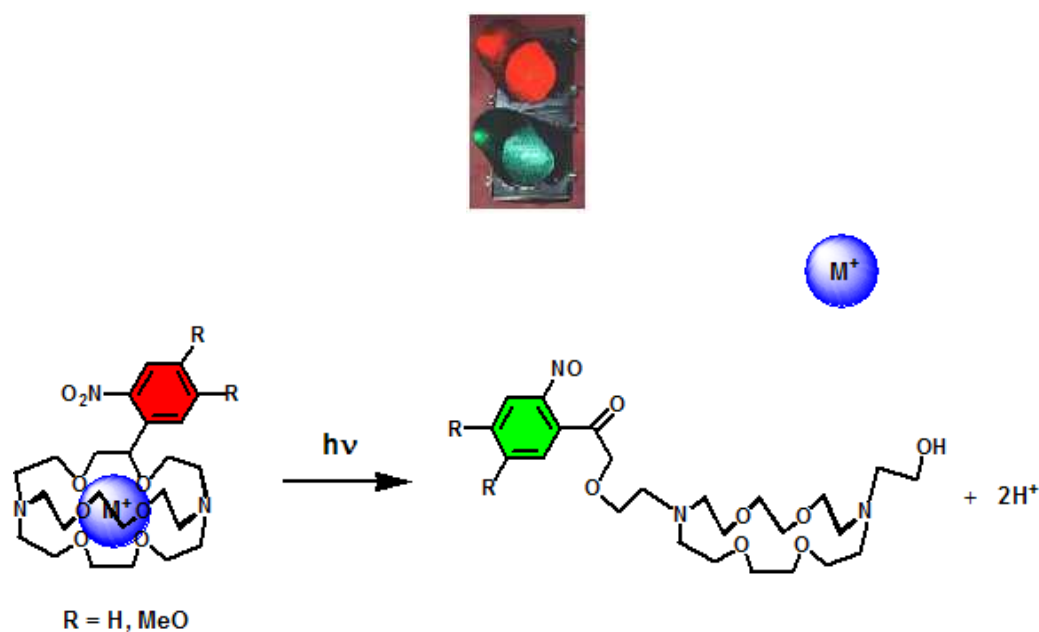


Fig I-11-Photocleavable cryptands

Host-Guest systems

Life is based on molecular recognition, transformation, and translocation processes carried out by extremely complicated chemical systems (enzymes, genes, antibodies, etc...). The fundamental discovery of crown ether by Pedersen^[36] in 1967 opened the way to the study of molecular recognition, transformation, and translocation processes with simple synthetically accessible molecular species. In the last years, most of the attention was focused on the synthesis of polyammonium macrocyclic receptors able to receive organic molecules non-covalently linked inside the macrocycle. The work of Stoddart^[37] is a elegant example of host-guest system using this time two weakly-bonded organic molecules, one for the first example is a dibenzo[24]-crown-[8] ether which is able to accept a dimethyl-4,4'-bipyridinium guest, the second example shows a dibenzo-4,4'-bipyridinium cyclic dimer which plays the role of host and guest.

6. Host-Guest systems using Ru(II)-Polypyridine systems.

Supramolecular species whose components are connected by means of non-covalent forces can be disassembled and reassembled by modulating the interactions that keep the component together, thereby allowing switching of electron- or energy transfer processes. Ru(II) bipyridine complexes can be useful components to build up this kind of systems^[38].

Proton-driven assembling process

1,4,8,11-Tetraazacyclotetradecane (cyclam), which is one of the most extensively investigated ligands in coordination chemistry, in its protonated forms can play the role of host towards cyanide metal complexes. Balzani and Vögtle^[39] have investigated the acid-driven adducts formed in acetonitrile-dichloromethane solution between $[\text{Ru}(\text{bpy})(\text{CN})_4]^{2-}$ and 1,4,8,11-tetrakis(naphthylmethyl)cyclam and a dendrimer consisting of a cyclam core appended with 12 3,5-dimethoxybenzene and 16 naphthyl unit (*Fig I-12*). $[\text{Ru}(\text{bpy})(\text{CN})_4]^{2-}$, with the two

cyclamic ligands exhibiting characteristic absorption and emission bands that are strongly affected by addition of acid. When a solution containing equimolar amounts of $[\text{Ru}(\text{bpy})(\text{CN})_4]^{2-}$ and the two ligands are titrated with TFA, the adduct in Fig I-12 is formed with a quenching of the fluorescence of naphthyl units by very efficient energy transfer to the metal complex. This adduct $[\text{Ru}(\text{bpy})(\text{CN})_4]^{2-} + \text{cyclam}$ can be disrupted by addition of a base (1,4-diazabicyclo[2.2.2]octane), yielding the starting species $[\text{Ru}(\text{bpy})(\text{CN})_4]^{2-}$ and the cyclams. The stimulation with two chemical inputs (acid and base) both exhibit two distinct optical outputs (naphthalene-based and $\text{Ru}(\text{bpy})$ -based emissions) that behave according to an XOR and an XNOR logic, respectively.

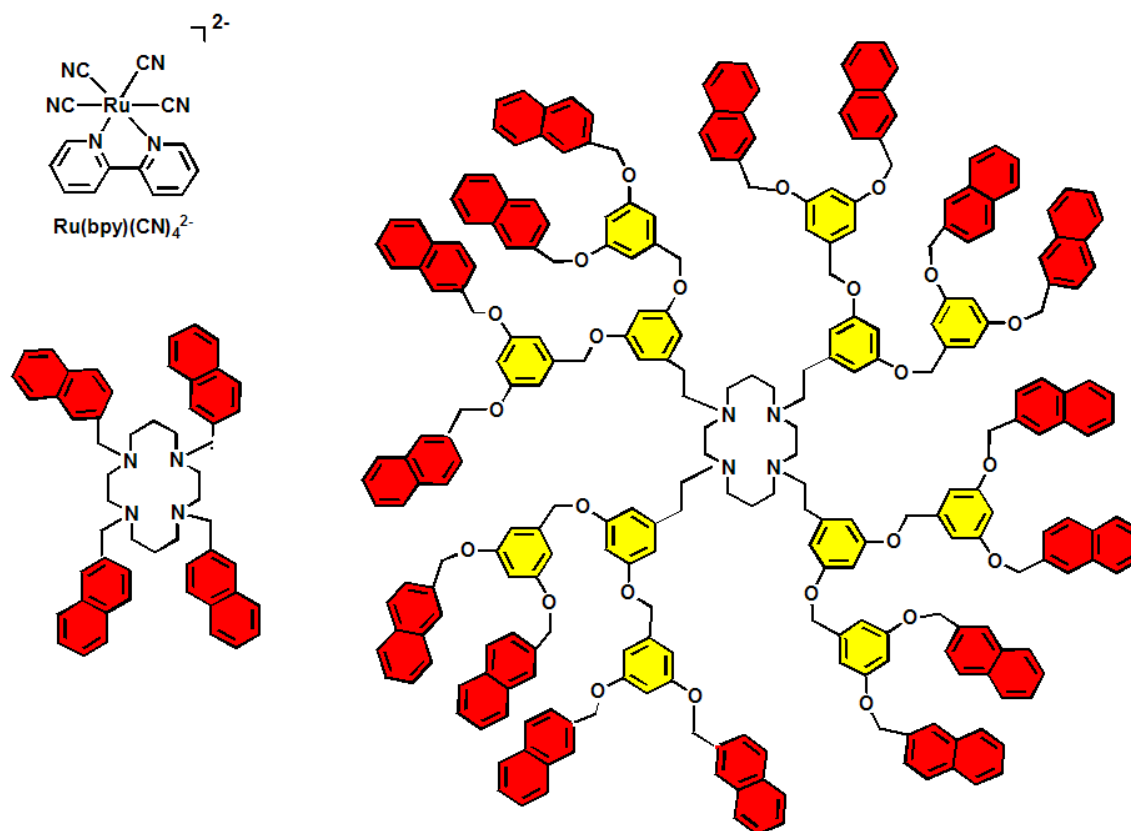


Fig I-12- Structure of $[\text{Ru}(\text{bpy})(\text{CN})_4]^{2-}$ complex and of two cyclam-cored dendrimers

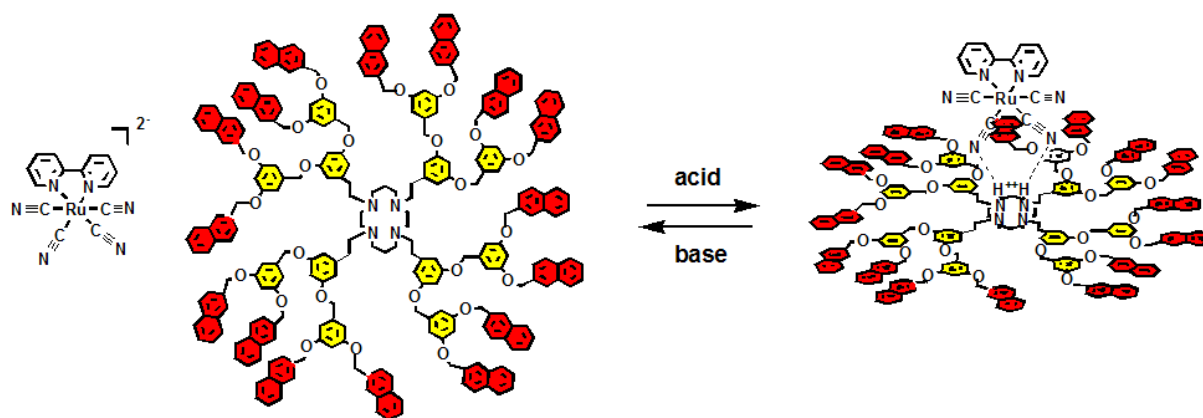


Fig I-13-Schematic representation of the formation of the $[\text{Ru}(\text{bpy})(\text{CN})_4]^{2-}$ (Cyclam) adduct

II-Supramolecular systems using Ru(II)-polypyridine complexes

Molecular Machines

Supramolecular self-assembly

1.) *Rotaxanes, pseudorotaxanes and catenanes.*



Rotaxanes and catenanes are molecular (multicomponent) species^[1,2,40] strictly related to, but very different from, pseudorotaxanes (*Fig I-14*). Pseudorotaxanes can be dissociated into their wirelike and macrocycle components, whereas rotaxanes and catenanes are interlocked species, whose dissociation requires breaking of a covalent bond. The general strategy to prepare rotaxanes and catenanes with high yields is based on the template effect^[41], which relies on the presence of molecular recognition sites in the components to be assembled. Rotaxanes (*Fig I-14*) are formed by a ring which is threaded by a linear fragment with bulky groups on either end. Catenanes (*Fig I-14*) are species composed of interlocked rings. Catenanes, rotaxanes and related species like knots are molecular architectures^[42] very attractive from a design point of view. This architectures have received the attention, but only

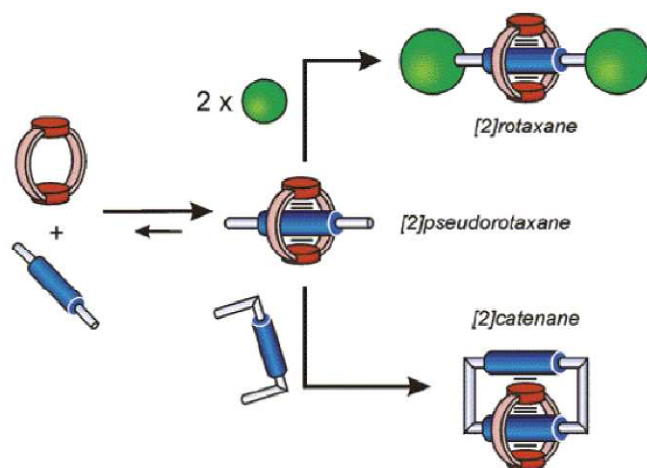


Fig-I-14 Formation of [2]rotaxane, [2]pseudorotaxane and [2] catenane with simple building elements

recent achievements in synthetic and analytic methods have made possible their synthesis and characterisation. Nowadays several catenanes, rotaxanes, knots, helicates, etc... have been prepared and their photochemical and photophysical properties have been investigated^[8,9]. Fig (I-14) shows the routes by which components bearing suitable recognition sites leads to the formation of rotaxanes. Way (1) shows the threading of a molecule through a preformed ring, followed by capping the end(s) of the thread follow by a capping operation with a preformed dumbbell-shaped component.

Catenanes

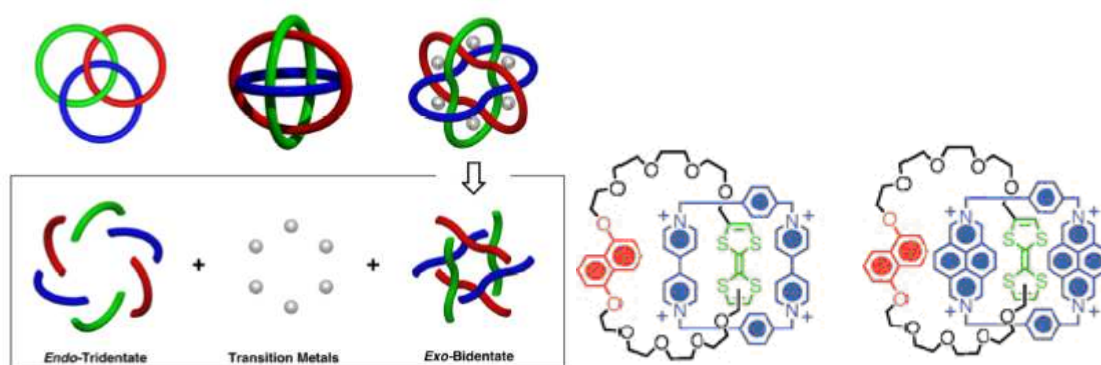




Fig I-15 Example of catenanes Borromean rings^[43] self-assemblies^[44,45], Olympiadane^[46].

Chemically controllable catenanes

Stoddart and coworkers have performed template-directed synthesis of a catenane using an electron donor-acceptor interaction. The groups involved in the electron donor-acceptor interaction are the electron rich hydroquinol unit and the electron deficient bipyridinium (paraquat) unit (*Fig I-16*)

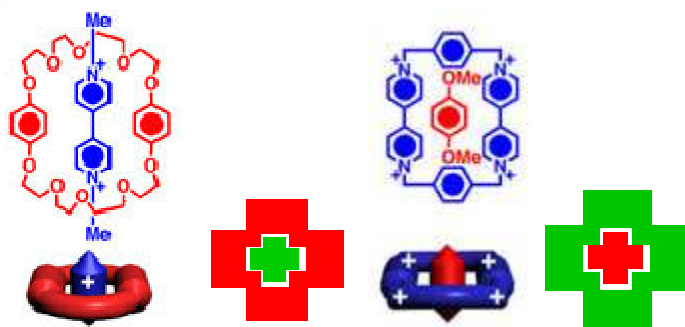


Fig I-16-Host-Guest system containing a dibenzo[24]crown[8] and a paraquat moieties, and its inverse species^[41,42]

Using this template effect, Stoddart has build catenanes (*Fig I-17*) using the most rational synthetic strategy by clipping the macrocycle onto a preformed one . A double-clipping procedure was used^[43], for the synthesis of the [2]catenane^[44, 45] (*Fig I-17*) which incorporates a bipyridinium-based tetracationic cyclophane and a π -electron-rich macrocyclic polyether comprising a tetrathiafulvalene ring system in the solid state.

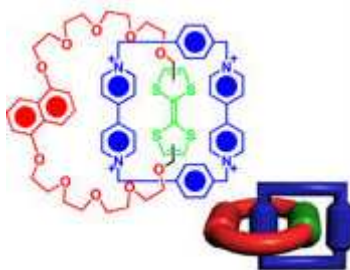


Fig-I-17 Stoddart's [2]catenane

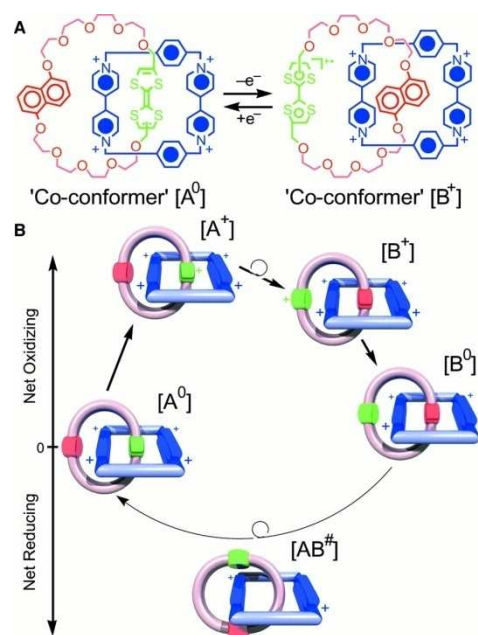


Fig-I-18- Redox controllable [2]catenane

Photochemical control of catenane movement

One intriguing aspect of the bacterial photosynthetic reaction center is the redox asymmetry of the cofactors; electron transfer proceeds exclusively along one branch of an almost symmetrical pair of reagents^[47, 48]. The catenane structure can be exploited to reproduce such an asymmetry with artificial systems; in catenane (*Fig I-19*)^[49], the two bipyridinium electron acceptors, linked to a $[\text{Ru}(\text{bpy})_3]^{2+}$ -type primary electron donor, possess different reduction potential because one of them is encircled by an electron donor crown ether that both attenuates its electron acceptor affinity via charge transfer interactions and hinders access by solvent molecules. Indeed, in CH_3CN solution at 293 K, a very fast ($k = 5.9 \times 10^{10} \text{ s}^{-1}$) electron transfer takes place from the photoexcited $[\text{Ru}(\text{bpy})_3]^{2+}$ moiety to a bipyridinium unit. Although it can be anticipated with thermodynamic arguments that the redox asymmetry of the two acceptor branches (*Fig I-19*) should result in a fivefold difference in rate constants^[49], there is no means to distinguish between the two electron transfer paths by time-resolved spectroscopic techniques. In such a system, back electron transfer is also extremely rapid ($k = 2.4 \times 10^{10} \text{ s}^{-1}$) owing to the close proximity of the reactants, despite the fact that it should fall in the Marcus “inverted” region.

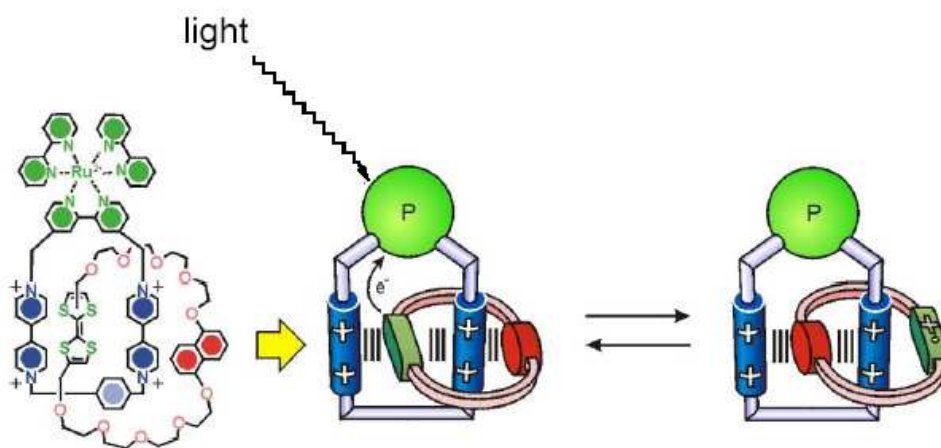


Fig I-19- Photoinduced rotation in [2]catenane^[49]

Pseudorotaxane

Defintion

A pseudorotaxane according the Stoddart definition^[50] “ ..is an interwoven inclusion complex in which a molecular thread is encircled by one or more beads (macrorings) so that the thread’s extremities are directed away from the bead’s center. At least one of the thread’s extremities are directed away from the bead center. At least one of the thread’s extremities does not possess a bulky stopper group. Hence, the constituents of the assemblage, like any complex, are at liberty to dissociate into separate molecular species. In contrast with rotaxanes, there is no attendant mechanical bond to maintain the system’s integrity”.

Complexes which are good candidates for chemical switching include those that rely upon hydrogen-bonding interactions between ammonium ions and crown ethers. It has long been known that organic ammonium ions can forms adducts with crown-ethers^[51,52]. More recently, it has been found^[53-56] that suitable threadlike dialkyl ammonium ions, for example, the dibenzylammonium cation, can interpenetrate suitably sized crown ethers, for example, dibenzo[24]crown-[8] in non polar solvents to form pseudorotaxanes^[50].

Piston/Cylinder systems



Fig I-20- Donor and acceptor moieties in a [2]pseudorotaxane

Dethreading/rethreading of the wire and the ring components of a pseudorotaxane resembles the movement of a piston in a cylinder^[9] (Fig I-21). The first attempts at designing a photochemically driven molecular machine of this type were carried out on pseudorotaxanes stabilized by donor/acceptor interaction (Fig I-21). In such systems, the donor/acceptor interaction introduces low-energy charge transfer (CT) excited states responsible for absorption bands in the visible region. Light excitation in these CT absorption bands leads formally to the transfer of an electron from the donor to the acceptor component, as illustrated in (Fig I-21) for the pseudorotaxane formed in H₂O or CH₃CN solution by the electron donor thread **26** and the electron acceptor **25**⁴⁺. As a consequence, particularly when this process leads to formation of charges of the same sign in the two components, one can expect destabilization of the pseudorotaxane structure followed by dethreading. In practice, however,

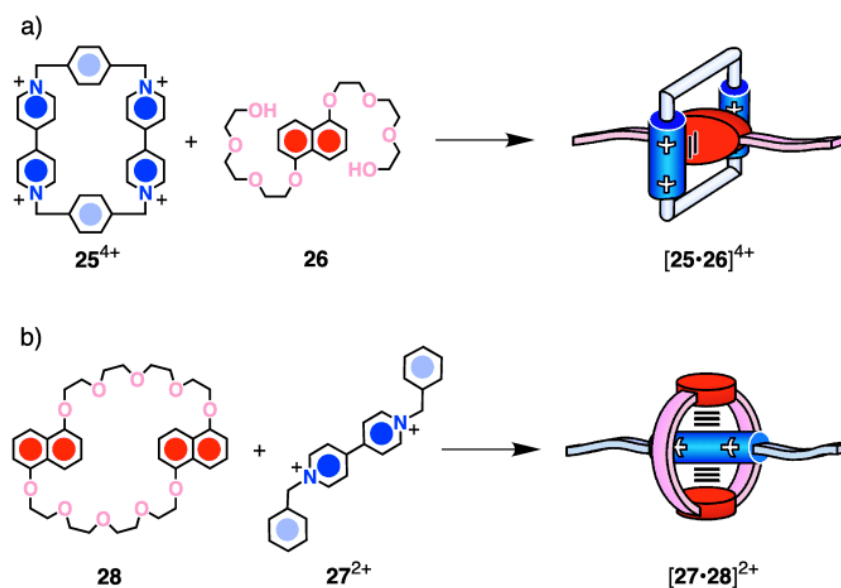


Fig I-21- Photochemical processes associated with [2]pseudorotaxane **[25·26]**⁴⁺ **[27·28]** upon excitation in its charge transfer absorption band^[57,58].

This simple approach does not work because the back electron transfer process is much faster than the separation of the molecular components, a process that requires extended nuclear motions and solvent rearrangement. In some particular cases ^[59,60], laser flash photolysis (LFP) experiments have suggested that a small fraction of the irradiated pseudorotaxane may undergo dissociation.

Photoisomerization reactions, particularly the well-known reversible cis/trans photoisomerization of the azobenzene group, have long been used to exert photochemical control on chemical systems^[61]. Azobenzene-containing compounds have been employed both

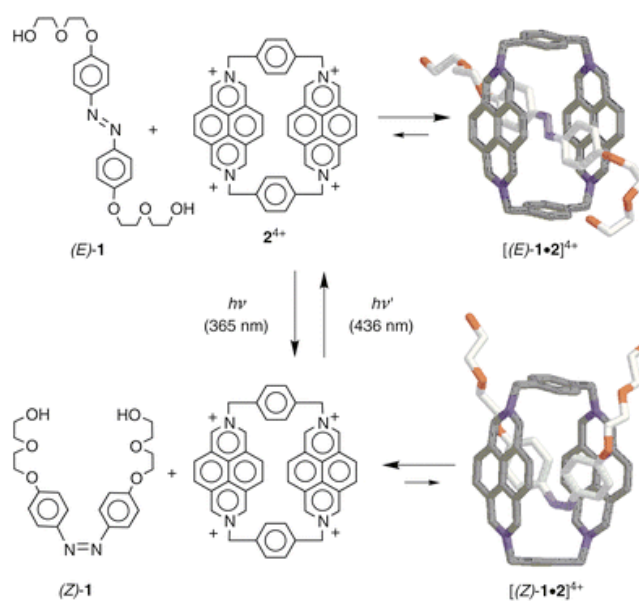


Fig I- 22- (Z) and (E) geometry control in a Pseudo-rotaxane^[62]

Molecular plug/socket and extension cable

Hydrogen-bonding interactions between ammonium ions and crown ethers are particularly convenient for constructing molecular-level plug/socket devices since they can be switched on and off and quickly and reversibly by means of acid-base inputs (*Fig I-23*)^[63].

The plug/socket concept can then be extended to design molecular systems which mimic the function played by a macroscopic electrical extension cable. An extension cable is more complex than a plug/socket device since there are three components held together by two connections that have to be controllable reversibly and independently; in the fully connected system, an electron or energy flow must take place between the remote donor and acceptor units (*Fig I-24*)

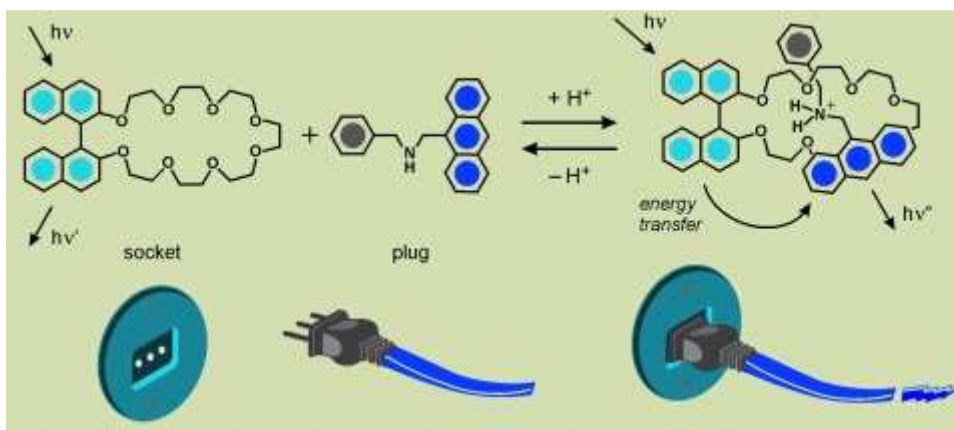


Fig I-23- A plug-socket system: switching of photoinduced energy transfer by acid/basedcontrolled plug in/plug out of suitable molecular components^[63].

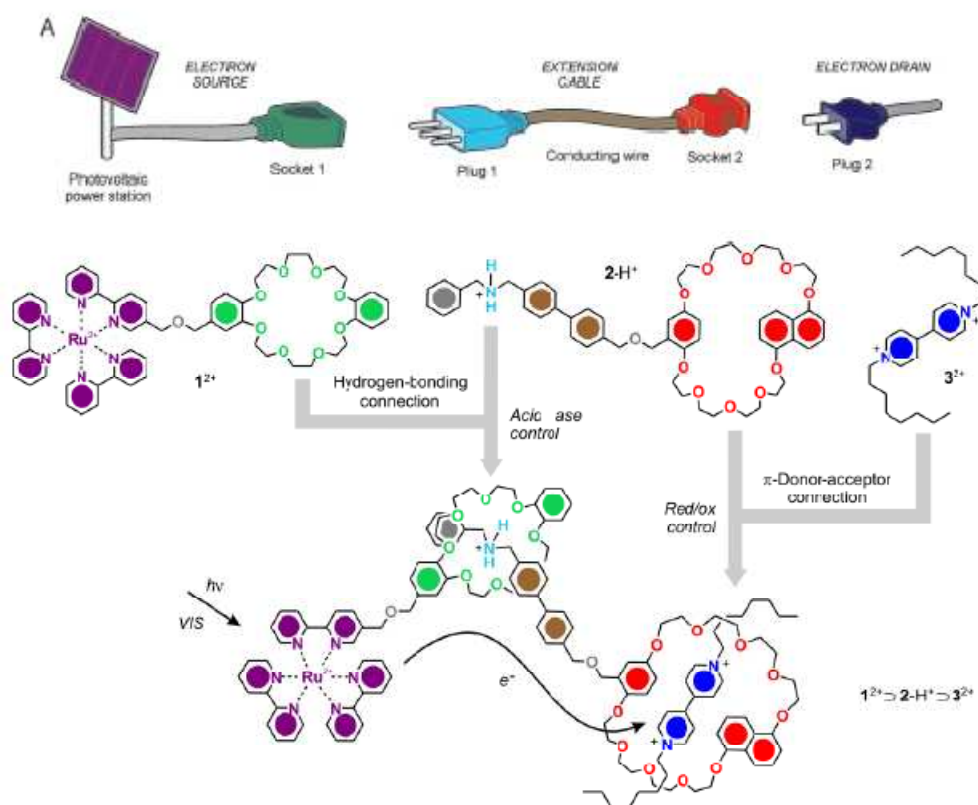


Fig I-24- Elongation in a photoinduced [2+2]-Pseudorotaxaneformation^[64,65]

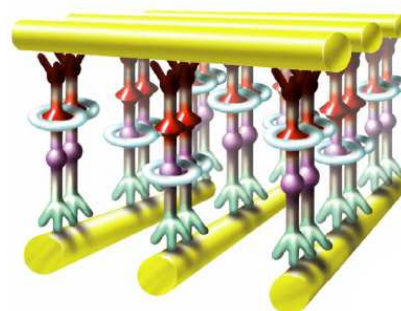
In the attempt of constructing a molecular-level extension cable, the [3]pseudorotaxane shown in (Fig I-24), made of three components 1^{2+} , $[2H]^+$, 3^{2+} . In the fully connected triad light excitation of the $[Ru(bpy)_3]^{2+}$ unit of the component 1^{2+} is followed by electron-transfer to the ammonium unit of $[2H]^+$ and to the bipyridinium unit unit of component 3^{2+} . This process can be photocontrolled reversibly and independently.

Rotaxanes: Molecular shuttles



Chemically controllable molecular shuttles.

The [2]rotaxane in *fig* I-24 incorporates a π -electron-deficient macrocycle and a π -electron-rich-dumbbell^[66]. In solution the macrocycle resides around the benzidine or the biphenol recognition site. The two conformations are stabilised by π - π stacking interactions between the bipyridinium units of the macrocycle and the sandwiched π -electron-rich recognition site of the dumbbell, as well as by C-H \cdots O interactions between the bipyridinium hydrogen atoms and the polyether oxygen atoms (Fig-I-25). The [2]rotaxane of *Fig* I-26 incorporate a dialkylammonium and a bipyridinium recognition site in their dumbbell-shaped components^[67,68]. The preference of the macrocycle for the ammonium recognition site is a result of a combination of $^+N-H\cdots O$ and C-H \cdots O interactions between the $CH_2NH_2^+$ hydrogen atoms of the dumbbell and the oxygen atoms of the macrocycle. Upon addition of an excess of iPr_2Net to a solution of one of these [2]rotaxanes in $(CD_3)_2CO$, deprotonation of the ammonium recognition site occurs. As a result, the intercomponent hydrogen bonds are destroyed and the macrocycle shuttles to the bipyridinium recognition site in a and b. However, the original co-conformation is restored after the addition of CF_3CO_2H , since the protonation of the ammonium recognition site is followed by the shuttling of the macrocycle back to encircle the NH_2^+ center.



Upon addition of an excess of iPr_2Net to a solution of one of these [2]rotaxanes in $(CD_3)_2CO$, deprotonation of the ammonium recognition site occurs. As a result, the intercomponent hydrogen bonds are destroyed and the macrocycle shuttles to the bipyridinium recognition site in a and b. However, the original co-conformation is restored after the addition of CF_3CO_2H , since the protonation of the ammonium recognition site is followed by the shuttling of the macrocycle back to encircle the NH_2^+ center.

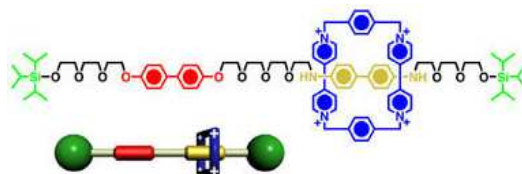


Fig I-25- The shuttling of the macrocyclic component along its dumbbell-shaped component can be controlled chemically or 33immer33chemically by protonating/deprotonating or oxydizing/reducing the benzidine unit^[66].

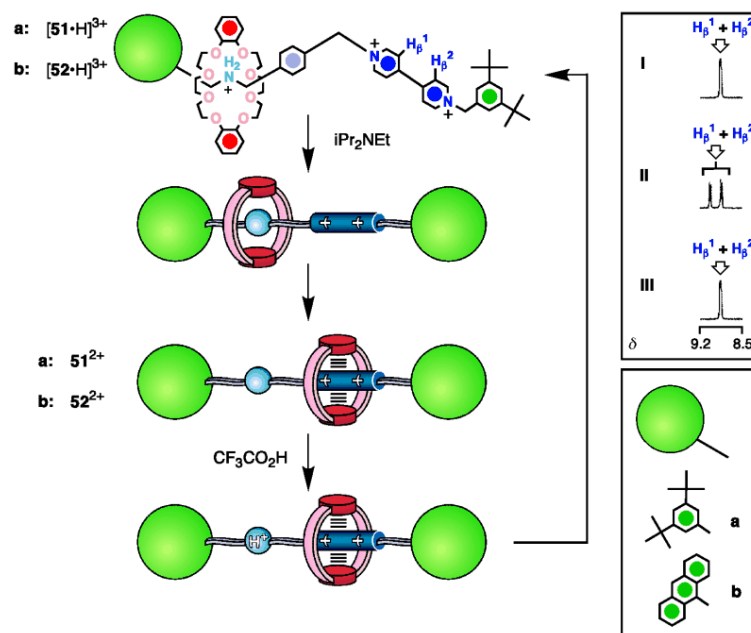


Fig I- 26-Chemically controllable^[67,68] molecular shuttles

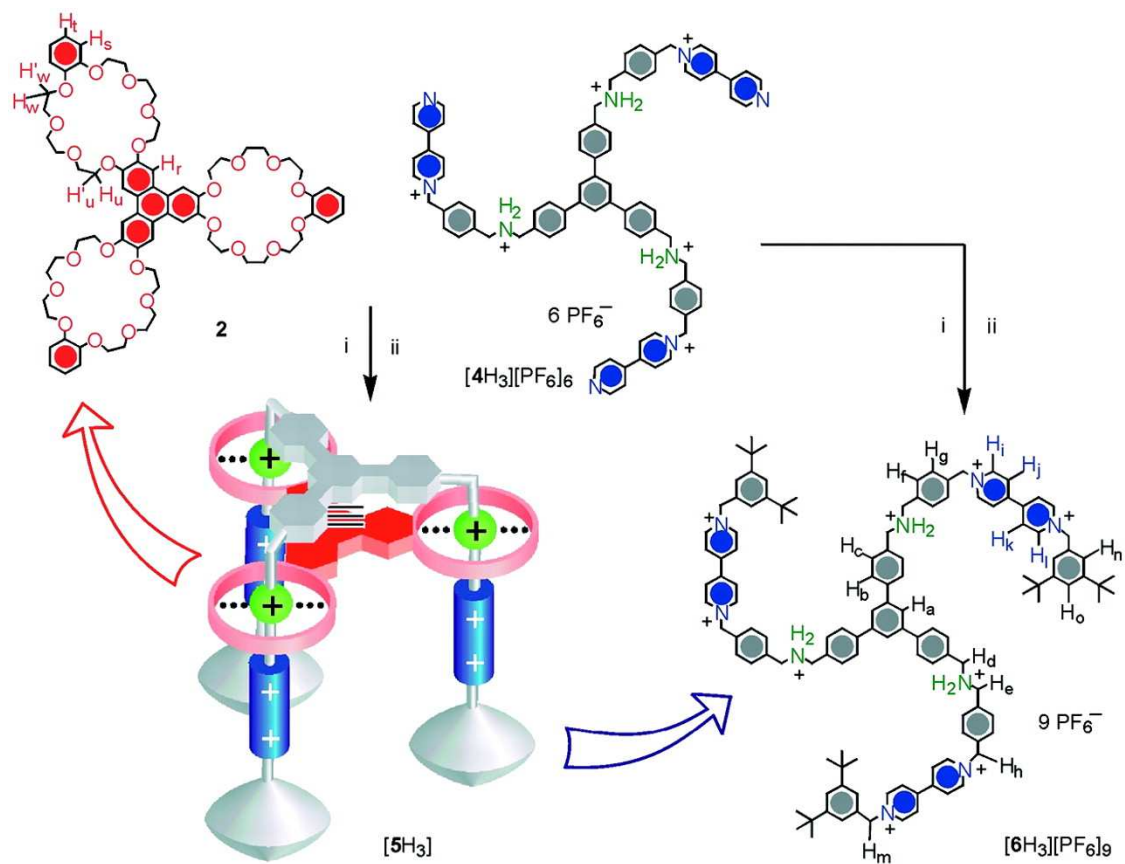


Fig I-27- Nanoelevator using chemically controllable pseudo-rotaxane^[69]

Photochemically controllable molecular shuttles

This year Balzani and Stoddart have reported^[70] an example of photoinduced shuttling movement of [2]rotaxane photosensitized by a $[\text{Ru}(\text{bpy})_3]^{2+}$ complex, This was synthesized^[71] and its mechanism was photochemically and electrochemically studied. The mechanism is based on a “four-stroke” synchronized sequence of electronic and nuclear processes. At room temperature the deactivation time of the high-energy charge transfer state obtained by light excitation is about $10 \mu\text{s}$, and the time period required for the ring-displacement process is on the order of $100 \mu\text{s}$. The rotaxane behaves as an autonomous linear motor and operates with a quantum efficiency up to $\sim 12\%$. The investigated system is a unique example of an artificial linear nanomotor because it gathers together the following features: (i) it is powered by visible light (sunlight), (ii) it exhibits autonomous behaviour, like motor proteins, (iii) it does not generate waste product, (iv) its operation can rely only on intramolecular processes, allowing in principle operation at the single-molecule level, (v) it can be driven at a frequency of 1 kHz , (vi) it works in mild environmental conditions (fluid solution at ambient temperature), (viii) it is stable for at least 10^3 cycles.

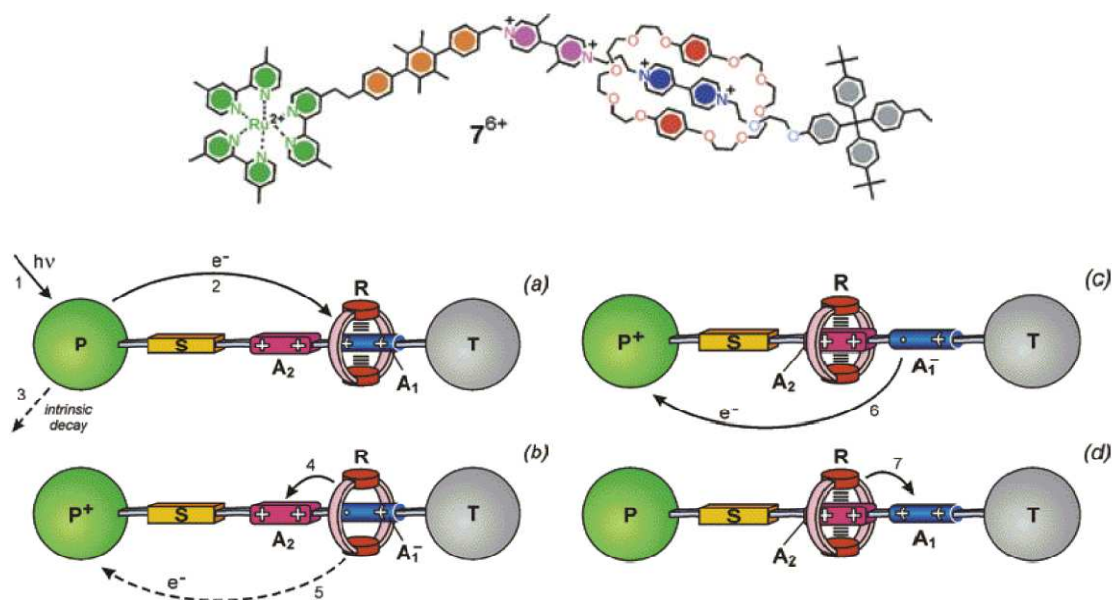


Fig I-28- Autonomous artificial nanomotor powered by sunlight^[70,71].

The $[\text{Ru}(\text{bpy})_3]^{2+}$ - type unit P (*Fig I-28*) is capable of playing the role of a photosensitizer for ring shuttling because visible light excitation leads to the formation of a long-lived strongly reducing excited state. Each phase corresponds, in kind to the fuel injection and combustion (a), piston displacement (B), exhaust removal (C), and piston replacement (D) of a four-stroke engine. The timing of the strokes is intrinsic to the molecular motor and cannot be tuned up externally as in fuel-injected car engines.

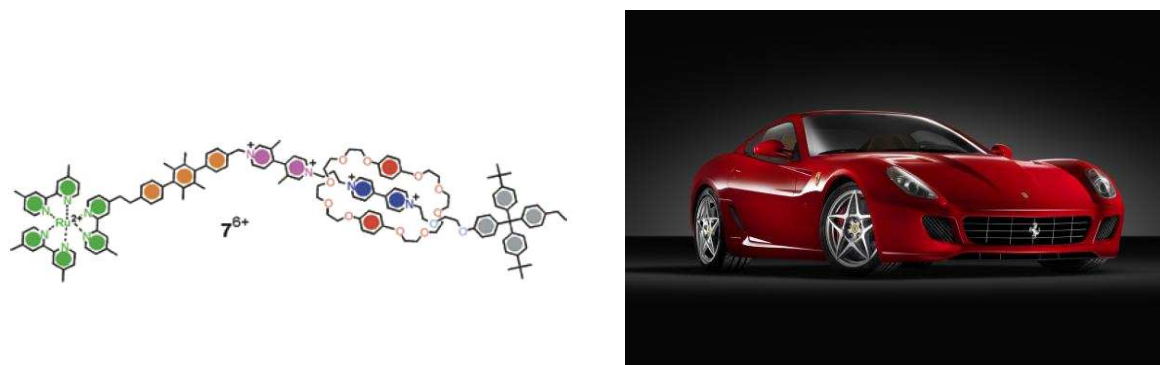


Fig I-29 – Nanopiston faster than highly performant motorsport cars

Besides being powered by sunlight and operating as an autonomous motor, this nano piston shows other very interesting properties. It is operational in mild condition, it is stable, and can be driven at high frequency (1 kHz) approximately 60000 rpm. If we compare to high performant motorsport cars (max 10000 rpm), the rotation performance is higher for the nanopiston.

Another light driven shuttle using the same process has been reported by Leigh^[72]. The [2]rotaxane (*Fig I-30*) consists of a benzylic cyclic macrocycle that surrounds an axle featuring two hydrogen-bonding stations, namely, a succinimide unit and a naphthylimide unit, separated by a long alkyl chain. Initially, the macrocycle resides on the succinimide station because the naphthalimide unit, which undergoes high-yield intersystem crossing to the triplet excited state. Such a triplet state can be reduced in bimolecular encounters by an electron donor (D) added to the solution in a sufficiently large amount. Because the back electron transfer process is spin forbidden and thus slow, the photogenerated ion pair can efficiently dissociate; the naphthylimide radical anion survives for hundreds of microseconds

before it decays by bimolecular charge recombination with D radical cation. Since the naphthylimide anion is a much stronger hydrogen-bonding station compared to the succinamide, upon reduction of the naphthylimide unit the macrocycle is expected to shuttle from the latter to the former station; this has been demonstrated by cyclic voltammetric experiments. Laser flash photolysis studies have demonstrated that this is indeed the case; the time required for ring shuttling ($\sim 1 \mu\text{s}$) (with D = DABCO) is much shorter than the lifetime of the naphthylimide radical anion ($\sim 100 \mu\text{s}$). After charge recombination, the macrocycle moves back to its starting position. This [2]rotaxane constitutes an other example of a linear motor driven exclusively by light, although its operation still relies on the presence of external reactants, which however are not consumed.

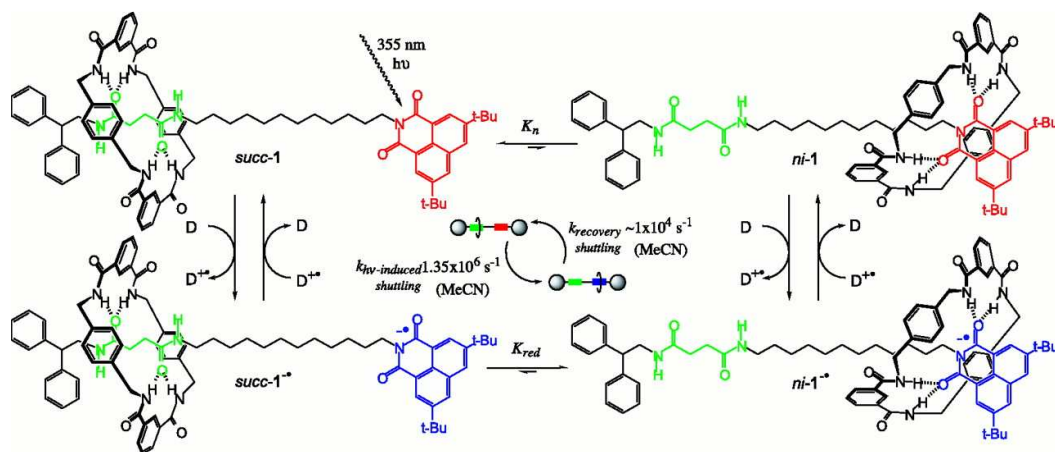


Fig-I-30- Leigh's light powered [2]-rotaxane^[72]

Photochemically induced conformational motion

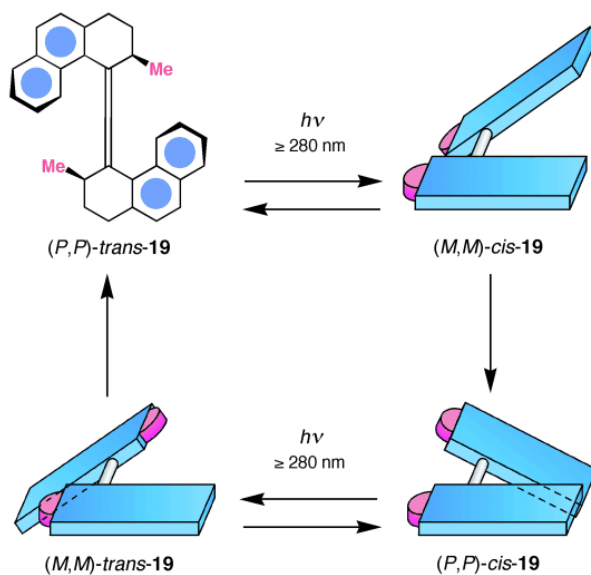


Fig I-31- The light-fueled rotary motor 19 undergoes unidirectional rotation in n-hexane at 333K upon irradiation at appropriate wavelengths

In order to generate a light-driven unidirectional molecular rotor, the design of this molecular switch was studied^[73,74] (*Fig I-31*) with using a chiral 38immer of tetrahydrophenanthrene. Each of the two helical subunits of the resulting compound 19 can adopt a right handed (P) or a left-handed (M) helicity. As a result, a total of four stereoisomers are possible for this compound. However, the cis/trans isomerisation are reversible and occur upon irradiation at appropriate wavelengths. By contrast the inversions of helicities, while maintaining a cis or a trans configuration, occur irreversibly under the influence of thermal energy. Upon irradiation (> 280 nm, 218 K) of a solution of (P,P)-obtained in a ratio 5:95. By warming the solution up to 293 K, (M,M)-cis 19 interconverts irreversibly to (P,P)-cis-19. Subsequent irradiation (>280 nm) of the solution produces a mixture of (P,P)-cis-19 and (M,M)-trans-19 in a ratio of 10:90. Upon increasing the temperature further (333 K), (M,M)-trans-19 in a ratio of 10:90. Upon increasing the temperature further (333 K), (M,M)-(P,P)-trans-19. Thus, a sequence of light- and temperature- induced isomerizations can be exploited to move this molecular rotor in one direction only. The unidirectional motion in this system is dictated by the stereogenic centers associated with the two methyl substituent. Tour^[75] has used this motion to build motorised nanocars which used light as fuel.

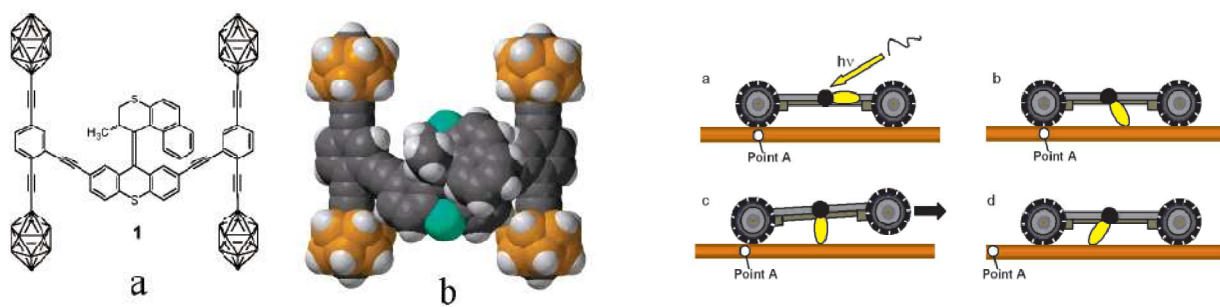


Fig I-32- Carboborane based nanochassis^[75]

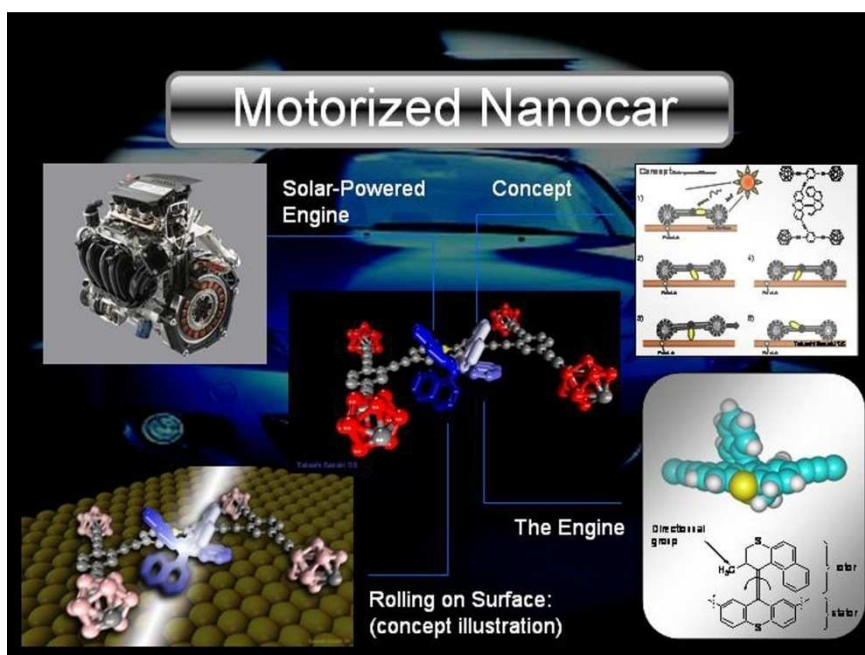


Fig I-33- Light motioned nano-chassis for molecular nanocar^[75].

Covalently-linked molecular components.

Photosynthesis, the natural process where sunlight is converted into chemical energy (food, firewood, fossil fuels) that maintains life on the earth, is based on photoinduced energy and electron transfer processes. In green plants, light is absorbed by ordered arrays of pigments, and the resulting excitation energy is channelled to specific sites (reaction centers) where a charge separation reaction takes place. The reducing and oxidizing species so obtained give rise to secondary chemical reactions which lead to the final products. An important aim of current chemical research is the design of supramolecular species to be used for building up artificial photosynthetic systems.

The supramolecular species can also be obtained by linking molecular components via covalent bonds (*Fig I-3*). In this way it is possible to synthesize linear or bi- and tri-dimensional arrays of molecular components where photoinduced electron and energy transfer processes can take place in a controlled manner

In the last few years many experimental and theoretical investigations have explored the mechanism of photoinduced electron and energy transfer processes and the state of the art can be found in several books and reviews^[1,5,10].

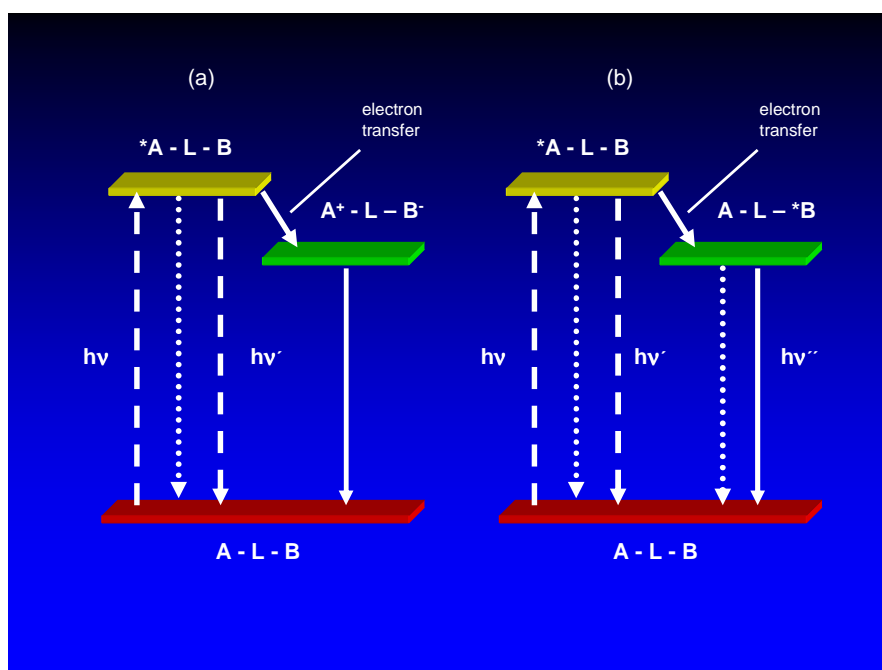


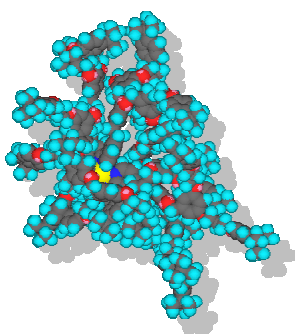
Fig I-34- Schematic representation of photoinduced electron (a) and energy (b) transfer processes in a supramolecular system made of two components (A and B) linked by a connector (L)

Photoinduced electron and energy processes in supramolecular species made of two covalently-linked molecular components can be schematized as in *Fig I-34*. In general, photoinduced electron transfer is followed by a fast back electron transfer process, and energy transfer is followed by the radiative. Detailed investigations have shown that in the compounds with larger spacers there are conformers where energy transfer does not take place and conformers where energy transfer is very fast.

Dendrimers.

Definition.

Dendrimers are a new class of well-defined macromolecules exhibiting a tree-like structure ^[76]. Dendrimer chemistry was initially developed in the field of organic chemistry. More recently,



a number of dendrimers based on metal complexes have been synthesized ^[77]. Metal complexes are



characterized by a precise molecular geometry related to the characteristic coordination number of the metal ion and can exhibit valuable properties such as absorption of visible light, luminescence and reduction and oxidation at low potentials. By using metal complexes it is possible to

incorporate in the dendritic structure specific ‘pieces of information’ that, when placed in suitable sites of the array, can be used to perform valuable functions. From a structural viewpoint, most of the metal-containing dendrimers can be classified according to four categories:

- (i) dendrimers built around a metal complex as a core;
- (ii) dendrimers containing metal complexes as peripheral units;
- (iii) dendrimers containing metal complexes in the branches;
- (iv) dendrimers based on metals as branching centers ^[76];

Examples of dendrimers synthesized by Balzani and coworkers ^[78], shows in some cases some complexes assembly architectures containing polypyridine metal complexes like Ru and Os. The design of such polynuclear metal complexes capable of exhibiting interesting photophysical and electrochemical properties. Using polypyridine ligands like 2,3-dpp and 2,5-dpp as bridging ligands (dpp = bis(2-pyridyl)pyrazine), Ru(II) and Os(II) as metal centers, and bpy or biq (biq=2,2'-biquinoline) as terminal ligands (Fig I-) and the so called

complexes-as-metals and complexes-as-ligands synthetic strategy^[78,79], Balzani has prepared a series of homo- and heterometallic di-^[80], tri-^[81], tetra-^[82,83], hexa-^[84,85], hepta-^[86], deca-^[87], trideca-^[88], and docosanuclear^[89] complexes. The structure of a decanuclear complex of this family is schematized in (Fig I-35). Such complexes, which have a dendrimer-type structure are very interesting because depending on the number and location of the metal and the ligand components, predetermined energy migration (Fig I-36 right) and redox patterns (Fig I-36) can be obtained^[77,90]. The use of this kind of dendrimers as molecular-level antennas to harvest sunlight has been recently reviewed^[91].

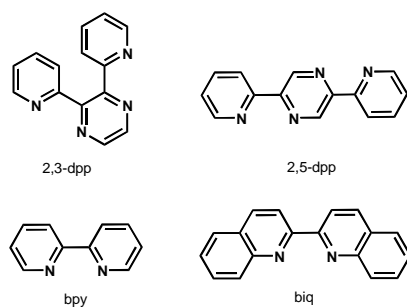


Fig I-35- Polypyridine ligands employed to obtain polynuclear complexes of large nuclearity^[78].

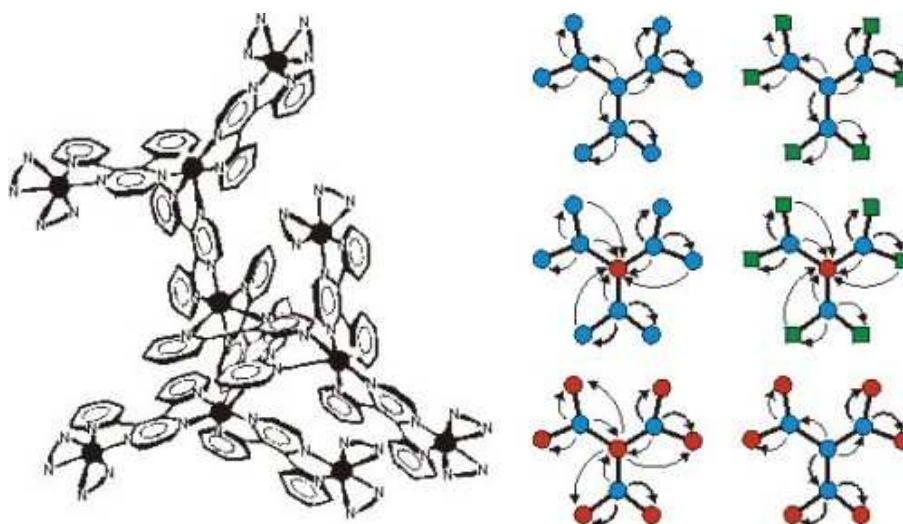


Fig I-36- Schematic view of the structure of a decanuclear complex containing Ru and Os ions^[87]

The group of Vögtle has synthesised a dendrimer built around a $\text{Ru}(\text{bpy})_3^{2+}$ core. In the dendritic complex (Fig I-37), the bpy ligands of the $[\text{Ru}(\text{bpy})_3]^{2+}$ type core carry branches

containing 3,5-dimethoxybenzene and 2-naphthyl-type chromophoric units^[92]. Since such units are separated by aliphatic connections the interchromophore interactions are weak and the absorption spectra of the dendrimer is substantially equal to the sum of the spectra of the groups present. The three types of chromophoric groups, namely, $[\text{Ru}(\text{bpy})_3]^{2+}$, dimethoxybenzene, and naphthalene, are potentially luminescent species. In the dendrimer, however the fluorescence of the dimethoxybenzene and naphthyl-type units is almost completely quenched in acetonitrile solution, with sensitization of the luminescent core ($\lambda_{\text{max}} = 610 \text{ nm}$). These results show that a very efficient energy-transfer process takes place converting the very short lived UV fluorescence of the aromatic units of the wedges to the long-lived orange emission of the metal-based dendritic core. In aerated solution the luminescence intensity of the dendrimer core is more than twice as intense as that of $[\text{Ru}(\text{bpy})_3]^{2+}$ parent compound because the dendrimer branches protect the Ru-bpy-based core from dioxygen quenching^[93]. In conclusion, because of the very high absorbance of the naphthyl groups in the UV spectral region, the high energy-transfer efficiency, and the strong emission of the $[\text{Ru}(\text{bpy})_3]^{2+}$ type core, the dendrimer exhibits a strong visible emission upon UV excitation even in very dilute ($10^{-7} \text{ mol. L}^{-1}$) solutions.

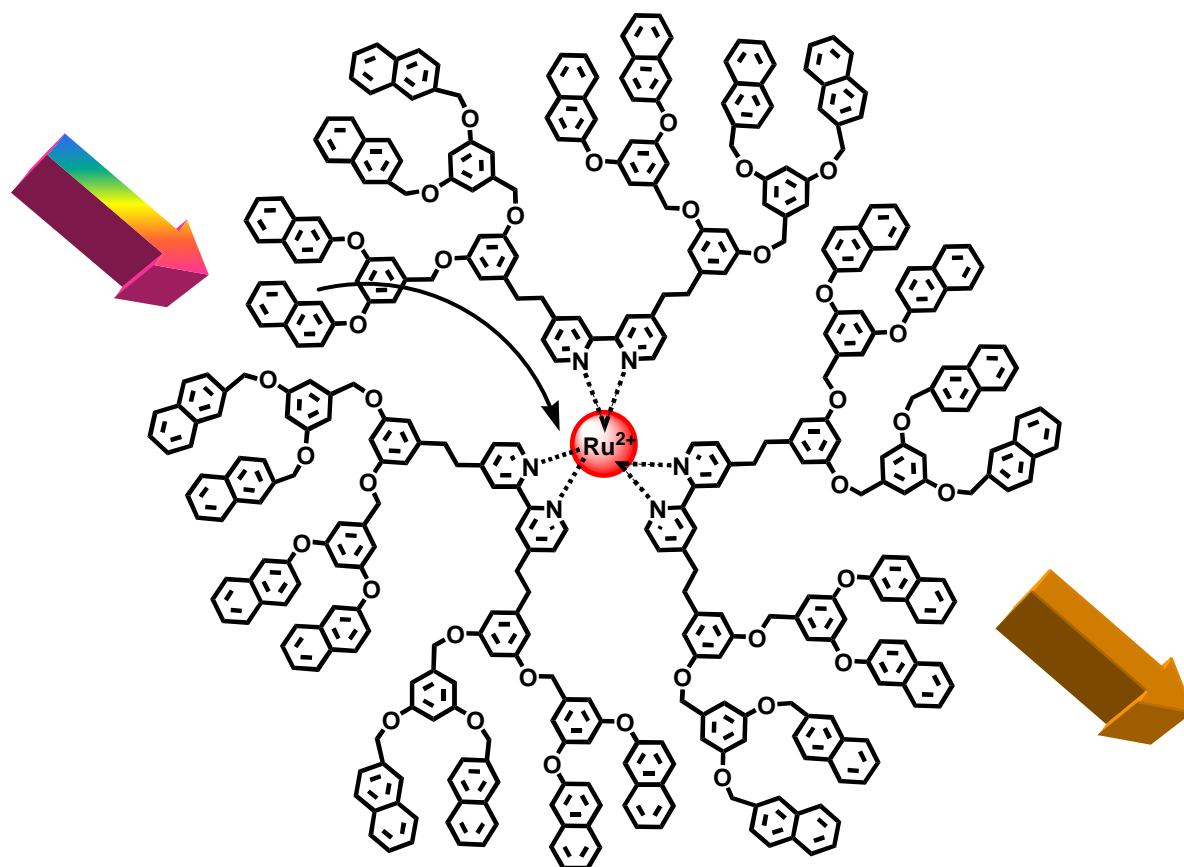
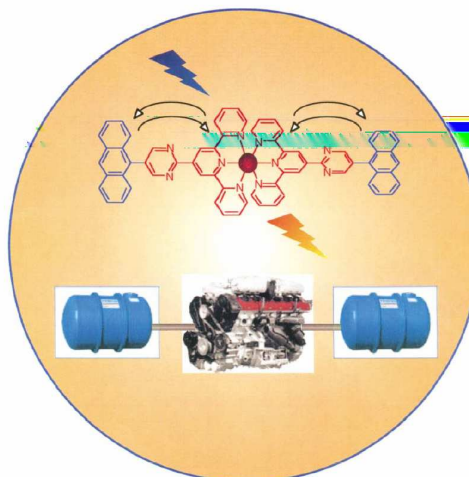


Fig I-37- Antenna effect in a dendrimer^[91]

Metallosupramolecular chemistry

2,2':6',2''-terpyridine complexes



The 2,2':6',2''-terpyridine ligands have very interesting chemical properties due to the possible linear functionalisation at the 4'-position^[93-99]. In the course to synthesise molecules which are potential molecular-wire at nano-scale, the usefulness of 4'-substituted tpy ligand is of great interest because the bridging spacer formed after complexing with transition metal can have a linear geometry. However that is not the case with the

2,2'-bipyridine ligands which have several problems when used for devices with well-defined geometries, and after complexation and formation of heteroleptic complexes, the problem of enantiomer formation appears. Octahedral complexes $[M(tpy)_3]^{2+}$ are achiral and the substitution in 4'-position does not generate enantiomers

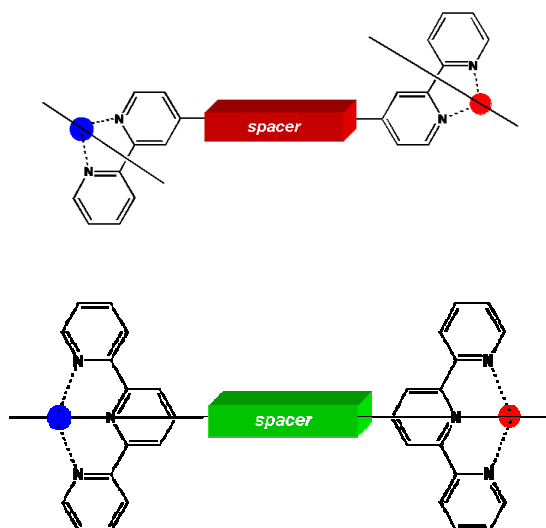


Fig I-38- Geometrical representation of dinuclear complexes containing bpy ligand and tpy ligand

Metallostars

According to the definition of Constable^[12], metallostars are first generation metallodendrimers and it is convenient to consider them as a separate class^[12] because the majority of compounds of this class have been specifically prepared as first-generation species without the structural development of the ligands that would be required for the separation of a dendrimer. In the literature, the distinction between metallostars and metallodendrimers is not usually clearly made.

Metallostars based on terpyridines

A series of heptanuclear metallostars based upon central $\{M(\text{bpy})_3\}$ motifs and bearing pendant $\{M'(\text{tpy})_2\}$ units has been prepared by Constable and co-workers making extensive use of the reactions of coordinated bpy and tpy ligands. In a convergent approach, the complex (Fig I-39) was obtained by the reaction of 4,4'-(HO)₂bpy with $[\text{Ru}(\text{tpy})(\text{tpy}-\text{Cl})]^{2+}$.

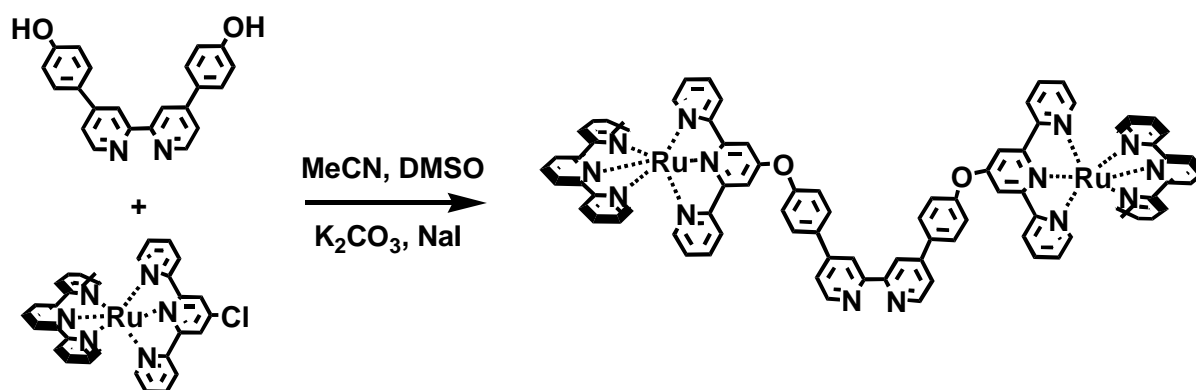


Fig I-39-Heteroleptic bpy based dinuclear complex^[99]

Reaction of coordinated ligands have been extensively used in the preparation of higher-generation star compounds based upon hexasubstituted benzene as core (Fig I-40). Using the same strategy and a trinuclear nucleophilic unit, reaction with hexakis(bromomethyl)benzene yielded the beautiful octadecanuclear 36^+ charged metallostar.

The inherent chirality of the $\{M(\text{bpy})_3\}$ motif is a disadvantage when it comes to multinuclear compounds as these will be formed as mixtures of diastereoisomers unless special conditions

are used to optimize stereospecificity. In contrast, $\{M(\text{tpy})_2\}$ units linked through the 4'-position are achiral and are an ideal motif for the linear extension of achiral metallostars

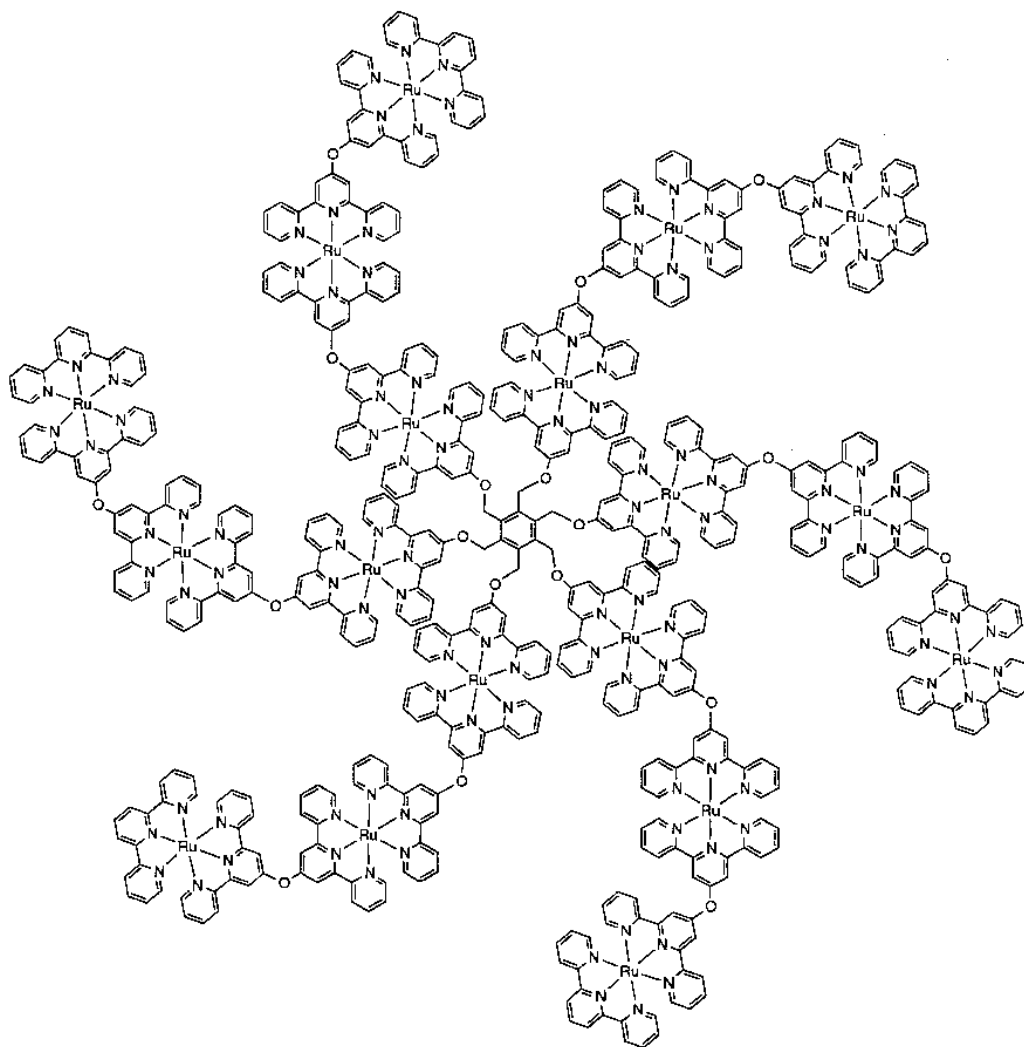


Fig I-40- Octadecanuclear Ru (II) terpyridine based metallostar^[100,101].

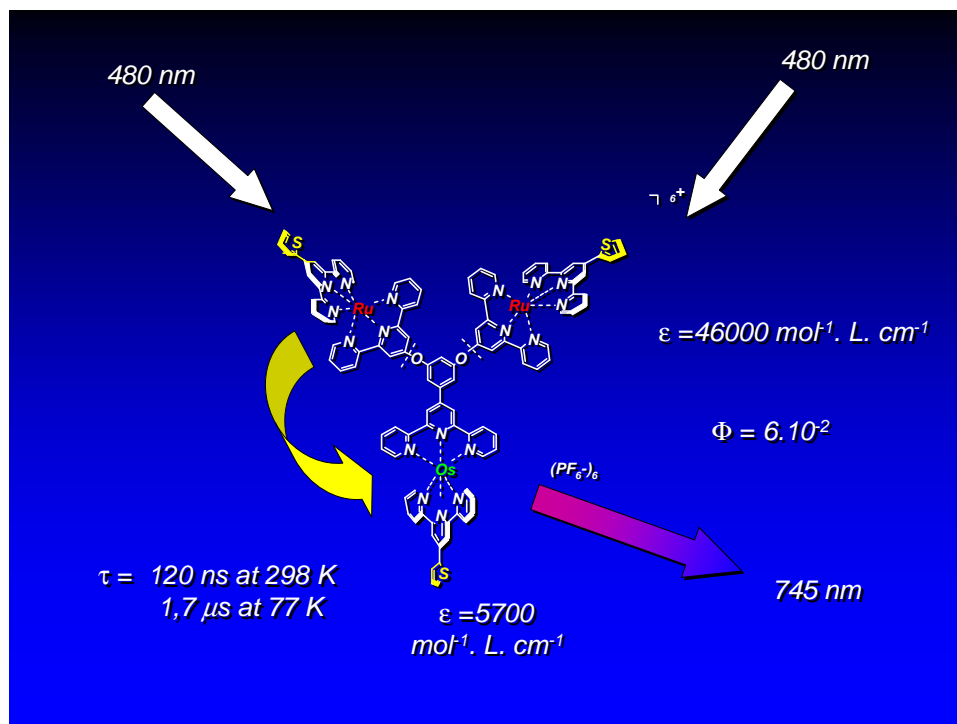


Fig I-41- Photoinduced energy transfer through a Ru-Os Y shaped metallostar^[102,103]

Multiinuclear oligopyridine complexes are important in metallosupramolecular chemistry and species such as rods or wires, helicates and dendrimers are well established. The investigation of photoinduced energy- and electron-transfer (Metal-to-Ligand) in geometrically well defined polynuclear systems allows the electronic and nuclear factors governing these processes to be investigated. The exploitation of the spectroscopic (particularly luminescence) properties of transition metal-oligopyridine complexes for ion sensing, light harvesting or energy collection using high-nuclearity dendrimers is of intense current interest^[101, 102]

References.

- [1]. Lehn, J.-M., *Supramolecular Chemistry*, VCH, Weinheim, **1995**.
- [2]. Balzani, V., Scandola, F., *Supramolecular Photochemistry*, Ellis Horwood Chichester U.K., **1991**.
- [3]. Ringsdorf, H., Schlarb, B., Venzmer, J., *Angew. Chem. Int. Ed. Engl.* **1988**, 27, 113.
- [4]. Balzani, V., Moggi, L., Manfrin, M. F., Boletta, F., Laurence, G. S., *Coord. Chem. Rev.* **1975**, 15, 321.
- [5]. Karvanos, G. J., Turro, N. J., *Chem. Rev.* **1986**, 86, 401.
- [6]. Lehn, J.-M., *Angew. Chem. Int. Ed. Engl.* **1990**, 29, 1304.
- [7]. Balzani, V., *Tetrahedron* **1992**, 48, 10443
- [8]. Sauvage, J.-P., Dietrich-Buchecker, C. O., Eds, *Molecular Catenanes, Rotaxanes and knots*, Wiley-VCH, Weinheim, **1999**.
- [9]. Balzani, V., Credi, A., Raymo, F. M., Stoddart, J. F., *Angew. Chem. Int. Ed. Engl* **2000**, 39, 3348.
- [10]. Sauvage, J.-P., Collin, J.-P., Chambron, J.-C., Guillerez, S., Coudret, C., Balzani, V., Barigelletti, F., De Cola, L., Flamigni, L., *Chem. Rev.* **1994**, 94, 993.
- [11]. Vögtle, F., *Supramolecular Chemistry*, Wiley, Chichester, U.K., **1991**.
- [12]. Constable, E. C., in *Comprehensive Coordination Chemistry II, Vol 7* (Eds: Fujita, M., Powell, A., Creutz, C., ; Series Eds: McCleverty, J. A., Meyer, T. J.), Elsevier, Oxford, **2003**, p 263.
- [13]. Ballardini, R., Balzani, V., Credi, A., Gandolfi, M. T., Venturi, M., *Acc. Chem. Res.* **2001**, 34, 445.
- [14]. Klassen, D. M., Crosby, G. A., *J. Chem. Phys.* **1965**, 43, 1498.
- [15]. Crosby, G. A., Watts, R. J., Carstenes, D. H. W., *Science* **1970**, 170, 1195.
- [16]. Gafney, A. D., Adamson, A W., *J. Am. Chem. Soc.* **1972**, 94, 8238.
- [17]. Sabbatini, N., Balzani, V., *J. Am. Chem. Soc.* **1972**, 94, 7587.
- [18]. Natarajan, P., Endicott, J. F., *J. Phys. Chem.* **1973**, 77, 971.
- [19]. Navon, G., Sutin, N., *Inorg. Chem.* **1974**, 13, 2159.
- [20]. Balzani, V., Moggi, L., Boletta, F., Manfrin, M. F., *Science* **1975**, 189, 852.
- [21]. Watts, R. J., *J. Chem. Educ.* **1983**, 60, 814.
- [22]. Balzani, V., Scandola, F., *J. Chem. Educ.* **1983**, 60, 834.
- [23]. Sutin, N., Creutz, C., *J. Chem. Educ.* **1983**, 60, 809.

- [24]. Juris, A., Balzani, V., Barigelletti, F., Campagna, S., Belser, P., von Zelewsky, A., *Coord. Chem. Rev.* **1988**, *84*, 85.
- [25]. De Armond, M. K., Carlin, C. M., *Coord. Chem. Rev.* **1981**, *36*, 325.
- [26]. Vlcek, A. A., *Coord. Chem. Rev.* **1982**, *43*, 39.
- [27]. Roffia, S., Casadei, R., Paolucci, F., Paradisi, C., Bignozzi, C. A., Scandola, F., *J. Electroanal. Chem.* **1991**, *302*, 157.
- [28]. Marcaccio, M., Paolucci, F., Paradisi, C., Carano, M., Roffia, S., Fontanesi, C., Yellowlees, L. J., Serroni, S., Campagna, S., Balzani, V., *J. Electroanal. Chem.* **2002**, *532*, 99.
- [29]. Balzani, V., *Photochem. Photobiol. Sci.* **2003**, *2*, 459.
- [30]. Balzani, V., Credi, A., Venturi, M., *Molecular Devices and Machines. A Journey into the Nano World*, Wiley-VCH, Weinheim, **2003**, p. 1.
- [31]. Lehn, J.-M., *Struct. Bond.* **1973**, *16*, 1.
- [32]. Lehn, J.-M., Sauvage, J.-P., *J. Am. Chem. Soc.* **1975**, *97*, 6700.
- [33]. Warmuth, R., Grell, E., Lehn, J.-M., Bats, J. W., Quinkert, G., *Helv. Chim. Acta* **1991**, *74*, 671.
- [34]. Adams, S. R., Kao, J. P. Y., Grienkiewicz, G., Minta, A., Tsien, R. Y., *J. Am. Chem. Soc.* **1988**, *110*, 3212.
- [35]. Ellis-Davies, G. C. R., Kaplan, J. H., *J. Org. Chem.* **1988**, *53*, 1966
- [36]. Pedersen, C. J., *J. Am. Chem. Soc.* **1967**, *89*, 2495.
- [37]. Ashton, P. R., Goodnow, T. T., Kaifer, A. E., Reddington, M. V., Slawin, A. M. Z., Spencer, N., Stoddart, J. F., Vicent, C., Williams, D. J., *Angew. Chem. Int. Ed. Engl.* **1989**, *28*, 1396.
- [38]. Balzani, V., Credi, A., Venturi, M., *Proc. Natl. Acad. Sci. USA.* **2002**, *99*, 4814.
- [39]. Bergamini, G., Saudan, C., Ceroni, P., Maestri, M., Balzani, V., Gorka, M., Lee, S.-K., van Heyst, J., Vögtle, F., *J. Am. Chem. Soc.* **2004**, *126*, 16466.
- [40]. Sauvage, J.-P., *Acc. Chem. Res.* **1990**, *23*, 319.
- [41]. Busch, D. H., Vance, A. L., Kolchinski, A. G., in *Comprehensive Supramolecular Chemistry*, Vol 9, Pergamon, Oxford, **1996**, p. 1.
- [42]. Schill, G. *Catenanes, Rotaxanes, and knots*, Academic: New York, USA, **1971**.
- [43]. Cantrill, S. J., Chichak, K. S., Peters, A. J., Stoddart, J. F., *Acc. Chem. Res.* **2005**, *38*, 1.
- [44]. Balzani, V., Credi, A., Mattersteig, G., Menzer, S., Montalti, M., Spencer, N., Stoddart, J. F., Venturi, M., Williams, D. J., *J. Org. Chem.* **2000**, *65*, 1924.

- [45]. Asakawa, M., Ashton, P. R., Boyd, S. E., Brown, C. L., Gillard, R. E., Kocian, O., Raymo, F. M., Stoddart, J. F., Tolley, M. S., White, A. J. P., Williams, D. J., *J. Org. Chem.* **1997**, *62*, 26.
- [46]. Amabilino, D. B., Ashton, P. R., Reder, A. S., Spencer, N., Stoddart, J. F., *Angew. Chem. Int. Ed. Engl.* **1994**, *33*, 1286.
- [47]. Deisenhofer, J., Michel, H., *Angew. Chem. Int. Ed. Engl.* **1989**, *28*, 829.
- [48]. Huber, R., *Angew. Chem. Int. Ed. Engl.* **1989**, *28*, 848.
- [49]. Ashton, P. R., Balzani, V., Credi, A., Kocian, O., Pasini, D., Prodi, L., Spencer, N., Stoddart, J. F., Tolley, M. S., Venturi, M., White, A., Williams, D. J., *Chem. Eur. J.* **1998**, *4*, 590.
- [50]. Ashton, P. R., Phillip, D., Spencer, N., Stoddart, J.F., *J. Chem. Soc. Chem. Commun.* **1991**, 1677.
- [51]. Dietrich-Buchecker, C. O., Sauvage, J.-P., *Chem. Rev.* **1987**, *87*, 795.
- [52]. Amabilino, D. B., Stoddart, J. F., *Chem. Rev.* **1995**, *95*, 2725.
- [53]. Kolchinski, A. G., Busch, D. H., Alcock, N. W., *J. Chem. Soc. Chem. Commun.* **1995**, 1289.
- [54]. Ashton, P. R., Campbell, P. J., Chrystal, E. J. T., Glink, P. T., Menzer, S., Philp, D., Spencer, N., Stoddart, J. F., Tasker, P. A., Williams, D. J., *Angew. Chem. Int. Ed. Engl.* **1995**, *34*, 1865.
- [55]. Ashton, P. R., Chrystal, E. J. T., Glink, P. T., Menzer, S., Schiavo, C., Spencer, N., Stoddart, J. F., Tasker, P. A., White, A., Williams, D. J., *Chem. Eur. J.* **1996**, *2*, 709.
- [56]. Glink, P. T., Schiavo, C., Stoddart, J. F., Williams, D. J., *Chem. Commun.* **1996**, 1483.
- [57]. Ballardini, R., Balzani, V., Gandolfi, T., Prodi, L., Venturi M., Philp, D., Ricketts, H. G., Stoddart, J. F., *Angew. Chem. Int. Ed. Engl.* **1993**, *32*, 1301.
- [58]. Ashton, P. R., Ballardini, R., Balzani, V., Boyd, E., Credi, A., Gandolfi, M. T., Gómez-López, M., Iqbal, S., Philp, D., Preece, J. A., Prodi, L., Ricketts, H. G., Stoddart, J. F., Tolley, M. S., Venturi, M., White, A. J. P., Williams, D. J., *Chem. Eur. J.* **1997**, *3*, 152
- [59]. Benniston, A. C., Harriman, A., Philp, D., Stoddart, J. F., *J. Am. Chem. Soc.* **1993**, *115*, 5298.
- [60]. Benniston, A. C., Harriman, A., Yufit, D. S., *Angew. Chem. Int. Ed. Engl.* **1997**, *36*, 2356.
- [61]. Shinkai, S., Manabe, O., *Top. Curr. Chem.* **1984**, *121*, 76.
- [62]. Balzani, V., Credi, A., Marchioni, F., Stoddart, J. F., *Chem. Commun.* **2001**, 1861.
- [63]. Ishow, E., Credi, A., Balzani, V., Spadola, F., Mandolini, L., *Chem. Eur. J.* **1999**, *5*, 984.

- [64]. Ballardini, R., Balzani, V., Clemente-Léon M., Credi A., Gandolfi M. T., Ishow E., Perkins J., Stoddart, J. F., Tseng, H.-R., Wenger, S., *J. Am. Chem. Soc.* **2002**, *124*, 12786.
- [65]. Ferrer, B., Rogez, G., Credi, A., Ballardini, R., Gandolfi, M. T., Balzani, V., Liu, Y., Stoddart, J. F., *Proc. Natl. Acad. Sci. USA.* **2006**, *103*, 18411.
- [66]. Bissel, R. A., Córdova, E., Kaifer, A. E., Stoddart, J. F., *Nature* **1994**, *369*, 133.
- [67]. Martinez-Diaz, M.-V, Spencer, N., Stoddart, J. F., *Angew. Chem. Int. Ed. Engl.* **1997**, *36*, 1904.
- [68]. Ashton, P. R., Ballardini, R., Balzani, V., Baxter, I., Credi, A., Fyfe, M. C. T., Gandolfi, M. T., Gómez-López, M., Martinez-Diaz, M.-V., Piersanti, A., Spencer, N., Stoddart, J. F., Venturi, M., White, A. J. P., Williams, D. J., *J. Am. Chem. Soc.* **1998**, *120*, 11932.
- [69]. Badjic, J. D., Ronconi, C. M., Stoddart, J. F., Balzani, V., Silvi, S., Credi, A., *J. Am. Chem. Soc.* **2006**, *128*, 1489.
- [70]. Balzani V., Clemente-Leon M., Credi A., Ferrer B., Venturi M., Flood A. H., Stoddart J. F., *Proc. Natl. Acad. Sci. USA* **2006**, *102*, 1843.
- [71]. Ashton P. R., Ballardini R., Balzani V., Credi A., Dress K. R., Ishow E., Kleverlaan C. J., Kocian O., Preece J. A., Spencer N., Stoddart J. F., Venturi M., Wenger S., *Chem. Eur. J* **2000**, *6*, 3558.
- [72]. Brouwer, A. M., Frochot, C., Gatti, F. G., Leigh, D. A., Mottier, L., Paolucci, F., Roffia, S., Wurpel, G. W. H., *Science* **2001**, *291*, 2124.
- [73]. Komura, N., Zijlstra, R. W. J., van Delden, R. A., Harada, N., Feringa, B. L., *Nature* **1999**, *401*, 152.
- [74]. Feringa, B. L., van Delden, R. A., Komura, N., Geertsema, E. M., *Chem. Rev.* **2000**, *100*, 1789.
- [75]. Morin, J. F., Shirai, Y., Tour, J. M., *Org. Lett.* **2006**, *8*, 1713.
- [76]. Newkome, G. R., Morefield, C. N., Vögtle, F., *Dendritic Macromolecules: Concepts and Perspectives*, VCH, Weinheim, **1996**.
- [77]. Venturi, M., Serroni, S., Juris, A., Campagna, S., Balzani, V., *Top. Curr. Chem.* **1998**, *197*, 193.
- [78]. Denti, G., Serroni, S., Juris, A., Ciano, M., Balzani, V. in A. F. Williams, C. Floriani, A. Merbach (Eds.), *Perspectives in Coordination Chemistry*, VCH, Basel **1992**, p. 153.
- [79]. Serroni, S., Juris, A., Venturi, M., Campagna, S., Resino, I. R., Denti, G., Credi, A., Balzani, V., *J. Mater. Chem.* **1997**, *7*, 1227.
- [80]. Campagna, S., Denti, G., De Rosa G., Sabatino, G., Ciano, M., Balzani, V., *Inorg. Chem.* **1989**, *28*, 2565.

- [81]. Campagna, S., Denti, G., Sabatino, L., Serroni, S., Ciano, M., Balzani, V., *Gazz. Chim. Ital.* **1989**, *119*, 415.
- [82]. Campagna, S., Denti, G., Sabatino, L., Serroni, S., Ciano, M., Balzani, V., *J. Chem. Soc. Chem. Commun.* **1989**, 1500.
- [83]. Serroni, S., Juris, A., Campagna, S., Venturi, M., Denti, G., Balzani, V., *J. Am. Chem. Soc.* **1994**, *116*, 9086.
- [84]. Campagna, S., Denti, G., Serroni, S., Ciano, M., Balzani, V., *Inorg. Chem.* **1991**, *30*, 3728.
- [85]. Denti, G., Serroni, S., Campagna, S., Ricevuto, V., Juris, A., Ciano, M., Balzani, V., *Inorg. Chim. Acta.* **1992**, *507*, 198.
- [86]. Denti, G., Campagna, S., Sabatino, L., Serroni, S., Ciano, M., Balzani, V., *Inorg. Chim. Acta.* **1990**, *176*, 175.
- [87]. Denti, G., Campagna, S., Serroni, S., Ciano, M., Balzani, V., *J. Am. Chem. Soc.* **1992**, *114*, 2944.
- [88]. Campagna, S., Denti, G., Serroni, S., Ciano, M., Juris, A., Venturi, M., Ricevuto, V., Balzani, V., *Chem. Eur. J.* **1995**, *1*, 211.
- [89]. Serroni, S., Denti, G., Campagna, S., Juris, A., Ciano, M., Balzani, V., *Angew. Chem. Int. Ed. Engl.* **1992**, *31*, 1493.
- [90]. Balzani, V., Juris, A., Venturi, M., Campagna, S., Serroni, S., *Chem. Rev.* **1996**, *96*, 759.
- [91]. Balzani, V., Campagna, S., Denti, G., Juris, A., Serroni, S., Venturi, M., *Acc. Chem. Res.* **1998**, *31*, 405.
- [92]. Plevoets, M., Vögtle, F., De Cola, L., Balzani, V., *New. J. Chem.* **1999**, *23*, 63.
- [93]. Constable E. C., Cargill Thompson, A. M. W., *J. Chem. Soc., Chem. Commun.* **1992**, 617.
- [94]. Constable, E. C., Thompson, A. M. W., *J. Chem. Soc., Dalton Trans.* **1992**, 3467.
- [95]. Maestri, N., Armaroli, N., Balzani, V., Constable, E. C., Cargill Thompson, A. M. W., *Inorg. Chem* **1995**, *34*, 2759.
- [96]. Ashton, P. R., Balardini, R., Balzani, V., Constable, E. C., Credi, A., Kocian, O., Langford, S. J., Preece, J. A., Prodi, L., Schofield, E. R., Spencer, N., Stoddart, J. F., Wenger, S., *Chem. Eur J.* **1998**, *4*, 2413.
- [97]. Armaroli, N., Barigelletti, F., Constable, E. C., Encinas, S., Figgmeier, E., Flamigni, L., Housecroft, C. E., Schofield E. R., Vos, J. G., *Chem. Commun.* **1999**, 869.

- [98]. Encinas, S., Flamigni, L., Barigelletti, F., Constable, E. C., Housecroft, C. E., Schofield, E. R., Figgemeier, E., Fenske, D., Neuburger, J. G., Vos, M., Zehnder, M., *Chem. Eur. J.* **2002**, *8*, 137.
- [99]. Constable, E. C., Housecroft, C. E., Neuburger, M., Poleschak, I., Zehnder, M., *Polyhedron* **2003**, *22*, 93-108.
- [100]. Constable, E. C., Harverson, P., *Inorg. Chim. Acta.* **1996**, *252*, 9.
- [101]. Constable, E. C., Harverson, P., *Chem. Commun.* **1996**, 33.
- [102]. Constable, E. C., Handel, R. W., Housecroft, C. E., Morales A. F., Ventura, B., Flamigni, L., Barigelletti, F., *Dalton Trans.* **2003**, 1220.
- [103]. Constable, E. C., Handel, R. W., Housecroft, C. E., Morales A. F., Ventura, B., Flamigni, L., Barigelletti, F., *Chem. Eur. J.* **2005**, *11*, 4024.

Chapter II : Synthesis of ruthenium(II) complexes of 4,4'-bis(phenyl)-2,2'-bipyridine ligands.

I. Introduction

The study of the luminescence and redox properties of oligopyridine metal complexes has interested supramolecular chemists during the past twenty years^[1-15]. The bpy^[2] and tpy-ligand^[10] metal complexes are of particular interest as possible redox activator for water photosplitting^[5], have long phosphorescence lifetimes^[4], and could be used as photosensitizers or energy information transmitters in supramolecular systems^[13]. Numerous ruthenium(II) bpy complexes have been studied, and their redox and photophysical properties in the excited state are well known. Our interest is in the synthesis of new complexes using new substituted ligands and studying the possible modification of redox potential and increasing the phosphorescence lifetime and quantum yield of the metal-to-ligand charge transfer at triplet excited state (³MLCT)^[6]. To tune the photophysical properties of triplet excited state relaxation through their phosphorescence lifetimes and luminescence quantum yields, we changed the chemical functionality of the 2,2'-bipyridine ligands in the 4 and the 4'-positions by adding 4-methoxyphenyl, 3,5-dimethoxyphenyl or 4-(1-naphthyl) substituents.

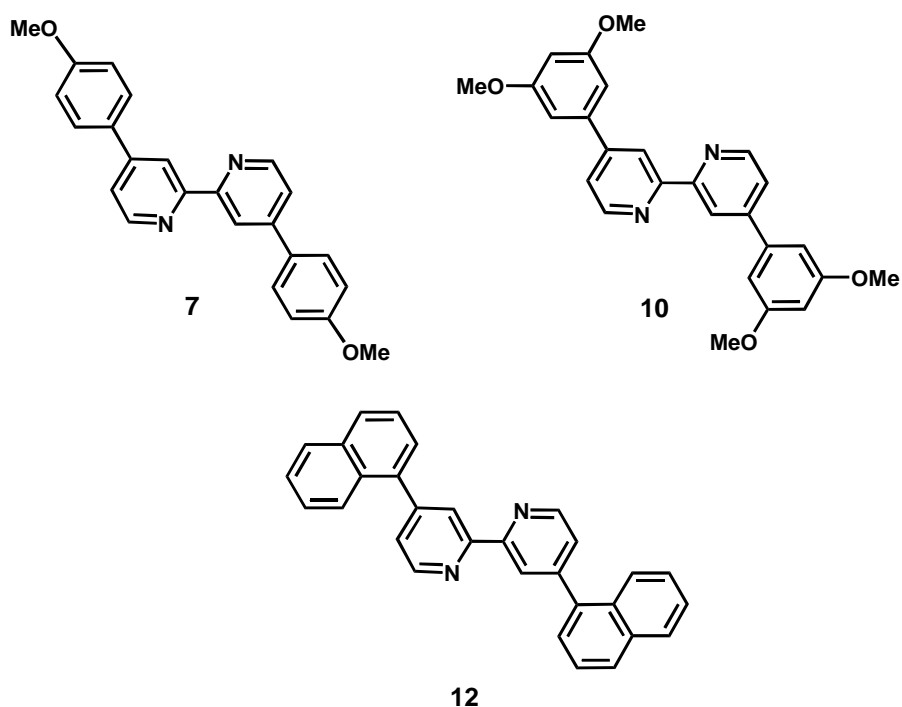


Fig II-1- The three substituted 2,2'-bipyridines.

II. Synthesis of 4,4'-bis(4-methoxyphenyl)-2,2'-bipyridine 7, and 4,4'-bis(3,5-dimethoxyphenyl)-2,2'-bipyridine 10.

1) *The synthetic strategy*

The general synthetic methods for 4,4'-substitued-2,2'-bipyridines are well known and give good yields for the synthesis of halide, amino or hydroxy substituted bpy ligands. The preparation of aryl substituted ligands necessitates the synthesis of bpy ligands containing a good leaving-group for coupling following Pd(0) catalysed cross-couplings.

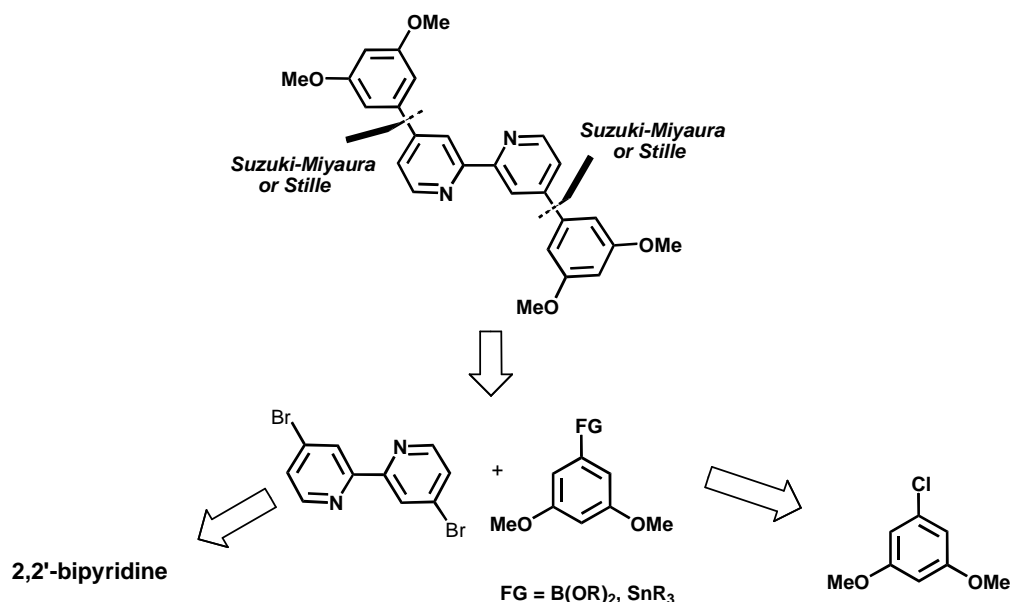


Fig II-2- Retrosynthetic analysis for the synthesis of **10**.

The theoretical synthetic route shows us two possible synthetic ways : the first ligand synthesis is according a C-C bond formation via Suzuki-Miyaura^[16] or Stille^[17] coupling between a 4,4'-dihalo-2,2'-bipyridine such as 4,4'-dibromo-2,2'-bipyridine, and an organometallic derivative of 4-methoxy or 3,5-dimethoxybenzene. We have two possible C-C bond couplings: the first is a Suzuki-Miyaura^[16] cross-coupling between a boronic acid or ester and the halo compound and the second is a Stille^[17,18] cross-coupling between a organotin both in the presence of Pd (0) catalyts in organic solvent.

2) *The Suzuki-Miyaura cross-coupling.*

The principle of the Suzuki-Miyaura coupling^[16] consists in the formation of a C-C bond, with help of a boronic acid or a boronic ester derivative and a haloaromatic or haloalkene in presence of Pd(0) catalyst and a biphasic solvent containing a base in aqueous solution.

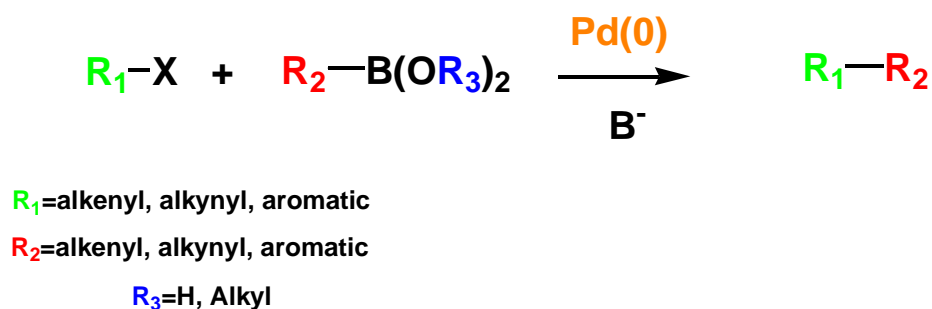


Fig II-3- The Suzuki-Miyaura cross coupling

This reaction was performed the first time by the group of Suzuki^[16] and the reaction mechanism follows the catalytic cycle in Fig 4. The palladium(0) catalyst most commonly used is [Pd(PPh₃)₄].

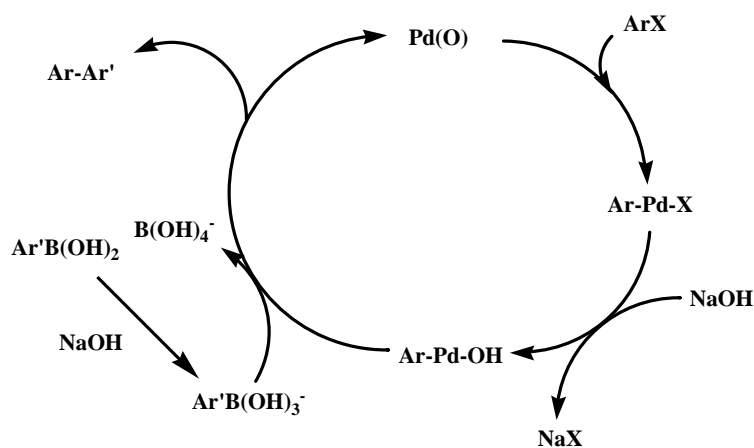


Fig 4- Catalytic cycle for cross-coupling of organic halides and organoboranes

This insertion compound Ar-Pd-X gives in presence of base (NaOH) a hydroxyaryl palladium(II) complex (Ar-Pd-OH). The boronic acid in presence of base give a anionic arylborate product which react with Ar-Pd-OH and after reductive elimination of palladium, we obtain the desired coupling compound Ar-Ar' .

3) Synthesis of 4,4'-dibromo-2,2'-bipyridine.

We need the presence of an efficient leaving group at the 4,4'-positions and the choice of bromo substitution is due to the high reactivity of bromide in the Pd(0)-catalysed cross-coupling. In our case, we used the Suzuki-Miyaura coupling with the bromo-substituent favouring the insertion of palladium.

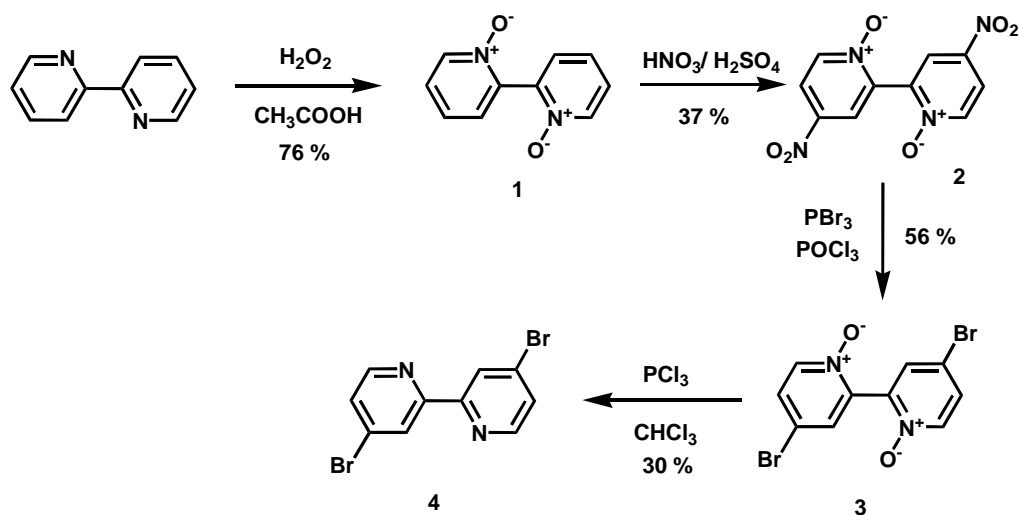


Fig II-4- Synthesis of 4,4'-dibromo-2,2'-bipyridine **4**.

The 4,4'-dibromo-2,2'-bipyridine synthon is obtained from 2,2'-bipyridine as starting material which is activated at first by oxidation of the two nitrogens with H₂O₂ in glacial acetic acid giving the 1,1'-dioxide (bpydio), which was then treated for 20 hours with H₂SO₄-HNO₃ to give the 4,4'-dinitro compound **2**. The reaction of **2** with PBr₃ in POCl₃ gives the 4,4'-dibromo compound **3** which was converted to **4** by 12 hours of treatment with PCl₃ in chloroform with 30% yield. The free ligand was characterised by NMR ¹H, ¹³C spectroscopy FAB-MS and the crystal structure was elucidated.

Crystal structure of 4

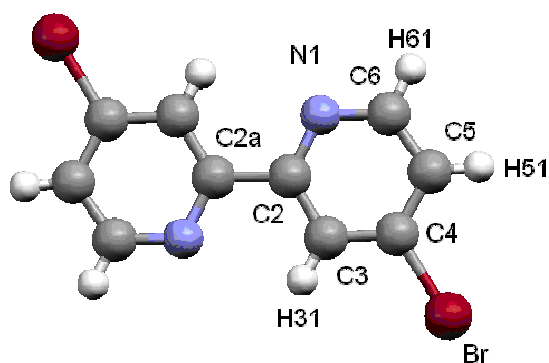


Fig II-5- The solid state structure of **4** (collection data, annexe A1).

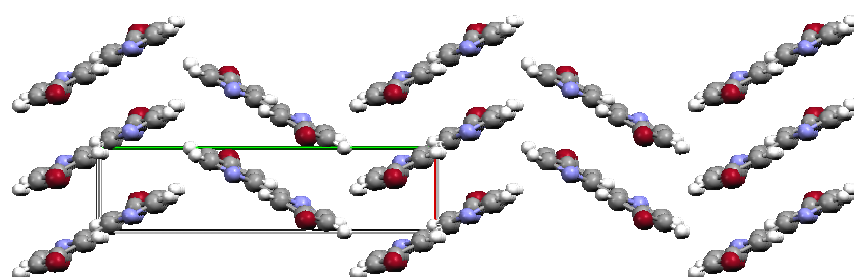


Fig II- 6- Structure packing of **4** along the c crystal axis.

4) Synthesis of 4,4'-bis-(4-methoxyphenyl)-2,2'-bipyridine (7).

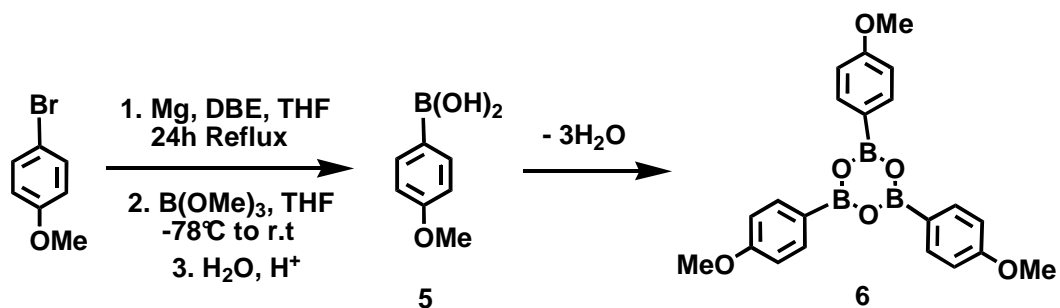


Fig II-7 – Synthesis of 4-methoxy phenylboronic acid anhydride **6**^[19].

The synthesis of 4-methoxyphenylboronic acid is in two steps according the method of Dol^[19] starting with a Grignard reaction of 4-bromomethoxybenzene with magnesium turnings in THF using 1,2-dibromoethane as activator. Then a brown slurry of the Grignard reagent is then converted to the boronic acid by addition to a solution of B(OMe)₃ in THF cooled to -78°C over 24 hours. The 4-methoxyphenylboronic acid **6** is obtain after hydolysis in acidic condition. After extraction and purification we obtained the trimeric anhydride in 19 % yield. The formation of this trimer is a principal cause of the low yields of the Suzuki-Miyaura coupling and 4,4'-dibromo-2,2'-bipyridine, because the formation of B(OH)₄⁻ in the catalytic cycle from the anhydride is more difficult than starting from the corresponding boronic acid.

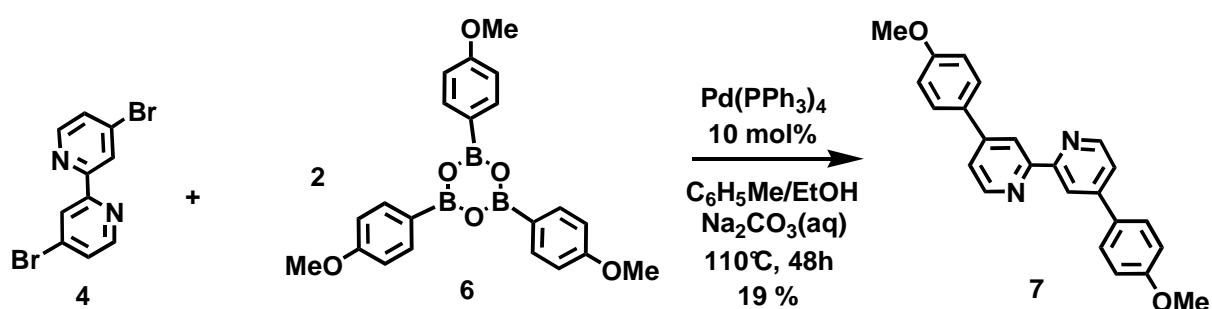


Fig II-8- Synthesis of ligand **7**

The synthesis of 4,4'-di(4-methoxyphenyl)-2,2'-bipyridine **7** was according to the literature^[9]. We used an excess of anhydride **6**.

5) Synthesis of 4,4'-bis-(3,5-dimethoxyphenyl)-2,2'-bipyridine **10**.

The preferred way for the synthesis of **10** is to use the Suzuki-Miyaura coupling as the key step because the synthesis of the 4,4'-dibromo-2,2'-bipyridine synthon is easy and the 3,5-dimethoxyphenylboronic acid corresponding to the second synthon is accessible after a three steps synthesis according Dol^[19] in 38 % yield.

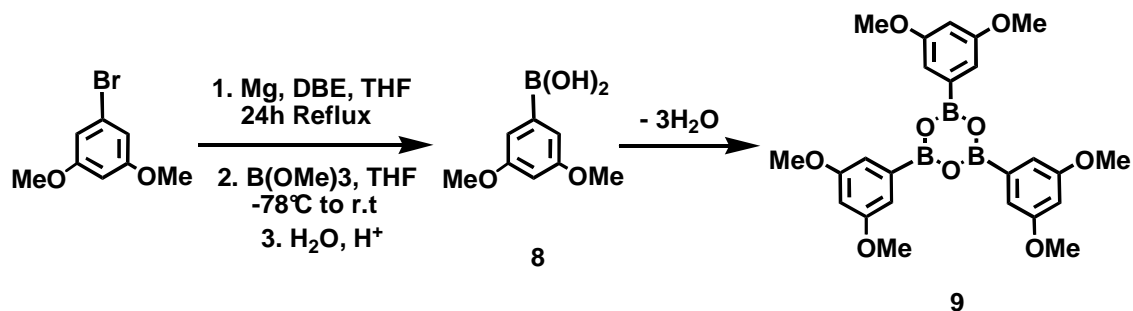


Fig II-9- Synthesis of 3,5-dimethoxyphenylboronic acid anhydride **9**.

The $^1\text{H-NMR}$ spectrum shows signals corresponding to the methoxy group at $\delta=3.90$ ppm in acetone, two singlets at $\delta=6.53$ and $\delta=7.05$ ppm corresponding to aromatic protons at the para- and ortho position of the phenyl rings. The spectrum shows the no peaks which can be assigned to the acidic protons of the boronic acid. This could be due to exchange with the deuterated solvent or the presence of the trimeric form, resulting from the condensation of three 3,5-dimethoxyphenylboronic acid monomers. This ring formation is confirmed by the mass spectrum which exhibits a molecular peak at $m/z = 492.2$.

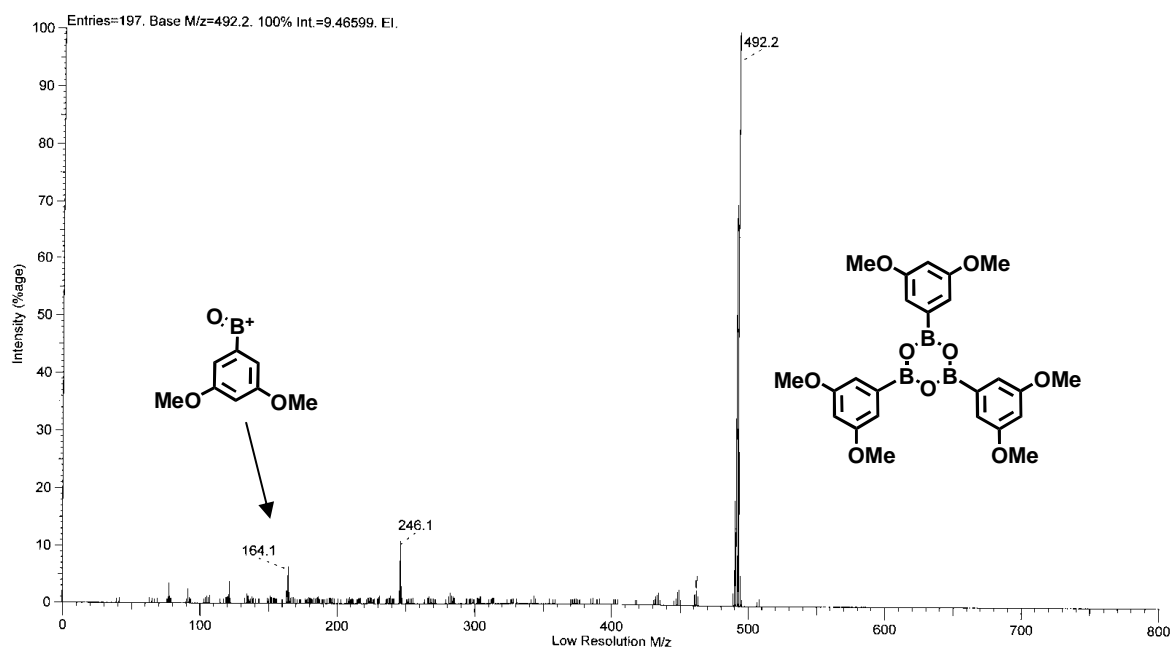


Fig II-10- FAB-MS showing 9.

This spectrum shows also the presence of the two other fragments at $m/z = 246.1$ which corresponding to the half molar mass of the trimer and at $m/z = 164.1$ which corresponding to the fragment $(\text{MeO})_2\text{C}_6\text{H}_3\text{BO}^+$. The trimer was crystallised from acetone and the X-ray solid state structure is presented in *Fig II-11*.

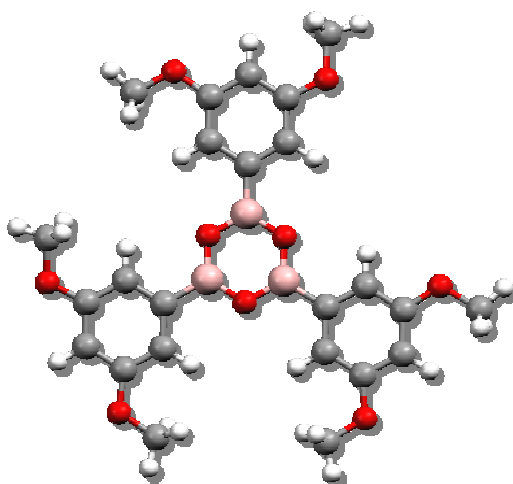


Fig II-11- X-ray structure of 9

The trimer **9** crystallised in a monoclinic system and in space group is $C2/c$.

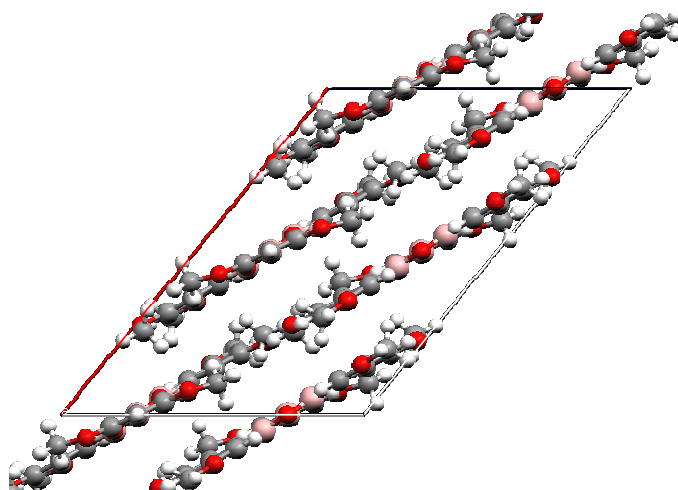


Fig II-12 – 9 packing along the b axis

The *Fig II-12* shows the packing configuration, we can see with the flat structure of the trimer the interstitial separation between the molecules. The intermolecular distance

The palladium catalysed coupling of compound **4** and **9** is according to the Suzuki-Miyaura method ^[20], using $[Pd(PPh_3)_4]$ as catalyst (0.1 equivalent) in biphasic toluene/ H_2O / Na_2CO_3 solvent at reflux over 2 days and yielded ligand **10** (characterised by 1H and ^{13}C NMR spectroscopy FAB mass spectroscopy) in is 20 % yield.

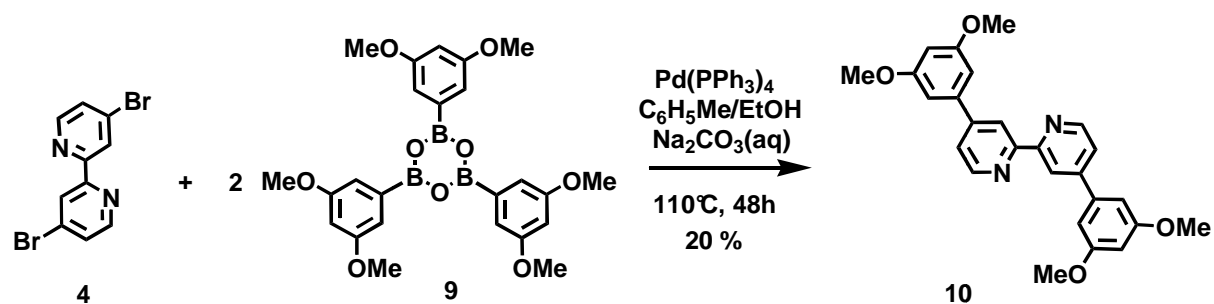


Fig II-13- Synthesis of **10** by Suzuki-Miyaura coupling of **4** and **9**.

The synthesis of the “locked” version of the analogous compound with 6,6'-dimethyl-substituents follows a different route.^[20]

¹H-NMR and ¹³C-NMR spectra of **10**.

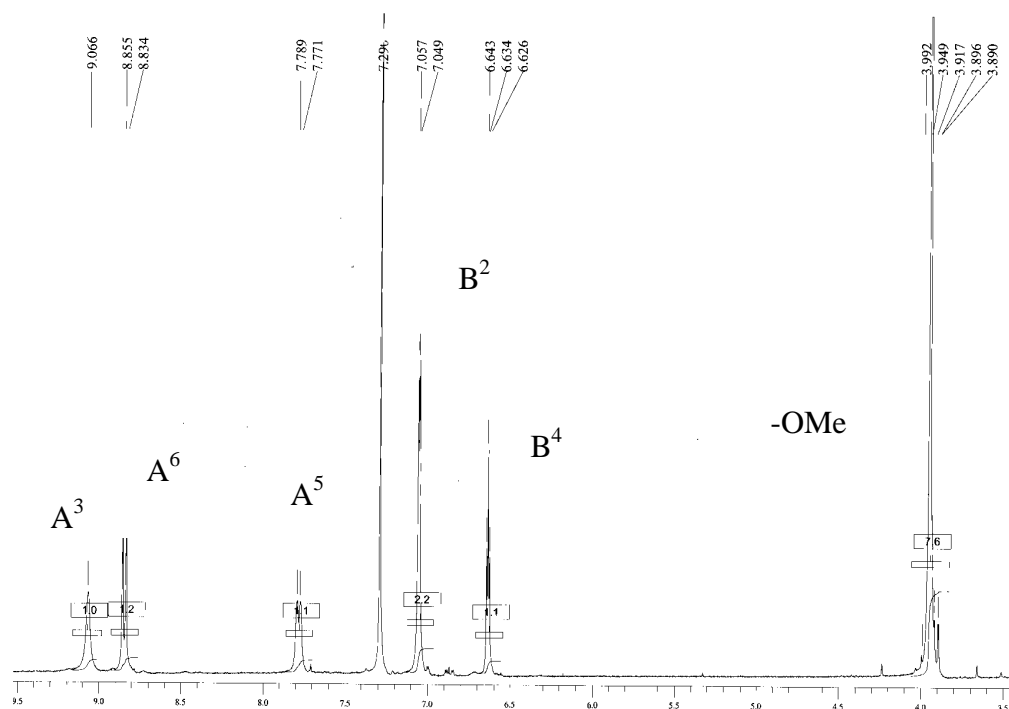


Fig II-14 - ¹H-NMR 250 MHz spectrum of **10** in CDCl₃ at 298 K

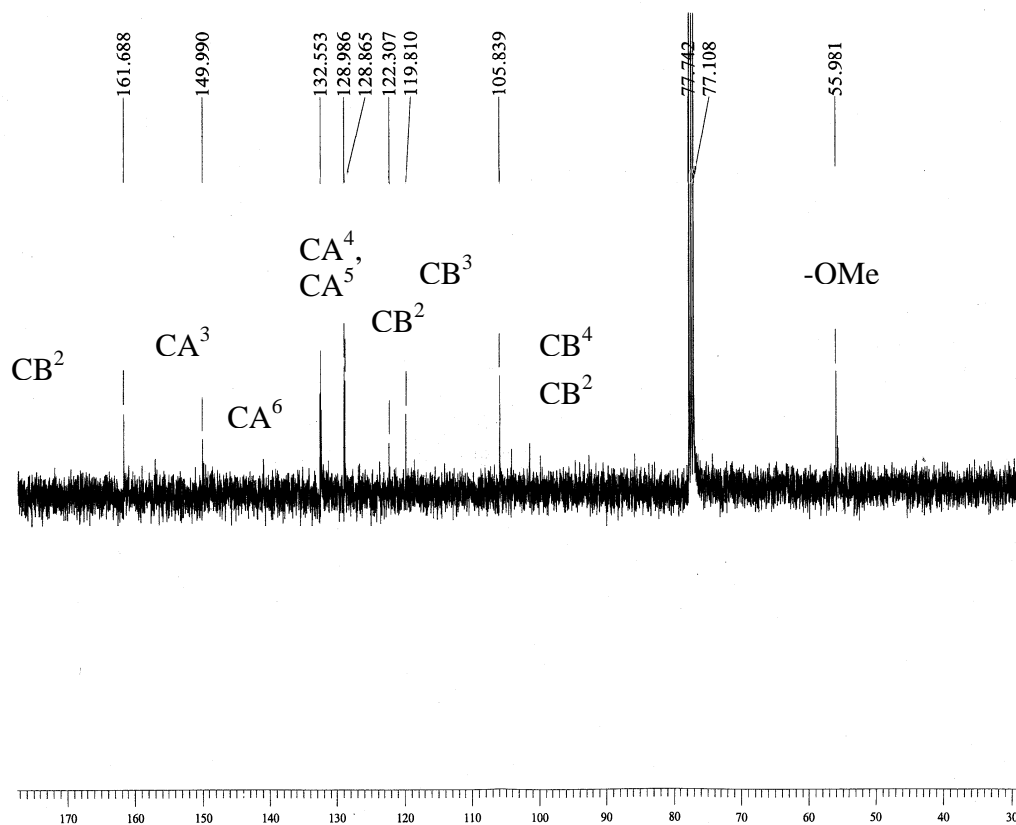


Fig II-15- ^{13}C spectra of **10** in CDCl_3 at 67.5 MHz at 298 K

Protons	A₃	A₆	A₅	B₂	B₄	OMe
δ ppm	9.07	8.84	7.78	7.05	6.63	3,95
signal	<i>s</i>	<i>d</i>	<i>d</i>	<i>d</i>	<i>t</i>	<i>s</i>
J (Hz)		5.25	4.5	2	2.25	
integration	2H	2H	2H	4H	2H	12H

Fig II-16- ^{13}C and ^1H chemicals shift assignment of ligand **10**, in CDCl_3 at 298 K.

The ligand **10** was also characterised by FAB-MS, and exhibited a molecular peak at $m/z = 429$, corresponding to the calculated mass.

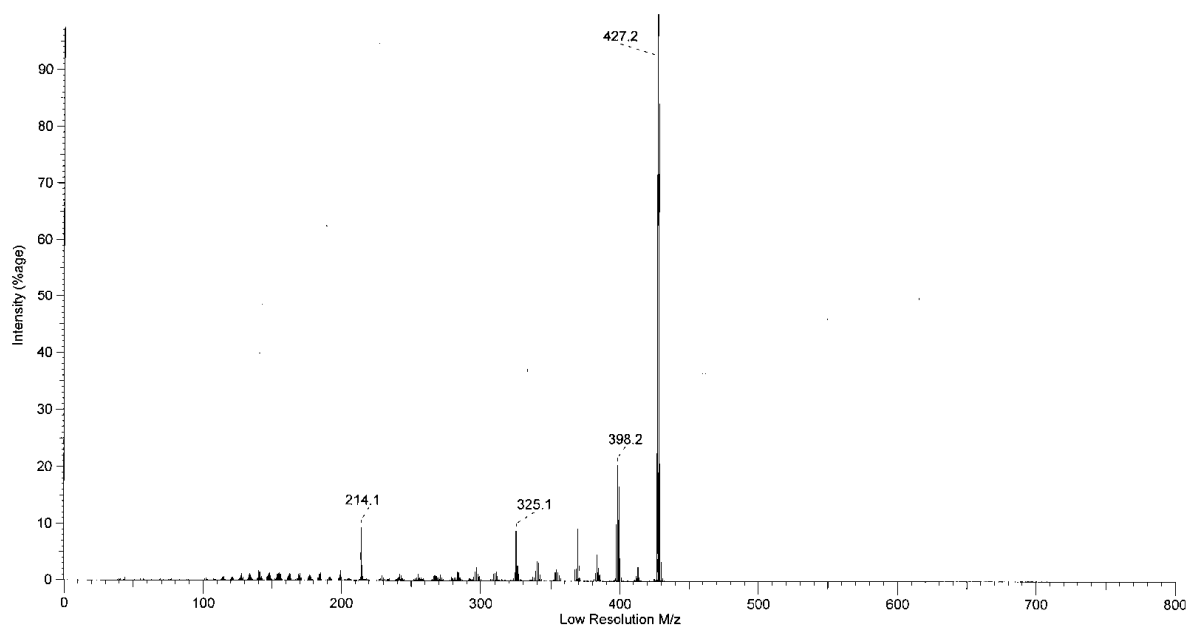


Fig II-17- EI-MS of **10**.

6) Synthesis of 4,4'-bis-(1-naphthyl)-2,2'-bipyridine **13**.

The addition of polyaromatic groups at the 4 and 4' positions of the 2,2'-bipyridine is necessary for studying if the presence of electron rich substituent, play a role photochemical properties of the the free ligand. The synthetic way of 4,4'-bis-(1-naphthyl)-2,2'-bipyridine is by Suzuki-Miyaura cross coupling (Fig II-18).

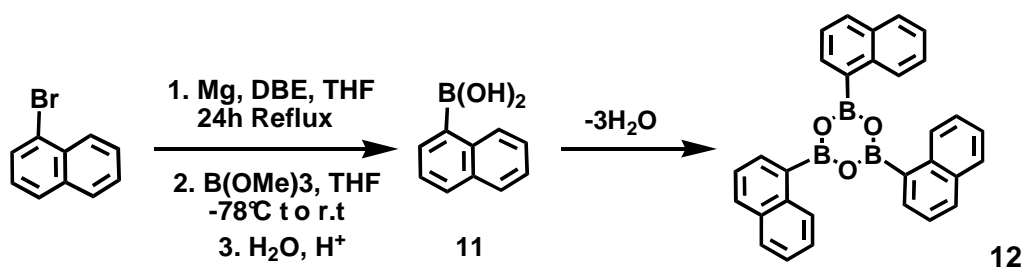


Fig II-18- Synthesis of **12**^[19].

The synthesis of 1-naphthylboronic acid **11** is according to the same procedure as previously seen: 1-bromonaphthalene gave in 27 % the anhydride **12**. The trimeric form of **11** was characterised by ¹H NMR spectroscopy in CDCl₃ FAB-MS spectrum show a molecular peak $m/z = 462$.

This boron species **12** reacts with 4,4'-dibromo-2,2'-bipyridine in the presence of $[\text{Pd}(\text{PPh}_3)_4]$ catalyst in basic conditions in a biphasic solution containing toluene and water, and forms with a low yield (11%) the coupling product 4,4'-bis(1-naphthyl)-2,2'-bipyridine.

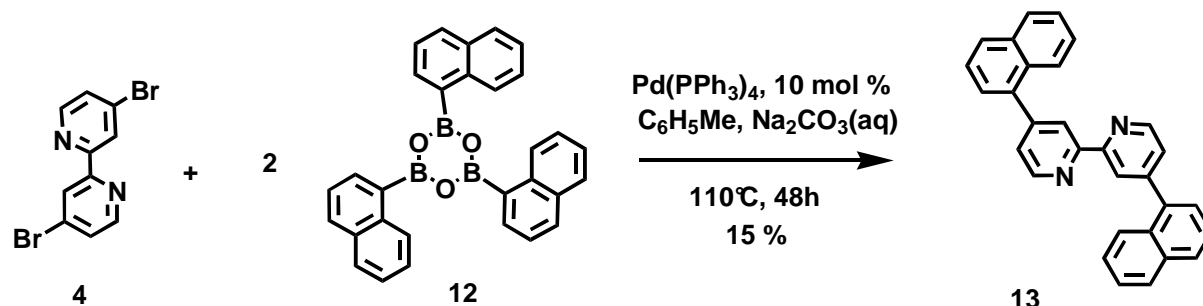


Fig II-19-Synthesis of **13**.

The ligand **13** was characterised by NMR spectroscopy FAB mass spectroscopy.

III. Synthesis of $[\text{Ru}(\text{bpy})_2(\mathbf{7})][\text{PF}_6]_2$ and $[\text{Ru}(\text{bpy})_2(\mathbf{9})][\text{PF}_6]_2$.

1) *Synthesis of $[\text{Ru}(\text{bpy})_2(\mathbf{7})][\text{PF}_6]_2$ **15**.*

The reaction of bis(2,2'-bipyridine)dichlororuthenium (II) with 4,4'-bis(4-methoxyphenyl)-2,2'-bipyridine in ethanol at reflux give the complex $[\text{Ru}(\text{bpy})_2(\mathbf{7})][(\text{PF}_6)_2]$ **15** in 80 % yield^[20]. This complex is characterised by ^1H NMR spectroscopy, and ES-MS in acetonitrile.

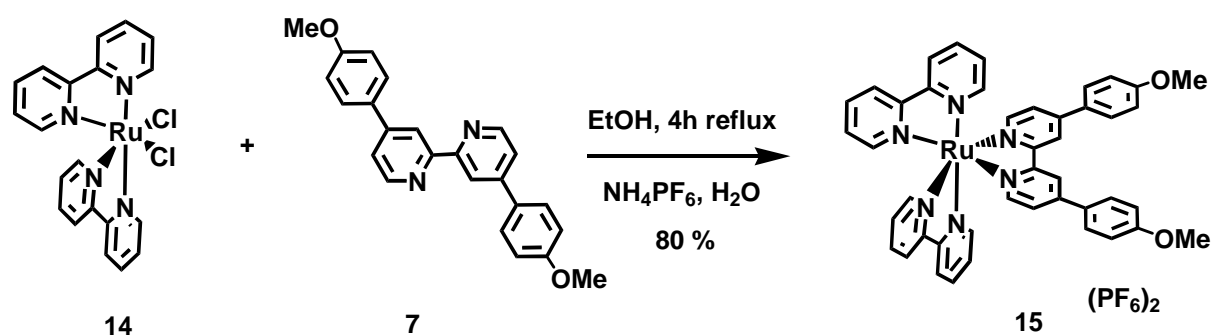


Fig II-22- Synthesis of **15**.

2) Synthesis of $[(Ru(bpy)_2(\mathbf{10}))][PF_6]_2$ **17**.

The complexation of $[Ru(bpy)_2Cl_2]$ with the ligand **10** give after 4 hours reaction in refluxing ethanol a very luminescent orange species which was precipitated as the salt $[(Ru(bpy)_2(\mathbf{10}))][PF_6]_2$. This complex contains four methoxy functional groups. This complex was also obtained from the coupling reaction between $[(Ru(bpy)_2(\mathbf{4}))][PF_6]_2$ and the anhydride of 3,5-dimethoxyphenylboronic acid under Suzuki-Miyaura conditions in the presence of $[Pd(PPh_3)_4]$ catalyst (Fig II-23) with 32 % overall yield which is higher than the coupling reaction on the ligand and the complexation which have 15 % yield of two steps reaction.

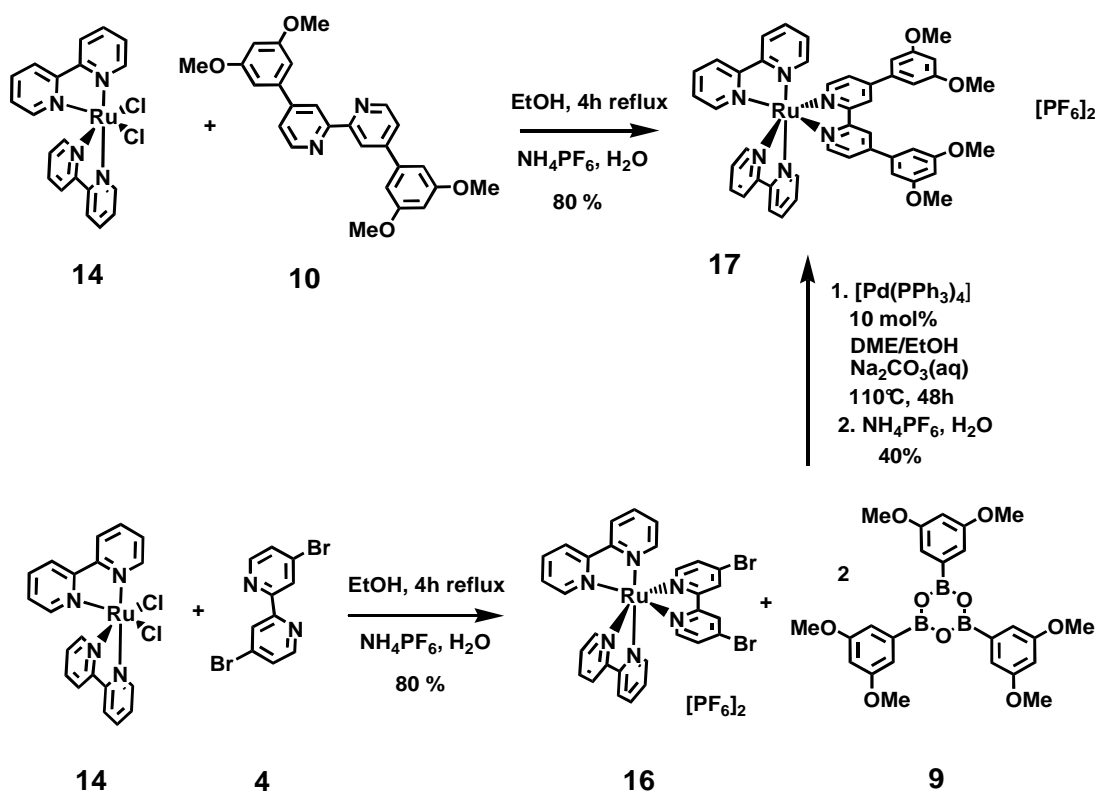


Fig II-23- Synthesis of complex **17**.

The complex $[(Ru(bpy)_2(\mathbf{10}))][PF_6]_2$ was analysed by 1H NMR spectroscopy using COSY H-H, and NOESY spectroscopy in CD_3CN and electrospray mass-spectroscopy. The 1H NMR spectrum shows protons corresponding to the methoxy group at δ 3,90 ppm and protons corresponding to the bpy ligands between 6.70 and 8.92 ppm. The different signal have been identified and assigned by the 2D COSY H-H and NOESY spectroscopy.

¹H NMR spectrum of **17**

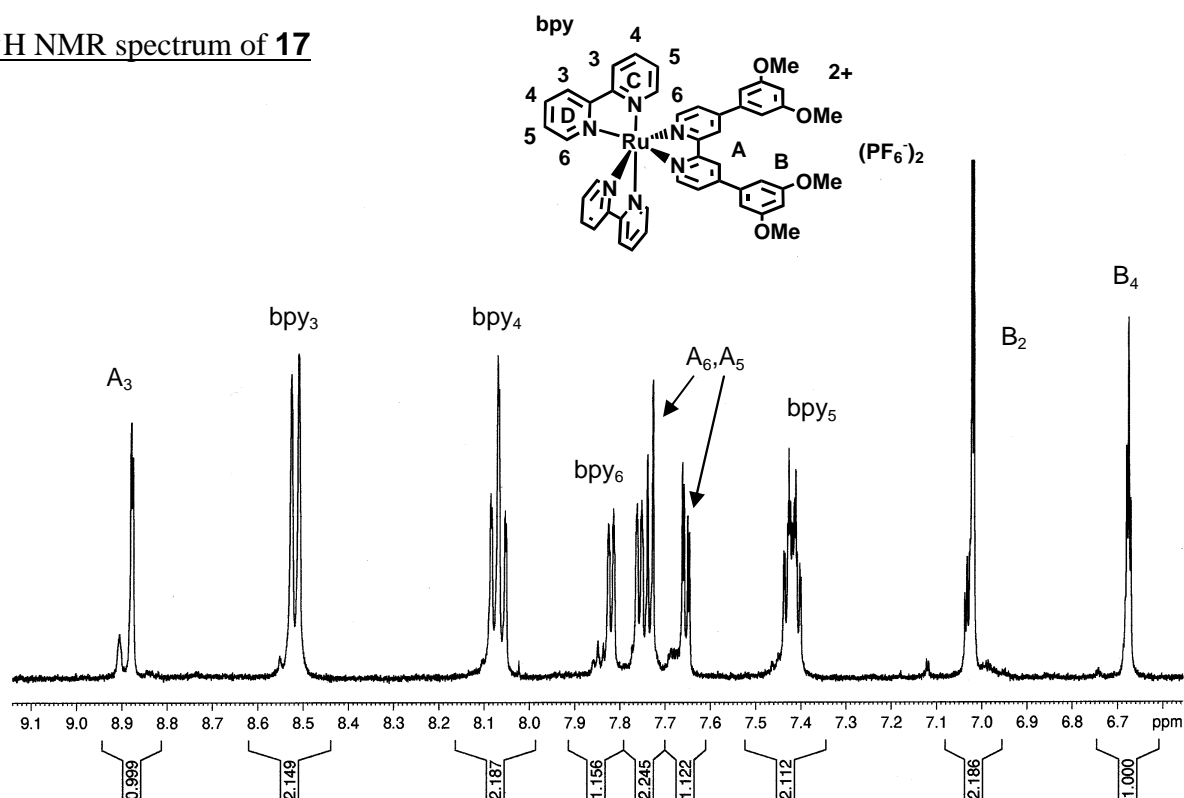


Fig II-24- ¹H-NMR spectrum of the aromatic zone of **17** at 500 MHz in CD₃CN at 298 K.

	bpy ₃	bpy ₄	bpy ₅	bpy ₆	A ₃	A ₅	A ₆	B ₂	B ₄	OMe
Ru(bpy) ₂ (17)(PF ₆) ₂ δ (ppm)	8.56	8.10	7.46	7.87	8.91	7.70	7.79	7.06	6.71	3.90
Spin multiplicity	<i>d</i>	<i>t</i>	<i>m</i>	<i>d</i>	<i>s</i>	<i>d</i>	<i>d</i>	<i>d</i>	<i>s</i>	<i>s</i>
Integration	2H	4H	4H	4H	2H	2H	2H	2H	2H	12H
J (Hz)	8.5	3.9		6		6	6	2.5	2	

The ¹H NMR spectrum show two bpy₃, bpy₄, bpy₅ and bpy₆ types of signals between, δ 6,71 and δ 8,56 ppm . The first type of protons are assigned to the protons of **10** which are denoted A₃, A₅, A₆, B₂, B₄. The aromatic protons B₂ and B₄ have respectively chemical shifts of δ 6.71 and δ 7.06 ppm which is normal for protons of phenyl groups. The bpy protons of **10** A₃, A₅ and A₆ have signals at δ 8.91, 7.70 and 7.79 ppm respectively. The assignment of the protons complexes are confirmed with COSY H-H and nOESY spectra at 500 MHz . The C and D rings of bpy ligands are not equivalent but the two environments are not fully resolved other than in the case of the H₆ protons.

COSY H-H spectrum of **17**.

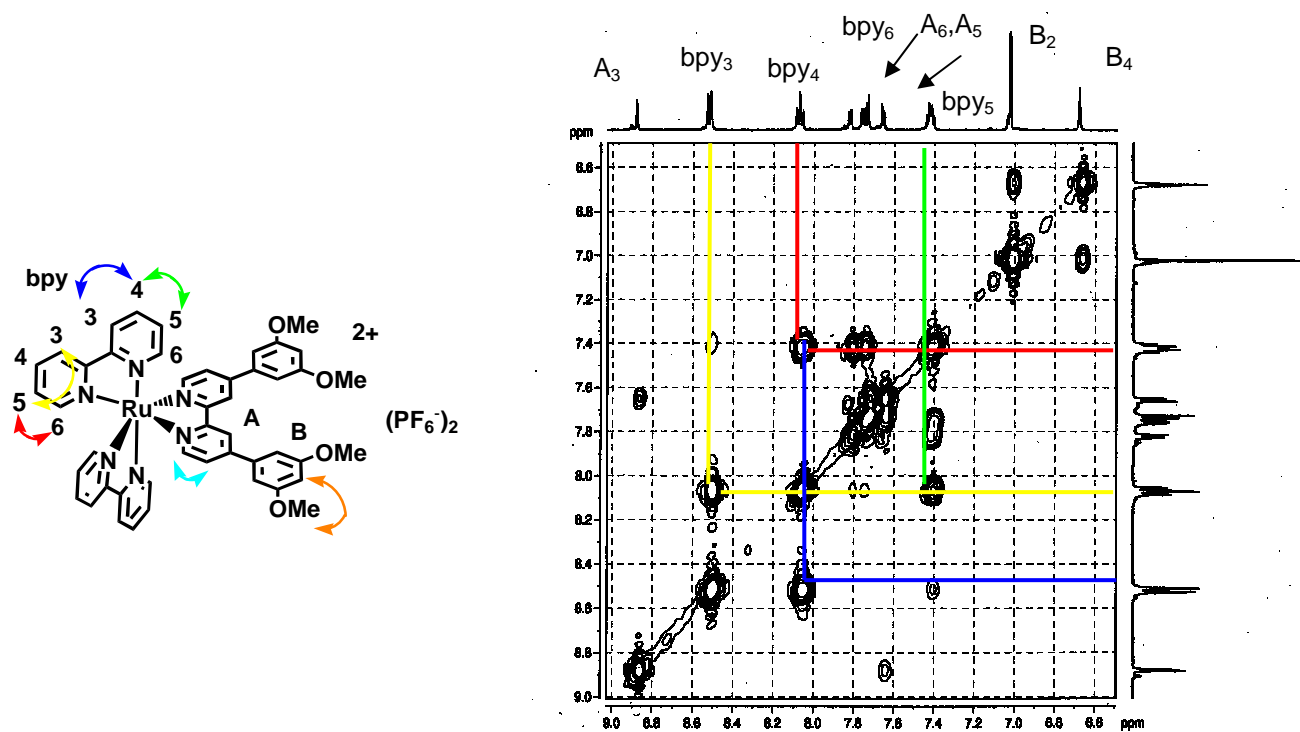


Fig II-25- COSY H-H spectrum of **17** in CD₃CN at 500 MHz at 298 K.

The COSY H-H spectrum show strong correlation signals between H3 and H4, H4 and H5, H5 and H6 of non substituted bipyridine ligands , and A5 and A6 of bpy proton of **10**.

nOESY spectrum of **17**.

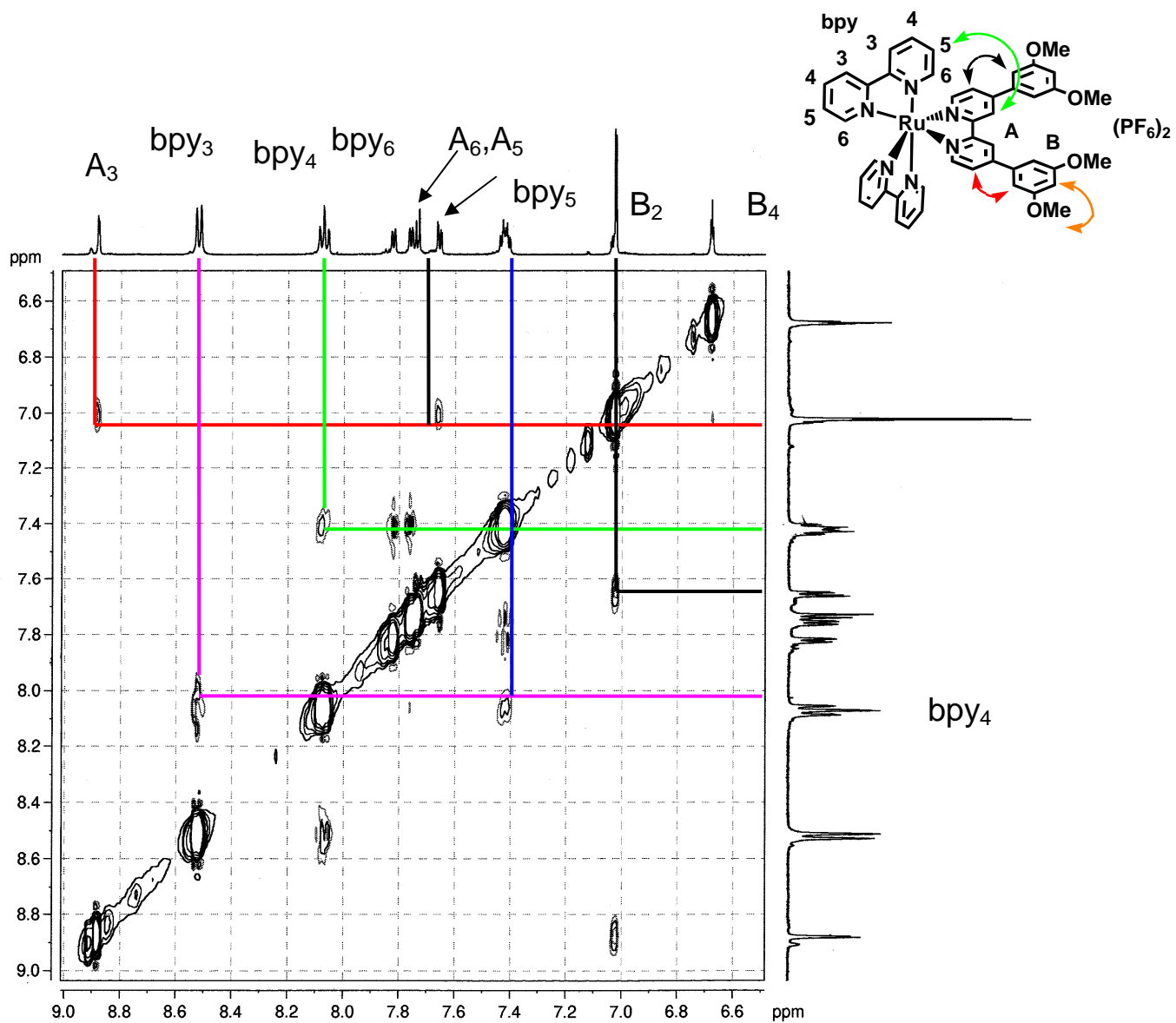


Fig II-26- NOESY spectrum of **17** in CD₃CN at 500 MHz at 298 K.

The NOESY spectrum shows the spatial proximity correlation of A₃ and B₂ protons, the bpy₃ and A₅ and B₂.

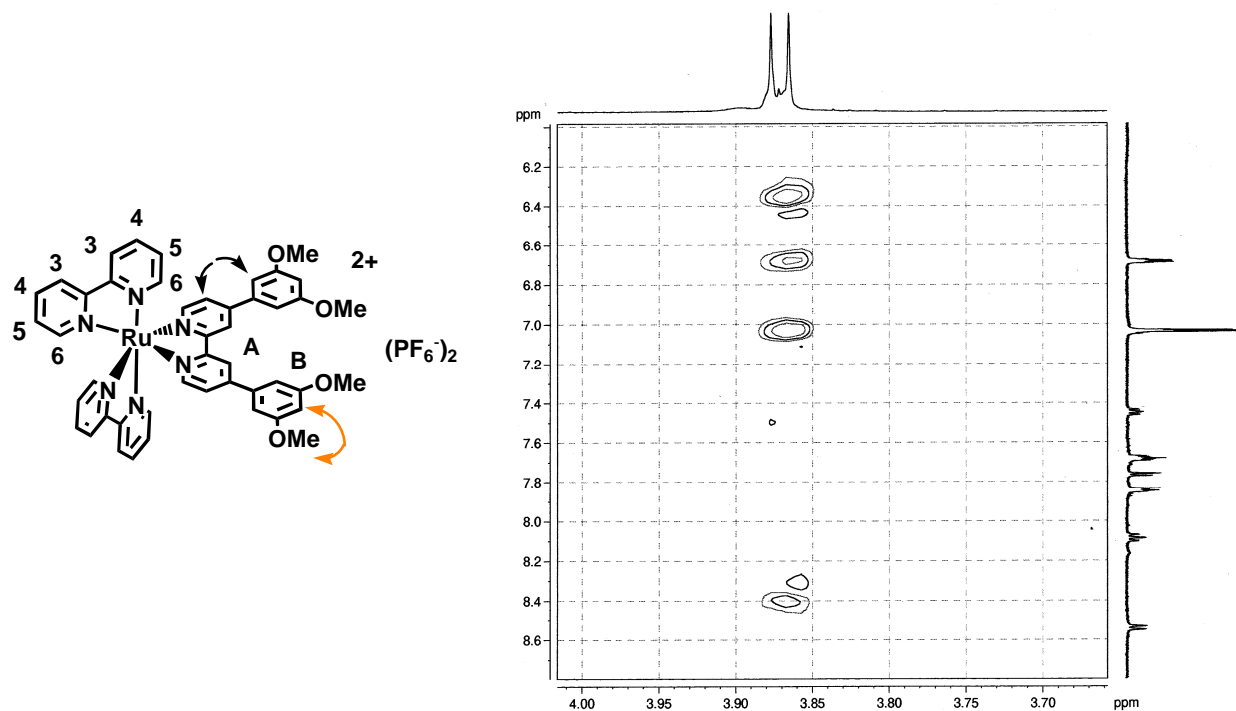


Fig II-27- NOESY spectrum of **17** in the -OMe region

ES Mass spectroscopy of **17**.

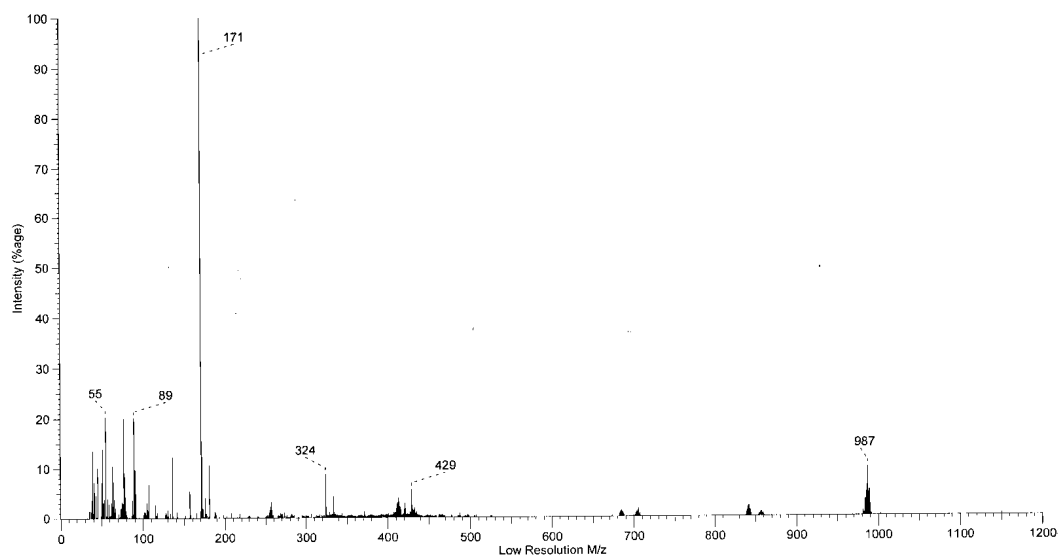


Fig II-28- ES Mass Spectrum of **17** in CH₃CN.

IV. Synthesis of [Ru(bpy)(10)₂][PF₆]₂ **19** and [Ru(10)₃][PF₆]₂ **20**.

1) *Synthesis of [Ru(bpy)(10)₂][PF₆]₂ **19**.*

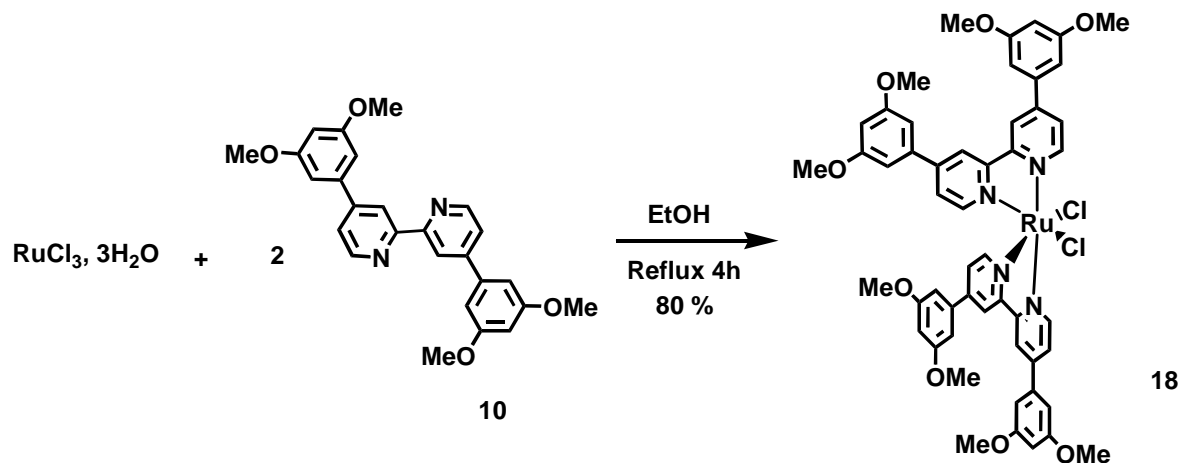


Fig II-29– Synthesis of [Ru(10)₂Cl₂] **18**.

The synthetic way is in two complexation reaction steps. The first is the complexation of RuCl₃ by two equivalents of **10** and forming [Ru(10)₂Cl₂] complex **18**. This complex without characterisation is by directly complexing one equivalent of 2,2'-bipyridine to form after 4 hours of reaction, purification over SiO₂ column and recrystallisation in methanol and precipitation with NH₄PF₆, the nice red complex [Ru(bpy)(10)₂][PF₆]₂ in (75%) yield. This new complex containing 8 methoxy functionalities in the para position of the 4,4' substituent phenyl group and was characterised by ¹H NMR spectroscopy in CD₃CN and ES-MS.

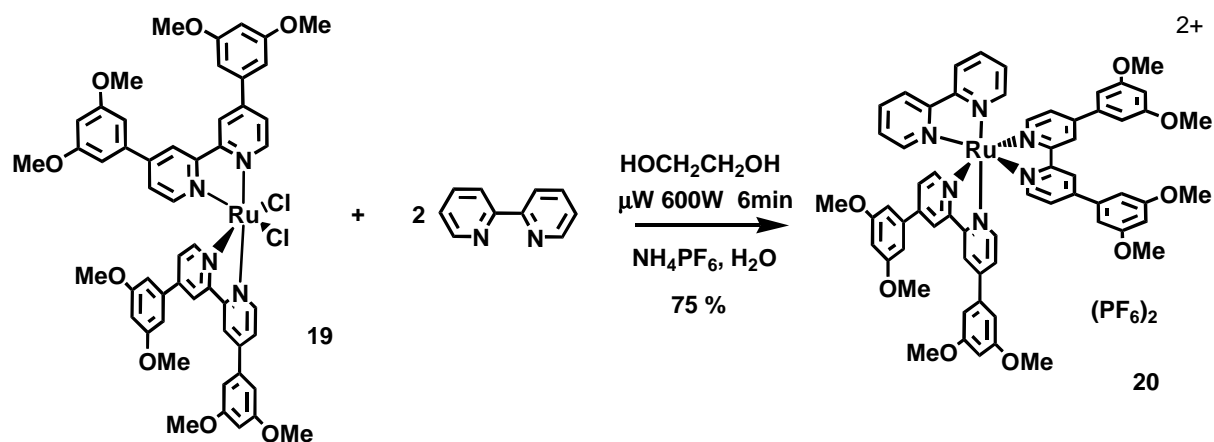


Fig II-30- Synthesis of **19**.

^1H NMR spectrum of **19** in CD_3CN

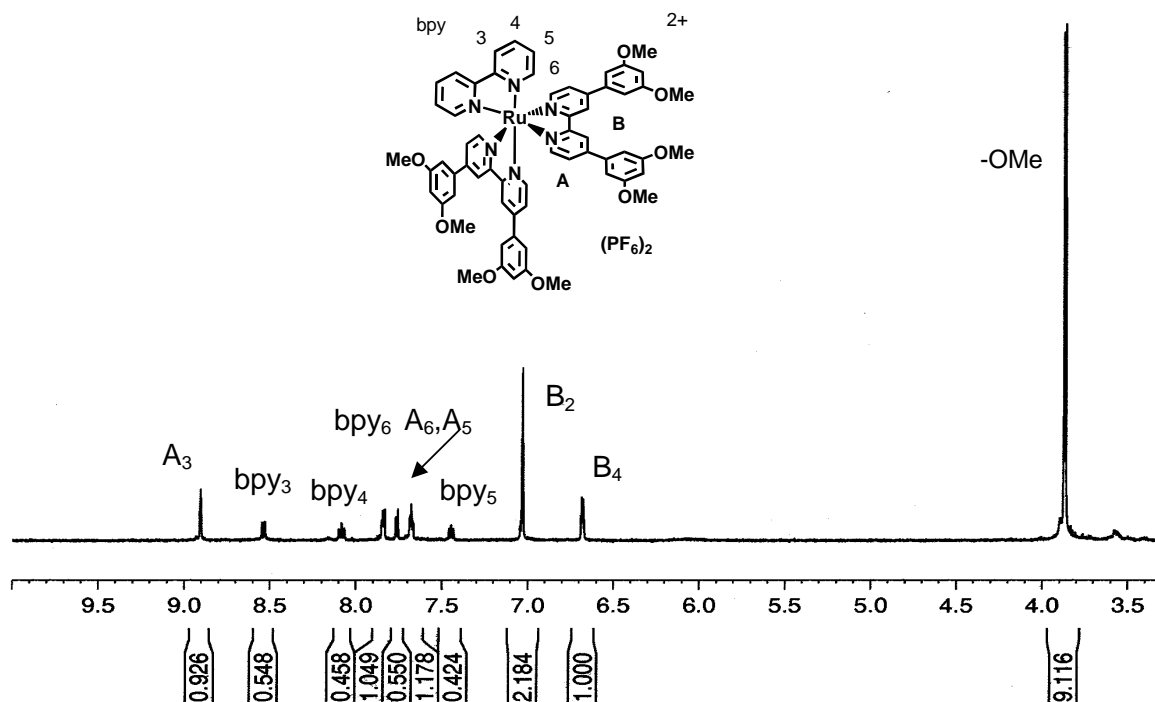


Fig II-31– ^1H NMR spectrum of **19** at 500 MHz in CD_3CN at 298 K

Table- ^1H NMR data of **19**.

attribution	bpy ₃	bpy ₄	bpy ₅	bpy ₆	A ₃	A ₅	A ₆	B ₂	B ₄	OMe
Ru(bpy)(10) ₂ (PF ₆) ₂										
δ ppm	8.58	8.12	7.49	7.88	8.95	7.72	7.81	7.07	6.71	3.91
Spin multiplicity	<i>d</i>	<i>t</i>	<i>t</i>	<i>d</i>	<i>d</i>	<i>d</i>	<i>d</i>	<i>t</i>	<i>m</i>	<i>s</i>
Integration	2H	2H	2H	2H	4H	4H	4H	8H	4H	24H
<i>J</i> (Hz)	8	7.5	5.75	8	1.75	4.5	6	1		

The ^1H NMR spectrum at 500 MHz showed a peak at 3,90 ppm, corresponding to the methoxy protons. In the aromatic zone we found also the signals corresponding to the protons of the phenyl substituent B₂ and B₄ respectively at 7.07 and 6.71 ppm, the bipyridine protons of **10** at ppm, and the free bpy ligand bpy₃, bpy₄, bpy₅ and bpy₆ at respectively 8.58, 8.12, 7.49, 7.88 ppm. The assignments of this protons were confirmed by 2D spectroscopies.

COSY H-H spectroscopy of **19** in CD₃CN

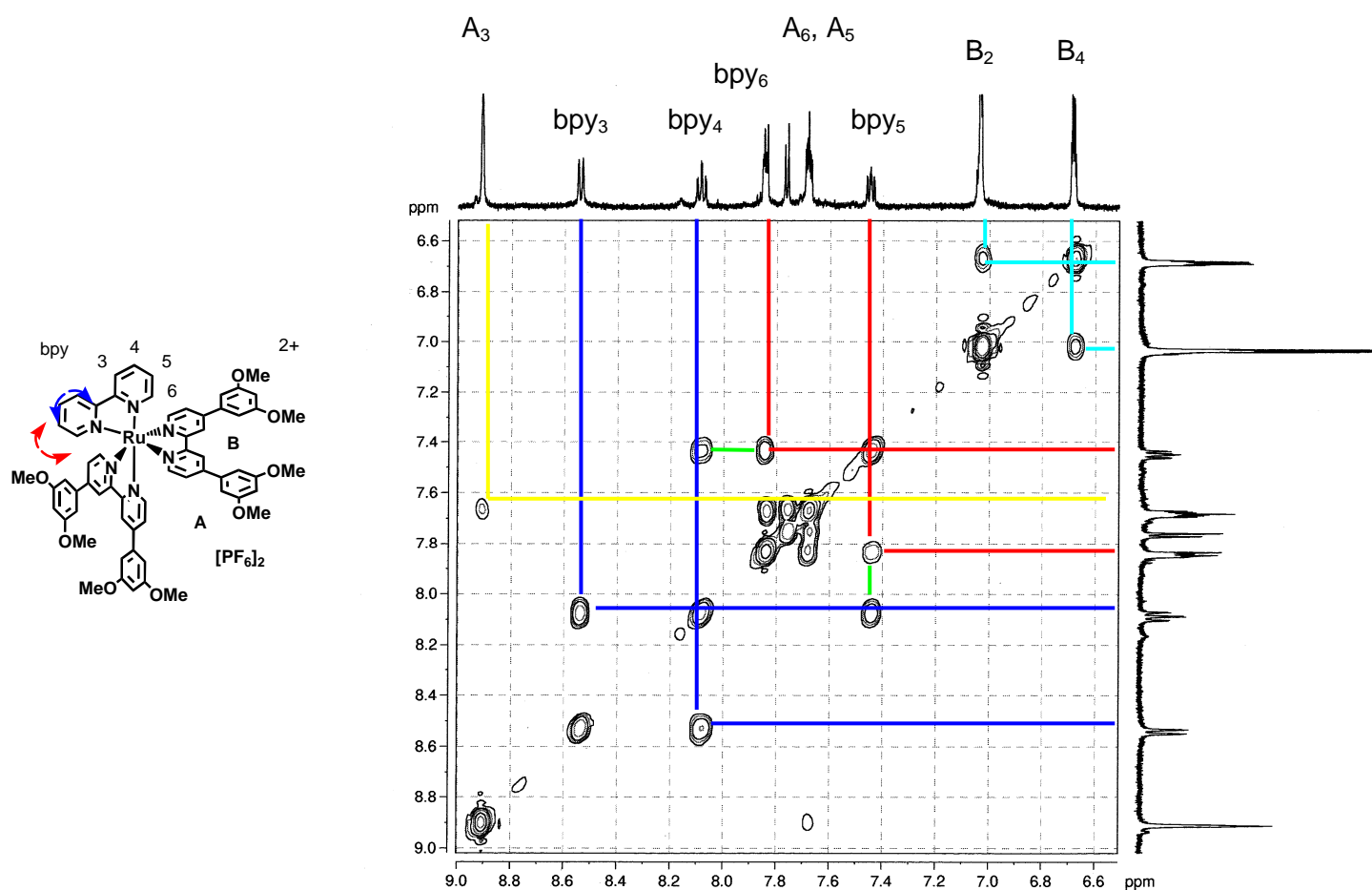


Fig II-32– COSY H-H spectrum of **19** at 500 MHz in CD₃CN at 298 K.

The correlation spectroscopy at 500 MHz showed coupling between neighbouring protons of the free bpy ligands bpy₃ and bpy₄, bpy₄ and bpy₅, bpy₅ and bpy₆.

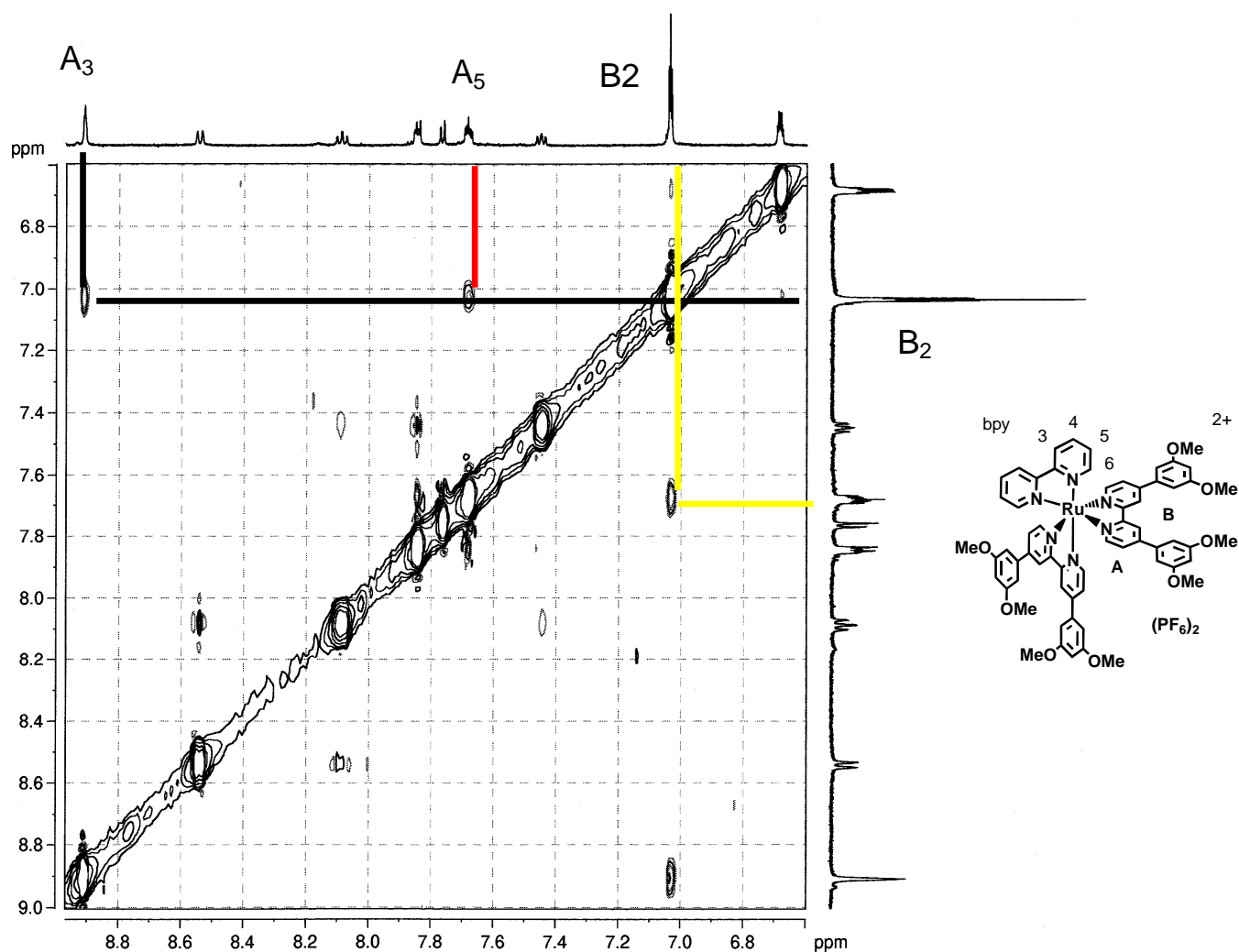


Fig II-33- nOESY spectrum of **19** at 500 MHz in CD₃CN at 298 K

The NOESY spectrum showed long distance correlations the **10** ligands, between A₃ and B₂, A₅ and B₂ which confirms the protons assignments. The NOE spectrum also showed the equivalence of the B₂ protons of **10** establishing the rotation of this ring about the C-C interannular bond.

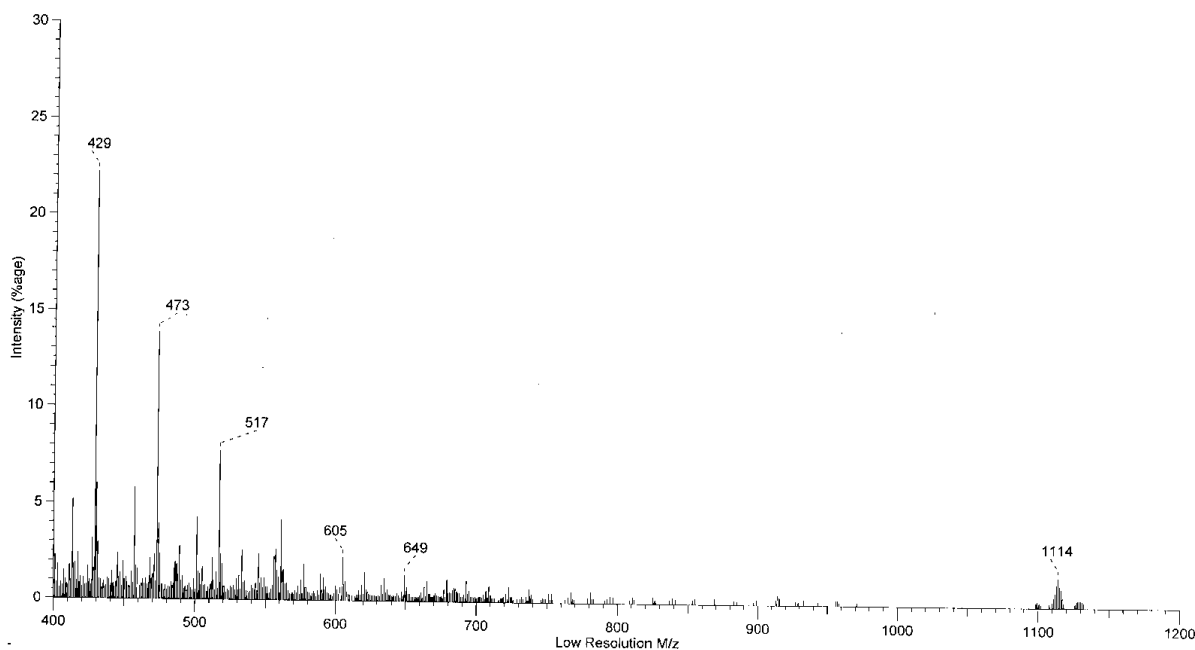


Fig II-34- ES-Mass spectrum of **19** in CH₃CN.

2) Synthesis of [Ru(**10**)₃][PF₆]₂ **20**.

The complex **20** was obtained after treatment of RuCl₃ · 3H₂O with three equivalent of the free ligand **10** are dissolved in diethyleneglycol, the mixture is the carry at reflux during 6 min with a microwave oven. After precipitation, filtration and purification with a chromatography on SiO₂ column using A_{sol} as eluent, the complex **20** (Fig II-35). **20** was obtained and characterised by ¹H NMR spectroscopy and electro-spray mass spectrometry.

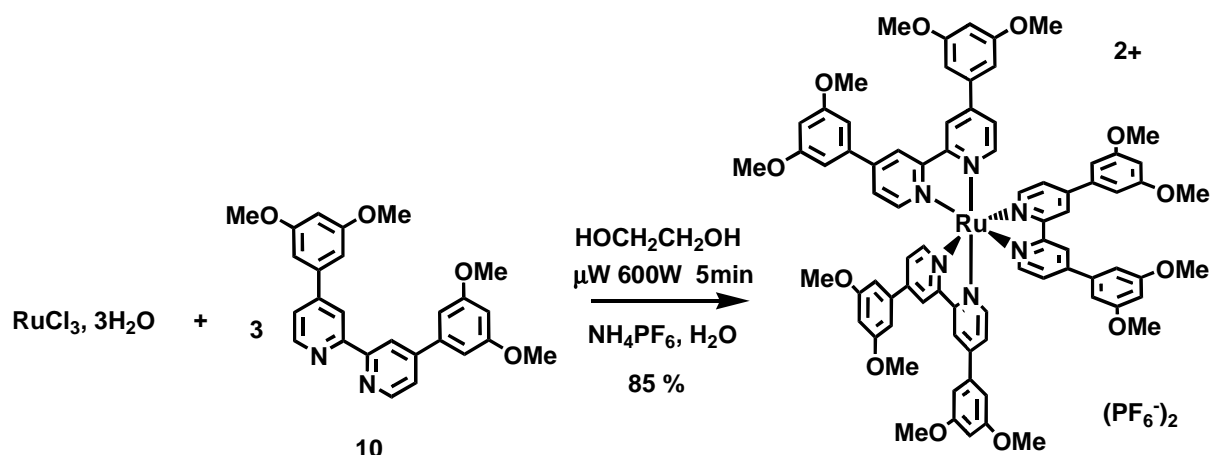


Fig II-35- Synthesis of **20**.

This complex contains 12 methoxy functionalities on the three ligands. The complex is symmetrical and this is confirmed by the NMR spectroscopy which showed only one ligand environment for ligand **10**.

Table- ^1H NMR data of **20**.

Proton	A ₃	A ₅	A ₆	B ₂	B ₄	-OMe
δ ppm	8.97	7.91	7.74	7.08	6.72	3.90
Spin multiplicity	d	d	d	d	s	s
Integration	6H	6H	6H	8H	4H	36H
J (Hz)	3.2	4.8	7.8	3.6	2.6	

Fig II-36 - ^1H NMR values of **20** in CD_3CN at 298 K at 500 MHz.

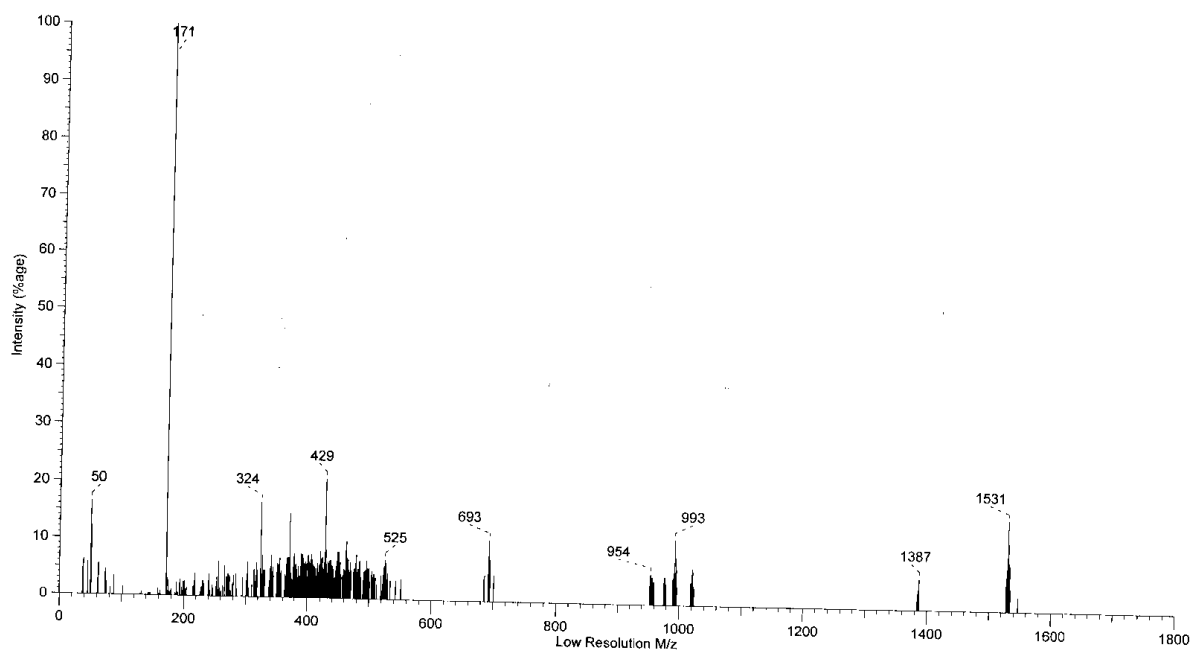


Fig II-37- ES-Mass spectra of compound **20** in CH_3CN .

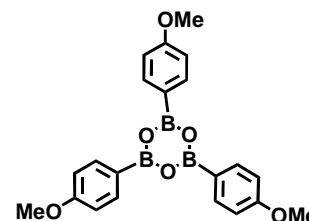
IV. Conclusion and perspectives

In this chapter two new 4,4'-substitued 2,2'-bipyridine ligands have been synthesised, containinig respectively a 3,5-dimethoxyphenyl **9** and a 1-naphtyl **13** fonctionnal group. Four complexes have been obtained, containing a mono, and bis bpy liganded ruthenium (II) metal center and complexed with one **17**, two **19**, and three **21** 3,5-dimethoxyphenyl substituted bpy ligands. This complexes have been obtained after complexation reaction and have been fully characterized. Now such complexes have been studied electrochemically and photochemically afford to mesure the influence of 3,5-dimethoxyphenyl fonctionnalisation in Ru(II)-bipyridine type complex.

Experimental Section.

Synthesis of 6^[19].

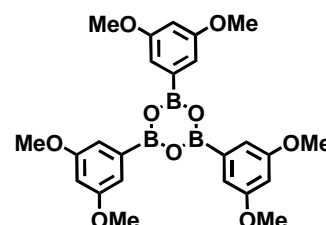
4-Bromoanisole (5.00 g, 29.3 mmol) and magnesium turnings (2.00 g, 82.3 mmol) were dissolved in THF (25 ml) and 1,2-dibromoethane (1 ml) was added. After 24 hours the brown slurry was collected by filtration and added to trimethylborate (5.00 ml) in THF (10 ml) cooled to -78°C and the mixture allowed to warm to room temperature 12 hours. After this, the reaction mixture was quenched in aqueous HCl (1M, 30 ml) of HCl and diethyl ether (50 ml). The organic phases are separated and the aqueous phase is again extracted with diethyl ether (25 ml). The combined organic phases were washed with aqueous NaOH (10 ml, 2 M) aqueous solution, then the aqueous phases are washed with dichloromethane (10 ml) and after separation neutralised with concentrated HCl solution. The mixture was then extracted with dichloromethane (3 x 10 ml). After evaporation under vacuum, the residue is purified by recrystallisation from acetone to give white crystal. (m = 760 mg, yield = 19 %).



Experimental datas : $^1\text{H NMR}$ (250 MHz) in CDCl_3 δ (ppm): 8.205 (d, 2H, $J = 8.75$ Hz) **Ph-H²**, 7.093 (d, 2H, $J = 8.5$ Hz) **Ph-H³**, 3.908 (s, 3H)-**OCH₃**. $^{13}\text{C NMR}$ in CDCl_3 δ (ppm). 163.6, 137.9, 113.9, 55.6, 31.3. **IR** : 2800-3000(w), 1599, (m), 1334 (s), 1242 (s), 1166 (s), 1022 (m), 829 (m) **EI-MS** (m/z): 402.2 ($[(\text{C}_6\text{H}_5\text{OMe})_3\text{B}_3\text{O}_3]^+$), 225.1, 134.1($[\text{C}_6\text{H}_5\text{OMe-B=O}]^+$). **m.p.**: 110°C .

Synthesis of 9^[19].

3,5-dimethoxychlorobenzene (1.65 g, 5.80 mmol) and magnesium turnings (600 mg, 24.7 mmol) were dissolved in THF (10 ml) and 1,2-dibromoethane (1 ml) were added. After 24 hours the brown slurry was collected by filtration and added to trimethylborate (1.70 ml) in THF (5 ml) cooled at -78°C and the mixture allowed to warm to room temperature 12 hours. After this, the reaction mixture was quenched in aqueous HCl (1M, 15 ml) and diethyl ether (25 ml). The organic phases are separated and the aqueous phase is again extracted with diethyl ether. The combined organic phases were washed with aqueous NaOH (5 ml, 2 M) aqueous solution, then the aqueous phases are washed with dichloromethane (10 ml) and after separation neutralised with

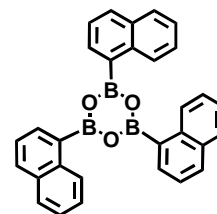


concentrated HCl solution. The mixture was then extracted with dichloromethane (3 x 10 ml). After evaporation under vacuum, the residue is purified by recrystallisation from acetone to give white crystal. (m = 590 mg, yield = 38 %).

Experimental datas : $^1\text{H NMR}$ (250 MHz) in acetone: δ (ppm): 7,05 (s, 2H) **Ph-H₂**, 6,52 (s, H) **Ph-H₄**, 3,70 (s, 6H) **-OMe**. **IR** : ν (cm⁻¹): 3009-2840, ν C_{sp2}-H 1588, 1419, 1344, 1201, 1154, 1056 **ES-MS** : 492.2 ($[(\text{C}_6\text{H}_4(\text{OMe})_2)_3\text{B}_3\text{O}_3]^+$), 246.1, 164 ($[\text{C}_6\text{H}_5(\text{OMe})_2\text{-B=O}]^+$).

Synthesis of 11^[19].

1-bromonaphtalene (5.00 g, 24.1 mmol) and magnesium turnings (2 mg, 82.3 mmol) were dissolved in THF (25 ml) and 1,2-dibromoethane (1 ml) were added. After 24 hours the brown slurry was collected by filtration and added to trimethylborate (5 ml) in THF (10 ml) cooled at -78°C and the mixture allowed to warm to

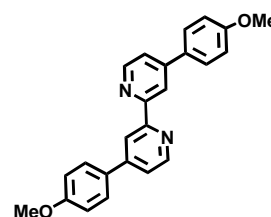


room temperature 12 hours. After this, the reaction mixture was quenched in aqueous HCl (1M, 30 ml) of chlorhydric acid and diethylether (50 ml). The organic phases are separated and the aqueous phase is again extracted with diethylether. The combined organic phases were washed with aqueous NaOH (10 ml, 2 M) aqueous solution, then the aqueous phases are washed with dichloromethane (10 ml) and after separation neutralised with concentrated HCl solution. The mixture was then extracted with dichloromethane (3 x 10 ml). After evaporation under vacuum, the residue is purified by recrystallisation from acetone to give white crystal. (m = 1.09 g, yield = 26 %).

Experimental datas : $^1\text{H NMR}$ (250 MHz) in CDCl₃: δ (ppm): 8,615 (s, 2H) **ph-H₂**, 7,92 (t, H, $J_1 = 5.2$ Hz) **nap-H₃, H₇, H₈**, 7,495 (m, 6H) **nap-H₄, H₆, H₉**. **IR** : (ν cm⁻¹): 3009-2840, ν C_{sp2}-H 1588, 1419, 1344, 1201, 1154, 1056 **ES-MS** : 462 ($[(\text{C}_{10}\text{H}_7\text{BO})_3]^+$), 231, 154 ($[(\text{C}_{10}\text{H}_7\text{-B=O})]^+$).

Synthesis of 7.

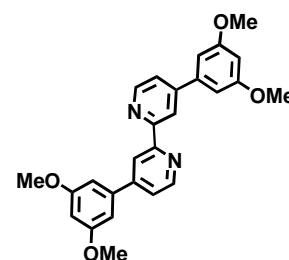
4 (100 mg, 0.32 mmol) and was dissolved in toluene (10 ml) then [Pd(PPh₃)₄] (26 mg, 0.002 mmol) dissolved under an inert atmosphere in ethanol (10 ml) are added to the mixture, then 10 ml of an aqueous solution of Na₂CO₃ (2M) was added. The biphasic mixture was purged with nitrogen and then **6** (85 mg, 0.21 mmol) in ethanol (5 ml) were added slowly and the mixture refluxed at 110°C for 2 days. The resulting dark solution was diluted with water (10 ml) and of toluene (20 ml). Ethanol was removed in vacuo and the phases were separated. The aqueous phase was extracted twice with chloroform. The combined organic phases were washed with saturated aqueous sodium chloride twice and evaporated under vacuum. (m = 24 mg Yield = 20%).



Experimental datas: ¹H NMR in CDCl₃ at 250 MHz at 298 K(δ ppm), 8.738 (*d*, 2H, *J*= 5Hz) **bpy-H⁶**; 8.716 (*d*, 2H, *J* = 2Hz) **bpy-H³**, 7.788 (*d*, 2H, *J* = 8.75 Hz) **Ph-H²**; 7.557 (dd, 2H, *J*₁= 5.25 Hz, *J*₂= 1.75 Hz) **bpy-H⁵**, 7.057 (*d*, 4H, *J* = 4.5 Hz); 3.91 (*s*, 12H) **-OMe**. ¹³C NMR in CDCl₃ (δ ppm) 160.6 ; 156.7, 149.6, 148.8 , 130.6, 128.4, 121.1, 118.5, 114.5, 55.4 ; (-**OMe**): EI-MS : 369.2 [M⁺]; 353.2, 325.1, 282.1, 184.1, 162.6, 141.1. IR: UV-vis: aspect white off solid.

Synthesis of **10**.

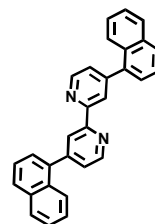
4 (100 mg, 0.32 mmol) are dissolved in toluene (10 ml) then 26 mg of [Pd(PPh₃)₄] are dissolved under inert atmosphere in ethanol are added to the mixture then 10 ml of an aqueous solution of Na₂CO₃ (2M) was added. The biphasic mixture was purged with nitrogen and then **9** (105 mg, 0.21 mmol) in ethanol (5 ml) were added slowly and the mixture refluxed at 110°C for 2 days. The resulting dark solution was diluted with water (10 ml) and of toluene (20 ml). Ethanol was removed in vacuo and the phases were separated. The aqueous phase was extracted twice with chloroform. The combined organic phases were washed with saturated aqueous sodium chloride twice and evaporated under vacuum. (m = 27.3 g, Yield = 20%).



Experimental datas: ^1H NMR (250 MHz) in CDCl_3 (δ ppm), 9.07 (s, 2H) **bpy-H³**, 8.84 (d, 2H, $J = 5.25$ Hz) **bpy-H⁶**, 7.78 (d, 2H, $J = 4.5$ Hz) **bpy-H⁵**, 7.05 (d, 4H, $J = 2$ Hz) **Ph-B2**, 6.63 (t, 2H, $J = 2.25$ Hz) **Ph-B4**, 3.91 (s, 6H) **-OMe**. ^{13}C NMR in CDCl_3 (δ ppm) 161.7, 150.0, 132.5, 129.0, 128.9, 105.8, 56.0 **EI-MS** : $[\text{M}^+]$ 427.2, 398.2, 325.1, 214.1. **IR** (ν cm^{-1}) : 2941(w), 1589(w), 1434(w), 1119(w), 1062(w), 815(s) aspect white off solid.

Synthesis of 12.

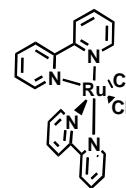
4 (1.0 g, 3.2 mmol) are dissolved in toluene (25 ml) then 367 mg of $\text{Pd}(\text{PPh}_3)_4$ are dissolved under inert atmosphere ethanol are added to the mixture then 10 ml of an aqueous solution of Na_2CO_3 (2M) was added. The biphasic mixture was purged with nitrogen and then **12** (985 mg, 2.1 mmol) in ethanol (10 ml) were added slowly and the mixture refluxed at 110°C for 2 days. The resulting dark solution was diluted with water (10 ml) and of toluene (20 ml). Ethanol was removed in vacuo and the phases were separated. The aqueous phase was extracted twice with chloroform. The combined organic phases were washed with saturated aqueous sodium chloride twice and evaporated under vacuum. The residue was chromatographed on $\text{SiO}_2/\text{CHCl}_3$ column and a white solid was obtained and recrystallised from ethanol ($m = 195$ mg, Yield = 15 %).



Experimental datas: ^1H NMR in CDCl_3 at 250 MHz at 298 K (δ ppm), 8.810 (d, 2H, $J = 5$ Hz); **bpy-H⁶**, 8.710 (s, 2H) **bpy-H³**; 7.485-7.606 (m, 14H) **nap-H**; 7.03 (s, 2H) **bpy-H⁵**. ^{13}C NMR in CDCl_3 (δ ppm) 207.4, 134.2, 131.2, 129.3, 128.9, 127.5, 127.1, 126.5, 125.8, 125.7. **EI-MS** : 407.1 $[\text{M}^+]$; 204. **IR**: 3033, 1737, 1585, 1365, 1217, 918. **Mass-Analysis**, Formula $\text{C}_{28}\text{H}_{20}\text{N}_2$ (% Calculated): 85.54% (88.21%), 5.09% (4.93%), 5.93% (6.86%). aspect white off solid.

Synthesis of **14**.

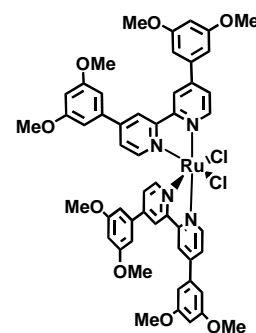
RuCl₃·3H₂O (500 mg 1,91 mmol) and 2,2'-bipyridine (596 mg 3,82 mmol) are dissolved in 10 ml of ethanol. The reaction mixture is carried at reflux during 4 hours, and cooled at room temperature. A brown insoluble solid precipitated and is filtered over fritted (porosity 3), the solid is washed with few amount of ethanol, recuperated and dried with a dessicator under vacuum. The compound **14** was weighted and put in the following complexation reaction without characterisation (m = 750 mg Yield = 81 %).



Experimental Datas: IR: (v cm⁻¹) 2974 (w), 1602 (m), 1448 (m), 1043.4 (s), 879 (s).

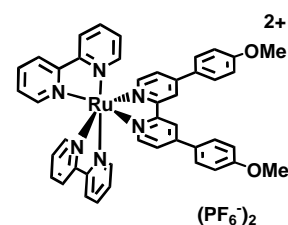
Synthesis of **18**.

RuCl₃·3H₂O (500 mg, 1.91 mmol) and **18** (596 mg, 3.82 mmol) are dissolved in ethanol (10 ml). The reaction mixture is carried at reflux during 4 hours, and cooled at room temperature. A brown insoluble solid precipitated and is filtered over fritted (porosity 3), the solid is washed with few amount of ethanol, recuperated and dried with a dessicator under vacuum. The compound **18** was weighted and put in the following complexation reaction without characterisation (m = 750 mg, Yield = 81 %).



Synthesis of **15**^[20].

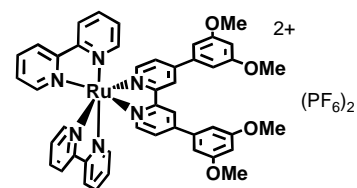
14 (23 mg, 0.047 mmol) and **7** (18 mg 0,047 mmol) were dissolved in EtOH (10 ml) and the reaction mixture heated at reflux for 4 h and then cooled at room temperature. The solution was extracted three times with CH₂Cl₂, and the solvent is removed under reduce pressure. The complex **15** was purified over column chromatography (SiO₂/A_{sol}) and recrystallised in refluxing methanol. We obtained the pure red complex **15** after precipitation with NH₄PF₆. (29.4 mg, 58 %).



Experimental Datas: ^1H NMR in CD_3CN (δ ppm), 9.04 (*s*, 2H) **A3**, 8.70 (*d*, 4H, $J = 8$ Hz) **bpy-H³**, 8.21 (*t*, 2H, $J_2 = 6.5$ Hz) **bpy-H⁴**, 8.07 (*d*, 4H, $J = 8.75$ Hz) **B2**, 8.00-7.92 (*d*, 4H, $J_2 = 1.5$ Hz) **bpy-H⁶**, 7.82 (*d*, 2H, $J = 6$ Hz) **A6**, 7.77 (*d*, 2H, $J = 6$ Hz) **A5**, 7.56 (*m*, 4H) **bpy-H⁵**, 7.27 (*d*, 4H, $J = 8.75$ Hz) **B3**, 3.91 (*s*, 6H) **-OMe**. **ES-MS** : $[\text{M}^+]$; 1056, 782, 624, 502, 369, 278, 176, 89, 50. **IR**: 1600 (*m*), 1580(*m*).

Synthesis of **17**.

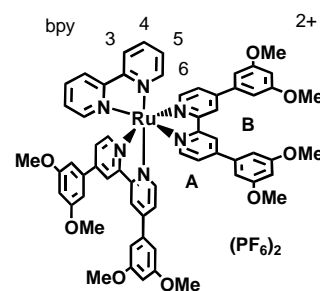
14 (20 mg, 0.076 mmol) and **10** (33 mg, 0.076) were dissolved in EtOH (10 ml) and the reaction mixture heated at reflux for 4 h and then cooled at room temperature. The solution was extracted three times with CH_2Cl_2 (10 ml), and the solvent is removed under reduce pressure. The complex **17** was purified over column chromatography ($\text{SiO}_2/\text{A}_{\text{sol}}$) and recrystallised in refluxing methanol. We obtained the pure red complex **17** after precipitation with NH_4PF_6 . (29.4 mg, 58 %).



Experimental datas : ^1H NMR (400 MHz) in CD_3CN : δ (*ppm*): 8.91 (*s*, 2H) **AH³**, 8.56 (*d*, 4H, $J = 8.5$ Hz) **bpy-H³**, 8.10 (*d*, 4H, $J = 7.5$ Hz) **bpy-H⁴**, 7.87 (*d*, 4H, $J = 6.0$ Hz) **bpy-H⁶**, 7.79 (*d*, 2H, $J = 6$ Hz) **AH⁶**, 7.70 (*d*, 2H, $J = 6$ Hz) **AH⁵**, 7.46 (*m*, 4H) **bpy-H⁵**, 7.06 (*s*, 4H, $J = 2.25$ Hz) **BH²**, 6.71 (*s*, 2H) **BH⁴**, 3.90 (*s*, 12H) **-OMe**. ^{13}C NMR in acetone δ (*ppm*): **IR** : ν (cm^{-1}): 1733(*w*), 1406(*m*), 1203(*w*), 1060(*w*), 824(*s*). **EI-MS** : 987 $[\text{M}^+ - \text{PF}_6^-]$, 842 $[\text{M}^+ - 2\text{PF}_6^-]$, 429, 307, 171, 154, 77. **UV/Vis** (MeCN): absorption : $\lambda_{\text{max}} = 458$ nm.

Synthesis of **19**.

18 (750 mg, 0.73 mmol) and **10** (312 mg, 0.73 mmol) were dissolved in EtOH (10 ml) and the reaction mixture heated at reflux for 4 h and then cooled at room temperature. The solution was extracted three times with CH_2Cl_2 (10 ml), and the solvent is removed under reduce pressure. The complex **19** was purified over column chromatography ($\text{SiO}_2/\text{A}_{\text{sol}}$) and

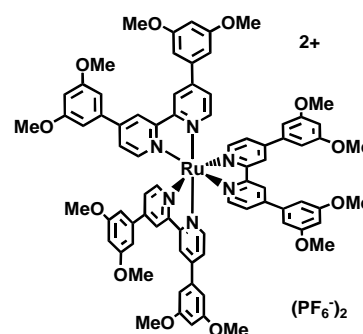


recrystallised in refluxing methanol. We obtained the pure red complex **19** after precipitation with NH_4PF_6 . (610 mg, 75 %). This new compound was analysed with ^1H NMR spectroscopy, and electrospray mass spectroscopy.

Experimental datas : ^1H NMR (500 MHz) in CD_3CN : δ (ppm): 8.95 (d, 2H, $J = 1.75$ Hz) AH^3 , 8.58 (d, 2H, $J = 8$ Hz) bpy-H_3 , 8.12 (t, 2H, $J = 7.5$ Hz) bpy-H^4 , 7.88 (d, 2H, $J = 8$ Hz) bpy-H^6 , 7.81 (d, 4H, $J = 6$ Hz) AH^6 , 7.72 (d, 4H, $J = 4.5$ Hz) AH^5 , 7.49 (t, 2H, $J = 5.75$ Hz) bpy-H^5 , 7.07 (t, 8H, $J = 1$ Hz) BH^2 , 6.71 (m, 4H) BH^4 , 3.91(s, 24H) $-\text{OMe}$. IR : ν (cm^{-1}): 1591(w), 1406(m), 1203(w), 1157(w), 1083(w), 1035(w), 824(s). ES-MS : 1114 [$\text{M}^+ - \text{PF}_6^-$], 987 [$\text{M}^+ - 2\text{PF}_6^-$], 429, 324, 171, 154, 77 UV/Vis (MeCN): absorption : $\lambda_{\text{max}} = 464$ nm.

Synthesis of **20**.

$\text{RuCl}_3 \cdot 3\text{H}_2\text{O}$ (5 mg, 0.0191 mmol) and **19** (24 mg 0.057 mmol) are dissolved in 6 ml of ethyleneglycol and the reaction mixture is carried at reflux for 6 minutes at 600 W. The brown-orange solution is extracted with 3 times CH_2Cl_2 (10 ml), after removing the solvent the complex was purified over SiO_2 column chromatography using A_{sol} as eluant, the compound **20** with a low R_f was isolated, and its solvent removed via evaporation under vacuum. The solid was recrystallised in methanol and after precipitation with aqueous solution of NH_4PF_6 we obtained a brown solid. (m = 24 mg, Yield = 81%).



Experimental datas : ^1H NMR (500 MHz) in CD_3CN : δ (ppm): 8.97 (d, 6H) AH_3 , 7.91 (d, 6H, $J = 5.2$ Hz) $-\text{AH}_6$, 7.75 (d, H, $J = 7.8$ Hz) AH_5 , 7.08 (d, 6H,) BH_2 , 6.72 (t, 6H, $J = 2.8$ Hz) BH_4 , 3.90 (s, 36 H) $-\text{OMe}$. IR : ν (cm^{-1}): 1588, 1419, 1344, 1201, 1154, 1056 FAB-MS : 1531 ([M]- PF_6^-), 1387 ([M]-2 PF_6^-), 1021, 993, 693, 429, 324, 171, 50. UV/Vis (MeCN): absorption : $\lambda_{\text{max}} = 476$ nm.

References.

- [1]. Lytle, F. E., Hercules, D. M., *J. Am. Chem. Soc.* **1969**, *91*, 253.
- [2]. Demas J. N., Diemente, D, Harris E. W., *J. Am. Chem. Soc.* **1973**, *91*, 6864.
- [3]. Hager, G. D., Watts, R. J., Crosby, G. A., *J. Am. Chem. Soc.* **1974**, *97*, 7037.
- [4]. Hager, G. D., Crosby, G. A., *J. Am. Chem. Soc.* **1975**, *97*, 7031.
- [5]. Balzani, V., Moggi, L., Boletta, F., Manfrin, M. F., *Science* **1975**, *189*, 852.
- [6]. Creutz, C., Chou, M., Netzel T. L., Okumura, M., Sutin, N., *J. Am. Chem. Soc.* **1980**, *102*, 1309.
- [7]. Durham, B., Caspar, J. V., Nagle J. K., Meyer T. J., *J. Am. Chem. Soc* **1982**, *104*, 4803.
- [8]. Juris, A., Balzani, V., Barigelletti, F., Campagna, S., Belser, P., von Zelewsky, A., *Coord. Chem. Rev.* **1988**, *84*, 85.
- [9]. Denti, G., Campagna, S., Scolastica, S., Ciano, M., Balzani, V., *J. Am. Chem. Soc.* **1992**, *114*, 2944.
- [10]. Sauvage, J.-P, Collin, J.-P, Chambron, J.-C, Guillerez, S., Coudret, C., Balzani, V., Barigelletti, F., De Cola, L., Flamigni, L., *Chem. Rev.* **1994**, *94*, 993.
- [11]. Maestri, N., Armaroli, N., Balzani, V., Constable, E. C., Cargill Thompson, A. M. W., *Inorg. Chem* **1995**, *34*, 2759.
- [12]. Balzani, V., Juris, M., Venturi, S., Campagna, S., Serroni, S., *Chem. Rev.* **1996**, *96*, 956
- [13]. Barigelletti, F., Flamigni, L., *Chem. Soc. Rev.* **2000**, *29*, 1.
- [14]. Encinas, S., Flamigni, L., Barigelletti, F., Constable, E. C., Housecroft, C. E., Schofield, E. R., Figgemeier, E., Fenske, D., Neuburger, J. G., Vos, M., Zehnder, M., *Chem. Eur. J.* **2002**, *8*, 137.
- [15]. Passalacqua, R., Loiseau, F., Campagna, S., Fang, Y. Q., Hanan, G. S., *Angew. Chem. Int. Ed.* **2003**, *42*, 1608.
- [16]. Miyaura, N., Suzuki, A., *Chem. Rev.* **1995**, *95*, 2457.
- [17]. Stille, J. K., *Angew. Chem. Int. Ed. Engl.* **1986**, *25*, 508.
- [18]. Scott, W. J., Crisp, G. T., Stille, J. K., *J. Am. Chem. Soc.* **1984**, *106*, 4630.
- [19]. Dol, G. C., Kamer, P. C. J., Van Leeuwen, P. W. N. M., *Eur. J. Org. Chem.* **1998**, 359.
- [20]. Constable, E. C., Housecroft, C. E., Neuburger, M., Poleschak, I., Zehnder, M., *Polyhedron* **2003**, *22*, 93.

Chapter III: Synthesis of 4'-phenylsubstitued-2,2': 6', 2'' -terpyridine complexes.

I. Introduction.

In the synthesis of metal bipyridine complexes, a problem appears when the desired complex contains different types of bipy ligands. The synthesis of 2,2':6',2''-terpy based complexes is of interest because the formed complexes will only be chiral if the terpy is asymmetrically substituted. In order to use Ru(II) oligopyridine type of complexes in supramolecular nano-devices, the linear geometry plays a crucial role in the construction of well defined systems using the metal complexes as electron donor. We have synthesized complexes containing 2,2':6'',2'-terpyridine ligands substituted on the 4-position of the terpy

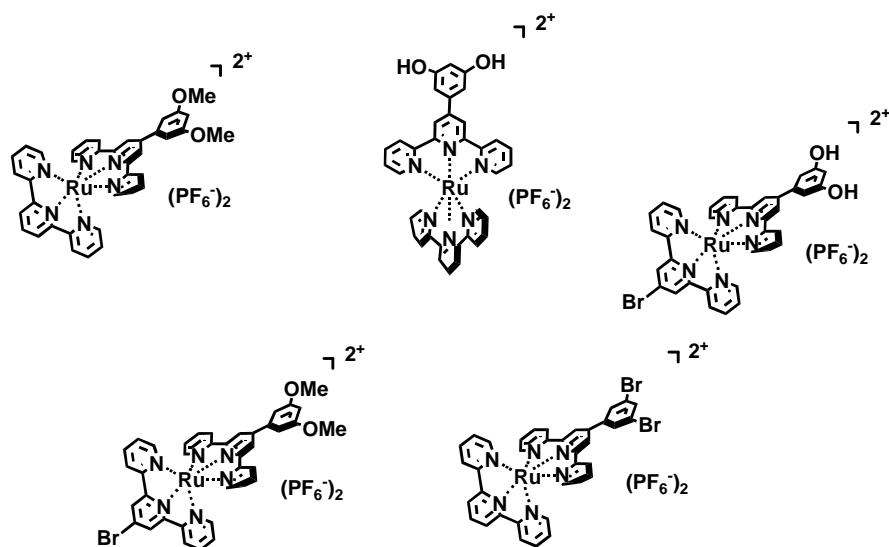


Fig III-1- 4-substituted terpyridine ruthenium (II) complexes

by a phenyl, 3,5-dihydroxyphenyl, 3,5-dimethoxyphenyl ligand or a 3,5-dibromophenyl group ligand. The heteroleptic complexes [Ru(tpy)L][PF₆]₂ were prepared in each case. In our goal to see the chemical influence in the electronic repartition of the photochemically induced excited state. The symmetrical series is well known and has been synthesized and studied in our group^[1-6], using 4-phenyl substituted terpyridines, hydroxy, chloro or methyl-substitued terpyridines^[3].

II. Synthesis of 4-substituted-2,2':6',2''-terpyridine ruthenium (II) complexes

The metal complexes containing terpyridine ligands have been studied in our labs because they showed (contrary to the bpy ligand based complexes) the absence of chirality. The linear properties of such complexes was interesting and offered possibilities of application in nano-molecular devices.

1) Synthesis of 4-bromo-2,2':6',2''-terpyridine **25**.

The synthesis of 4-bromo-2,2':6',2''-terpyridine was according to the Constable^[1] procedure. The pyridine-1,3,5-trione was obtained after reaction of two equivalents of 2-ethyl picolinate with acetone and NaH in 1,2-dimethoxyethane during 12 hours at reflux. After neutralisation of the excess base with water and dilute HCl, the yellow precipitate is filtered and washed with diethyl ether. This trione was ring closed by reaction

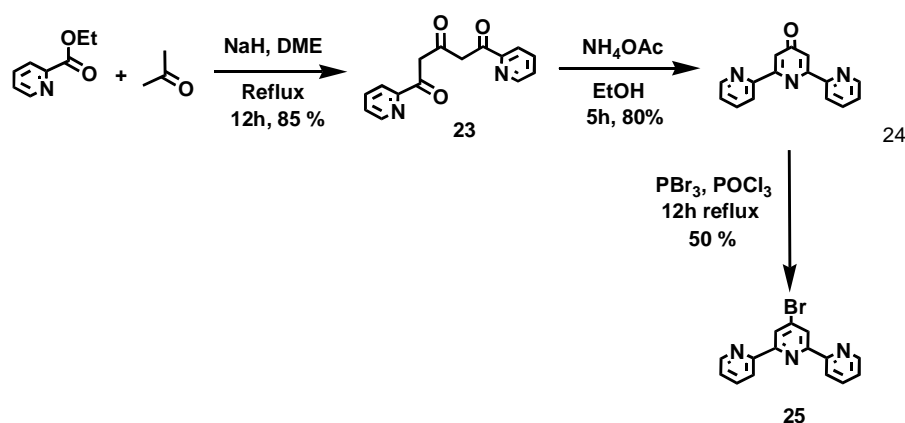


Fig III-2- Synthesis of **25**.

with NH₄OAc in EtOH during 5 hours at reflux and we obtained the 2,6-bis(2'-pyridyl)-pyridone which was in tautomeric equilibria with its 4-hydroxytypy form. This compound is then brominated by PBr₃ in POCl₃ during 12 hours at 100 °C, and after distillation of the POCl₃ and neutralisation of the reaction mixture, the compound is purified over Alox column compound **25** was recrystallised from CHCl₃ and obtained 50 % yield.

2) Synthesis of 4-phenyl-substituted -2,2':6',2''-terpyridine(tpy)

The synthesis of substituted terpyridine ligands is well known and often made by our group. Now we tried to synthesized the new 4-substitued-tpy ligands containing phenyl, 3,5-dimethoxyphenyl, 3,5-dihydroxyphenyl and 3,5-dibromphenyl functional groups. The synthesis of 4-phenyl substituted ligand is according the general synthetic method described before^[2].

The 3,5-dimethoxyphenyl tpy ligand, was obtained after reaction of 2-acetylpyridine with 3,5-dimethoxybenzaldehyde in presence of *t*-BuOK in EtOH at room temperature during 17 hours (*Fig III-3*). After the reaction mixture was treated with a solution of NH₄OAc in EtOH/CH₃CO₂H 2:1(v/v) and heated at reflux during 5 hours. The ligand **29** was obtained after cooling at room temperature and crystallisation onto ice, with 70 % yield. This

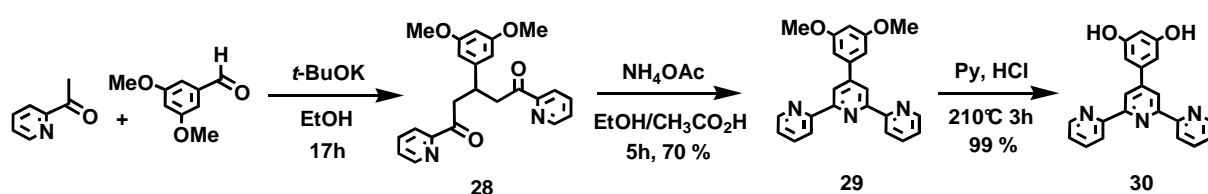


Fig III-3- Synthesis of tpy ligands **29** and **30**

compound is visualised on TLC with a solution of FeCl₂ in water. The ligand **29** is deprotected in presence of pyridine and concentrated HCl (*Fig III-3*) previously heated at 210 °C with the help of a distillation system which removed water. After stabilisation of the internal temperature during 2 hours, this solution is cooled to 150° C and the ligand introduced. The reaction mixture was heated during 3 hours at 210 ° C and cooled at 100 °C, then warm water added to the solution and after decreasing the temperature at 25 °C a white precipitate appeared. This one was filtered and recrystallised from DMF to obtain pure **30** with a near quantitative yield (99 %).

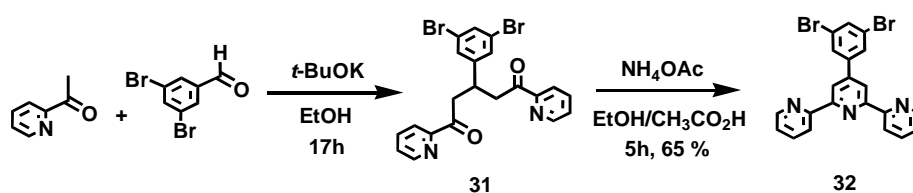


Fig III-4-Synthesis of **32**

The 3,5-dibromophenyl tpy ligand was synthesized in order to functionalise the 3,5 positions of the aromatic substituent by Pd(0) catalysed cross coupling. The synthesis of this ligand was done according to the same procedure as **29**. We obtained the light brown ligand **32** in 65 % yield (Fig III-4).

3) Synthesis of ruthenium(II) 4-phenyl-substituted -2,2':6',2''-terpyridine complexes

The synthesis of [Ru(tpy)(**25**)](PF₆)₂, **38** was according to the general procedure of ruthenium(II) tpy type complexes which consisted of, two steps. The first step consisted of synthesizing [Ru(tpy)Cl₃], starting with RuCl₃·3H₂O and tpy at reflux during 3 hours in ethanol. [Ru(tpy)Cl₃] was obtained after filtration and washing with ethanol to removed the excess of free tpy and RuCl₃. The second step consisted on the reaction between 1 equivalent of Ru(tpy)Cl₃ and 1 equivalent of **25** (Fig III-5) and after 4 hours of reaction and precipitation with NH₄PF₆ this gave the complex **38** in 53 % yield.

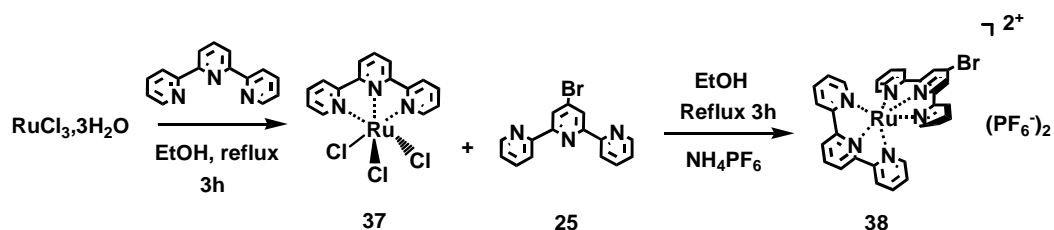


Fig III-5-Synthesis of **38**.

[Ru(tpy)Cl₃] reacted with 1 equivalent of **29** in ethanol in presence of NEM. The reaction mixture was treated with NH₄PF₆ and the complex precipitated, and was filtered and purified with SiO₂/Asol column chromatography. The complex [Ru(tpy)(**29**)](PF₆)₂, **39** was obtained in 79 % yield.

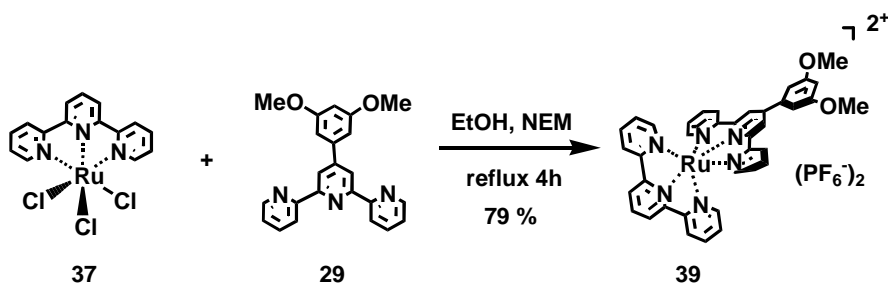


Fig III-6-Synthesis of **39**.

For the case of the complexation of **30** with $[\text{Ru}(\text{tpy})\text{Cl}_3]$, the reaction was made in the same conditions seen previously. **30** was dissolved with $[\text{Ru}(\text{tpy})\text{Cl}_3]$ in EtOH then the reaction mixture was heated at reflux during 4 hours. After precipitation with NH_4PF_6 and cooling to room temperature the complex was collected by filtration and column chromatography using SiO_2/Asol , we obtained a red-brown complex $[\text{Ru}(\text{tpy})(\mathbf{30})][\text{PF}_6]_2$, **40**. The lower solubility of **30**, decreased the final yield (65 %).

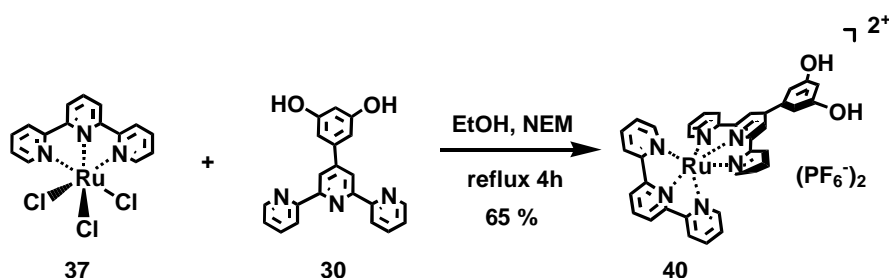


Fig IV-7-Synthesis of **40**.

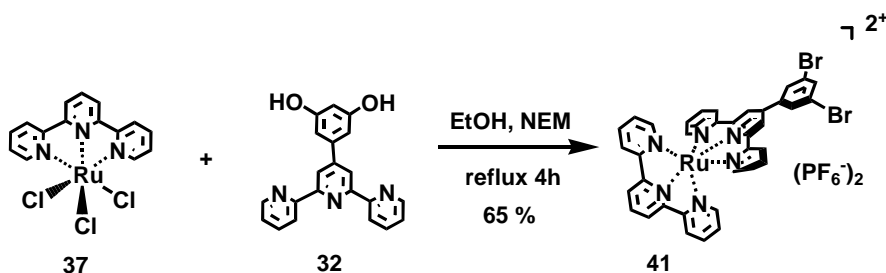


Fig III-8-Synthesis of **41**.

This complexes are characterised by ^1H NMR at 250 MHz. spectroscopy, and ES mass spectrometry.

III. Synthesis of ruthenium Y shaped 3,5-dioxyphenyl spaced metallostars.

Metallostars are dendrimeric structures containing several polymetallic centers such as Ru or Os. The most interesting topics of our metallostars are their electrochemical and photochemical properties. In our search for definite supramolecular systems which can have some light-harvesting properties, our research was focused on this type of architectures. In recent years some metallodendrimeric species have been synthesized in our group metal with

centers like ruthenium(II) and osmium(II) with bipyridine (bpy) or terpyridine (tpy) ligands as building blocks^[6-7].

1) Synthesis of Dendron A 45.

In order to increase the light-harvesting properties of our metallostars, the first synthetic modification was to add functionality at the periphery of the metallodendrimer. The last metallostars synthesized in our group lab contained as spacer a 3,5-dioxyphenyl spacer linking the different metal-terpyridine blocks. These monomers were substituted by H or 2-thiophenyl functional groups at the 4'-position of the terpyridine external ligands^[6-7]. In our case we want to add 3,5-dimethoxyphenyl functionality at the periphery, as a possible spacer

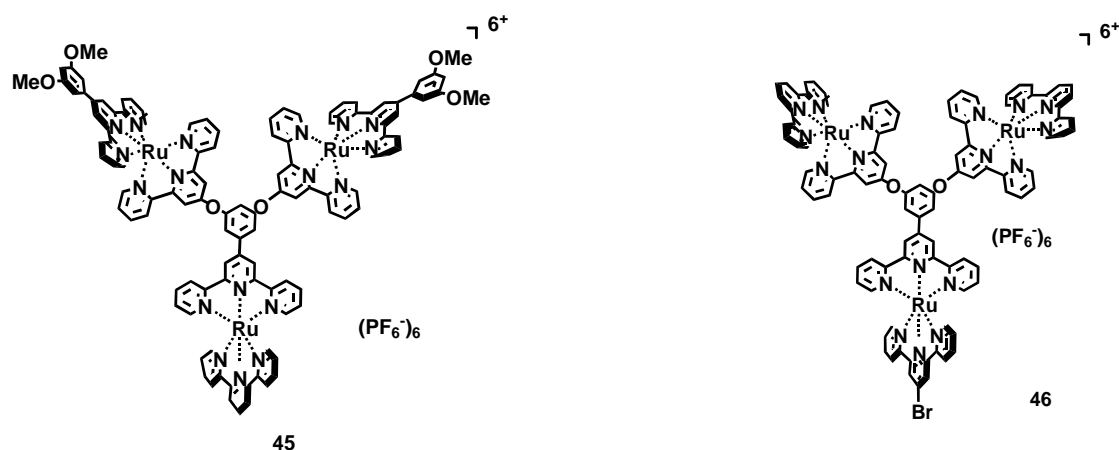


Fig-III-9- Two metallostars targets Dendron A 45 and Dendron B 46.

group for functionalised higher generation metallodendrimers in, and also to modify the light harvesting properties of these compounds.

The synthetic route was simple and consisted of the coupling of mononuclear precursors like $[\text{Ru}(\text{tpy})(\mathbf{30})]^{2+}$ and $[\text{Ru}(\mathbf{25})(\mathbf{29})]^{2+}$ by etherification of the 3,5-dihydroxy position with the bromine functionality and obtaining the trinuclear dendron A 45 (Fig III-9). The complex $[\text{Ru}(\text{tpy})(\mathbf{30})]^{2+}$ was obtained according the procedure described in II-3, and its synthesis is

described in the experimental procedure part. For the complex $[\text{Ru}(\text{tpy})(\mathbf{29})][\text{PF}_6]_2$, the synthesis is analogous.

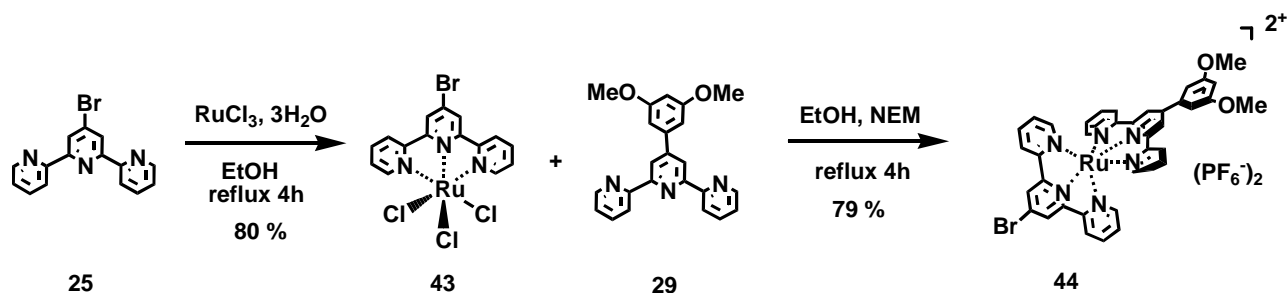


Fig III-10- Synthesis of **44**.

After reaction of **25** with $\text{RuCl}_3 \cdot 3\text{H}_2\text{O}$ in EtOH during four hours we obtained the complex **43** which was engaged in the second reaction with the ligand **29** in EtOH and NEM and heated at reflux during 4 hours and after precipitation with NH_4PF_6 , the complex $[\text{Ru}(\mathbf{25})(\mathbf{29})][\text{PF}_6]_2$, **44** was obtained.

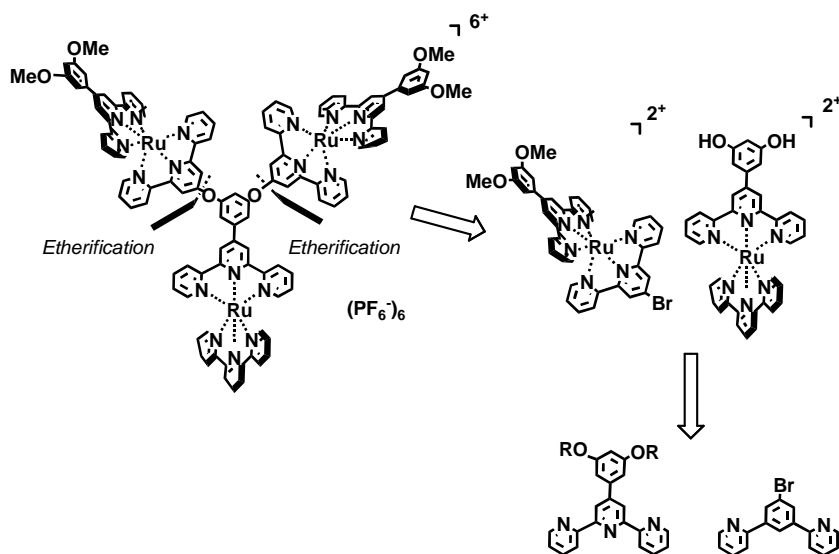


Fig III-11- Retrosynthetic analysis of **45**.

The trinuclear complex **45** was obtained after disconnection of the two 3,5-dimethoxy phenyl parts from the mononuclear complex core. This two mononuclear precursors were obtained by complexation of the ligands **25**, **29** and **30** with $\text{RuCl}_3 \cdot 3\text{H}_2\text{O}$.

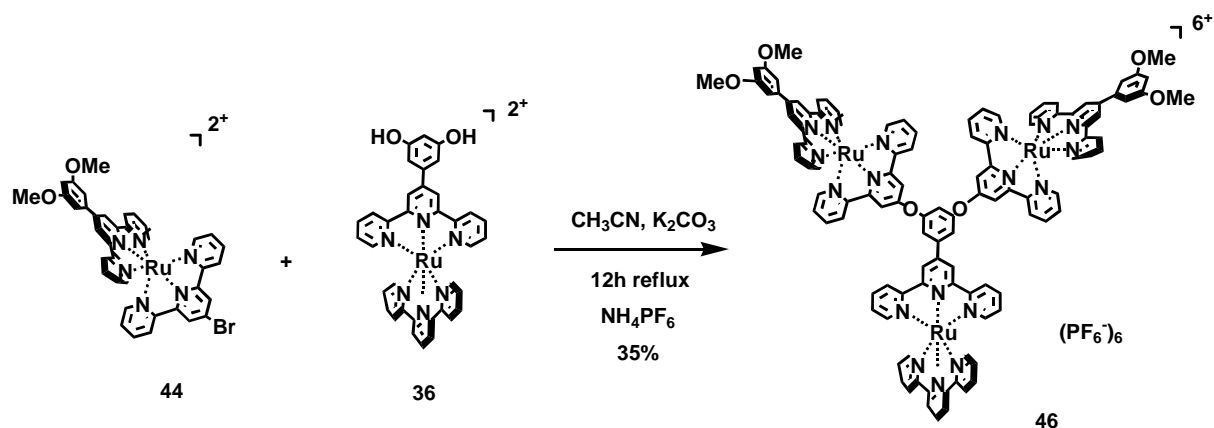


Fig III-12-Synthesis of **45** via etherfication reaction

The product **45** was obtained after reaction of two moles of complex **44** and with one equivalent of hydroxy complex **36**, after reaction in MeCN with K_2CO_3 during 12 hours at reflux in EtOH we obtained the coupling trinuclear product **45**. The compound was purified over SiO_2 column (230-400 Mesh) using A_{sol} as eluent. This compound was analysed by ^1H NMR at 500 MHz, ES mass spectrometry and IR spectroscopy.

^1H NMR spectrum of **45**.

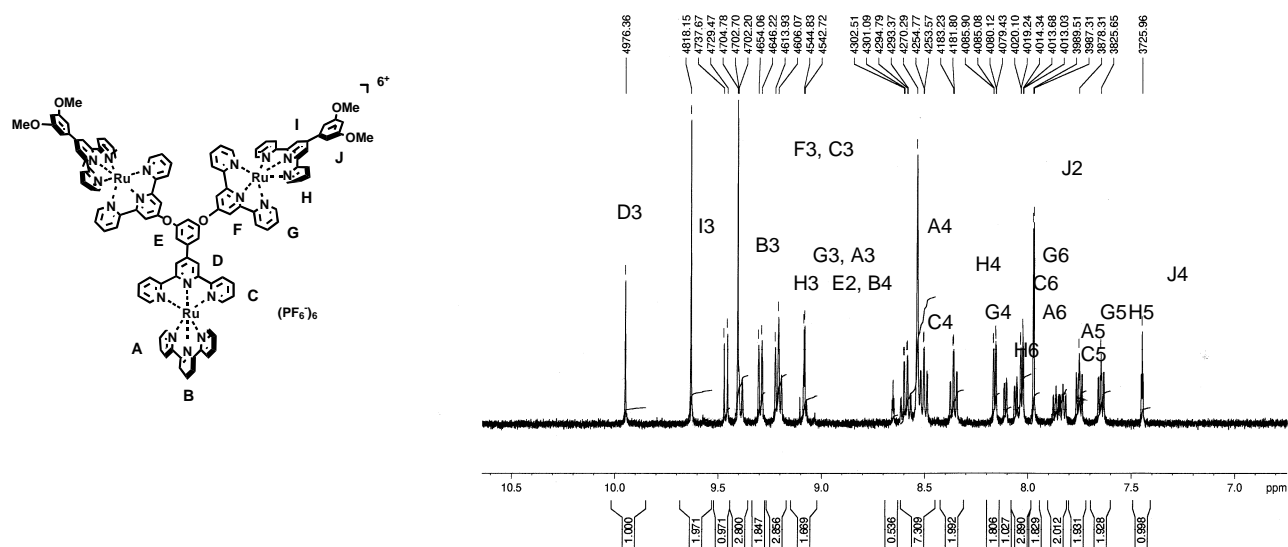


Fig III-13- ^1H NMR Spectrum of **45** in D_2O at 500 MHz at 298 K.

δ ppm	10.15	9.84	9.68	9.61	9.52	9.43	9.30	8.86	8.79	8.74	8.62	8.39
attribution	D3	I3	B3	F3	H3	G3,A3	E2,B4	C4	A4	H4	G4	H6
spin multiplicity	<i>s</i>	<i>s</i>	<i>d</i>	<i>d</i>	<i>d</i>	<i>t</i>	<i>d</i>	<i>dd</i>	<i>s</i>	<i>t</i>	<i>t</i>	<i>d</i>
integration	2H	2H	1H	2H	2H	3H	2H	2H	2H	2H	2H	2H
J (Hz)			6.6	9.1	8	8.5	2.1	$J_1=7.5$		8.75	8	5.25
								$J_2=9.9$				

δ ppm	8.32	8.27	8.26	8.20	8.09	8.07	7.98	7.88	7.68
attribution	A6	C6	G6	J2	C5	A5	G5	H5	J4
spin multiplicity	<i>d</i>	<i>d</i>	<i>d</i>	<i>d</i>	<i>t</i>	<i>t</i>	<i>t</i>	<i>t</i>	<i>t</i>
integration	1H	1H	2H	2H	1H	1H	2H	2H	1H
J (Hz)	6.5	6.5	6.5	2.5	6.5	6.6	7.4	7.1	2.2

The ^1H NMR spectrum of **45** showed different type of signals. corresponding to the aromatic region of phenyl spacers called **E** for core spacer and **J** for the protons of the phenyl group at the extremities. The others protons are characteristic of the pyridine protons of the tpy ligands (**A**, **B**, **C**, **D**, **F**, **G**, **H**) and **I** and assigned 3,4,5 or 6 following the proton position. The two protons of the spacer **E**₂ and **B**₄ of the core external ligand are both positioned at δ 9.09 ppm in the spectrum. The “H3” positioned protons of **D**₃, **I**₃, **B**₃, **F**₃, **C**₃, **H**₃, **G**₃, and **A**₃ have respectively δ 9.63, 9.47, 9.41, 9.40, 9.30, 9.28, 9.22 ppm. The vicinal protons were detected as doublet and triplet like **A**₃, **B**₃, **C**₃, **G**₃, **H**₃, and the isolated protons **I**₃, **F**₃, **J**₃ and are singlets.

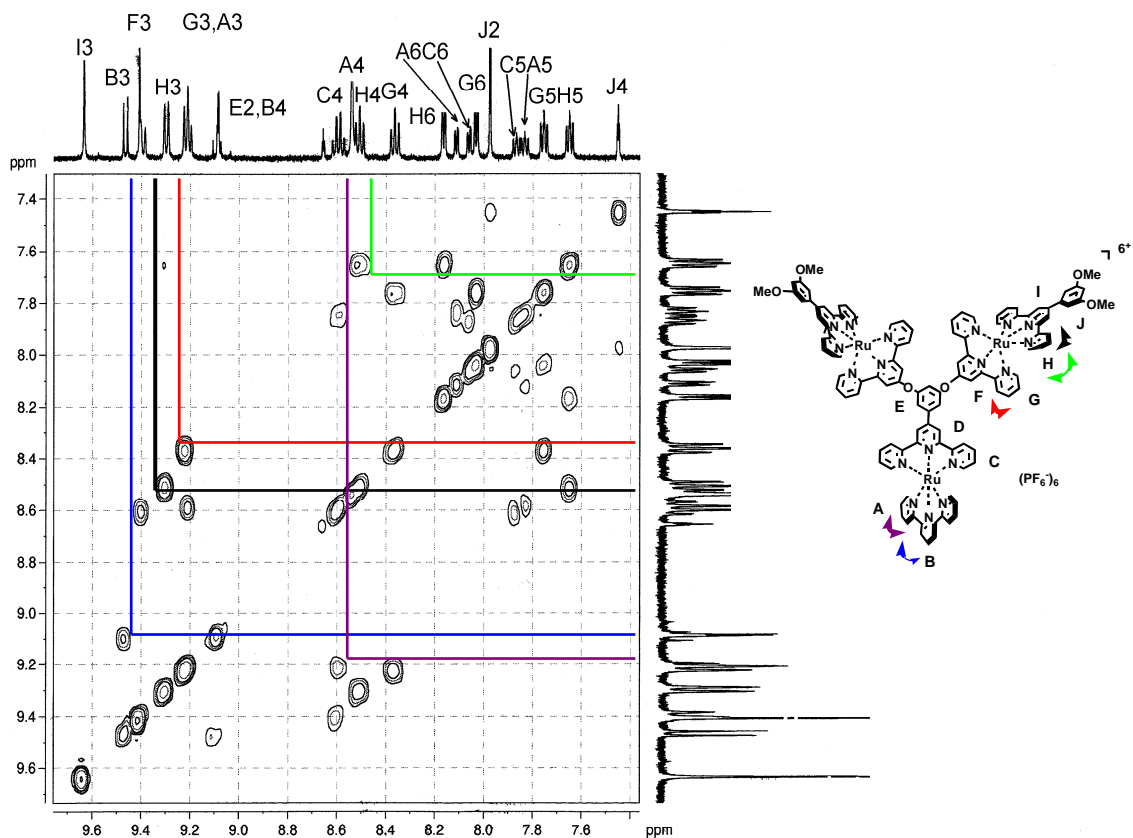


Fig III-14-COSY H-H spectrum of **45** in D₂O at 500 MHz at 298 K.

The COSY H-H spectrum showed vicinal correlations between exclusively pyridine proton, like **H₃-H₄** correlations **B₃:B₄**, **A₃:A₄**, **C₃:C₄**, **G₃:G₄**, **H₃:H₄**, the **H₄-H₅** **A₄:A₅**, **C₄:C₅**, **G₄:G₅**, **H₄:H₅**, and the **H₅-H₆** **A₅:A₆**, **C₅:C₆**, **G₅:G₆**, **H₅:H₆** confirming the proton assignment made previously. The position of the highly distant protons of the external 3,5-dimethoxyphenyl group of **45** was determined by nOe spectroscopy (Fig III-15), the spectrum showed long distance correlations between **D₃:C₃**, **E₂:D₃**, **F₃:E₄**, **I₃:H₂**, **J₂:I₃**. With the help of this spectrum, we could assigning the protons **I₃** and **F₃**.

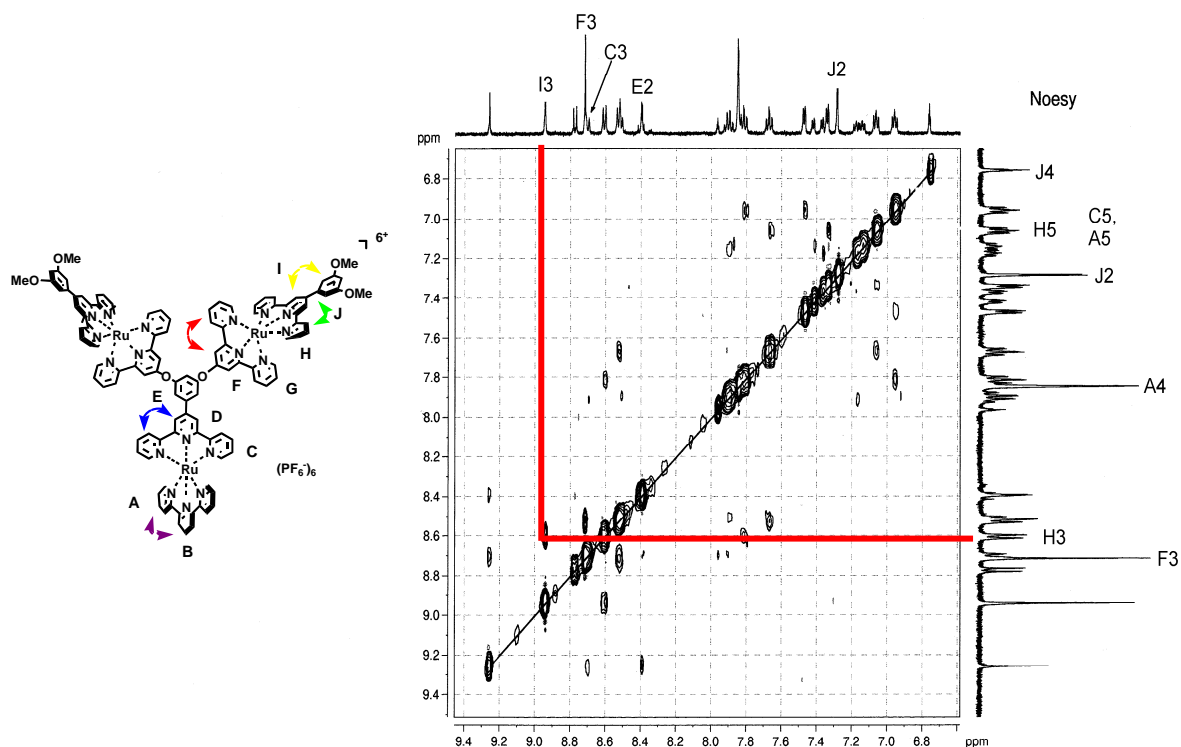


Fig III-15- nOESY spectrum of **45** in D₂O at 500 MHz at 298 K

The compound **45** was also analysed by ES mass spectroscopy, and the spectrum showed peaks corresponding to the cationic fragments of the compound **45** in the NO₃⁻ salt form; $m/z = 1163.5$ corresponding to the 2⁺ charged complex $m/z = 756.6$ correspond to the 3⁺ charged complex and at $m/z = 551.5$ the 4⁺ charged. The charged fragments are confirmed by the mass distribution of the peaks. The 2⁺ charged showed a $m/z = 0.5$ difference between peaks, 3⁺, 4⁺ charged showed respectively 0.3, 0.25 differences.

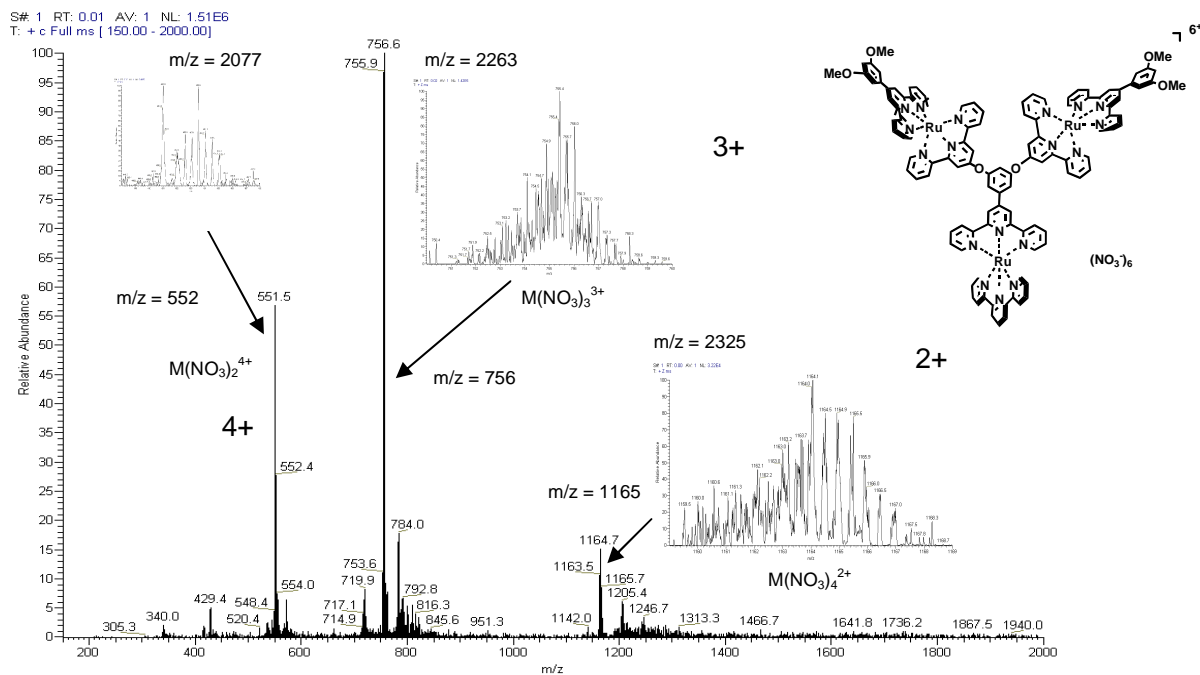


Fig III-16- ES-MS of **45**.

In order to functionalise the 3,5 positions of the compound **45**, requires prior a deprotection of the 3,5 – methoxy functional groups. The first method employed was a deprotection with a strong Lewis acid using a 1M BBr_3 in DCM cooled to $-78^\circ C$, **45** was heated at r.t. during 24 h. Water was added to the reaction mixture, and such was extracted three times with CH_2Cl_2 . The organic phases were evaporated and chromatographed through Alox column using A sol as eluant. The red fraction was isolated and analysed with

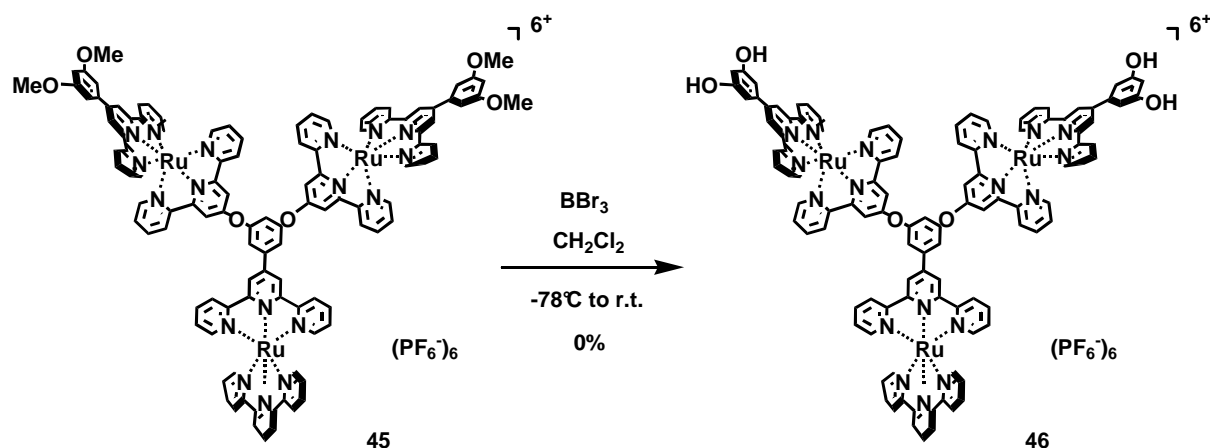


Fig III-17- Deprotection of **45**.

1H NMR and ES-MS spectroscopies which showed the only formation of Ru(II) mononuclear complexes which seems be the mononuclear fragments of **45**. The presence of brominated

mononuclear products confirms the ether cleavage, and the deprotection reaction had place essentially on such spacer.

2) Synthesis of Dendron B

Contrary to **45**, the compound dendron B has a terminal functional group in the 4 position of the core tpy. This functionality can later be useful for the coupling reaction with an other complex or metallostar unit. The synthetic way was retrosynthetically studied. The disconnection in the 3,5-dioxo position of the spacer gives the two fragments corresponding to

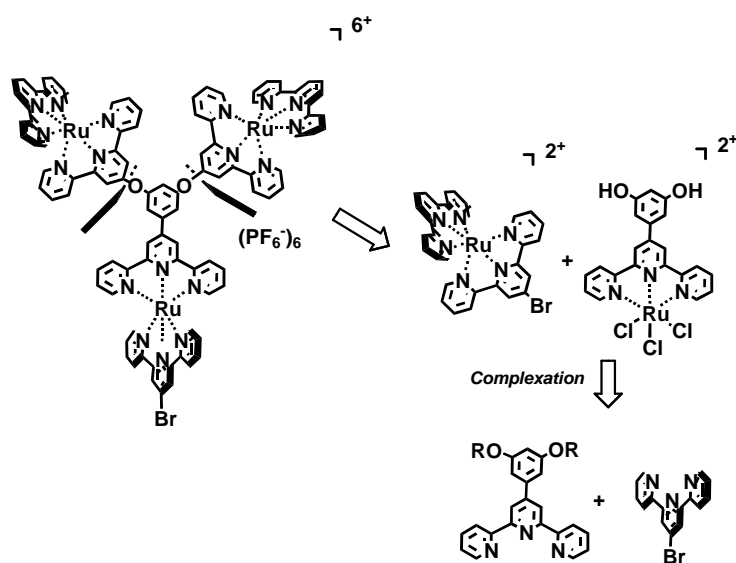


Fig III-20- Retrosynthetic analysis of Dendron B

the complex **36** and the ligand **30**. The reaction of two moles of complex **36** and ligand **30** with K_2CO_3 in excess at reflux during 12 hours led only formation of mononuclear complex **50** with 57 % yield (Fig III-20). This compound was purified through SiO_2/A_{sol} column and recrystallized in MeCN.

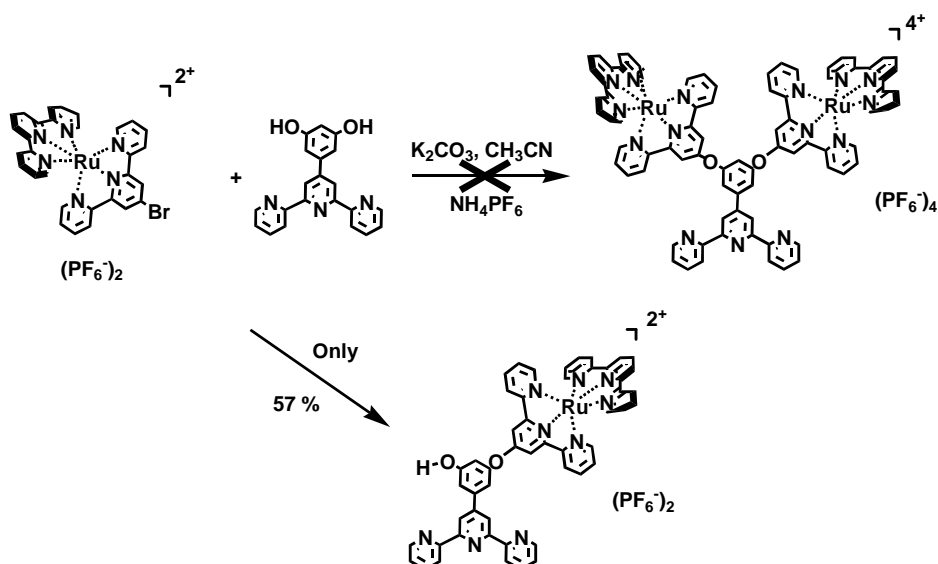


Fig III-21-Synthesis of **50**.

The compound **50** was analysed by ¹H NMR, ES-MS spectrometry.

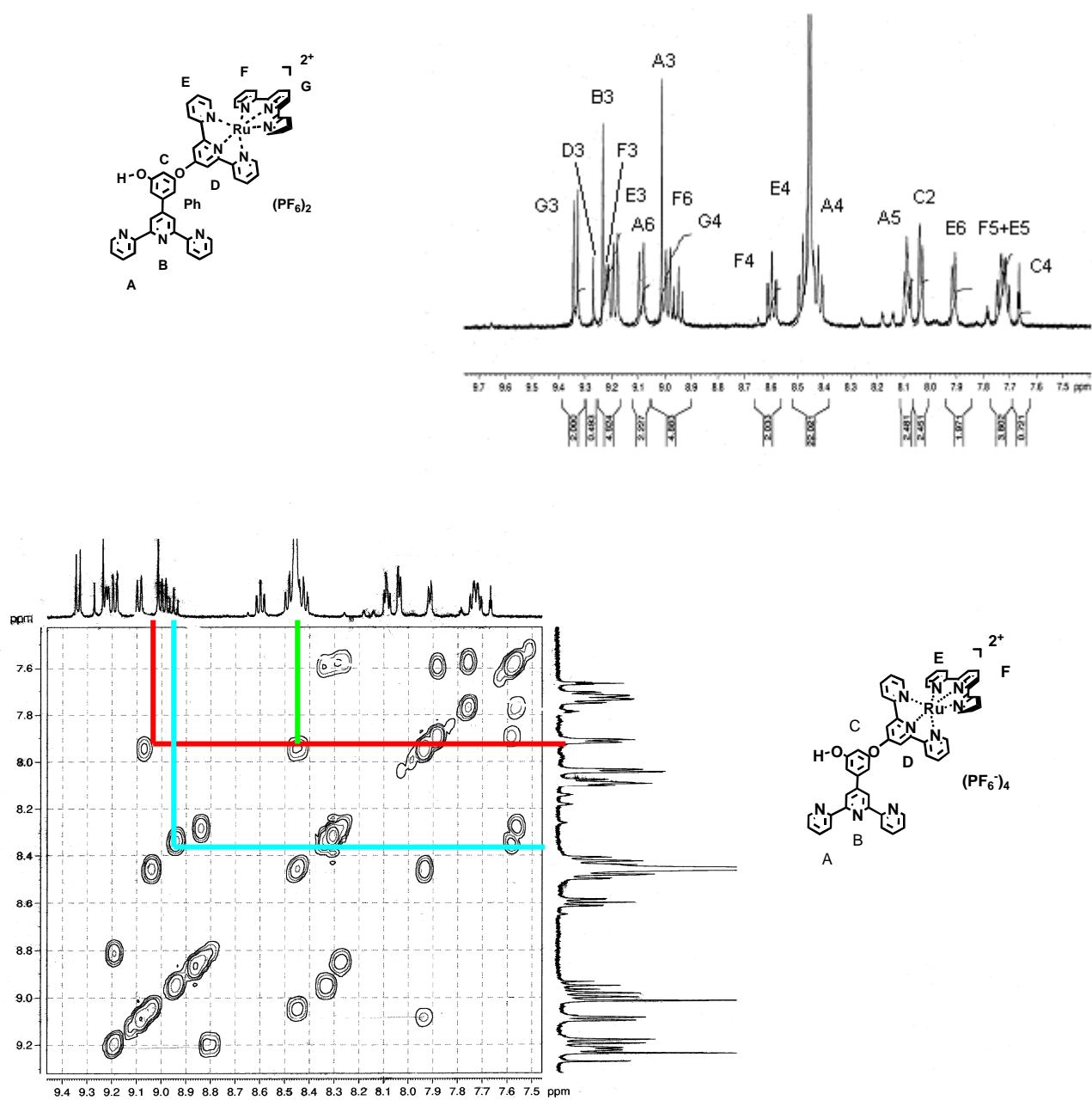
¹H NMR in CD₃CN of **50**

The ¹H NMR spectrum at 500 MHz showed peaks belonging to the pyridine protons between 7.6 and 9.4 ppm, these protons can be divided in two categories: the first belonging to the tpy protons of the Ru(II) complex, the second belonging to the free pendant ligand. This spectrum showed also protons of the phenyl spacer. The protons of the free ligand are called **A** and **B**; **C**, **D**, **E**, **F**, **G** belong to the Ru(II)-tpy protons.

δ ppm	9.35	9.27	9.25	9.23	9.19	9.09	9.02	8.99	8.95	8.60	8.52	8.43	8.09
attribution	G3	D3	B3	F3	E3	A6	A3	F6	G4	F4	E4	A4	A5
spin multiplicity	<i>d</i>	<i>s</i>	<i>s</i>	<i>d</i>	<i>d</i>	<i>d</i>	<i>s</i>	<i>d</i>	<i>t</i>	<i>t</i>	<i>t</i>	<i>t</i>	<i>t</i>
integration	2H	2H	2H	2H	2H	2H	2H	2H	2H	2H	2H	2H	2H
J (Hz)	8.2			5.95	8.1	8.0		7.9	8.3	7.75	7.8	4.4	3.6

δ ppm	8.04	7.91	7.74	7.67
attribution	C2	E6	F5+E5	C4
spin				
multiplicity	<i>d</i>	<i>d</i>	<i>m</i>	<i>t</i>
integration	2H	2H	4H	1H
J (Hz)	3.6	5.5		2.1

Fig III-22- ^1H NMR spectrum of **47** in CD_3CN at 500 MHz.



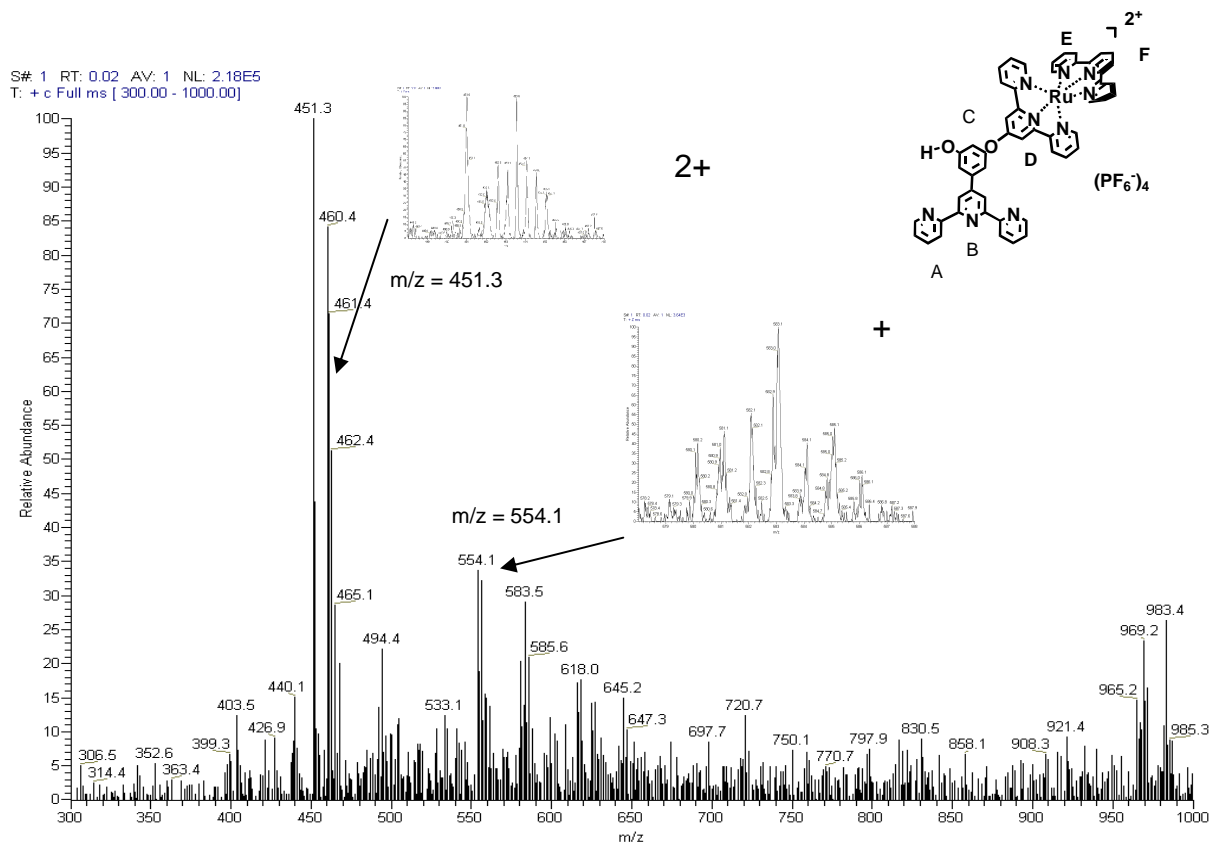


Fig III-24- ES mass spectrum of the complex **51** in NO_3^- salt form with mass distribution of the charged species.

The ES mass spectrum showed peaks assigned to charged fragments of **51**; m/z : 554.1 corresponds to the $[\text{M}^+-\text{NO}_3^-]$. The peak at m/z = 451.3 corresponds to the molecular weight distribution of the 1+ charged complex correspond to fragment $[\text{M}+2(\text{NO}_3^-)]$.

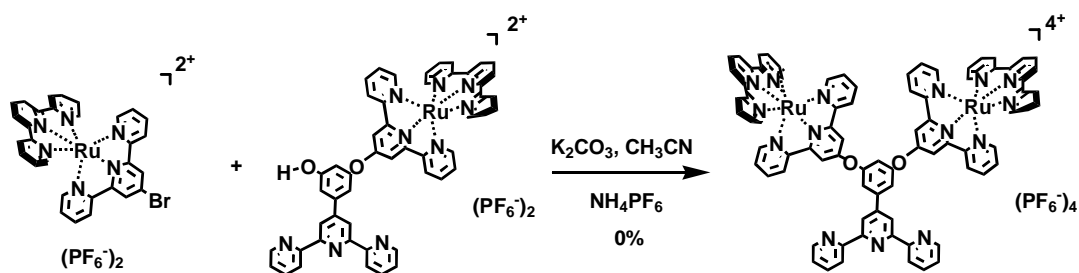


Fig III-25-Synthesis of dinuclear complex **52**.

The re-coupling via etherification in order to obtain the dinuclear species **52**, between complex **38** and complex **51** via etherification in the same coupling condition seen before (Fig III-25) has not fonctionnate and did not give the desired compound (Fig III-25).

In order to synthesize the trinuclear complex Dendron B **46**, we must change the synthetic strategy by using a way proceeding via a pentanuclear Fe(II)-tpy cored pentanuclear complex (III-26) obtain after coupling reaction of Ru(tpy)(**25**)(PF₆)₂ with the Fe(**30**)₂(PF₆)₂ complex **53**. The pentanuclear complex obtained, it can be decomplexed by oxidation to obtain the dinuclear fragment **48**, which can be easily complexed with [Ru(tpy)Cl₃].

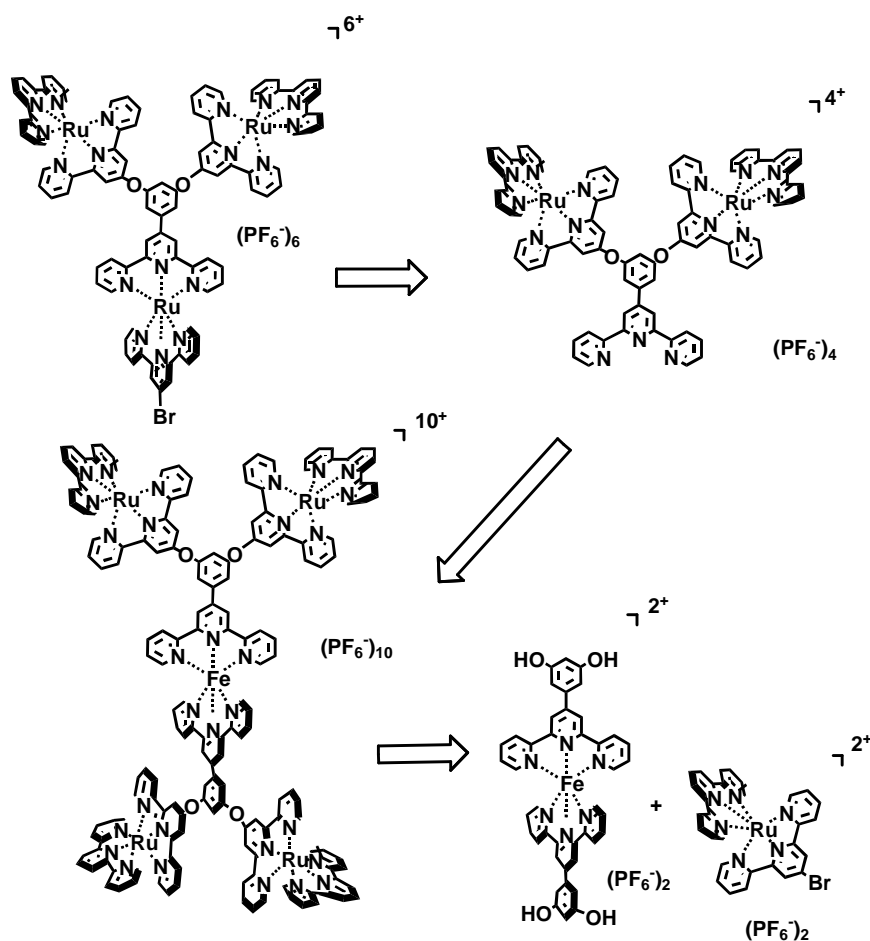


Fig III – 26 - Possible second way of Dendron B synthesis.

In order to synthesize the pentanuclear 10 + charged complex, we have to synthesize the Fe(II) complex **30**. This complex was obtained after reaction of FeCl₂·4H₂O with 2 moles of **30** (Fig III-27), to give the violet complex **53** after precipitation with NH₄PF₆ and purification over column using SiO₂/Asol. This compound was characterized by ¹H NMR spectroscopy in CD₃CN and ES-MS.

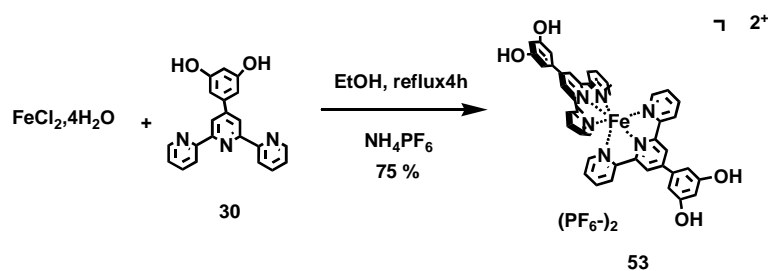


Fig III-27- Synthesis of **53**.

The second step was the coupling of the Fe(II) complex **53** with 4 equivalents of bromo complex **36** in the presence of K_2CO_3 in CH_3CN carry at reflux during 72 hours the reaction mixture was treated with NH_4PF_6 , and the resulting precipitate filtered under vacuo with

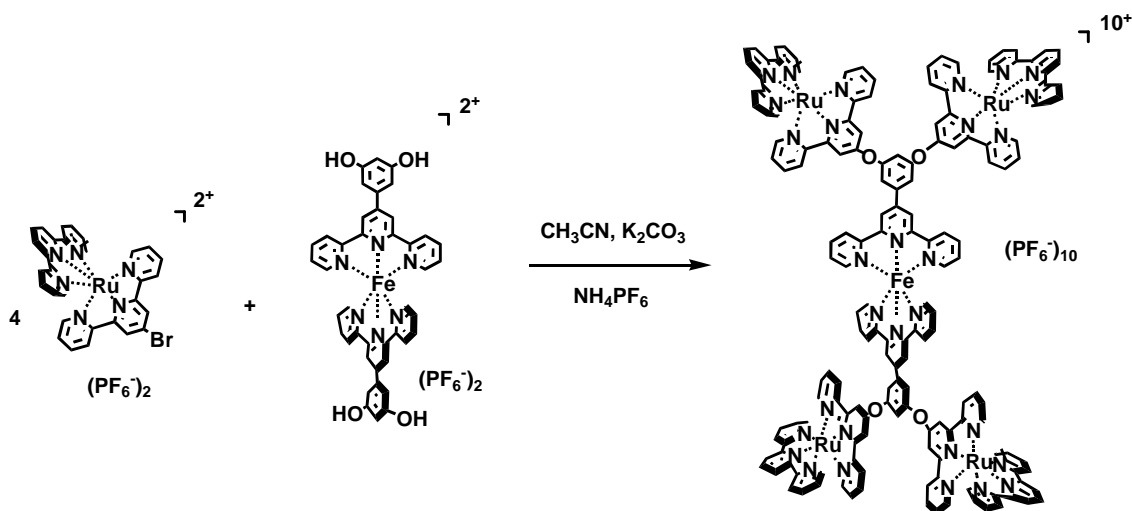


Fig III-28- Synthesis of pentauclear Fe(II)-Ru(II) complex **54**.

a fritted filter (porosity 4). The black residue was analysed by ^1H NMR and the spectrum showed the presence of starting material, especially the presence of mononuclear Fe(II) AND Ru(II) starting complexes, and products resulting of the oxidation of Fe(II) to Fe(III).

3) Synthesis of Dendron C and D.

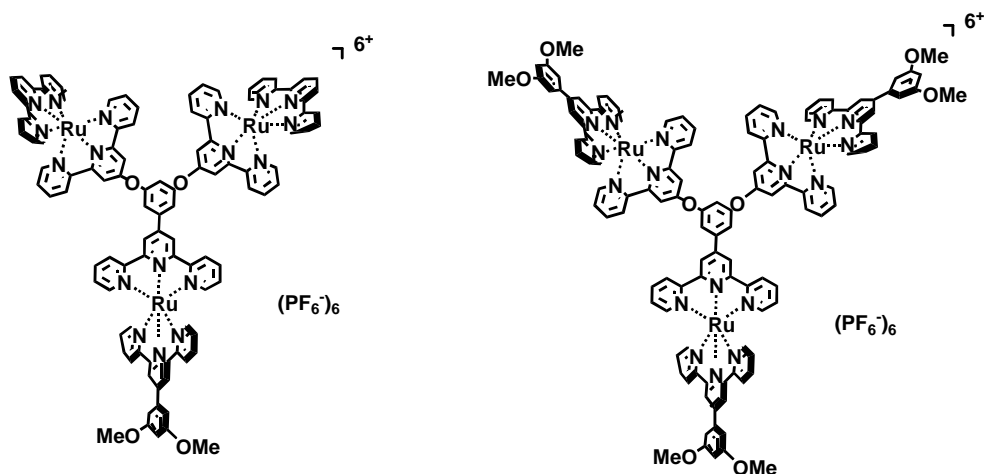


Fig III-29- Dendron C and D.

The possible synthesis of two other 3,5-methoxy substituted trinuclear Ru(II) complexes has been studied by coupling a 3,5-dimethoxy, 3,5-dihydroxy-4-phenyl substituted tpy with bromo complexes **38** and **45** via etherification. The core complex **56** was obtained after reaction of compound **55** with 1 eq of ligand **30** in EtOH during 4 hours in presence of NEM. This complex was characterised by NMR ^1H spectroscopy and ES-MS.

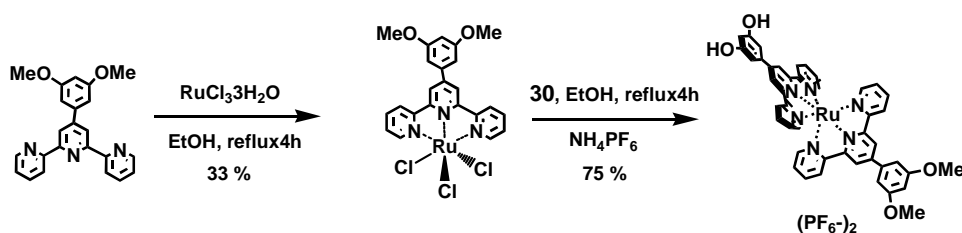


Fig III-30- Synthesis of **56**.

The spectrum showed the presence of H^3 protons signal labeled **A** and **B**; **A** and **B** correspond respectively to **30** and **29** protons. The aromatic signals of phenyl groups called here Ph and Ph' respectively corresponding to **30** and **29** are situated between 6.60 and 7.30 ppm.

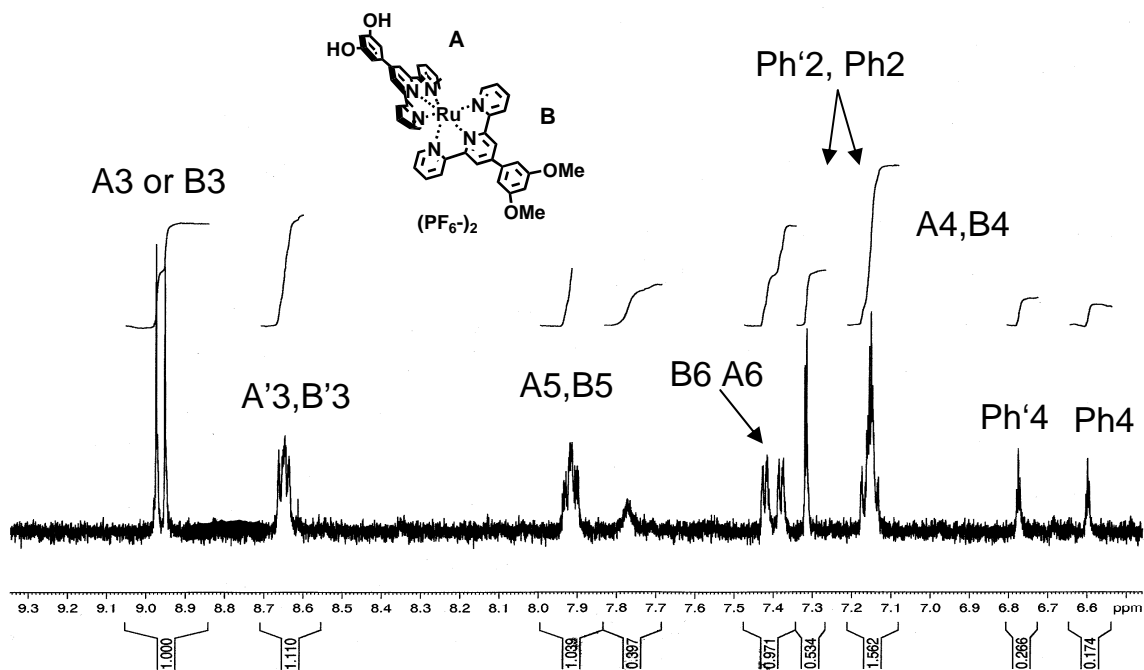


Fig III-31- ^1H NMR spectrum of **56** in CD_3CN at 500 MHz at 298 K.

	A3	B3	A'3,B'3	A5,B5	B6,A6	Ph '2	Ph2	A4,B4	Ph'4	Ph4	OMe
δ (ppm)	9.03	8.99	8.69	7.97	7.45	7.3 7	7.36	7.21	6.83	6.73	4.03
spin	<i>s</i>	<i>s</i>	<i>m</i>	<i>m</i>	<i>dd</i>	<i>s</i>	<i>s</i>	<i>m</i>	<i>s</i>	<i>s</i>	<i>s</i>
I	2H	2H	4H	4H	4H	2H	2H	4H	2H	2H	6H
J (Hz)					7.5 2						

Table III-3- Chemical shifts of ^1H NMR of compound **56** in CD_3CN .

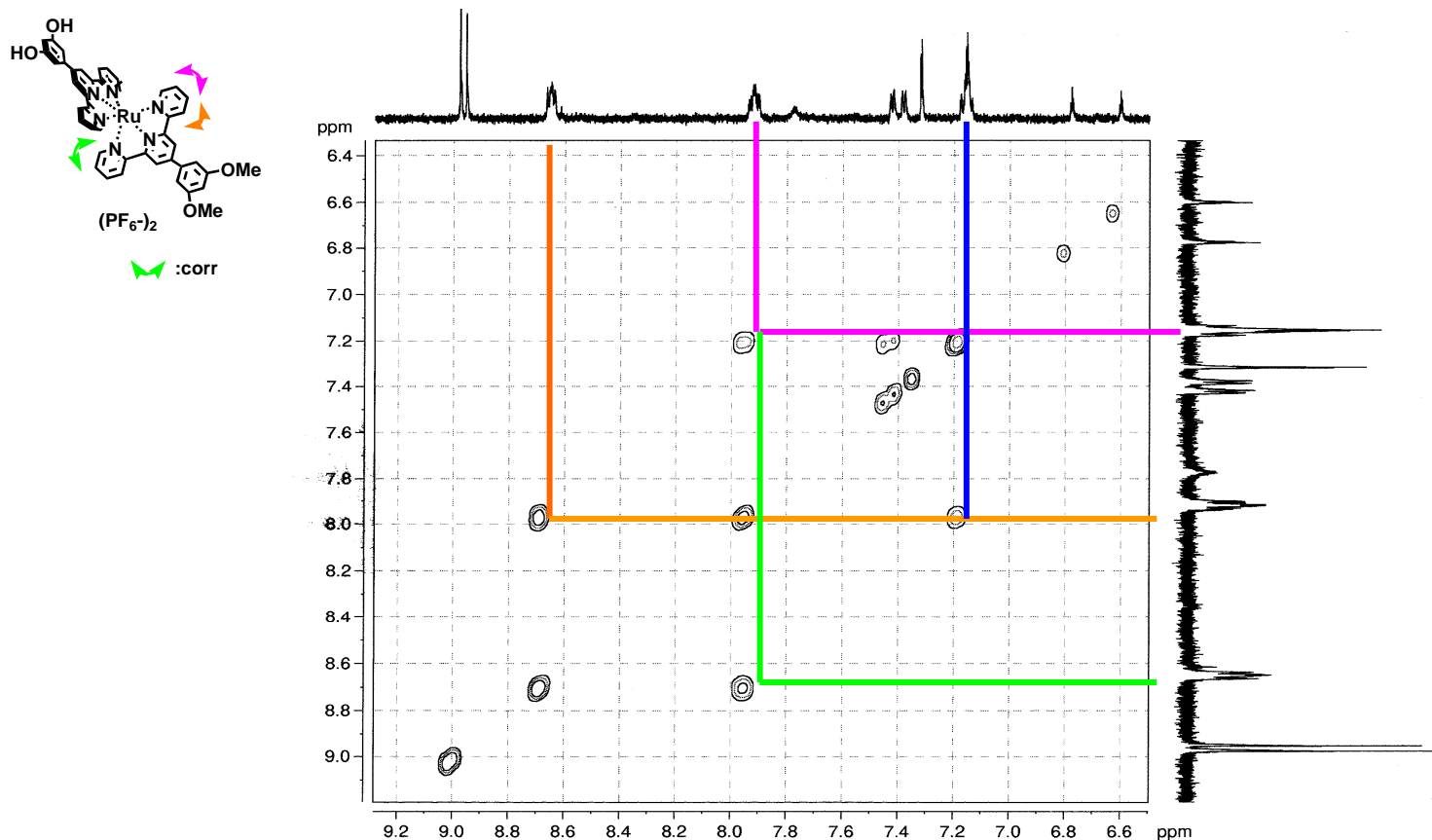


Fig III-32- COSY H-H spectrum of compound **56** in CD₃CN at 500 MHz.

In order to assign protons of the terpyridine ligands **29** and **30** of **56** the 2D COSY spectrum has been measured. Correlation of protons showed signals at 8.69, 7.97, 7.45, 7.21 ppm corresponding respectively to terpyridine A'3B' 3:A4,B4, A6B6:A5B5, A4B4:A5B5, protons correlation. We can affirm that the protons which are able to correlate are only in such case the terpyridine protons because the protons of the phenyl functional groups are isolated and showed no signal in the spectrum, only the long distance correlation detected by NOE spectroscopy can detect such couplings.

The NOE spectrum was measured at 500 MHz, this spectrum showed long distance correlations between **B3** and **Ph'2**, **A3** and **Ph2**, **A3** and **A'3**, **B3** and **B'3**, such measurements confirm very the assignment of the **B3** signal at 9.03 ppm and the **A3** signal at 8.99 ppm.

nOe spectrum of **56** in CD₃CN.

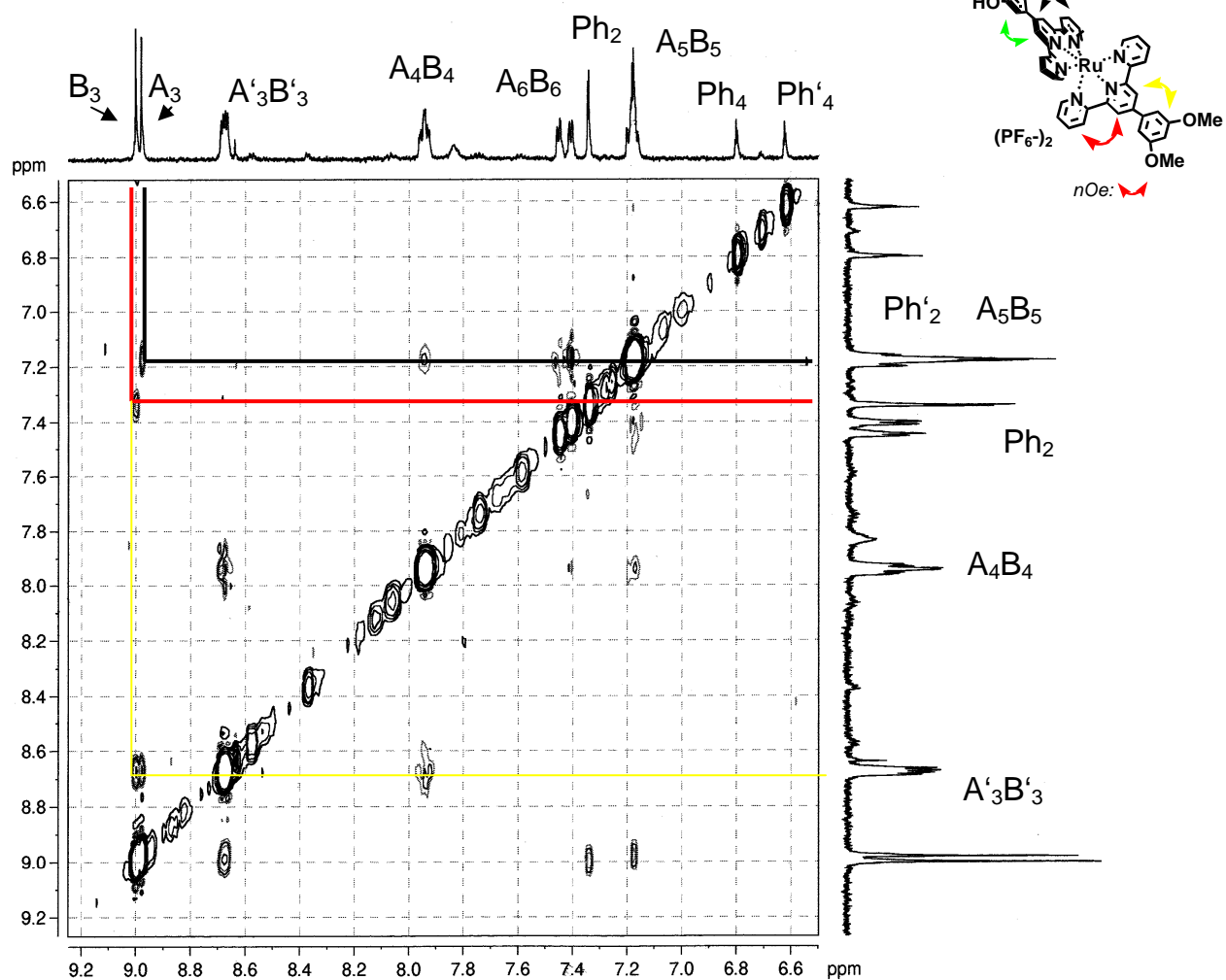


Fig III-33- nOesy spectrum of compound **56** in CD₃CN at 500 MHz.

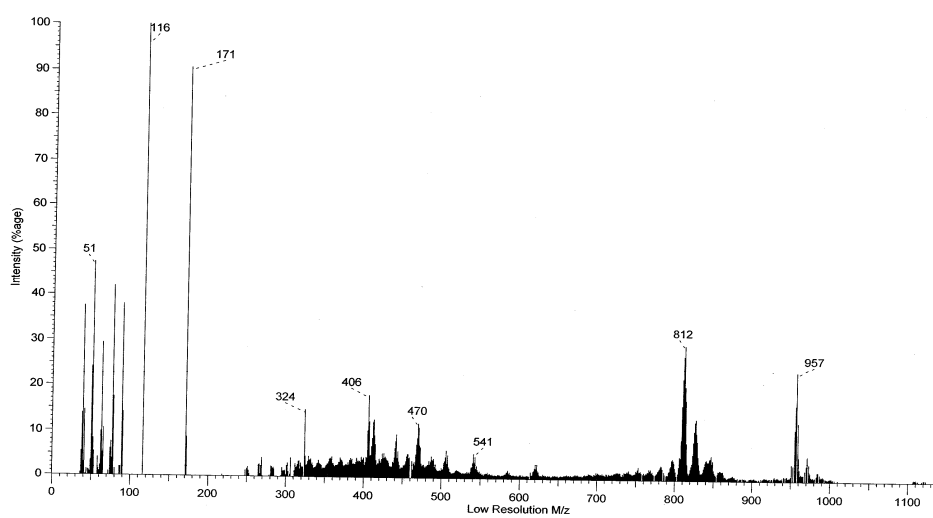


Fig III-34- ES-MS of complex **56**.

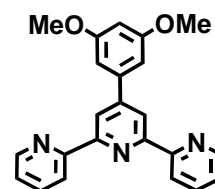
Conclusion.

In this section we have synthesized several Ru(II) heteroleptic tpy complexes which have different functional groups. We have also synthesized a trinuclear metallostar species which is interesting for photochemical and electrochemical studies. Such complexes are particularly interesting because they can be further functionalised.

Experimental procedures

Synthesis of 29.

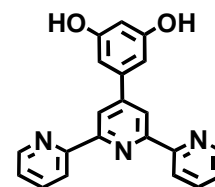
2-acetylpyridine (690 μ l, 5.8 mmol) were added dropwise a solution of t-BuOK (1.04 g, 9.3 mmol) in 50 ml of THF, the reactional mixture is stirring at room temperature during 30 min. The mixture got a yellow creamy colour. Then 3,5-dimethoxybenzaldehyde (508 mg, 3.0 mmol) in solution in THF was added and the mixture is stirring at room temperature overnight. A suspension of NH_4OAc (10 g) in EtOH/ CH_3COOH (2:1) (100 ml) is prepared and added to the mixture. The solution got a orange and turn to red color after the reactional mixture is heated to reflux during 5 hours. The mixture is cooled in a ice bath during 2 hours. Fresh distilled is added and a white light precipitate appears. The solid is filtered on Büchner and the free ligand is recrystallised in ethanol, dried in a desiccator on P_2O_5 . We obtained 2,7 g of white off solid (Yield = 70 %).



Experimental datas : $^1\text{H NMR}$ at 250 MHz in CDCl_3 : 8.77 (d, 2H, $J = 4.75$ Hz) H^6 , 8.72 (s, 2H) H^3 , 8.70 (d, 2H, $J = 8.1$ Hz) H^3 , 7.91 (dt, 2H, $J_1 = 1.9$ Hz, $J_2 = 7.7$ Hz) H^4 , 7.40 (m, 2H) H^6 , 7.09 (d, 2H, $J = 2.2$ Hz) Ph^2 , 6.59 (t, 1H, $J = 2.2$ Hz) Ph^4 , 3.94 (s, 6H) **-OMe** $^{13}\text{C NMR}$: **FAB-MS**: 369.2, 339.2, 324.1, 295.1, 184.6, 148.1, 78, 44. **IR** (v cm^{-1}): 2949 (w), 2365 (w), 1587.5 (s), 1476 (s), 1207 (s), 1153 (s), 799 (s). **M.P** ($^\circ\text{C}$): 215 $^\circ\text{C}$.

Synthesis of 30.

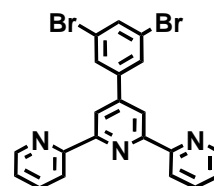
Concentrated HCl (17.6 ml) and pyridine (16 ml) are dissolved in a flask, with a distillation system for removing water, were heated at 210 $^\circ\text{C}$. After stabilisation of the temperature during 2 hours. The mixture was cooled at 150 $^\circ\text{C}$ and **29** (1.0 g, 2.7 mmol) was added to the reaction. The reactional mixture was heated during 3 hours. Before addition of warm water, the mixture is cooled at 150 $^\circ\text{C}$. After addition of water, a white light precipitate appears, after cooling at room temperature the solid is filtered on fritted filter (porosity 3) and washed with distilled water. The ligand **30** was purified by recrystallisation in DMF and we obtained a white solid (m = 93 mg, Yield = 100 %)



Experimental datas : $^1\text{H NMR}$ at 250 MHz in CDCl_3 : 8.94 (d, 2H, $J = 8$ Hz) **H3**, 8.89 (d, 2H, $J = 4.75$ Hz) **H6**, 8.76 (d, 2H, $J = 5$ Hz) **H3'**, 8.33 (t, 2H, $J = 8$ Hz) **H4'**, 7.79 (t, 2H, 6.5 Hz) **H5**, 6.87 (d, 1H, $J = 2.2$ Hz) Ph2, 6.41 (t, 1H, $J = 1.75$ Hz) **Ph4**. **FAB-MS**: 341 (M^+) **IR** (v cm^{-1}): 3050 (w $\text{v}_{\text{O-H}}$), 2850, 1594, 1232, 1155, 1006, 847, 784. **M.P** ($^\circ\text{C}$): 362 $^\circ\text{C}$.

Synthesis of **32**.

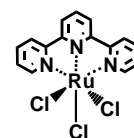
2-acetylpyridine (690 μl , 5.8 mmol) were added dropwise a solution of t-BuOK (1.04 g, 9.3 mmol) in 50 ml of THF, the reactionnal mixture is stirring at room temperature during 30 min The mixture got a yellow creamy colour. Then 3,5-dibromobenzaldehyde (790 mg, 3.0 mmol) in solution in THF was added and the mixture is stirring at room temperature overnight. A suspension of NH_4OAc (20 g mmol) in EtOH/ CH_3COOH (2:1) (100 ml) is prepared and added to the mixture. The solution got a orange and turn to red color after the reactionnal mixture is heated to reflux during 5 hours. The mixture is cooled in a ice bath during 2 hours. Fresh distilled is added and a white light precipitate appears. The solid is filtered on Büchner and the free ligand is recritallised in ethanol (10 ml) , dried in a dessicator on P_2O_5 . We obtained 981 mg of white off solid (Yield = 70 %).



Experimental datas : $^1\text{H NMR}$ at 250 MHz in CDCl_3 : 8.73 (d, 4H, $J = 3.8$ Hz) **H⁶**, 8.63 (s, 2H) **H^{3'}**, 7.95 (d, 2H, $J = 1.5$ Hz) **H⁶**, 7.89 (dt, 2H, $J_1 = 8.75$ Hz $J_2 = 1.5$ Hz) **H⁴**, 7.59 (s, 2H) **H⁵**, 375 (ddd, 2H, $J_1 = 5.25$ Hz $J_2 = 1.25$ Hz) **PhH²** , 7.29 (s, 1H) **PhH⁴**, **FAB-MS**: 467 [M^+], 388.1, 306.1, 229.1, 153.6, 78. **IR** (v cm^{-1}): 2885 (w), 2363 (w), 1476 (s), 1215 (s), 1153 (s), 818 (s).

Synthesis of $[\text{Ru}(\text{tpy})\text{Cl}_3]$.

Ruthenium(III) chloride trihydrate $\text{RuCl}_3 \cdot 3\text{H}_2\text{O}$ (500 mg, 3.82 mmol) and tpy (445 mg, 3.82 mmol) are added in EtOH (10 ml) and the mixture was heated at reflux during 3 hours. The solution got a brown dark coloration. After 3 h at heated at reflux, the reaction mixture is cooled at room temperature and the solidis filtered over fritted filter (porosity 3) and washed with few amount

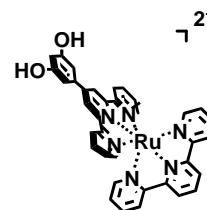


of ethanol. After drying we obtain the Ru(tpy)Cl₃ complex without chemical characterisation. (694 mg, Yield = 42 %).

Experimental datas: IR (ν cm⁻¹): 1600(w), 1451(w), 774(s).

Synthesis of **36**.

Ru(tpy)Cl₃ (45,3 mg 0,103 mmol) and **30** (35,3 mg 0,103 mmol) are dissolved in of EtOH (10 ml), then 4 droplets of NEM were added to the mixture. This was heated to reflux for 3 hours and followed by TLC (SiO₂). The product was precipitated by addition of aqueous NH₄PF₆.

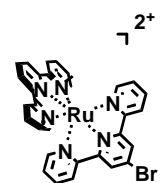


After purification with chromatography on column using SiO₂/Asol the product isolated is dissolved in methanol, filtered and reprecipitated with NH₄PF₆ to give a red complex. (m = 77 mg, Yield = 82 %)

Experimental datas : ¹H NMR at 250 MHz in CD₃CN: 8.97 (s, 2H) **B'3**, 8,78 (d, 2H) **A'3**, 8,66 (d, 2H, *J* = 8 Hz) **A3**, 8,52 (d, 2H, *J* = 7.75 Hz) **A3**, 8,44 (m, 1H) **A'4**, 7,95 (m, 4H) **A4+B4**, 7,44 (d, 2H, *J* = 5.75 Hz) **B6**, 7,36 (d, 2H, *J* = 4.75 Hz) **A6**, 7,14 (m, 6H) **A5+B5**, 6,64 (s, 2H) **Ph-H₂**, (s, 2H) **-OH**. IR (ν cm⁻¹): 3325 (w), 1600 (s), 1535 (w), 1415 (w), 1245 (w), 1161 (w), 817 (s), **FAB-MS:** 831 (M⁺-PF₆⁻), 676 (M⁺-2PF₆⁻).

Synthesis of **38**.

A mixture containing [Ru(tpy)Cl₃] (50 mg, 0.113 mmol) with **25** (34.2 mg , 0.110 mmol) was suspended in EtOH (10 ml). After the addition of 4 droplets of NEM the reaction mixture was heated at reflux for 3 hours and the reaction monitored by TLC. The product was precipitated by addition of aqueous NH₄PF₆. The product was isolated by column chromatography using SiO₂ A_{sol} and recrystallised in MeOH. (m = 54 mg, Yield = 52.3 %).

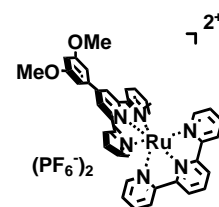


Experimental datas : ¹H NMR at 250 MHz in CD₃CN: 9.01 (s, 4H) **B'3**, 8.77 (d, *J* = 8.5 Hz 4H) **A'3**, 8.51 (d, 2H, *J* = 7.5 Hz) **A3+B4**, 8,44 (m, 4H) **A4+B4**, 7.95 (d, 2H, *J* = 4.5 Hz)

A6+B6, 7,19 (m, 4H) **A5+B5**. **FAB-MS**: 791 [M+-PF₆⁻], 646[M+-2PF₆⁻] **IR** (v cm⁻¹): 1749, 1558, 1439, 823.

Synthesis of **40**.

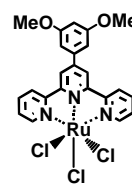
[Ru(tpy)Cl₃] (50 mg, 0.13 mmol) and **29** (47 mg, 0.13 mmol) are dissolved in EtOH (10 ml), then 4 droplets of NEM were added to the mixture. This was heated to reflux for 3 hours and followed by TLC (SiO₂). The product was precipitated by addition of aqueous NH₄PF₆. After purification with chromatography on column using SiO₂/Asol the product isolated is dissolved in methanol, filtered and reprecipitated with NH₄PF₆ to give a red complex. (m = 81 mg, Yield = 66 %)



Experimental datas : ¹H NMR at 250 MHz in CD₃CN: 9.02 (s, 2H) **H**^{3B}, 8.81 (d, 2H, J = 8 Hz) **H**^{3A}, 8.70 (d, 2H, J = 8 Hz) **H**^{3'B}, 8.54 (d, 2H, J = 8.5 Hz) **H**^{3'A}, 8.48 (t, 1H, J = 8.5 Hz) **H**^{4B}, 7.97 (m, 4H) **H**^{5A}+**H**^{5B}, 7.39 (dd, 2H, J₁ = 7.75 Hz, J₂ = 5.75 Hz) **H**^{6A}+**H**^{6B}, 7.36 (s, 2H) **Ph**², 7.20 (t, 4H, J = 6.25 Hz) **H**^{4'A}+**H**^{4'B}, 6.82 (s, 2H) **Ph**⁴, 4.03 (s, 6H) -OMe. ¹³C NMR: **FAB-MS**: (M+-PF₆⁻) 800, (M+-2PF₆⁻) 655, **IR** (v cm⁻¹): 3074 (w), 1595 (s), 1411 (w), 1150 (w), 781 (s).

Synthesis of Ru(**29**)Cl₃.

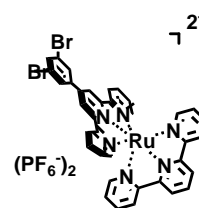
Ruthenium(III) chloride trihydrate RuCl₃·3H₂O (500 mg, 3.82 mmol) and tpy (445 mg, 3.82 mmol) was added in EtOH (10 ml) and the mixture was heated at reflux during 3 hours. The solution got a brown dark coloration. After reaction, the reaction mixture is cooled at room temperature and the dark brown solid filtered over fritted filter (porosity 3) and washed with few amount of ethanol. After drying we obtain the Ru(**29**)Cl₃ complex without chemical characterisation. (694 mg, Yield = 42 %).



Experimental datas: **IR** (v cm⁻¹): 1596(m), 1411 (w), 1150 (w), 1015 (w), 857 (w), 781 (w).

Synthesis of **41**.

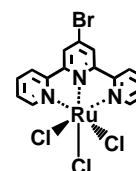
[Ru(tpy)Cl₃] (50 mg, 0.113 mmol) and **32** (56.1 mg, 0.113 mmol) are dissolved in 10 ml of EtOH, then 4 droplets of NEM were added to the mixture. This was heated to reflux for 3 hours and followed by TLC (SiO₂). The product was precipitated by addition of aqueous NH₄PF₆. After purification with chromatography on column using SiO₂/Asol the product isolated is dissolved in methanol, filtered and reprecipitated with NH₄PF₆ to give a red complex. (m = 95 mg, Yield = 75%).



Experimental datas : ¹H NMR at 250 MHz in CD₃CN: 9,04 (s, 2H) **B'3**, 8,82 (d, 2H) **H6**, 8,69 (d, 2H, J = 8.25 Hz) **A'3**, 8,56 (d, 2H, J = 7,8 Hz) **A3**, 8,45 (d, 2H) **A'4**, 7,97 (dd, 4H) **A4+B4**, 7,41 (t, 4H) **A5+B5**, 7,20 (dd, 4H). **FAB-MS**: (M+PF₆⁻) 946, (M+2PF₆⁻) 801, 510, 370, 201, 91, 41. **IR** (ν cm⁻¹): 2985 (w), 2370 (w), 1489 (s), 1237 (s), 1100 (s), 830 (s).

Synthesis of **43**.

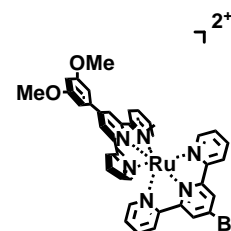
Ruthenium(III) chloride trihydrate RuCl₃·3H₂O (76 mg, 0.288 mmol) and tpy-Br (88.8 mg, 0.288 mmol) is added and the mixture is heated at reflux during 3 hours. The solution got a brown dark coloration. After 3 h at heated at reflux, the reaction mixture is cooled at room temperature and the solid is filtered over fritted filter (porosity 3) and washed with few amount of ethanol. After drying we obtain the complex **43** without chemical characterisation. (140 mg, Yield =94 %).



Experimental datas: IR (ν cm⁻¹): 1594(w), 1218(w), 872(w), 795(m).

Synthesis of **44**.

Ru(**25**)Cl₃ (48,5 mg, 0.0932 mmol) and **29** (34,5 mg 0.0932 mmol) were suspended in EtOH (15 ml). After addition of 4 droplets of N-ethylmorpholine (NEM) the reaction mixture was heated to reflux for 4 hours. The reaction mixture is followed during reaction by TLC SiO₂, after reaction the solution is cooled at room temperature, the

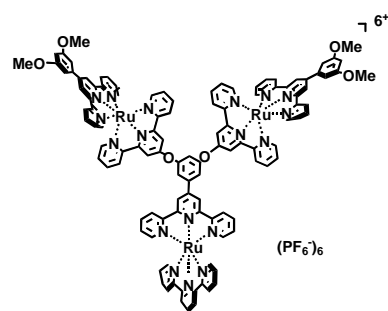


solvent removed and the residue is chromatographed on SiO₂ column using A sol as eluant. After recrystallisation in MeOH, and precipitation with NH₄PF₆ the brown complex **45** was obtained. (m = 100 mg, Yield = 72 %).

Experimental datas : ¹H NMR at 250 MHz in CD₃CN: 8.99 (d, 4H, *J* = 4.8 Hz) **A'3+B'3**, 8.67 (d, 2H, *J* = 7.5 Hz) **A3**, 8.48 (d, 2H, *J* = 7.8 Hz) **B3**, 7.94 (t, 4H, *J* = 8.75 Hz), 7.46 (d, 6H, *J* = 4,5 Hz) **A6**, 7.41 (d, 2H, *J* = 4.4 Hz) **B6**, 7.36 (s, 2H) **Ph-2**, 7.22 (m, 4H) **A5+B5**, 6.84 (m, 1H) **Ph-4**, 4.03 (s, 6H) **-OMe**. **FAB-MS**: (M⁺-PF₆⁻) 929, (M⁺-2PF₆⁻) 782 , 469, 412, 307, 171, 154, 77 , **IR** (ν cm⁻¹): 2888(w), 1600(w), 1419(w), 1120(w), 827(w).

Synthesis of **45**.

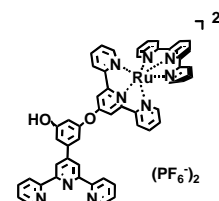
Ru(**25**)(**29**)](PF₆)₂ (182 mg, 0.17 mmol) and [Ru(tpy)(**30**)](PF₆)₂ (89 mg 0,085 mmol) and dried K₂CO₃ are dissolved in of CH₃CN (15 ml) and of DMF (3 ml). The reaction mixture is carry at reflux during 12 h and monitoring with TLC SiO₂/Asol. After refluxing the mixture is quenched with NH₄PF₆. Then the mixture is removed of its solvent, and separated with chromatography on column using SiO₂ (230-400 Mesh) and A sol as eluant. A intense orange product with R_f = 0,55 is isolated, dissolved in MeOH, filtrated and precipitated with NH₄PF₆. The orange complex is obtained after filtration on fritted.(m = 61,2 mg, Yield = 35%).



Experimental datas : ¹H NMR at 500 MHz in D₂O: 10.15 (s, 2H) **D3**, 9.84 (s, 2H) **I3**, 9.68 (d, 1H, *J* = 6.6 Hz) **B3**, 9.61 (d, 2H, *J* = 9.1 Hz) **F3**, 9.52 (d, 2H, *J* = 8 Hz) **H3**, 9.43 (t, 3H, *J* = 8.5 Hz) **G3+A3**, 9.30 (d, 2H, *J* = 2.1 Hz) **E2+B4**, 8.86 (*dd*, 2H, *J*₁ = 7.5 Hz, *J*₂ = 9.9 Hz) **C4**, 8.79 (s, 2H) **A4**, 8.74 (t, 2H, *J* = 8.75 Hz) **H4**, 8.62 (t, 2H, *J* = 8Hz) **G4**, 8.39 (d, 2H, *J* = 8Hz) **H6**, 8.32 (d, 2H, *J* = 8Hz) **A6**, 8.27 (d, 1H, *J* = 6.5 Hz) **C6**, 8.26 (d, 2H, *J* = 6.5 Hz) **G6**, 8.20 (d, 2H, *J* = 2.5 Hz) **J2**, 8.09 (d, 1H, *J* = 6.5 Hz) **C5**, 8.07 (t, 1H, *J* = 6.6 Hz) **A5**, 7.98 (t, 2H, *J* = 7.4 Hz) **G5**, 7.88 (t, 2H, *J* = 7.1 Hz) **H5**, 7.68 (t, 1H, *J* = 2.2 Hz) **J4**, **3.90** (s,12H) **-OMe**. **EI-MS** in MeCN: 1164.7(M²⁺, -2NO₃⁻), 756.6 (M³⁺, -3NO₃⁻), 551.5. **IR** (ν cm⁻¹): 3130 (w), 2835 (w), 1595 (w), 1418.6 (s), 1232 (w), 1066 (w), 954 (s), 886 (w), 697 (s). **UV** in CH₃CN: Absorption λ_{max} = 489 nm.

Synthesis of **47**.

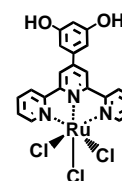
38 (24 mg, 0.026 mmol), **30** (4.4 mg, 0.013 mmol) and dried K_2CO_3 are dissolved in CH_3CN (10 ml) then 4 droplets of DMF and are added to the mixture. This one is carry at reflux during 12 hours and monitoring with TLC using $SiO_2/Asol$. After cooling at room temperature, NH_4PF_6 is added and the precipitated complex was filtered. **47** was obtained as major product after purification with chromatography on column using SiO_2 (230-400 Mesh) and $Asol$ as eluant. The complex **47** with a $R_f = 0.75$ is obtained after recrystallisation in MeOH. (m = 23.4 mg, Yield = 57 %).



Experimental datas : 1H NMR at 500 MHz in CD_3CN : 9.35 (d, 2H, $J = 8.2$ Hz) **G3**, 9.27 (s, 2H) **D3**, 9.25 (s, 2H) **B3**, 9.23 (d, 2H, $J = 5.95$ Hz) **A6**, 9.19 (d, 2H, $J = 8.1$ Hz) **F3**, 9.09 (d, 2H, $J = 8.0$ Hz) **E3**, 9.02 (s, 2H) **B3**, 8.99 (d, 2H, $J = 7.9$ Hz) **A3**, 8.95 (t, 2H, $J = 8.3$ Hz) **G4**, 8.60 (t, 2H, $J = 7.8$ Hz) **A4**, 8.48 (t, 2H, $J = 7.75$ Hz) **E4**, 8.43 (t, 2H, $J = 7.8$ Hz) **F4**, 8.09 (t, 2H, $J = 4.4$ Hz) **A5**, 8.04 (d, 2H, $J = 3.6$ Hz) **C2**, 7.91 (d, 2H, $J = 3.6$ Hz) **E6**, 7.74 (m, 2H) **E5+E5**, 7.67 (t, 4H, $J = 2.1$ Hz) **C4**. **EI-MS** in MeCN : 983.4, 554.1 ($M^+-PF_6^-$), 460.4 ($M^+-2PF_6^-$). **IR** (ν cm^{-1}): 3065 (w), 1617 (w), 1583 (w), 1429 (w), 1343 (s), 1216 (m), 823 (s).

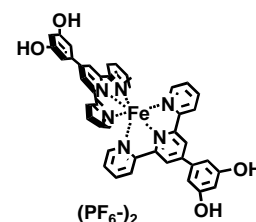
Synthesis of $Ru(\mathbf{30})Cl_3$ **49**.

Ruthenium(III) chloride trihydrate $RuCl_3 \cdot 3H_2O$ (500 mg, 3.82 mmol) and tpy (445 mg, 3.82 mmol) is added and the mixture was heated at reflux during 3 hours. The solution got a brown dark coloration. After 3 h at heated at reflux, the reaction mixture is cooled at room temperature and the solid was filtered over fritted filter (porosity 3) and washed with few amount of ethanol. After drying we obtain the $Ru(\mathbf{30})Cl_3$ complex without chemical characterisation. (694 mg, Yield = 42 %).



Synthesis of **53**.

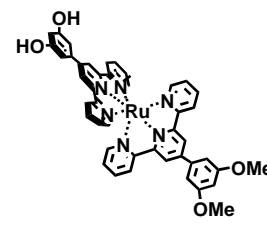
FeCl₂·4H₂O (45.3 mg, 0.103 mmol) and **30** (70.6 mg, 0.206 mmol) were dissolved in EtOH (10 ml), then 4 droplets of NEM were added to the mixture. This was heated to reflux for 3 hours and followed by TLC (SiO₂). The product was precipitated by addition of aqueous NH₄PF₆. After purification with chromatography on column using SiO₂/Asol the product **53** was isolated and dissolved in methanol, filtered and reprecipitated with NH₄PF₆ to give a violet complex. (m = 93 mg, Yield = 75 %).



Experimental datas : ¹H NMR at 250 MHz in CD₃CN: 9.13 (s, 4H) **H'3**, 8.63 (d, 4H, *J* = 8 Hz) **H3**, 7.92 (t, 4H, *J*₁ = 7.5 Hz) **H⁴**, 7.28 (s, 4H) **H⁶**, 7.22 (d, 4H *J* = 6.25 Hz) **Ph²**, 7.11 (t, 4H, *J*₁ = 6.5 Hz) **H⁵**, 6.78 (t, 2H, *J* = 2 Hz) **Ph⁴**. **FAB-MS**: (M⁺-PF₆⁻) 1050.9, [M²⁺-2(PF₆⁻)], 369.6 **IR** (ν cm⁻¹): 3201 (w), 2821 (w), 1605 (m), 1418 (m), 968 (s), 829 (s).

Synthesis of **56**.

[Ru(tpy)Cl₃] (45.3 mg, 0.103 mmol) and **30** (35.3 mg, 0.103 mmol) are dissolved in (10 ml) of EtOH, then 4 droplets of NEM were added to the mixture. This was heated to reflux for 3 hours and followed by TLC (SiO₂). The product was precipitated by addition of aqueous NH₄PF₆. After purification with chromatography on column using SiO₂/Asol the product isolated is dissolved in methanol, filtered and reprecipitated with NH₄PF₆ to give a red complex. (m = 84 mg, Yield = 74 %)



Experimental datas : ¹H NMR at 250 MHz in CD₃CN: 9.03 (s, 2H) **A3**, 8.99 (s, 2H) **B3**, 8.69 (t, 4H, *J* = 7.2 Hz) **A'3+B'3**, 7.97 (t, 4H, *J* = 7.8 Hz) **A5+B5**, 7.45 (dd, 4H, *J*₁ = Hz) **A6+B6**, 7.37 (s, 2H) **Ph²**, 7.36 (s, 2H) **Ph²**, 7.21 (m, 4H) **A4+B4**, 6.83 (s, 2H) **Ph⁴**, 6.73 (s, 2H) **Ph⁴**, 4.03 (s, 6H) **-OMe**. **FAB-MS**: (M⁺-PF₆⁻) 957, (M⁺-2PF₆⁻) 812, 541, 470, 406, 324, 171, 116, 51. **IR** (ν cm⁻¹): 3350 (w), 3082 (w), 1599 (s), 1535 (w) 1420 (w), 1248 (w), 1158 (w), 819 (s),

References:

- [1]. Constable E. C., Ward M. D., *J. Chem. Soc., Dalton Trans.* **1990**, 1405.
- [2]. Constable E. C., Cargill Thompson, A. M. W., *J. Chem. Soc., Chem. Commun.* **1992**, 617.
- [3]. Constable, E. C., Thompson, A. M. W., *J. Chem. Soc., Dalton Trans.* **1992**, 3467.
- [4]. Maestri, N., Armaroli, N., Balzani, V., Constable, E. C., Cargill Thompson, A. M. W., *Inorg. Chem* **1995**, *34*, 2759.
- [5]. Armaroli, N., Barigelletti, F., Constable, E. C., Encinas, S., Figgmeier, E., Flamigni, L., Housecroft, C. E., Schofield E. R., Vos, J. G., *Chem. Commun.* **1999**, 869.
- [6]. Constable, E. C., Harverson, P., *Inorg. Chim. Acta.* **1996**, 252, 9.
- [7]. Constable, E. C., Harverson, P., *Chem. Commun.* **1996**, 33.
- [8]. Constable, E. C., Handel, R. W., Housecroft, C. E., Morales A. F., Ventura, B., Flamigni, L., Barigelletti, F., *Dalton Trans.* **2003**, 1220.
- [9]. Constable, E. C., Handel, R. W., Housecroft, C. E., Morales A. F., Ventura, B., Flamigni, L., Barigelletti, F., *Chem. Eur. J.* **2005**, *11*, 4024.

Chapter IV : Photophysical and electrochemical investigations of the 4-methoxy and 3,5-dimethoxyphenyl substituted ruthenium (II) oligopyridine complexes.

I. Introduction.

The study of metal-organic complexes photochemistry and electrochemistry of transition metal complexes is of great interest, due to their highly efficient luminescence properties^[1]. The focus in this area has been reported for the bipyridine type complex family, with $[\text{Ru}(\text{bpy})_3]^{2+}$ as prototype which shows a good luminescent lifetime (860 ns at 298 K)^[2] and high quantum yield in acetonitrile. In the hope of increasing this luminescence lifetime and quantum yield, several hundreds of metal complexes using bipyridine ligands with different substituents at the periphery have been synthesized. The excited state reactivity tuning is essentially based on the change of the ligand functional groups substituting the periphery. For increasing the luminescence properties, we have to use complexes with ligands containing chromophoric^[3], π -conjugated^[4], electron-reservoir^[5], or light-harvesting^[6] functional groups. The essential photochemical phenomenon in metal polypyridine complexes is the metal-to-ligand charge transfer (MLCT), and the MLCT study of the is essential to understand how to control the excited state processes and to tune the luminescent properties of our complexes. At first we are going to define the photochemical process of the MLCT, then we investigate the luminescence properties of our new 4,4'-aryl substituted-2,2'-bipyridine ruthenium (II) complexes and investigate the electrochemical properties of this complexes in solution.

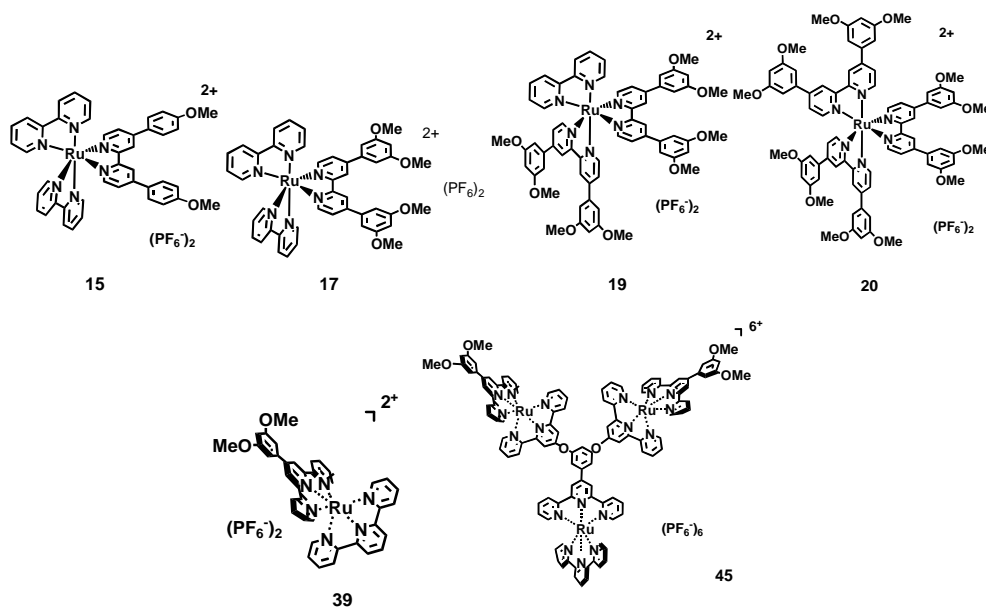
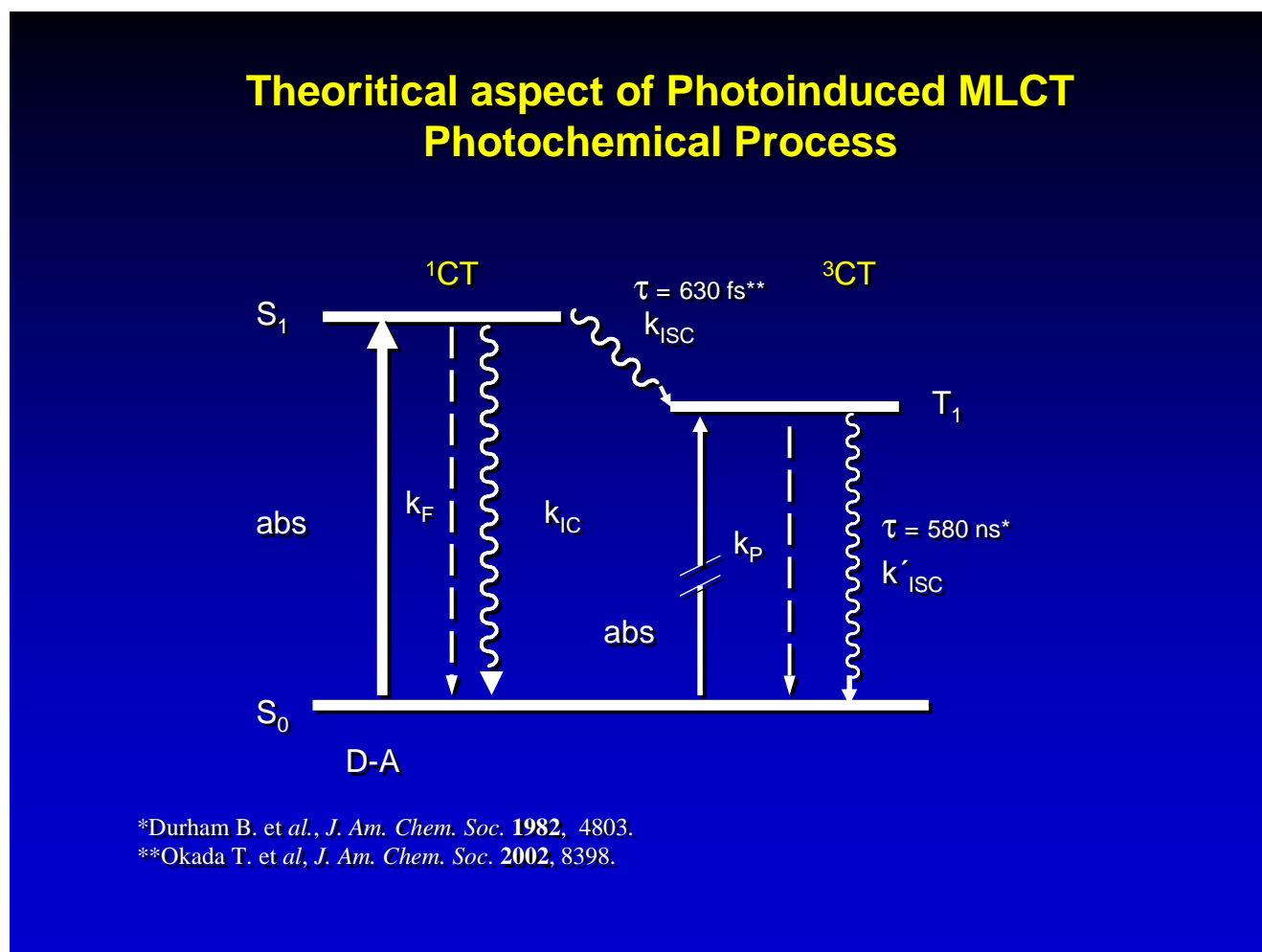


Fig IV-1-3,5-dimethoxyphenyl and 4-methoxyphenyl oligopyridine Ru(II) complexes studied.

II. Theoretical aspects of the metal-to-ligand charge transfer (MLCT).

II-1. The photoinduced metal-to-ligand charge transfer.

Photoinduced metal-to-ligand charge transfer is a phenomenon after the absorption of one photon by a metal complex. This is an electronic charge transfer from the metal to the ligand. The photochemical process for $[\text{Ru}(\text{bpy})_3]^{2+}$ is as following (Fig IV-2).



IV-2-Perrin-Jablonski diagram explaining the photochemical process of the MLCT, k_f (fluorescence rate constant), k_{ic} (internal conversion rate constant), k_p (phosphorescence rate constant), k_{isc} (intersystem crossing rate constant) ^1CT is the singlet excited state of the charge transfer, ^3CT is the triplet level.

The species after light energy absorption reach at first higher excited state named here ^1CT charge transfer at the singlet excited state. The complex can then fluoresce or reach a triplet excited state by intersystem crossing (isc) to further emit through phosphore light. The latter

transition have for consequences the relaxation of the triplet excited state and a phosphorescence emission.

The complexes have been excited by nanosecond laser and luminescence decays were measured.

The kinetic decays were measured with Laser Flash Photolysis (LFP) experiments and the lifetimes are determined using the formula below.

$$\tau = \frac{1}{\sum_i k_i}$$

The luminescence quantum yield is defined with this formula.

$$\phi_L = \frac{\text{number of luminescing molecules}}{\text{number of absorbed quanta}}$$

The experimental quantum yields have been calculated using the following formula established by Crosby^[6]. The reference used is the compound $[\text{Ru}(\text{bpy})_3]^{2+}$ with ($\phi_{\text{rL}} = 0.028$ in H_2O).

$$\frac{\phi_L}{\phi_{\text{rL}}} = \frac{\text{Abs } \eta^2 \text{ (area)}}{\text{Abs}_r \eta_r^2 \text{ (area)}_r}$$

with ϕ_{rL} : luminescence quantum yield of the reference.

ϕ_L : luminescence quantum yield.

Abs : Absorbance

Abs_r : Absorbance of the reference.

η : refraction index.

η_r : refraction index of the reference.

For the Laser Flash Photolysis (LFP) experiments the samples Pyrex quartz cell tubes were degassed three times by pump-freeze technical.

Laser Flash Photolysis experiments were carried out by exciting the sample solution with absorbances of $< 0.5 \text{ cm}^{-1}$ at 308 nm with the 20 ns, $\sim 75 \text{ mJ}$ output of a XeCl excimer laser. A pulsed Xenon arc lamp was used as the monitoring beam (4.5 cm path length, orthogonal to the excitation pulse). The detection system allowed monitoring of either the kinetics at a single wavelength using a transient digitizer or the whole transient spectrum, with an Optical Multichannel Array (OMA).

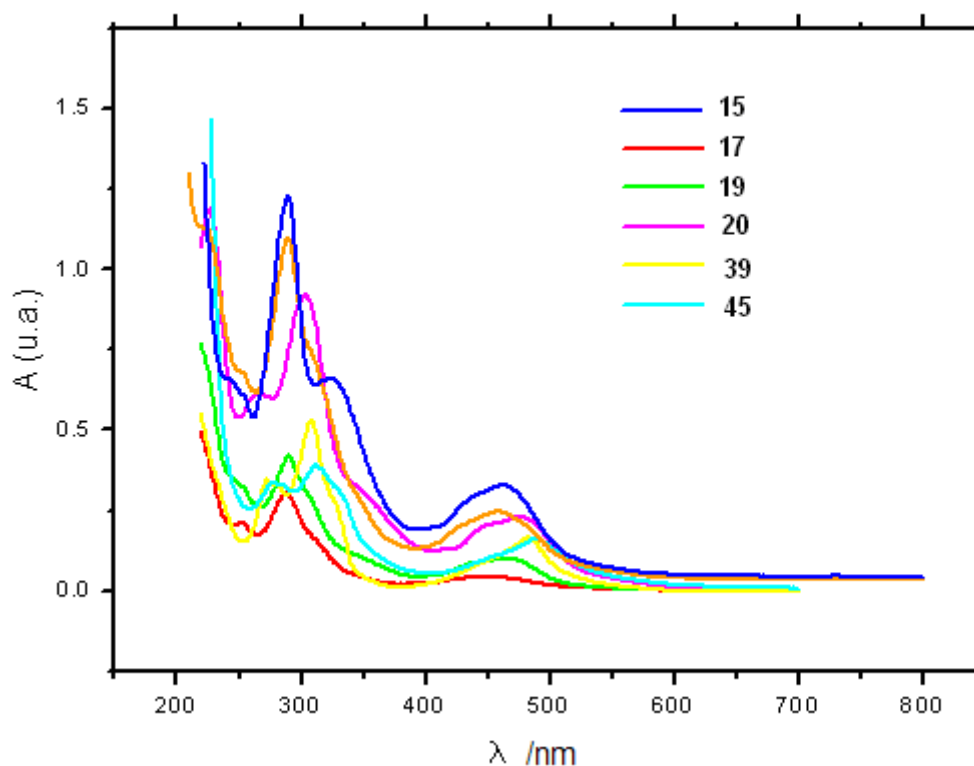


Fig IV-2- Absorption spectra of compounds **15, 17, 19, 20, 39, 45** in MeCN .

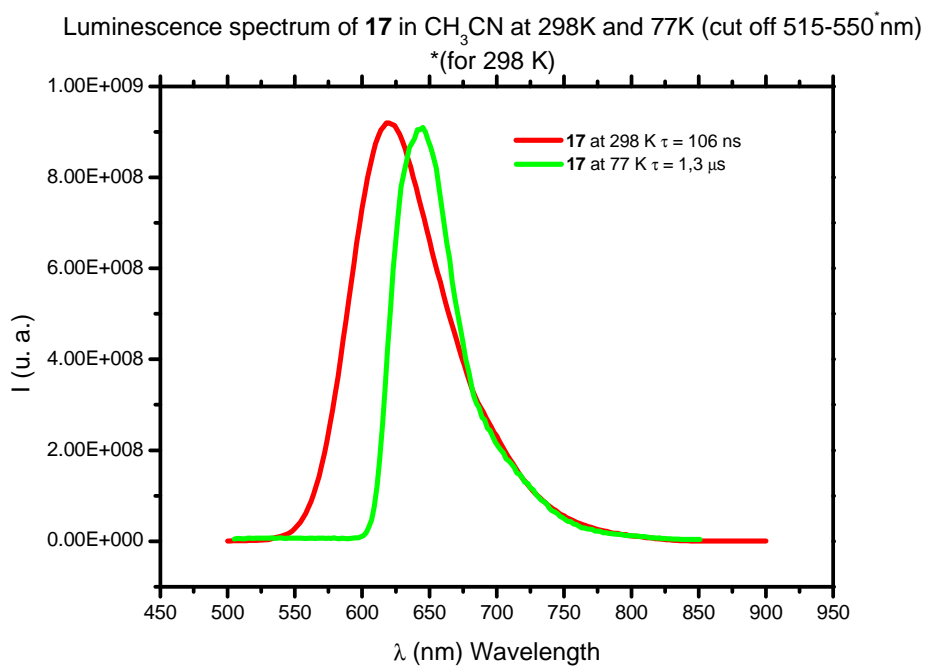


Fig IV-3- Steady-state emission of **17** in air saturated MeCN at 298 K and 77 K.

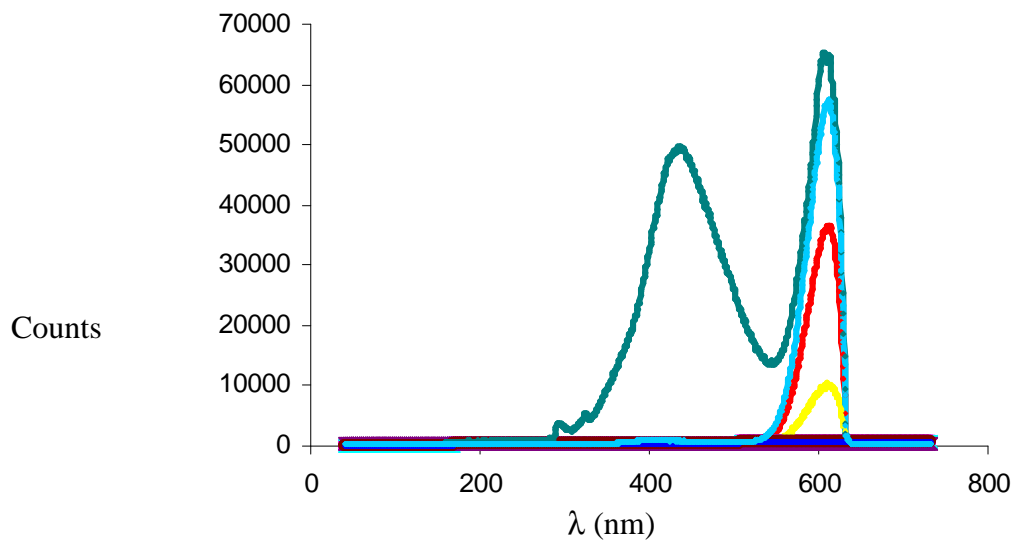


Fig IV-4- Emission spectra of the transients of **17** in degassed MeCN at 298 K 20 ns (deep blue), 200 ns (sky blue), 1 μs (red), 3 μs (yellow), 10 μs after the laser excitation.

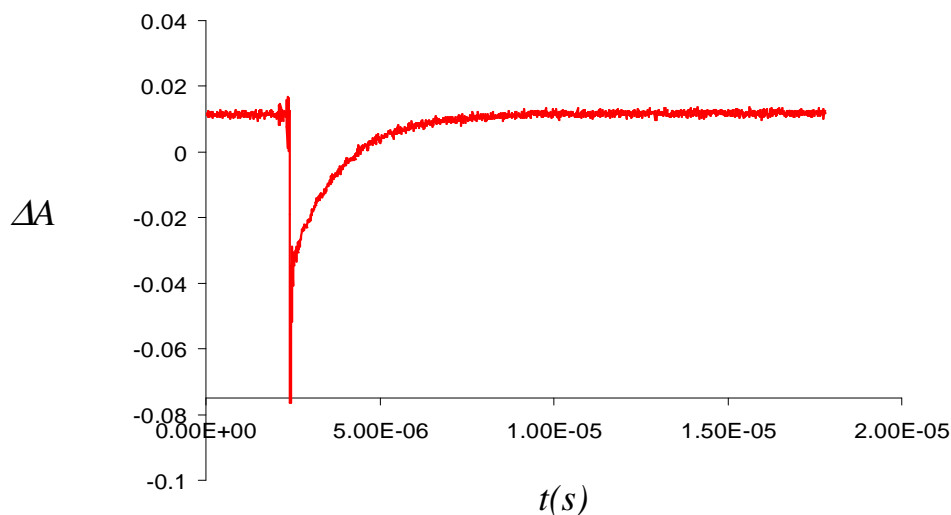


Fig IV-5- Kinetic trace of **17** luminescence observed at 612 nm in degassed MeCN at 298K.

Emission spectra of a solution of **17** in MeCN ($A_{351} = 0.40$) taken before and after a single flash show that the photochemical luminescence is very efficient: a massive emission band appears at 612 nm. Time resolved emission spectroscopy of **17** in degassed MeCN shows two bands with maxima 612 nm and ca 460 nm (Fig IV-4). One microsecond after the laser, we can still see the same band at 612 nm ca. but without the second band at 460 nm (instead 20 ns after pulse).

The kinetics of the band observed at 612 nm was probed (Fig IV-5). A slow growth (up than 1 μ s) is detected in degassed MeCN at 298 K. The introduction of air effects the 612 nm signal. We have assigned the band at 612 nm to triplet MLCT state of the complex **17** emission.

2. Photophysical properties of **19**.

Photophysical properties of complex **19** (described in the Chapter II), were determined. UV-Vis absorption and emission spectra were done by steady-state and transient spectroscopy at 298 K and in rigid matrix at 77 K using laser-flash photolysis and single-photon counting methods. The UV-Vis steady-state absorption spectrum of **19** showed different absorption bands characteristic of Ru(II)-bpy complexes with a MLCT absorption band. The steady-state emission spectrum were measured at 298 K and 77 K.

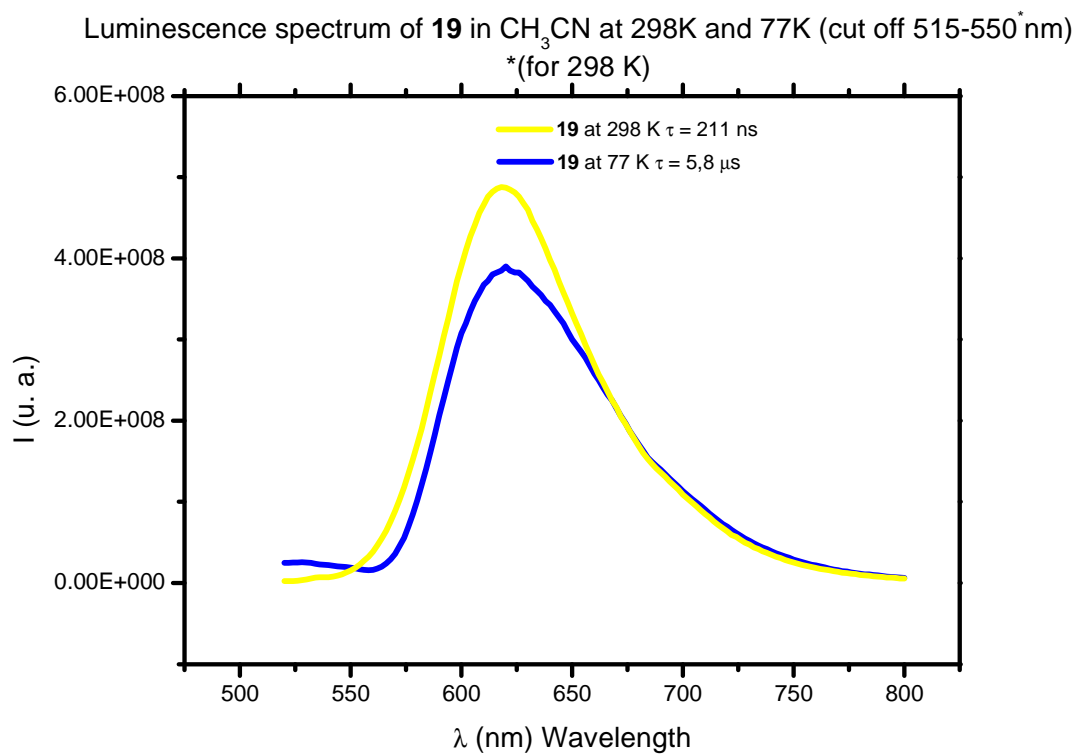


Fig IV-7- Steady-state emission spectra of **19** luminescence in air-equilibrated MeCN at 298 K (yellow curve) and 77 K (blue curve).

The emission spectrum shows two identical band at 298 K and 77 K

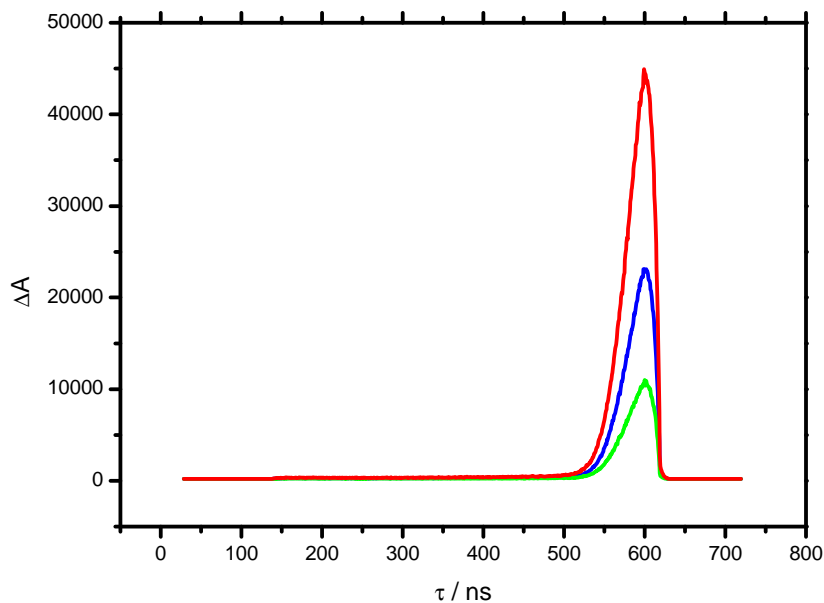


Fig IV-8- Emission spectra of the transient 80 ns (red), 1 μ s (blue), 2 μ s (green), after the laser excitation of **19** in degassed MeCN.

2. Photophysical and electrochemical properties of 20.

Complex **20** described in the Chapter II, was analysed by different spectroscopy methods for the photophysical properties similar to **17**, like UV-Vis absorption and emission spectroscopy, steady-state and transient spectroscopies at 298 K and with rigid matrix at 77 K using laser-flash photolysis and single-photon counting methods. The steady-state UV-Vis absorption spectrum at of **20** showed different absorption bands characteristic of Ru(II)-bpy complexes.

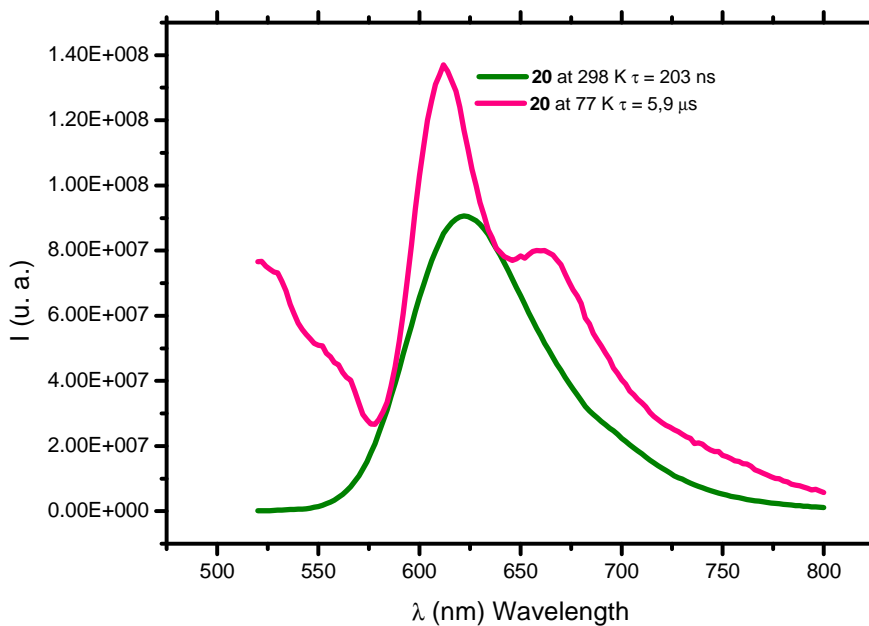


Fig IV-9- Steady-state emission spectra of **20** luminescence in air-equilibrated MeCN at 298 K and 77 K.

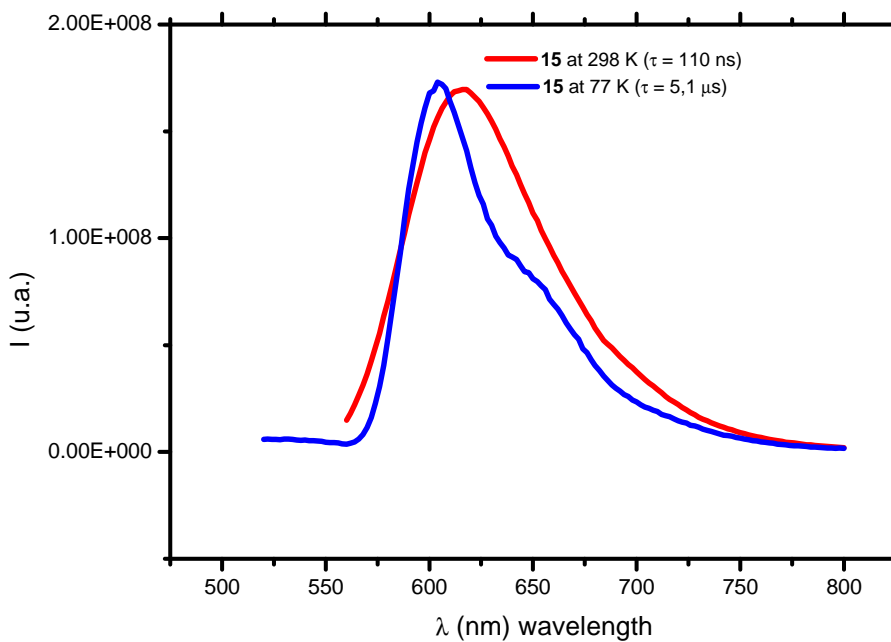


Fig IV-10- Steady-state emission spectra of **15** luminescence in air-equilibrated MeCN at 298 K and 77 K.

3. Electrochemistry.

Electrochemical measurement of all mononuclear and polynuclear compounds were performed in acetonitrile with 1.0 mM TBAPF₆ as electrolyte. The results are summarised in (table IV-1). Cyclic voltammetry (CV) was measured fully reversible metal-centered redox waves, and reversible or quasi reversible ligand reduction processes. Differential pulse voltammetry (DPV) was used to differentiate close redox processes and to distinguish one electron processes and two electron processes in polynuclear species.

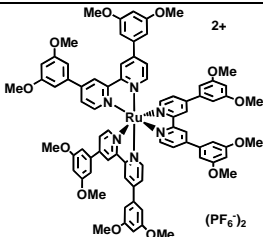
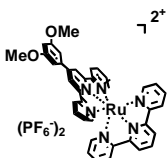
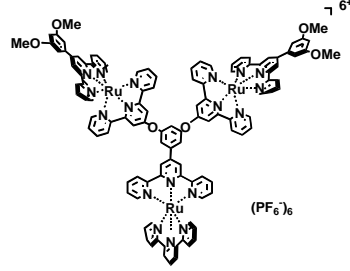
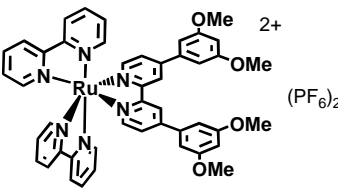
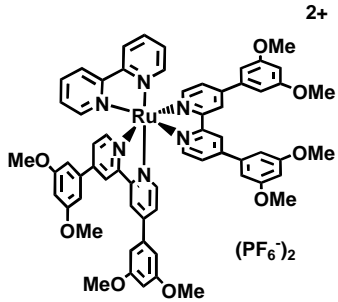
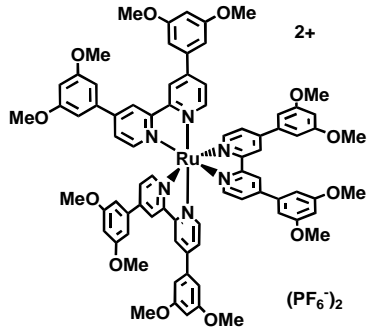
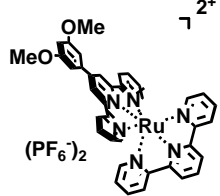
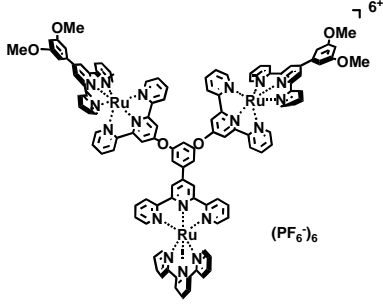
Compound	E _{red} (V)	E _{ox} (V)
	+ 0.590	-1.81
	+ 1.188	-1.964 , -2.311
	+1.319	-0.67V, -2.336

Table IV-I-Potential of complexes **20**, **42** and **45** 1 mM in MeCN + 1mM TBAPF₆, Glassy carbon, CE-Pt wire, RE-Ag wire, referenced vs F_c⁺/F_c from C_V.

Luminescence photophysical datas of 4-methoxyphenyl 3,5-dimethoxyphenyl substituted bpy and tpy ligand ruthenium complexes at 298 K in CH₃CN

Formula	Compound (solvent)	Absorption		Emission 298 K air equilibrated (deairated)*			Emission 77 K	
		λ_{\max} (nm)	ϵ (M ⁻¹ cm ⁻¹)	λ_{\max} (nm)	ϕ	τ (ns)	λ_{\max} (nm)	τ (μ s)
	17 (MeCN)	458	21800	616	0.016	380 (1.84 μ s)*	609	5,6
	19 (MeCN)	464	25000	618	0.02	211 (1.8 μ s)*	620	5,8

 <p>2+</p> <p>(PF₆)₂</p>	<p>20 (MeCN)</p>	<p>476</p>	<p>27500</p>	<p>622</p>	<p>0.018</p>	<p>203 (1.75 μs)*</p>	<p>660</p>	<p>5.9</p>
 <p>2+</p> <p>(PF₆)₂</p>	<p>39 (MeCN)</p>	<p>482</p>	<p>12400</p>	<p>638</p>	<p>2.8.10⁻⁴</p>	<p>0.65</p>	<p>634</p>	<p>8.5</p>
 <p>6+</p> <p>(PF₆)₆</p>	<p>45 (H₂O)</p>	<p>488</p>	<p>72500</p>	<p>640</p>	<p>18. 10⁻⁵</p>	<p>8.5</p>	<p>639</p>	<p>8.1</p>

<p>2+</p> <p>(PF₆)₂</p>	<p>15 (MeCN)</p>	<p>462</p> <p>21000</p>	<p>617</p> <p>9.10^{-3}</p> <p>110</p> <p>605</p> <p>(1.45 μs*)</p> <p>5.1</p>
---	-------------------------	-------------------------	--

IV-Conclusions and discussion.

The photophysical and electrochemical parameters of the 4-methoxy and 3,5-dimethoxyphenyl bpy and tpy ruthenium (II) complexes serie have been investigated. The steady-state absorption at room temperature and emission spectrums at 298 K and 77 K have been measured for the complexes **15**, **17**, **19**, **20**, **39** and **45**. The transient emission spectrum of the compound **15**, **17**, **19** and **20** have been measured with a streak-camera. The bpy type complexes **15**, **17**, **19**, **20** luminescence lifetimes have been determined at room temperature by nanosecond laser flash photolysis. The lifetime of this complexes for the such compounds are two time higher in degassed MeCN as the reference $[\text{Ru}(\text{bpy})_3]^{2+}$ (860 ns in MeCN) ^[2]. This mesurements have been confirmed by single-photon counting saturated and degassed. The quantum yield of the bpy type complexes have been determined with the Crosby method^[6].

References:

- [1]. Lytle, F. E., Hercules, D. M., *J. Am. Chem. Soc.* **1969**, *91*, 253.
- [2]. Durham, B., Caspar, J. V., Nagle J. K., Meyer T. J., *J. Am. Chem. Soc.* **1982**, *104*, 4803.
- [3]. Passalacqua, R., Loiseau, F., Campagna, S., Fang, Y. Q., Hanan, G. S., *Angew. Chem. Int. Ed. Engl.* **2003**, *42*, 1608.
- [4]. Armaroli, N., Barigelletti, F., Constable, E. C., Encinas, S., Figgmeier, E., Flamigni, L., Housecroft, C. E., Schofield E. R., Vos, J. G., *Chem. Commun.* **1999**, 869.
- [5]. Denti, G., Campagna, S., Scolastica, S., Ciano, M., Balzani, V., *J. Am. Chem. Soc.* **1992**, *114*, 2944.
- [6]. Demas, J. N., Crosby G. A., *J. Phys. Chem.* **1971**, *75*, 991.

Chapter V : Synthesis and photochemical investigation of 4,4'-bis(3,5-dimethoxyphenyl)-6,6'-dimethyl-2,2'-bipyridine copper (I) and ruthenium (II) complexes.

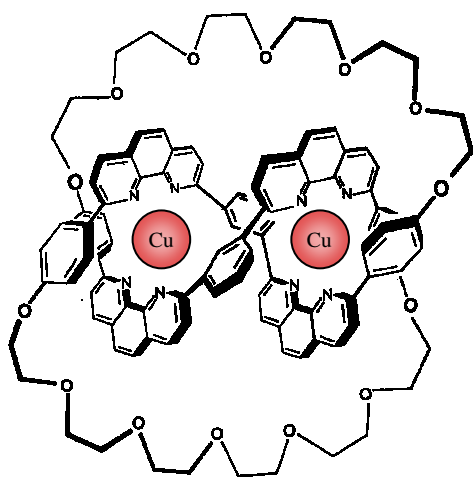


Fig V-1- Sauvage's copper (I)-phenanthroline based trefoil knot^[1].

I. Introduction

The investigation of the luminescence properties of bisphenanthroline complexes of copper (I), $[\text{Cu}(\text{NN})_2]^+$ has been the focus of many research reports that have been reviewed^[2-6]. The major motivation for this type of study has to do with practical applications for instance of the field of energy conversion and storage^[7-8]. In the area of supramolecular photochemistry other metal complexes, for instance those of the ruthenium(II)-oligopyridine family have attracted a great deal of attention since they can be useful for the design of supramolecular systems using photons as energy information. In this chapter, we will see the synthesis of 4,4'-bis(3,5-dimethoxyphenyl)-6,6'-dimethyl-2,2'-bipyridine copper (I), 4,4'-bis(3,5-dimethoxyphenyl)-2,2'-bipyridine copper (II) and 4,4'-bis(3,5-dimethoxyphenyl)-6,6'-dimethyl-2,2'-bipyridine ruthenium (II) complexes and their photophysical and electrochemical properties.

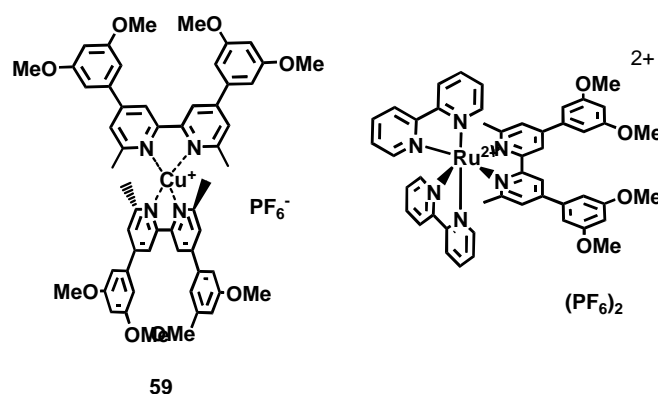


Fig V-I- Complexes synthesised in this chapter.

II. Synthesis of 4,4'-bis(3,5-dimethoxyphenyl)-6,6'-dimethyl-2,2'-bipyridine- copper (I) complex 59.

In order to synthesise this type of complexes we need first to synthesise the ligand **58**, this ligand is the 6,6'-dimethyl substituted ligand seen in chapter II and its synthesis was according the Kröhnke method used in the Constable procedure^[9]. Two equivalents of 3,5-dimethoxybenzaldehyde reacts with 2,3-butanedione to form the compound **56** and this compound reacts with **57** at reflux in EtOH during 5 hours.

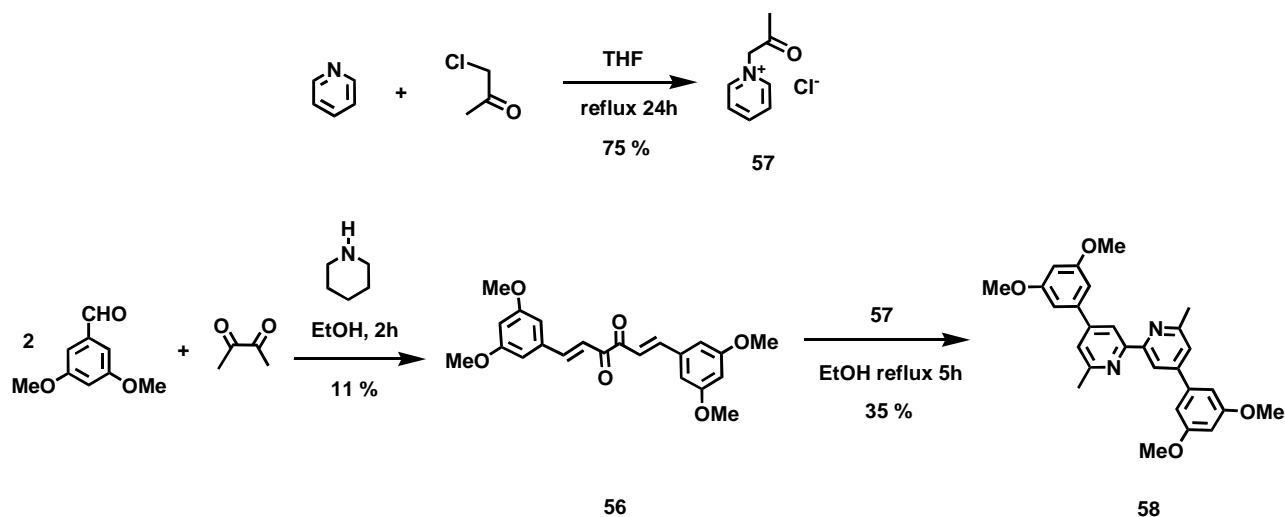


Fig V-3 - Synthesis of ligand **58** .

The synthesis of the “ locked ” version of the analogous with 6,6'-dimethyl-substituents follows a different route. The first step is a Michael condensation of 3,5-dimethoxybenzaldehyde and 2,3-butanedione with catalytic amounts of piperidine at reflux 4 hours and the resulting yellow solids is treated with the **57** salt according the Kröhnke method [8] .

^1H NMR spectrum of **59**.

The complex $\text{Cu}(\mathbf{58})_2(\text{PF}_6)$, **59** was obtained after complexation of the ligand with $[\text{Cu}(\text{MeCN})_4][\text{PF}_6]$ in EtOH during 4 hours. The complex **59** was characterised by ^1H NMR ^{13}C NMR spectroscopy in CD_3CN and ES-MS.

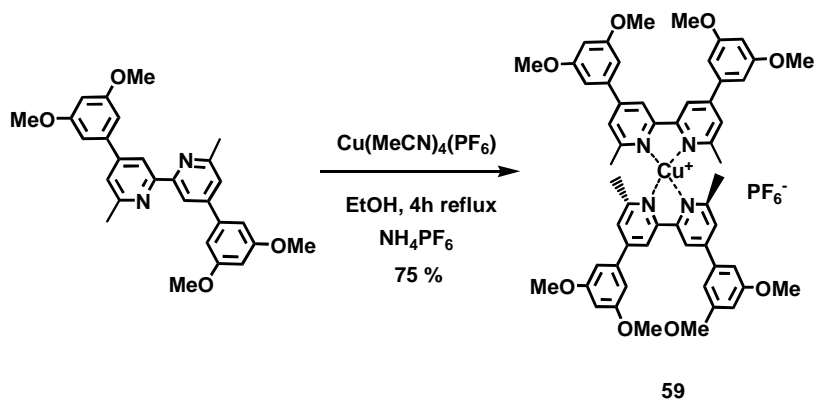


Fig V-4- Synthesis of complex $[\text{Cu}(\mathbf{58})][\text{PF}_6]$, **59**.

The ^1H NMR spectrum of **59** shows peaks corresponding to the ligand protons, at 8.66 ppm

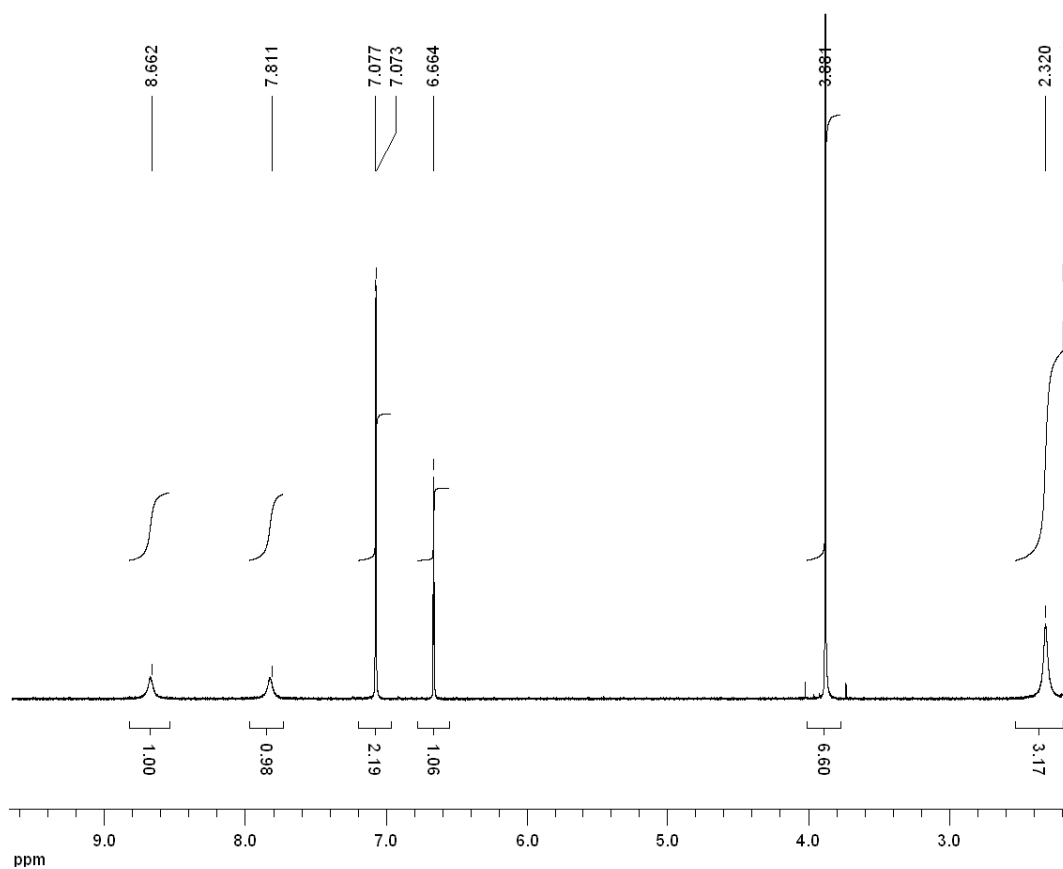


Fig V- 4- ^1H -NMR spectrum of complex **59** at 500 MHz at 298 K.

Proton	AH^3	AH^5	BH^2	BH^4	$-\text{OCH}_3$	$-\text{CH}_3$
δ ppm	8.66	7.81	7.08	6.66	3.89	2.32
type of signal	s	s	s	s	s	s
Integration	4H	4H	8H	4H	24H	12H

Table V- ^1H NMR signal values in CD_3CN at 500 MHz at 298 K.

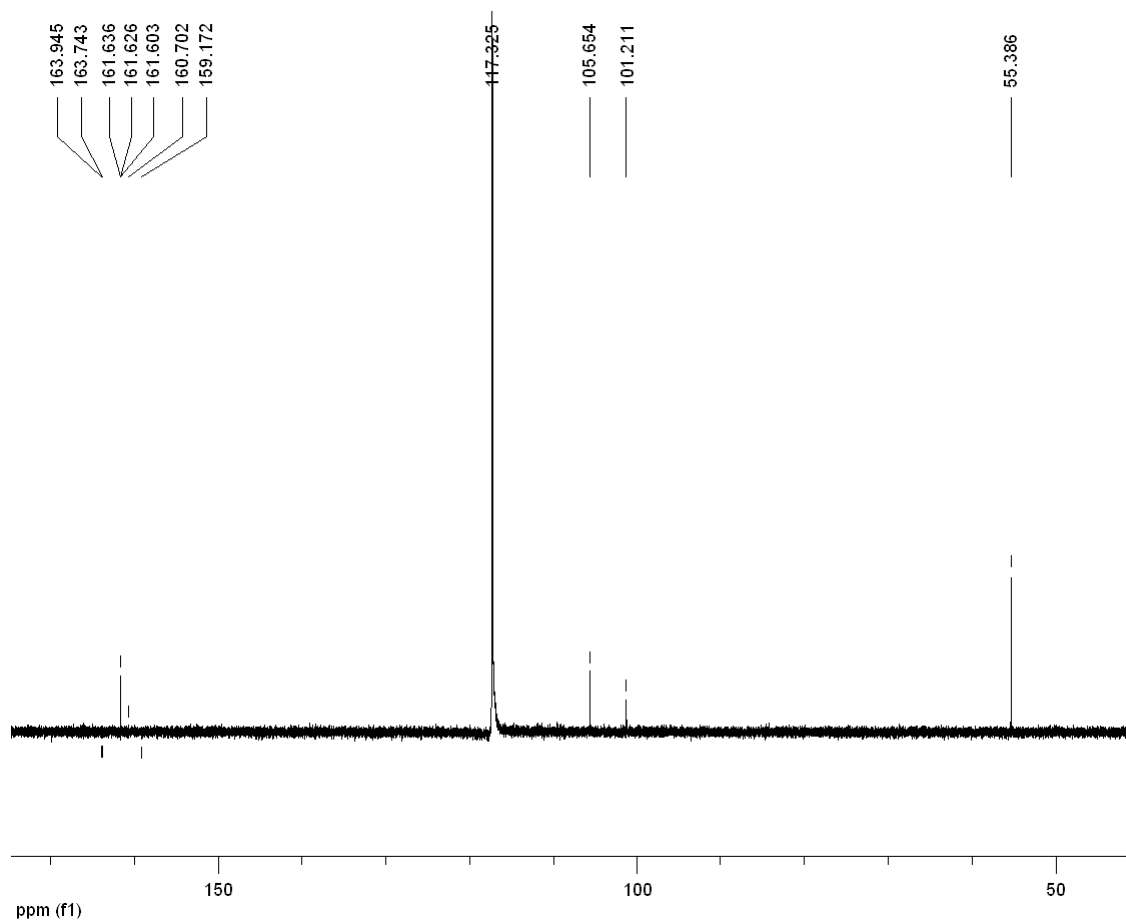


Fig V-5- ^{13}C NMR spectrum of **59** at MHz at 67.5 MHz in CD_3CN at 298 K.

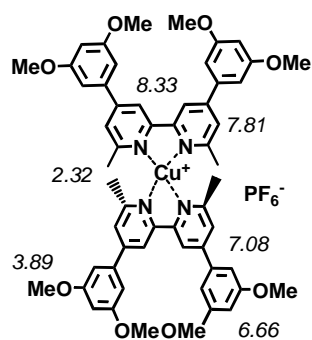
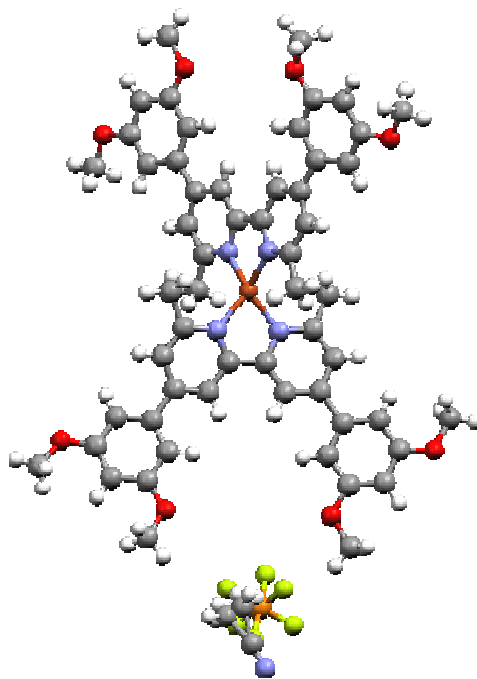
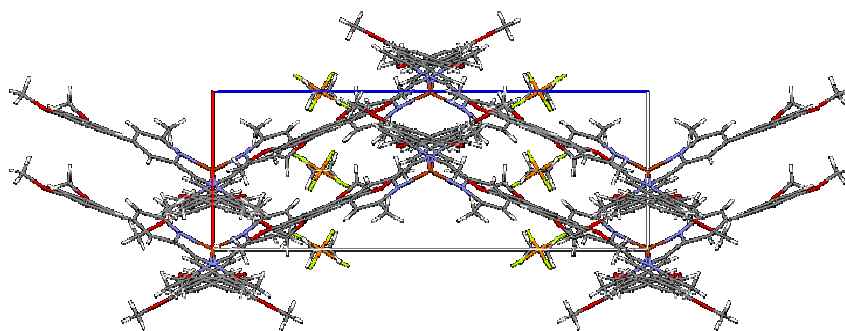


Fig V-6- ^1H NMR assignments of complex **59** in CD_3CN .

X-ray crystal structure of **59**.



*Fig V- 7- X-ray structure of complex **59** in CH₃CN.*



*Fig V- 8- Packing of complex **59** along the b axis.*

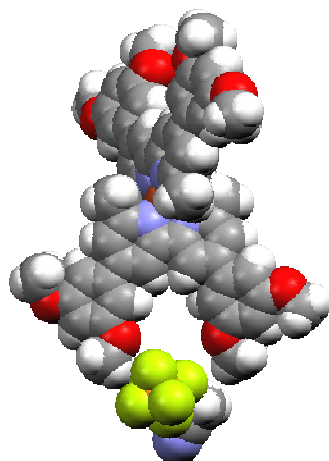


Fig V-9- Space filled representation of complex **59**.

III. Synthesis of Ru(bpy)₂(**58**)(PF₆)₂ complex **60**.

The synthesis was according the same procedure (Fig V-9) seen before in chapter II, [Ru(bpy)₂Cl₂] was dissolved with ligand **55** in EtOH and the mixture was carry at reflux during 4 hours. The complex was precipitated with NH₄PF₆ filtered and purified through SiO₂/A_{sol} column. The compound was characterised by ¹H NMR spectroscopy in CD₃CN, and ES-MS.

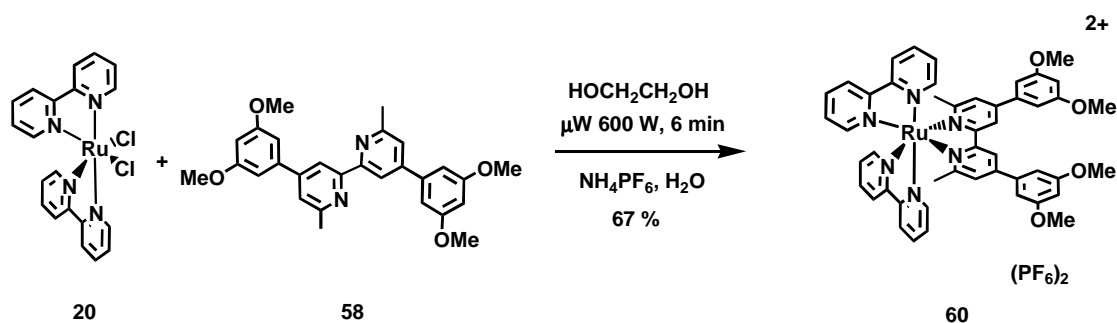


Fig V-10- Synthesis of complex **60**.

¹H NMR spectrum of complex **60**.

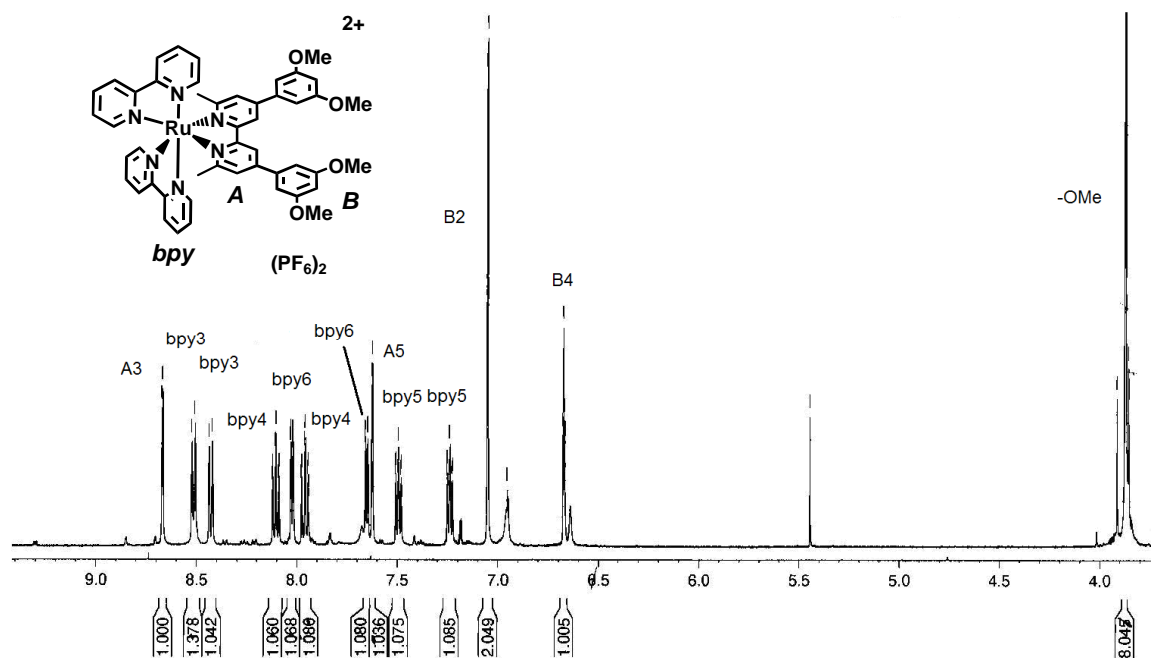


Fig V-11- ¹H NMR spectrum of complex **60** in CD₃CN at 500 MHz at 298 K.

NMR datas table of complex **60**.

δ (ppm)	8.67	8.52	8.43	8.11	8.02	7.96	7.66	7.63	7.50	7.24	7.05	6.67	3.87	1.68
spin mult	<i>d</i>	<i>d</i>	<i>d</i>	<i>t</i>	<i>d</i>	<i>t</i>	<i>d</i>	<i>d</i>	<i>t</i>	<i>t</i>	<i>d</i>	<i>t</i>	<i>s</i>	<i>s</i>
attribution	A ₃	bpy ₃	bpy ₃	bpy ₄	bpy ₆	bpy ₄	bpy ₆	A ₅	bpy ₅	bpy ₅	B ₂	B ₄	-OMe	-Me
Integration	2H	2H	2H	2H	2H	2H	2H	2H	2H	2H	4H	2H	12H	6H
<i>J</i> (Hz)	2	8	8	3.75	5.5	3.75	5.5	2	5.75	5.75	3.5	1.25		

Tab V-I- NMR-signal values of complex **60** in CD₃CN at 500 Mhz at 298 K.

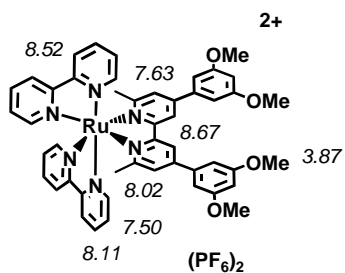


Fig V-12- ^1H NMR assignments of protons in CD_3CN at 500 MHz at 298 K.

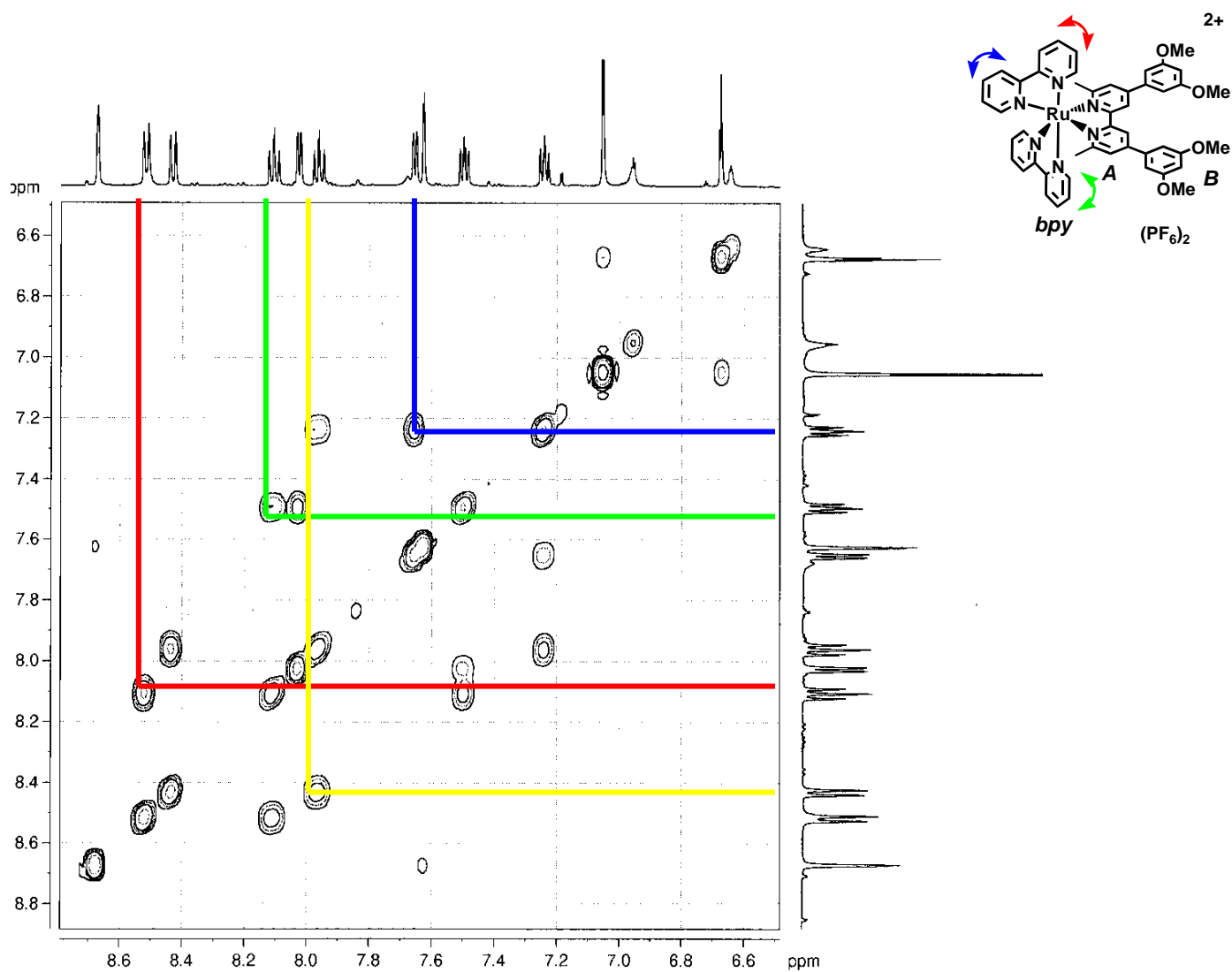


Fig V-13- H-H COSY spectrum of **60** complex in CD_3CN at 500 MHz at 298 K.

nOE spectrum of complex **60**.

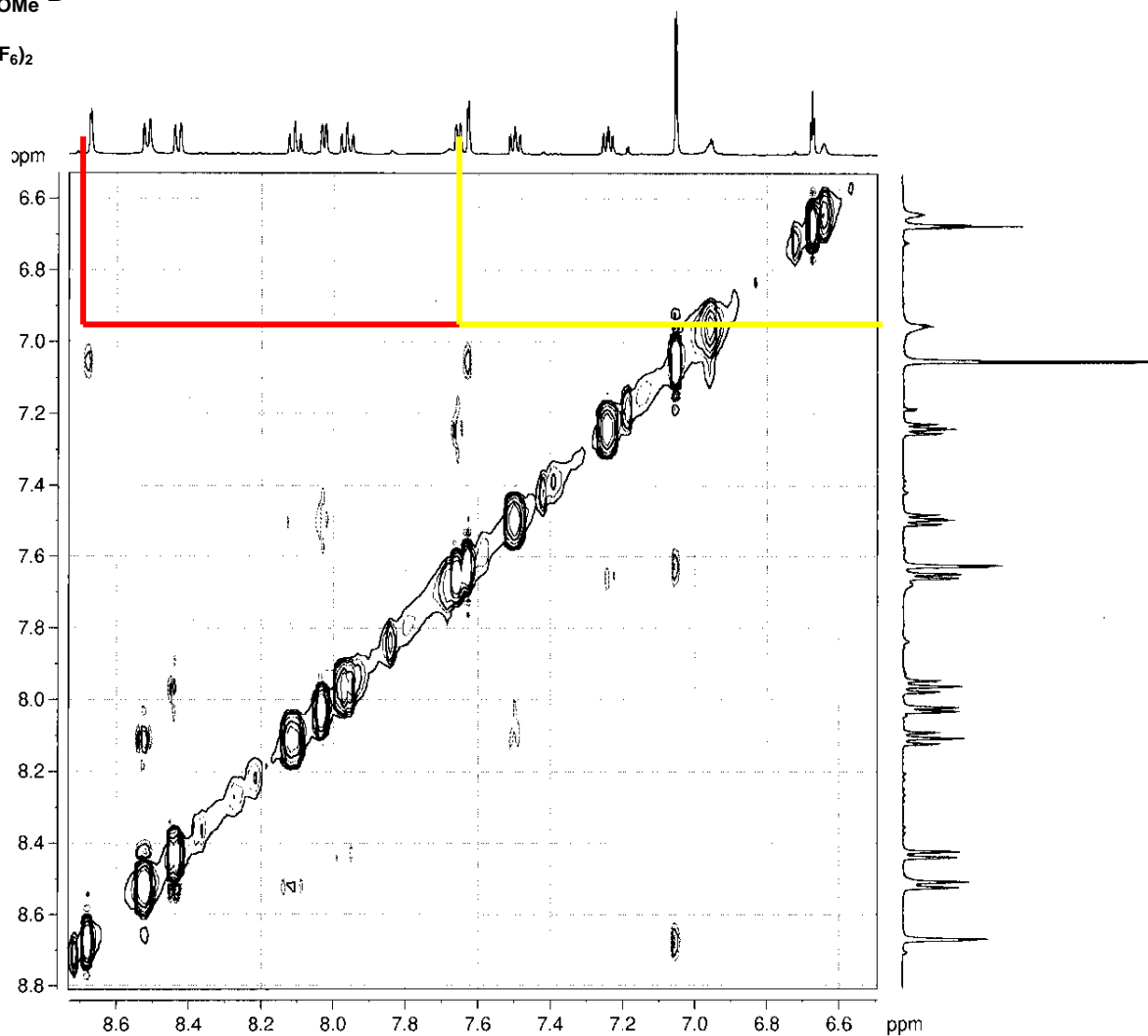
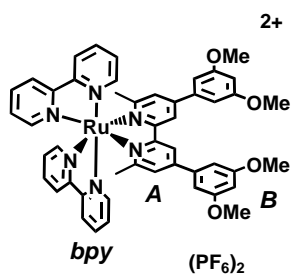


Fig V-14- nOesy spectrum of complex **60** in CD₃CN at 500 MHz at 298 K.

V-Photophysical and electrochemical properties of complexes 59, 60.

Absorption spectrum of 59.

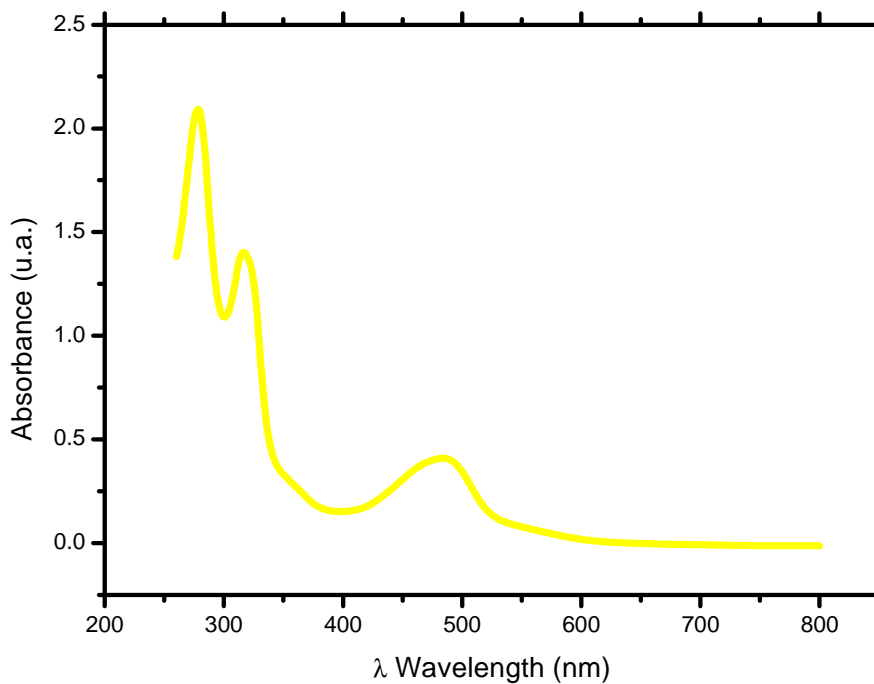


Fig -V-15- Emission spectrum of complex **59** in CH₃CN.

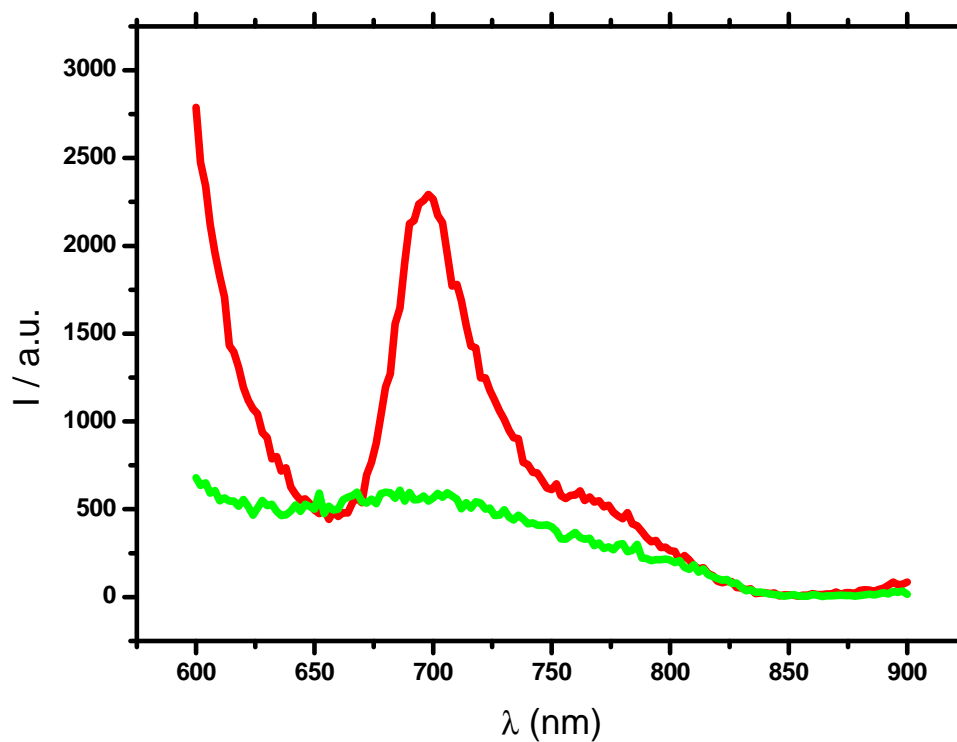


Fig -V-16- Emission spectrum of **59** green curve with C₆₀-malonate red curve.

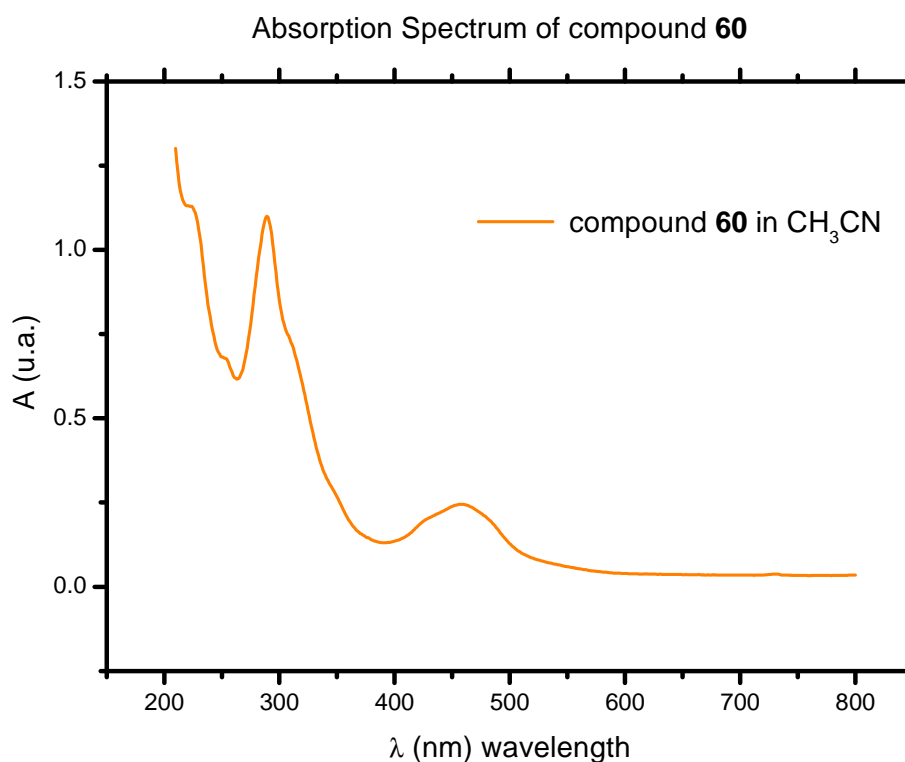


Fig V-17- Absorption spectrum of **60** compound in CH₃CN

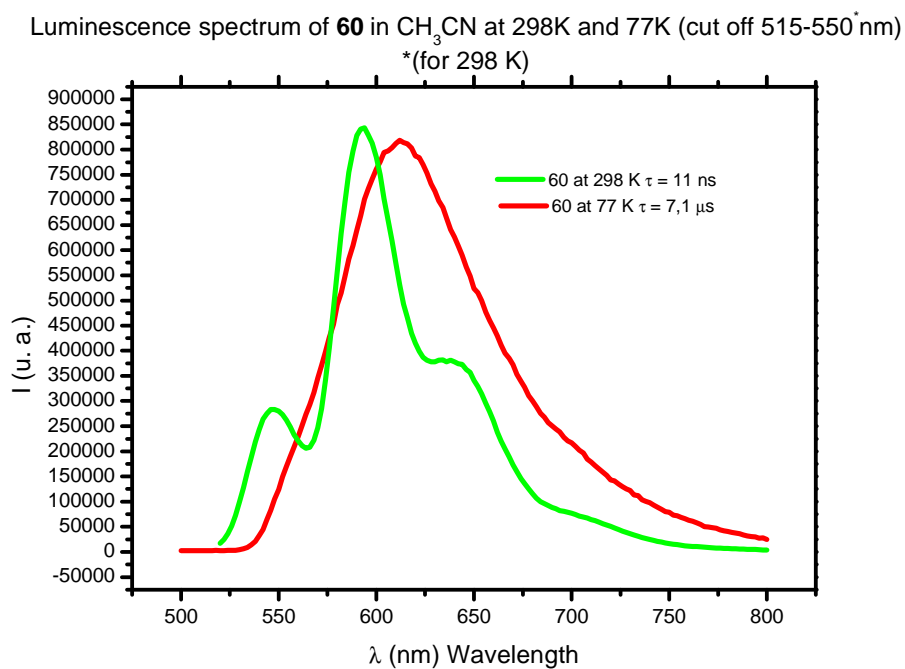


Fig V-18- Emission spectrum of compound **60** at 298 K green curve at 77 K red curve in CH₃CN

Kinetic investigations.

The kinetic investigations have been performed via single photon counting measurement at the maximum emission wavelength at 298 K and 77 K.

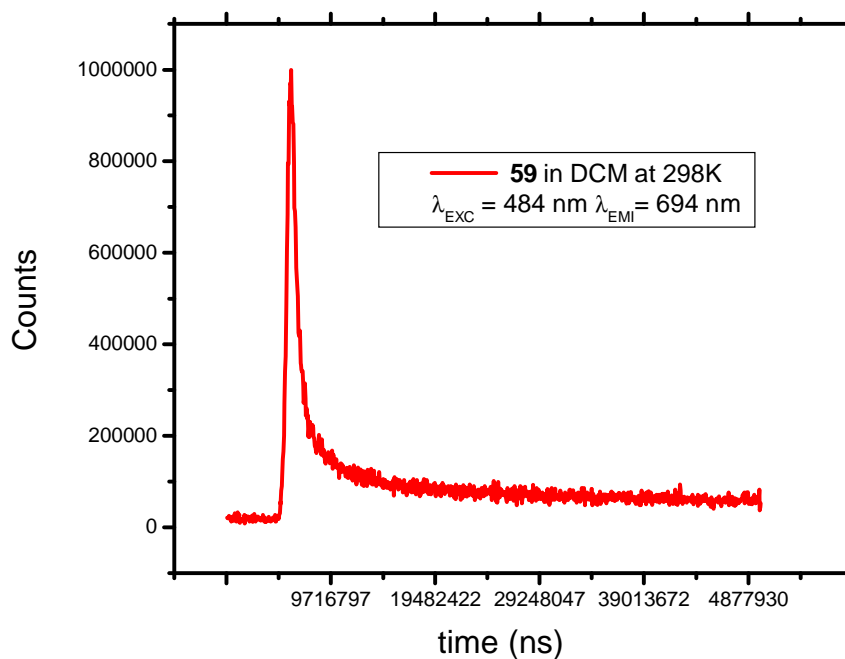


Fig V-19 - Kinetic trace of **59** in degassed DCM observed at 694 nm.

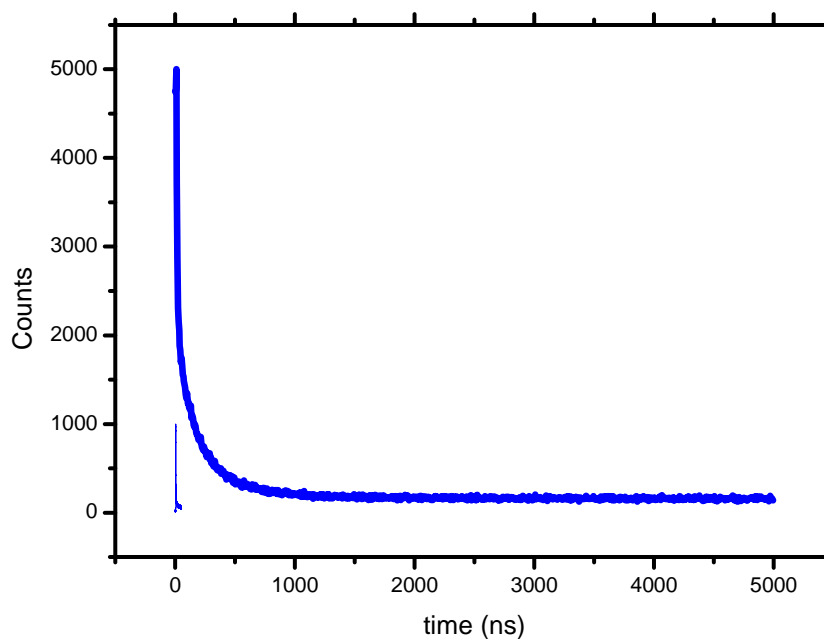


Fig V-20 - Kinetic trace of **59** in DCM rigid matrix at 77 K observed at 730 nm.

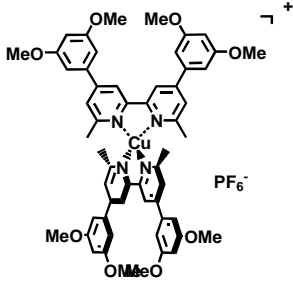
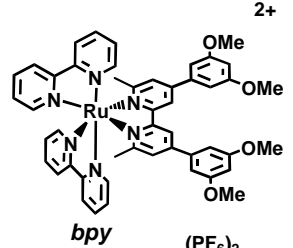
Formula	Name	Absorption		Emission 298 K air equilibrated			Emission 77 K air equilibrated	
		λ_{\max} (nm)	$\epsilon(\text{M}^{-1}\text{cm}^{-1})$	λ_{\max} (nm)	ϕ	τ (ns)	λ_{\max} (nm)	τ (μs)
	59	484	7800	694	$< 1.10^{-4}$	19	730	0,23
320		29600						
278		34300						
	60	457	14500	595	$1,7.10^{-4}$	19	637	4,1

Table V-II- Photophysical properties of complexes **59** and **60** in DCM.

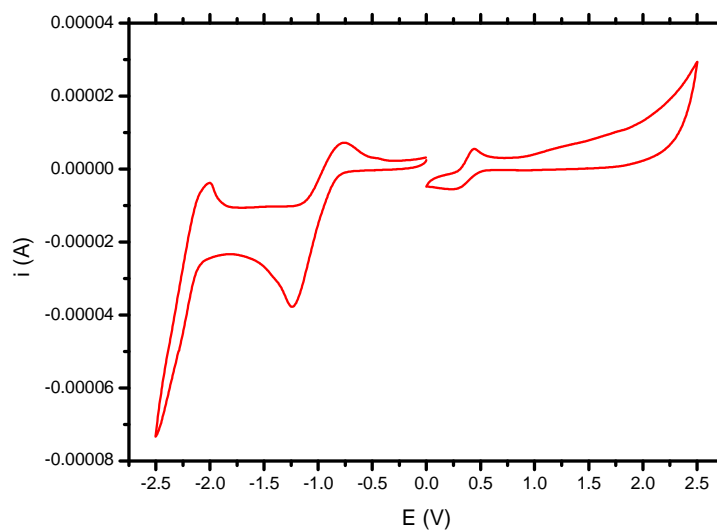


Fig V-21- Cyclic voltammetry of compound **59** in CH₃CN 1mM + 1 mM TBAPF₆ vs Fc⁺/Fc.

<u>Compounds</u>	<u>59</u>
<u>E_{red}</u>	+1.39 V
<u>E_{ox}</u>	-1.43 V

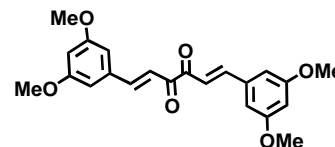
Conclusion.

In this chapter we have shown how to synthesized 4,4'-bis(3,5-dimethoxyphenyl)- 6,6'-dimethyl-2,2'-bipyridine **58** ligand and the corresponding copper (I) complex **59** and ruthenium (II) bis-bpy **60** complex. The photophysical studies in DCM have shown that the copper (I) complex **59** has a low quantum yield and a short lifetime, the Ru(II) corresponding complex has a higher quantum yield and a higher lifetime at 77 K comparing with **17** Ru(II) complexes have better luminescence properties.

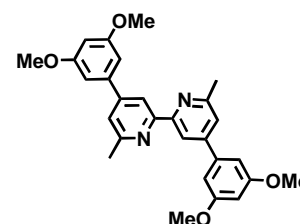
Experimental section:

Synthesis of 56 and 58.

A mixture of 3,5-dimethoxybenzaldehyde (10.0 g , 60 mmol), butan-2,3-dione (2.6 g, 30 mmol), EtOH (50 ml) and piperidine (0.5 ml) were heated to reflux for 2 h and then the solution allowed to cool.



After 24 h in the refrigerator, yellow crystals of 1,6-di(3,5-dimethoxyphenyl)hexa-1,5-diene-3,4-dione **56** were collected by filtration and washed with a little cold MeOH. (1.26 g, 3.3 mmol)., 1-pyridinopropanone chloride (1.14 g, 6.6 mmol) **57** and NH₄OAc (2.0 g) in EtOH (10 ml) were heated to reflux for 4 h. On cooling, 4,4'-di(3,5-dimethoxyphenyl)-6,6'-dimethyl-2,2'-bipyridine **58** crystallised and was collected by filtration. The product was washed with MeOH, dried under reduce pressure and recrystallised from EtOH/pentane to give colourless needles of **58** (m = 451 mg, yield = 30 %).

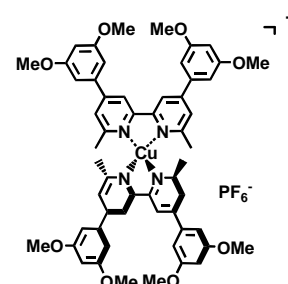


Experimental datas NMR ¹H at 400 MHz in CD₃CN: 7.80 (d, 2H, *J* = 16.2 Hz), 6.81 (d, 2H, *J* = 16 Hz) =C-H^{1,6}, 6.57 (t, 2H, *J* = 9.2 Hz) =C-H^{2,5}, 6.81 (d, 4H, *J* = 2.25 Hz) Ph-H², 6.57 (t, 2H) Ph-H⁴, 3.85 (s, 4H) -OMe. **FAB-MS** : 382. **IR** (ν cm⁻¹): 2909 (w), 2833 (w), 1585 (w), 1208 (s), 984 (s), 813 (s). **Mass-Analysis** : Formula C₂₂H₂₂O₆: C % 68.19 (69.10%), H % 5.76 (5.80%).

Experimental datas NMR ¹H at 400 MHz in CD₃CN: 9.04 (d, 2H) AH³, 7.66 (d, 2H, *J* = 9.2 Hz) AH⁵, 7.14 (d, 4H, *J*₁ = 8 Hz) BH², 6.65 (t, 2H) BH⁴, 3.97 (d, 9H, *J* = 5.6 Hz) H⁶, 3.03 (s, 6H , *J*₁ = 6 Hz) H⁵. **FAB-MS** : 457. **IR** (ν cm⁻¹): 2951 (w), 1593.5 (w), 1200 (s), 1157 (w), 831 (s). **Mass-Analysis** : Formula C₂₈H₂₈N₄O₄ (calculated): C % 71.82 (72.88%), H % 5.65 (5.75%), N % 6.54 (6.52%).

Synthesis of 59.

A solution of [Cu(MeCN)₄][PF₆] (0.025 g, 0.066 mmol) in EtOH (10 ml) was added dropwise to a solution of **58** (0.050 g, 0.13 mmol) in EtOH (25 mL) and the mixture stirred for 2 h at reflux after which H₂O

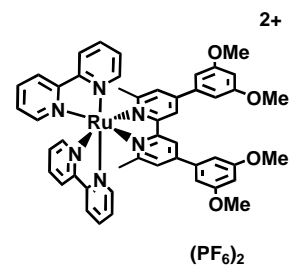


(50 mL) was added and the organic solvent removed in vacuo. The precipitate was collected over Celite, washed with water and redissolved in MeCN and purified by recrystallisation from acetone/ether to give dark red crystals of **59** (48.3 mg, 75 %).

Experimental datas NMR ^1H at 400 MHz in CD_3CN : 8.66 (s, 4H) AH^3 , 7.81 (s, 4H) AH^5 , 7.08 (s, 8H) BH^2 , 6.66 (s, 4H, $J_1 = 8$ Hz) BH^4 , 3.89 (s, 24H) -OMe , 2.32 (s, 12H) -CH_3 . .
ES-MS : 975.3, 457.3. **IR** (ν cm^{-1}): 2930 (w), 1598 (s), 1157 (s), 1045 (s), 839 (s). **Mass-Analysis** (% *calculated*): Formula $\text{C}_{56}\text{H}_{56}\text{N}_4\text{O}_8\text{CuPF}_6$: C 57.48 % (59.97%), 4.91 H % (4.99%), N 4.76 % (4.99%).

Synthesis of **60**.

$[\text{Ru}(\text{bpy})_2\text{Cl}_2]$ (100 mg, 0.21 mmol) and **58** (94.3 mg, 0.21 mmol) were dissolved in a in ethylene glycol (10 mL) and then the reaction mixture heated in a microwave oven for 6 min at 600 W. The reaction mixture was cooled to room temperature and extracted with CH_2Cl_2 (3 x 10 mL). The organic phases were collected and evaporated under reduce pressure. The solid was purified over SiO_2 chromatography using A_{sol} as eluant. The red complex obtained $[\text{Ru}(\text{bpy})_2(\text{58})_2][\text{PF}_6]_2$ **60** was obtained after recrystallisation from methanol (151 mg, yield = 71 %).



Experimental datas NMR ^1H at 400 MHz in CD_3CN : 8.67 (d, 2H, $J = 2$ Hz) A_3 , 8.52 (d, 2H, $J = 8$ Hz) bpy_3 , 8.43 (d, 2H, $J_1 = 8$ Hz) bpy_3 , 8.11 (t, 9H, $J_1 = 3.75$ Hz) bpy_4 , 8.02 (d, 4H, $J = 5.5$ Hz) bpy_6 , 7.96 (d, 4H, $J = 3.75$ Hz), 7.66 (t, 4H, $J_1 = 6$ Hz) bpy_6 , 7.63 (d, 4H, $J_1 = 6$ Hz) A_5 , 7.50 (t, 2H, $J = 5.75$ Hz) bpy_5 , 7.24 (t, 2H, $J = 5.75$ Hz) bpy_5 , 7.05 (d, 2H, $J = 3.5$ Hz) B_2 , 6.67 (t, 2H, $J = 1.25$ Hz) B_4 , 3.87 (s, 12H) OMe , 1.68 (s, 6H) Me . **FAB-MS** : 870 $[\text{M}^+ - (\text{PF}_6^-)]$, 725 $[\text{M}^+ - 2(\text{PF}_6^-)]$. **IR** (ν cm^{-1}): 2928 (w), 1591 (s), 1445 (w), 1202 (s), 1060 (w), 831 (s).

References:

- [1]. Dietrich-Buchecker, C. O., Nierengarten, J.-F., Sauvage, J.-P., Armaroli, N., Balzani, V., De Cola, L., *J. Am. Chem. Soc.* **1993**, *115*, 11237.
- [2]. Armaroli, N., *Chem. Soc. Rev.* **2001**, *30*, 113.
- [3]. Armaroli, N., *Photochem. Photobiol. Sci.* **2003**, *2*, 73.
- [4]. Felder, D., Nierengarten, J.-F., Barigelletti, F., Ventura, B., Armaroli, N., *J. Am. Chem. Soc.* **2001**, *123*, 6291.
- [5]. McMillin, D. R., McNett, K. M., *Chem. Rev.* **1998**, *98*, 1201.
- [6]. Scaltrito, D. V., Thompson, D. W., O'Callaghan, J. A., Meyer, G. J., *Coord. Chem. Rev.* **2000**, *208*, 243.
- [7]. Bignozzi, C. A., Argazzi, R., Kleverlaan, C. J., *Chem. Soc. Rev.* **2000**, *29*, 87.
- [8]. Schwab, P. F. H., Levin, M. D., Michl, J., *Chem. Rev.* **1999**, *99*, 1863.
- [9]. Constable, E. C., Housecroft, C. E., Neuburger, M., Poleschak, I., Zehnder, M., *Polyhedron* **2003**, *22*, 93.

Chapter VI: From pyrene to polymetallic dyads

I. Introduction.

The study of polymetallic systems based on polypyridine metal complexes is of great interest because this type of molecules possesses interesting photochemical and electrochemical properties. When the number of metal centers increases, the electrochemical potential and lifetime and quantum yields of luminescence change considerably. Many examples of dyads and triyads using rigid bridged ligands have been reported^[1-3] and their use as polymetallic molecular wires has been demonstrated^[1-3]. The photophysical parameters of a Ru/Os bpy based dyad change with the distance between the donor and the acceptor, and the charge separation in such a molecule is very efficient^[1]. Some recent examples of rod-like wires have been studied incorporating thiophenyl bridges between the metal centres^[2-3]. In order to control energy transfer and luminescence, it is interesting to study new spacers. In this chapter, we will discuss the possible formation of non covalently connected polyad, using possible non covalently bridged spacers based on pyrene excimer formation.

II. Wire type polyads.

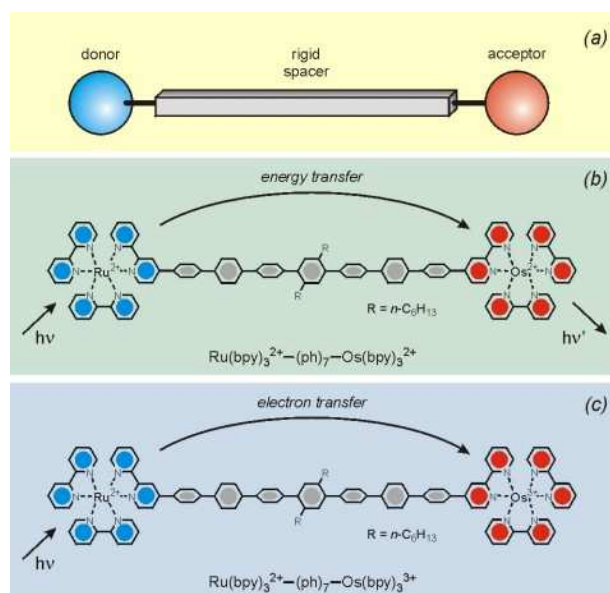


Fig VI-1- Examples of photoinduced energy (b) and electron (c) transfer processes over long distances^[1].

Photoinduced energy and electron-transfer over long distances and along predetermined directions is a very important function at the molecular level. This function can be obtained

by linking donor and acceptor components by a rigid spacer. For example, in the system $[\text{Ru}(\text{bpy})_3]^{2+}-(\text{ph})_n-[\text{Os}(\text{bpy})_3]^{2+}$ compounds (ph = 1,4-phenylene; n = 3, 5, 7) in which excitation of the $[\text{Ru}(\text{bpy})_3]^{2+}$ unit is followed by electronic energy transfer to the ground state $[\text{Os}(\text{bpy})_3]^{2+}$ unit, as shown by the emission of the latter (see Fig VI-I) schematic energy level diagram). For the compound (b) (Fig VI-1) with n = 7, the rate constant for energy transfer over 4.2 nm from Ru to Os is $1.3 \times 10^6 \text{ s}^{-1}$. In the $[\text{Ru}(\text{bpy})_3]^{2+}-(\text{ph})_n-[\text{Os}(\text{bpy})_3]^{3+}$ compounds, resulting from the chemical oxidation of the Os-based part, photoexcitation of the $[\text{Ru}(\text{bpy})_3]^{2+}$ unit cause the transfer of one electron to the Os-based one (see Fig VI-1) with a rate constant of $3.4 \times 10^6 \text{ s}^{-1}$ for n = 7 compound (c). Nevertheless the electron added to the $[\text{Os}(\text{bpy})_3]^{2+}$ unit is rapidly removed and a back electron transfer reaction (rate constant $2.7 \times 10^5 \text{ s}^{-1}$ for n= 7) takes place from the $[\text{Os}(\text{bpy})_3]^{2+}$ unit to the $[\text{Ru}(\text{bpy})_3]^{3+}$.

Spacers with energy levels or redox states in between those of the donor and acceptor may help energy or electron-transfer (hopping mechanism). Spacers whose energy or redox levels can be manipulated by an external stimulus can play the role of switches for the energy- or electron-transfer processes.

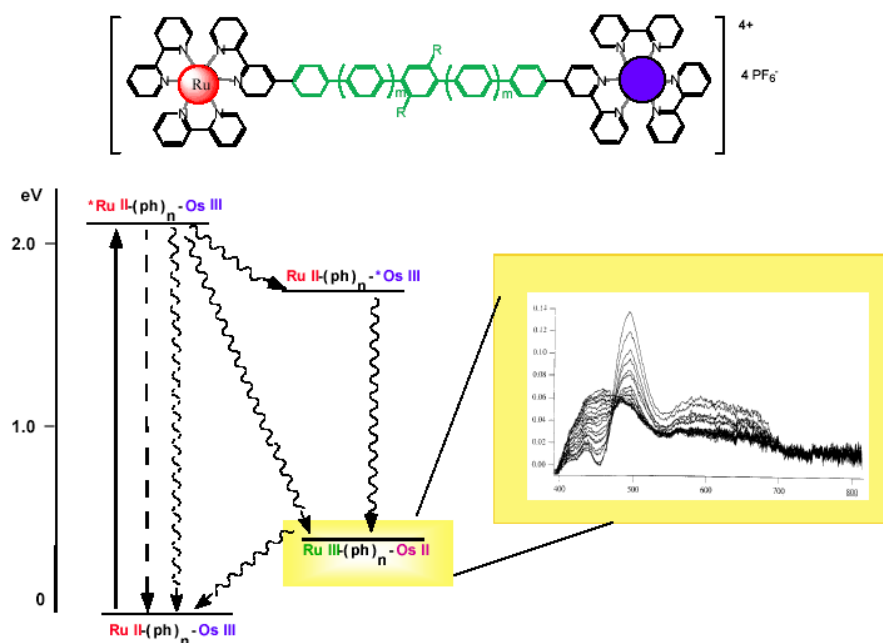


Fig VI-2- Binuclear Ru(II) polypyridine complexes built around bridges of varying degree of hybridization.

III. The pyrene excimer theory

What are excimer and exciplexes?

An excimer is an electronically excited state with highly polarizable species due to the electrophilic effect of the half-filled HOMO and the nucleophilic half-filled LUMO, and participate in charge-transfer interactions with other polar or polarizable species. These give a collision complex between an electronically excited species M^* , with any polar or polarizable ground state molecule, N , which will generally be stabilized by some charge transfer interaction. The collision complex M^*N is formed and possess a longer lifetime than the corresponding MN ground state collision complex. The M^*N collision complex has different properties to M^* . The M^*N collision complex can be considered as metastable species or new electronically excited state species. This electronically excited state is called an *exciplex*. When M and N are the same the excited complex M^*N is called an *excimer*.

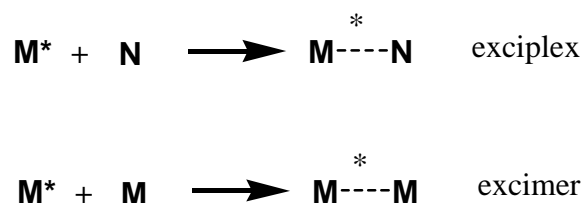


Fig VI-3- Exciplex and excimer theory

The typical properties of exciplexes are emission and production of light when they return from excited state to ground state. When the exciplexes are formed, they should in principle exhibit fluorescence (singlet exciplexes) or phosphorescence (triplet exciplexes). The emission of M^*N will in general be different from that of the M^* . The ground state collision complex MN is generally less bound than M^*N , and the exciplex emission shows that the collision complex is return to its ground state level or to an other weakly bound complex.

Example of excimers : Pyrene.

The pyrene excimer is a common example in this class of photochemical intermediates^[4]. *Fig VI-3* shows the fluorescence of pyrene in n-heptane as a function of pyrene concentration. At concentrations of 10^{-5} M or less, the fluorescence is concentration independent and is

composed of pure pyrene monomer fluorescence. When the pyrene concentration increases two effects are observed: (a) the monomer emission decreases in intensity, and (b) a new fluorescent emission due to the pyrene excimer, appears with a red shift compare to of the emission and its intensity increases.

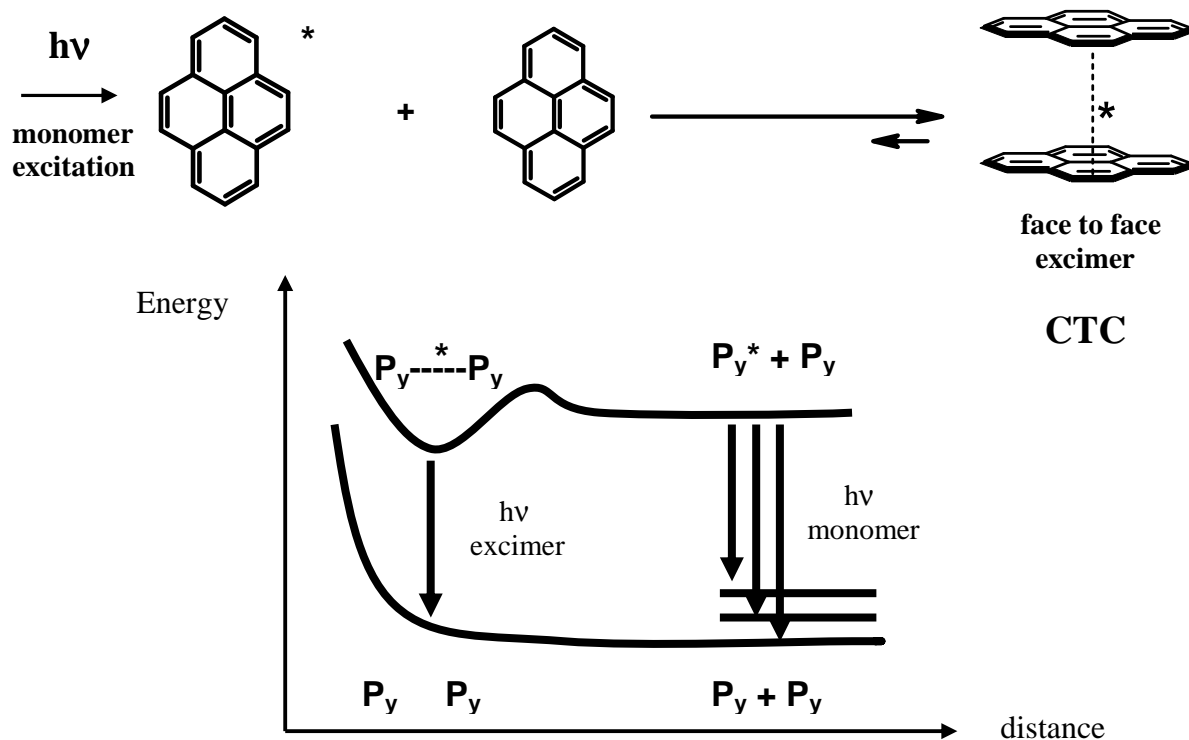


Fig VI-4- Pyrene excimer formation.

A potential-energy diagram for the formation of pyrene excimer is also shown in Fig VI-4. The diagram indicates how the energy of two pyrene molecules varies as a function of their internuclear separation. For the ground-state pair at large distance of separation ($\sim 10 \text{ \AA}$) the energy of the pair is constant, since intermolecular interactions are weak at this separation distance. At a separation of about 4 \AA , which is close to the equilibrium separation of the excimer, the energy of the ground state PyPy pair rises rapidly due to occupied π orbital repulsions. From the last figure it is easy to see why the pyrene excimer emission is structureless and why no absorption is observed corresponding to $\text{PyPy} \rightarrow \text{Py} \cdots \text{Py}^*$ absorption, the emission is to an unstable dissociative state. From a spectroscopic analysis of pyrene excimer

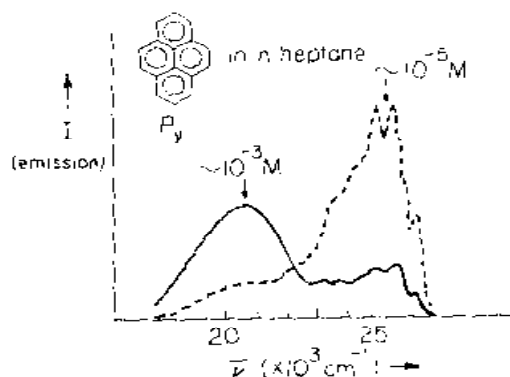


Fig VI-5- experimental example of the excimer emission of pyrene.

emission (Fig VI-5), and a correlation of this with the emission of pyrene crystals, it has been concluded that the structure of the “face to face” pyrene singlet excimer is favored. This structure is in agreement with expectations based on maximal overlap of π orbitals.

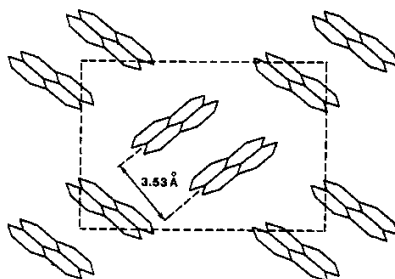


Fig VI-6-Arrangement of molecules in the (001) plane of a pyrene crystal.

IV-Synthesis of 1-pyrenyltpy Ru, Os and Ir complexes

The goal of our synthesis is to create excimers of two possible monomers containing one metal or two different metals (Ru+Os, Ru+Ir, Os+Ir) to form excited-state dimers (exciplexes) in the solid state or in solution which is more difficult with the probability of collision and the diffusion rate constant, or possible ordonated triyad containing respectively by hypothetic repartition order Ru->Os<-Ir (according to the possible energy levels of the ^3CT state and ($^3\pi\text{-}\pi^*$) state of Ru Os and Ir mono for Ru and Ir and Os dipyrenyl substituted for Os core-ligand as spacer. The formation of Ru-Ru Dimer Os-Os dimer is possible in solid state due to the possible natural $\pi\text{-}\pi^*$ stacking effect, for the dipyriddy substituted complex the packing was observed at solid state (Fig VI-7) (see Hannon literature^[5]) for the dipyriddy substituted

complex and the possible fluorescence analysis in the solid state should be interesting to study.

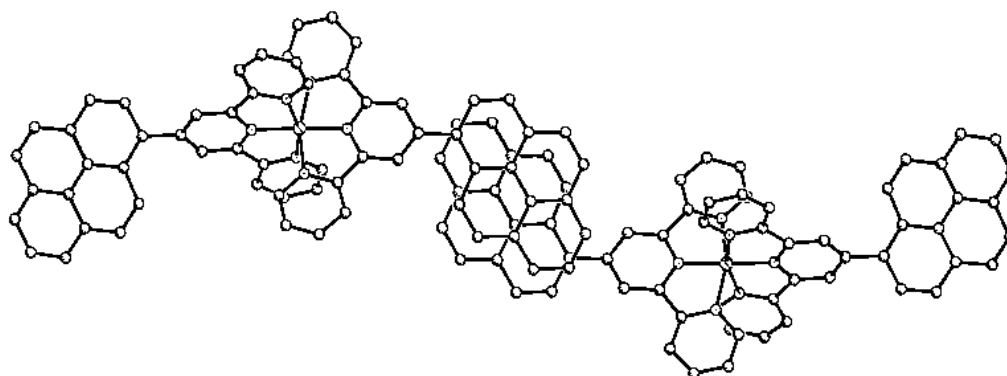


Fig VI-7- π -stacking of pyrenyl group in Fe(tpy-Pyr)₂(PF₆)₂ complex^[5].

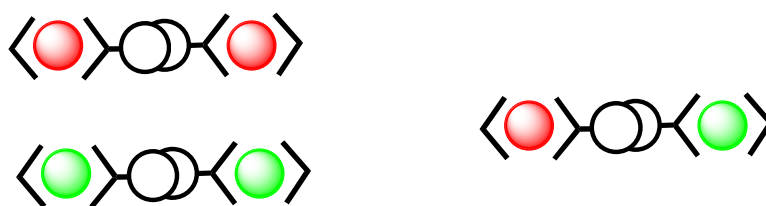


Fig VI-8 Excimer formation of two different complexes with photochemically induced excited state Ru (red), Os (green) nucleus

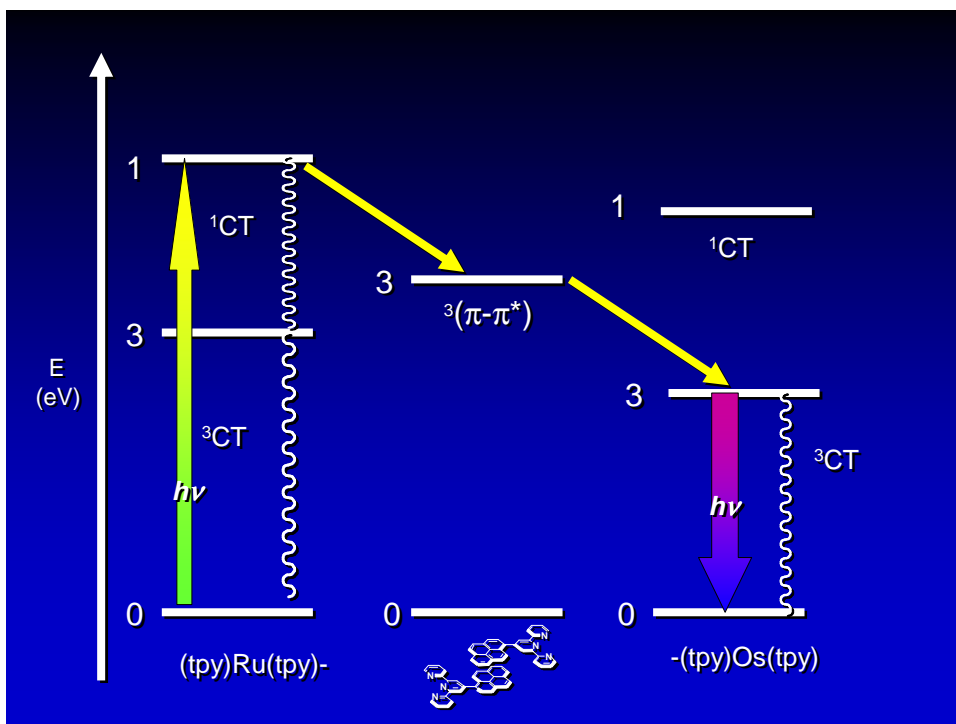
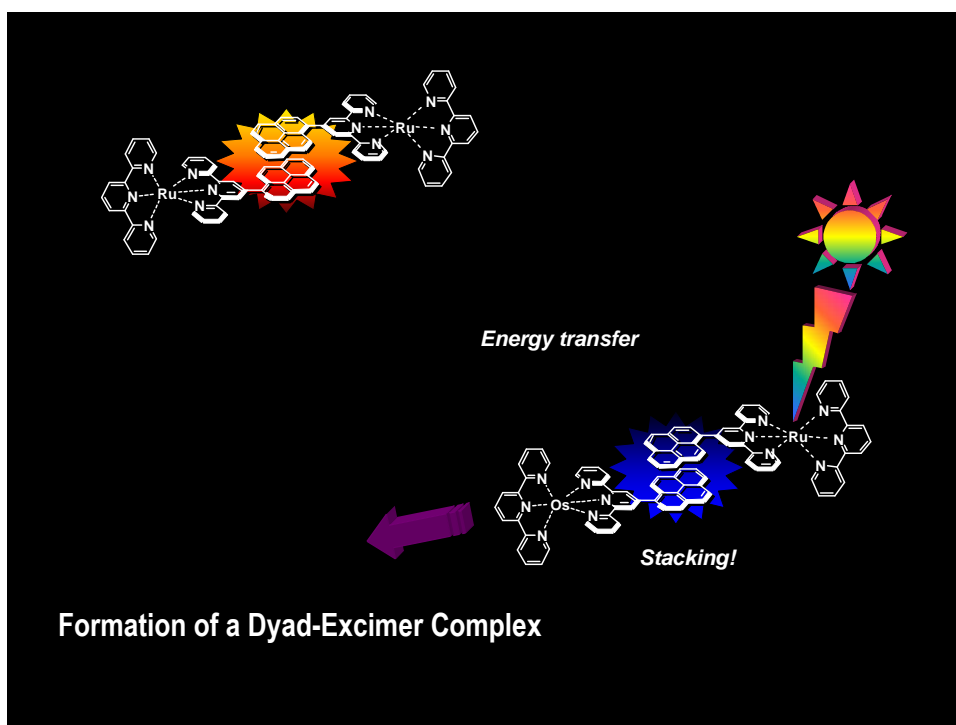


Fig VI-9 Hypothetic energy-level diagram of $\text{Ru}(\text{tpy})_2^{2+}$ -(Pyr...Pyr)- $\text{Os}(\text{tpy})_2^{2+}$



The excimer formation is possible after excitation by light of one monomer. The excited state can delocalise its electrons via MLCT from the metallic center to the pyrenic part of the ligand. If this pyrenic part reaches the $^3(\pi-\pi)^*$ excited state level the formation of dimer is possible (Fig IV-9). The heterodinuclear dyad formation between a Ru, Os tpy pyrene

complexes can be studied by excitation of the Ru based part of the system at the wavelength of its MLCT absorption.

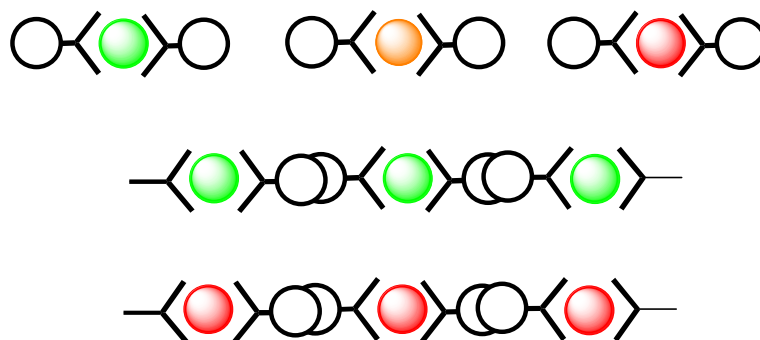


Fig VI-10 Excimer formation of two different complexes with photochemically induced excited state Ru (red), Os (green) nucleus

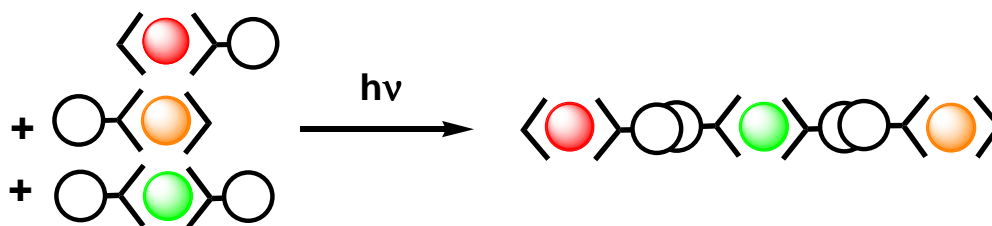


Fig VI-11- Photochemically induced excited state triad Ru (red), Os (green), Ir (orange) nucleus

V- Synthesis of Ru, Os and Ir complexes with 1-pyrenyl substituted tpy ligand.

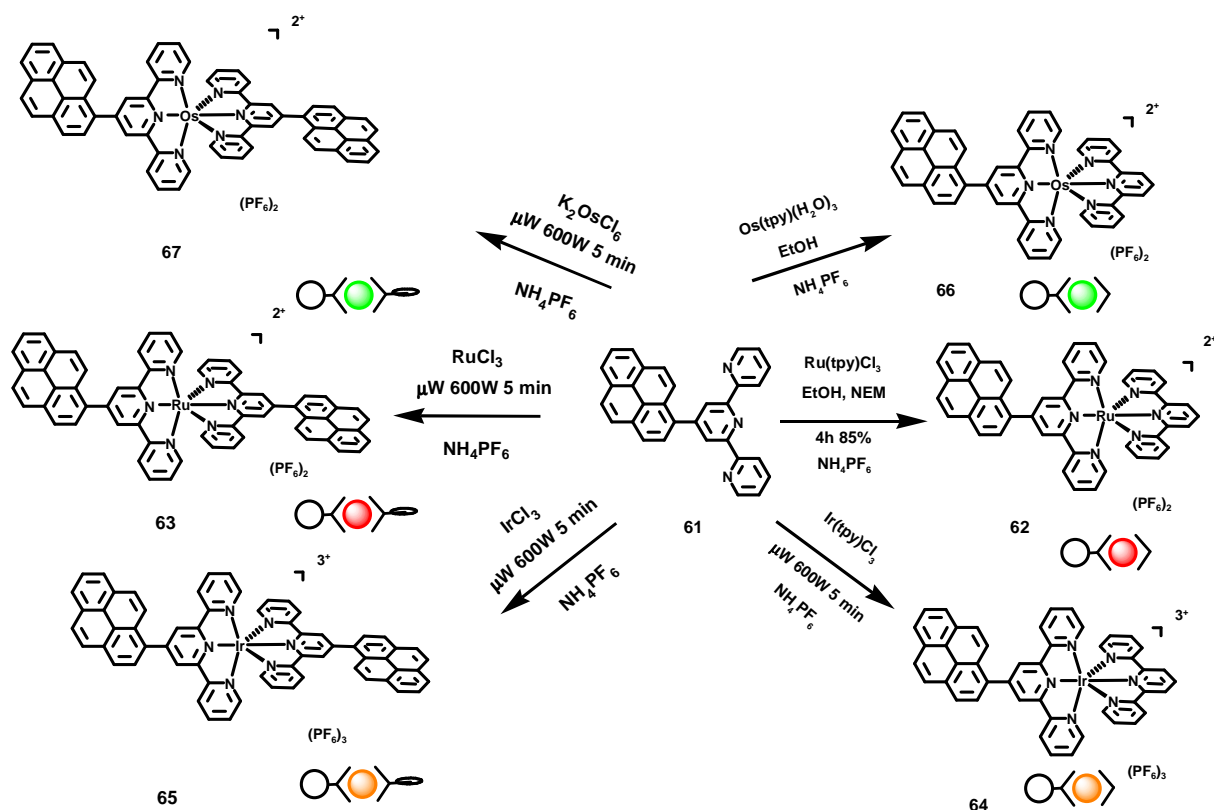


Fig VI-12-Synthesis of new 1-pyrenyl substituted tpy complexes.

The pyrenyl substituent can be employed in several configurations, and can play different roles in the ligands. To increase the quantum yield and the lifetime of the triplet state of the MLCT of bipyridine type metal-complexes, we can tune the functionality at the periphery of the ligand by adding a chromophoric substituent which can play a role of electron reservoir. Our strategy in the bipyridine functionalisation, is to connect directly a 1-pyrenyl substituent in the 4 and 4' position of a bpy ligand, or indirectly by using a π -electron system as spacer. These are (Fig VI-12) by example the complexes we want to synthesize. The ligand **61** was a 1-pyrenyl substituted tpy ligand. Such a ligand has potent π -stacking properties at solid state^[5] and in solution its excimeric properties can be interesting. The synthesis was according to the normal procedure for 4-tpy substituted ligand formation. We started with 1-pyrenecarbaldehyde which reacted with 2-acetylpyridine in basic medium, during 5 hours; the reaction mixture was then treated with NH_4OAc during 24 hours at 80°C and the compound **61** was obtained with 34 % yield.

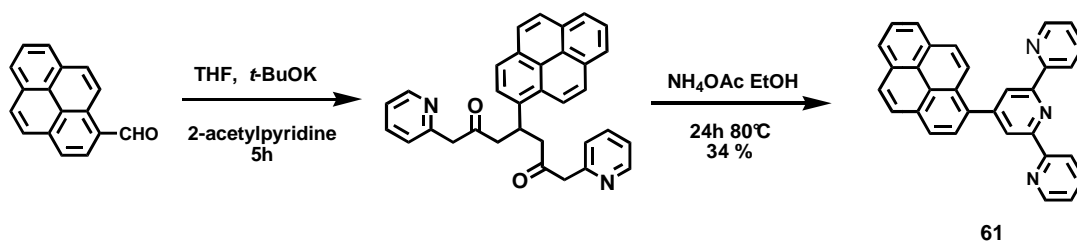


Fig VI-13-Synthesis of ligand **61**.

The compound **61** was characterised by ^1H NMR spectroscopy and FAB-MS and its crystal structure was elucidated.

Crystal Structure of **61**.

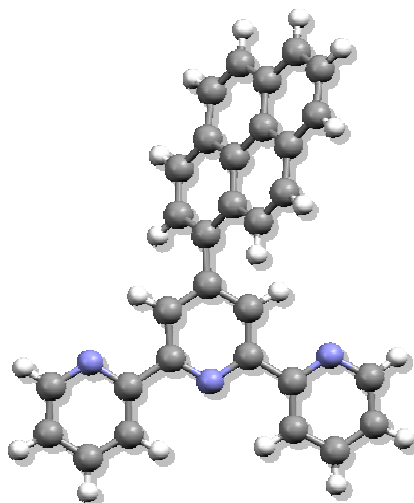


Fig VI- 14-X-Rays Crystal representation of **61** Interatomic distances (\AA)

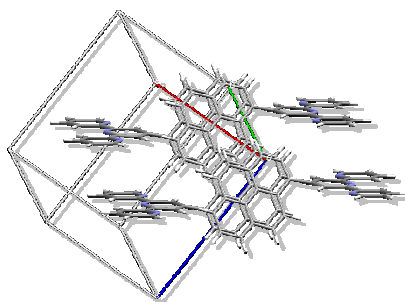


Fig VI- 15- π - π stacking between two **61** molecules.

H-Bond distance table

H-Bond	l(Å)	Angle (°)
C7--H7··N1	2.767(2)	100.00
C9--H9··N3	2.776(2)	100.00
C12--H12··N2	2.836(2)	100.00
C18--H18··N2	3.480(3)	153.00

Synthesis of [Ru(**61**)(tpy)][PF₆]₂

The mononuclear terpyridine complex containing a ruthenium metallic center and a 1-pyrenyl substituent is obtained after complexation of the free ligand tpy-pyr with the trischloroterpyruthenium complex, after 4 hours of reaction at reflux in ethanol, and after addition of NEM (Fig IV-). The red metallic complex [Ru(**61**)(tpy)][PF₆]₂ is obtained after precipitation of the reactional mixture with addition of NH₄PF₆. This complex was

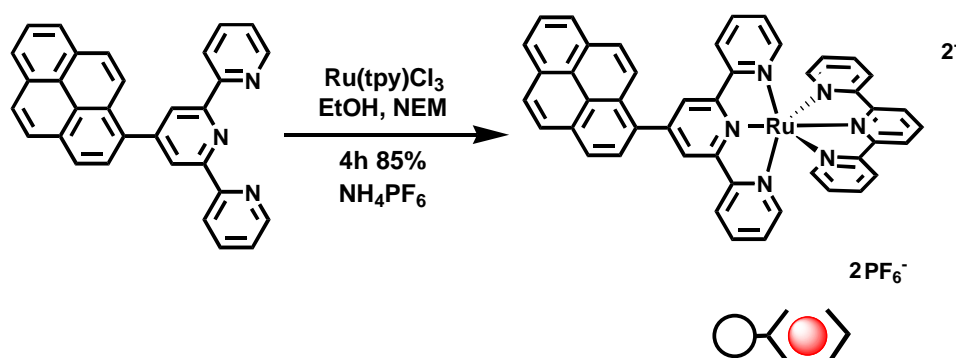


Fig IV-16-Synthesis of **62**.

characterised with ¹H and ¹³C NMR spectroscopies, ES-MS and mass analysis. The 2D spectras allowed us to assigned the differents protons from the two differets terpyridine systems.

COSY H-H spectrum at 500 MHz in CH₃CN.

The COSY spectrum of **62**, show vicinals coupling between H^{3A} and the pyrenyl Pyr-H² proton

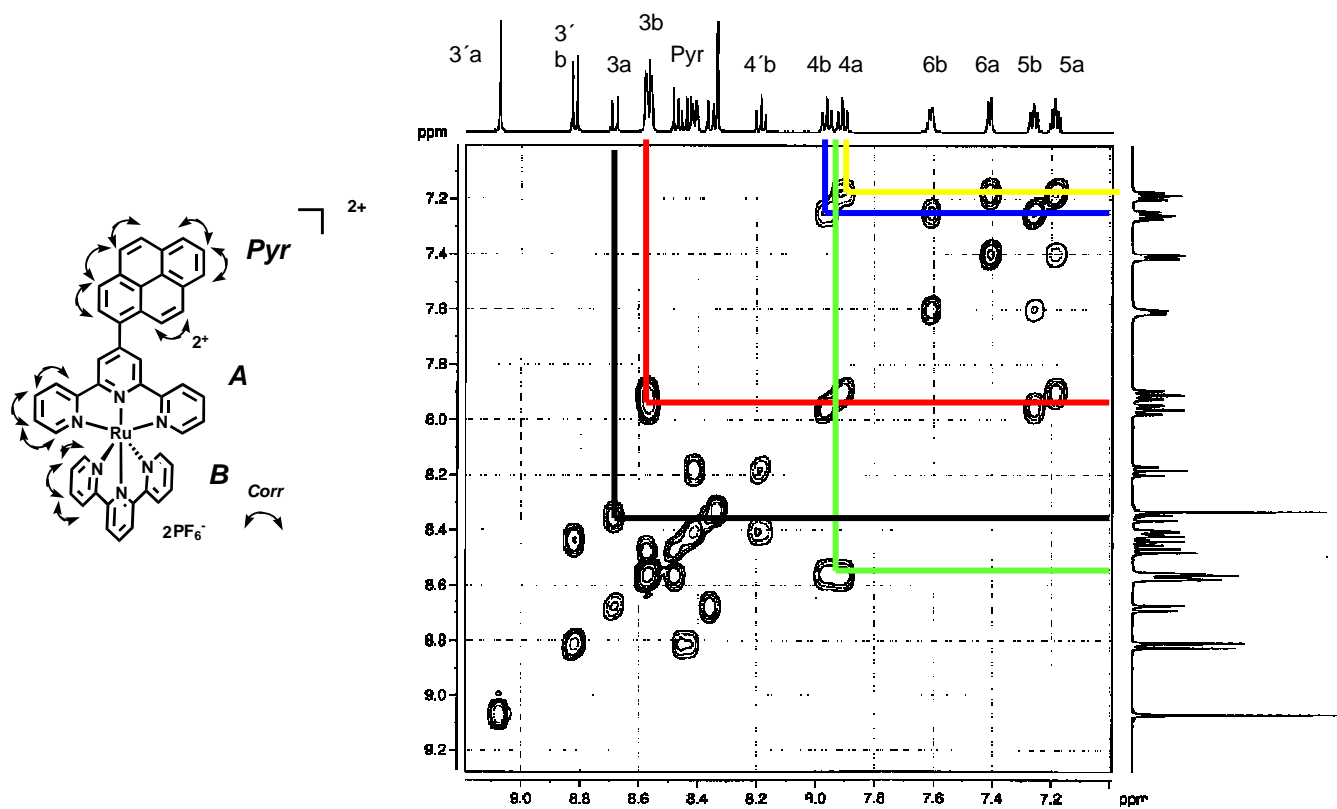
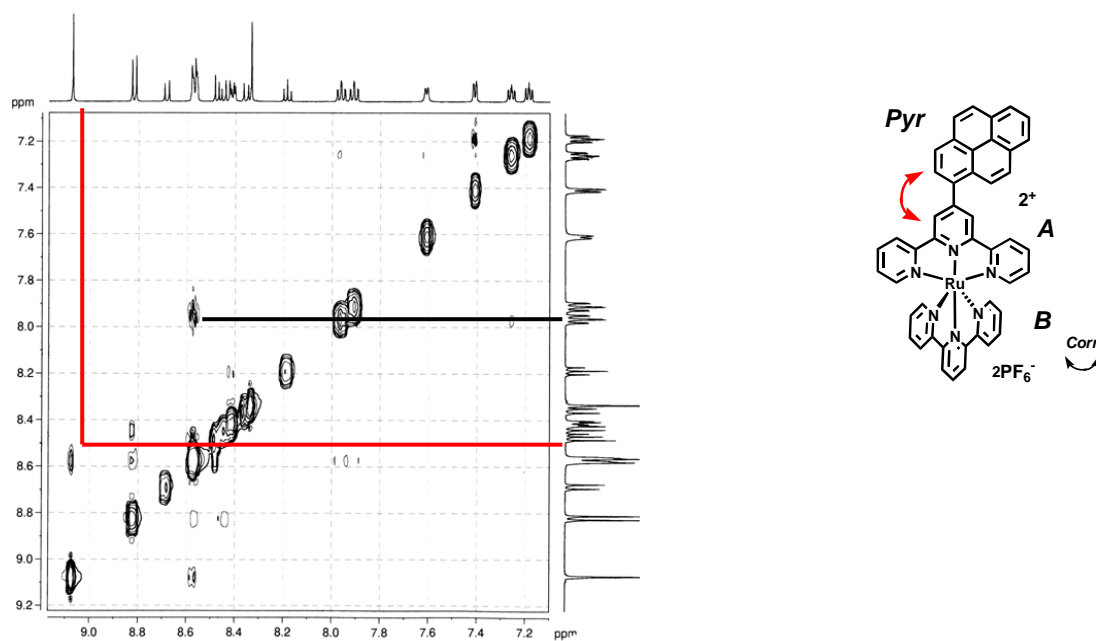


Fig VI-17-COSY H-H spectrum of **62** in CD_3CN at 500 MHz at 298 K.

nOesy spectrum of **62** at 500 MHz at 298 K in CD_3CN .



δ (ppm)	9.07	8.82	8.68	8.57	8.50-8.33	8.19	7.96	7.91	7.61	7.41	7.26	7.18
spin mult	<i>s</i>	<i>d</i>	<i>d</i>	<i>d</i>	<i>m</i>	<i>t</i>	<i>t</i>	<i>t</i>	<i>d</i>	<i>d</i>	<i>t</i>	<i>t</i>
attribution	3'A	3'B	3A	3B	Pyr	4'B	4B	4A	6B	6A	5B	5A
Integration	2H	2H	2H	2H	9H	2H	2H	1H	2H	2H	2H	2H
<i>J</i> (Hz)	2	8	9.5	8		7.5	8	8	5.4	5.3	6.6	6.7

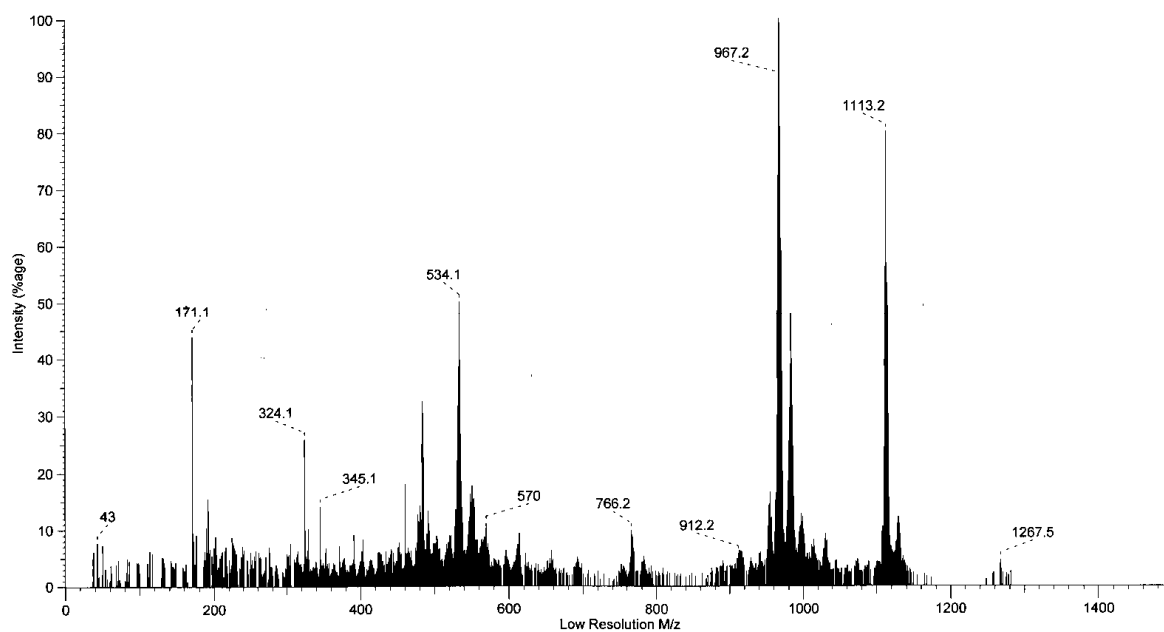


Fig VI-18- ES-MS of complex $[\text{Ru}(\mathbf{61})_2](\text{PF}_6)_2$

Synthesis of $[\text{Ir}(\mathbf{61})(\text{tpy})][\text{PF}_6]_2$.

The mononuclear terpyridine complex containing a ruthenium metallic center and a 1-pyrenyl substituent is obtained after complexation of the free ligand **61** with $[\text{Ir}(\text{tpy})\text{Cl}_3]$ complex, after 4 hours of reaction at reflux in ethanol, and after addition of (Fig IV-19). The red metallic

complex $[\text{Ir}(\mathbf{61})(\text{tpy})][\text{PF}_6]_2$ is obtained after precipitation of the reaction mixture with addition of NH_4PF_6 . This complex was

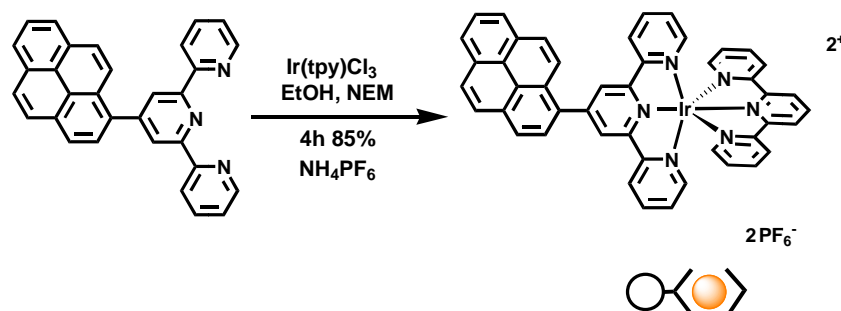


Fig IV-19- Synthesis of $[\text{Ir}(\mathbf{61})(\text{tpy})][\text{PF}_6]_2$.

characterised with ^1H and ^{13}C NMR spectroscopies, ES-MS and mass analysis. The 2D spectras allowed us to assigned the differents protons from the two differets terpyridine systems.

ES-MS of $[\text{Ir}(\mathbf{61})(\text{tpy})(\text{PF}_6)_3]$.

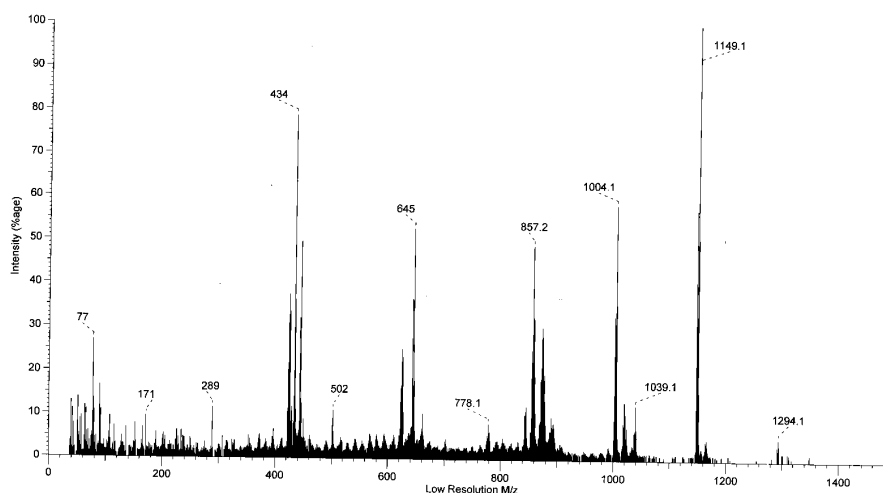


Fig VI-20-ES-MS of $[\text{Ir}(\mathbf{61})(\text{tpy})](\text{PF}_6)_3$.

The FAB mass spectrum showed differents peaks describing the $[\text{Ir}(\mathbf{61})(\text{tpy})](\text{PF}_6)_3$ structure with characteristic fragments of heteroleptic polypyridine complexes with PF_6^- as salt counterion. At m/z : 1294.1 we had the peak corresponding to the cationic fragment $[\text{Ir}(\mathbf{61})(\text{tpy})(\text{PF}_6)_2]^+$ with the lost of one PF_6^- of the molecular weight; at 1149.1

$[\text{Ir}(\mathbf{61})(\text{tpy})(\text{PF}_6)]^{2+}$, at m/z : 1004.1 that peak corresponded to the 3+ charged complex $[\text{Ir}(\mathbf{61})(\text{tpy})]^{3+}$.

Synthesis of 66.

The synthesis was according to the same procedure as $[\text{Ru}(\mathbf{61})(\text{tpy})](\text{PF}_6)_2$. To obtain the heteroleptic precursor we synthesised the complex $[\text{Os}(\text{tpy})(\text{H}_2\text{O})_3]\text{Cl}_2$. The complex $[\text{Os}(\text{tpy})\text{Cl}_3]$ was obtained after reaction of $\text{K}_2[\text{OsCl}_6]$ with tpy in MeOH:H₂O (4:1 v/v) at reflux during 6 hours. After cooling and filtration the black solid $[\text{Os}(\text{tpy})\text{Cl}_3]$ was reacted without purification with water and AgNO_3 solution during 3 days at reflux. After reaction the reaction mixture was removed of its half volume and treated with NH_3 (1M) solution and ultrasonic bath during 15 min. The compound $[\text{Os}(\text{tpy})(\text{H}_2\text{O})_3](\text{NO}_3)_3$ was obtained after filtration and recrystallisation in MeOH. This compound reacted with the free ligand **61** and heated in microwave oven during 5 min at 600 W in diethylene glycol. After cooling the reaction mixture the brown slurry was filtered over celite and solvent removed. The complex was recollected by washing the celite with CH_3CN and purification with column chromatography using SiO_2 A and Asol as eluant, recrystallised from MeOH and reprecipitated with NH_4PF_6 . The $[\text{Os}(\mathbf{61})(\text{tpy})](\text{PF}_6)_2$ complex structure was characterised by NMR ^1H , ES-MS spectroscopies.

Photophysical and electrochemical properties of the 4-pyrenyl-2,2':6',2''-terpyridine complexes.

The photophysical and the electrochemical properties of the ligand and the complexes have been studied by UV/Vis spectroscopy. The steady-state and the transient absorption and emission UV/Vis spectrum have been measured in DCM for the ligand, and in MeCN for the complexes emission spectrum. The lifetimes have been determined by single photon counting.

UV/Vis steady-state absorption spectroscopy.

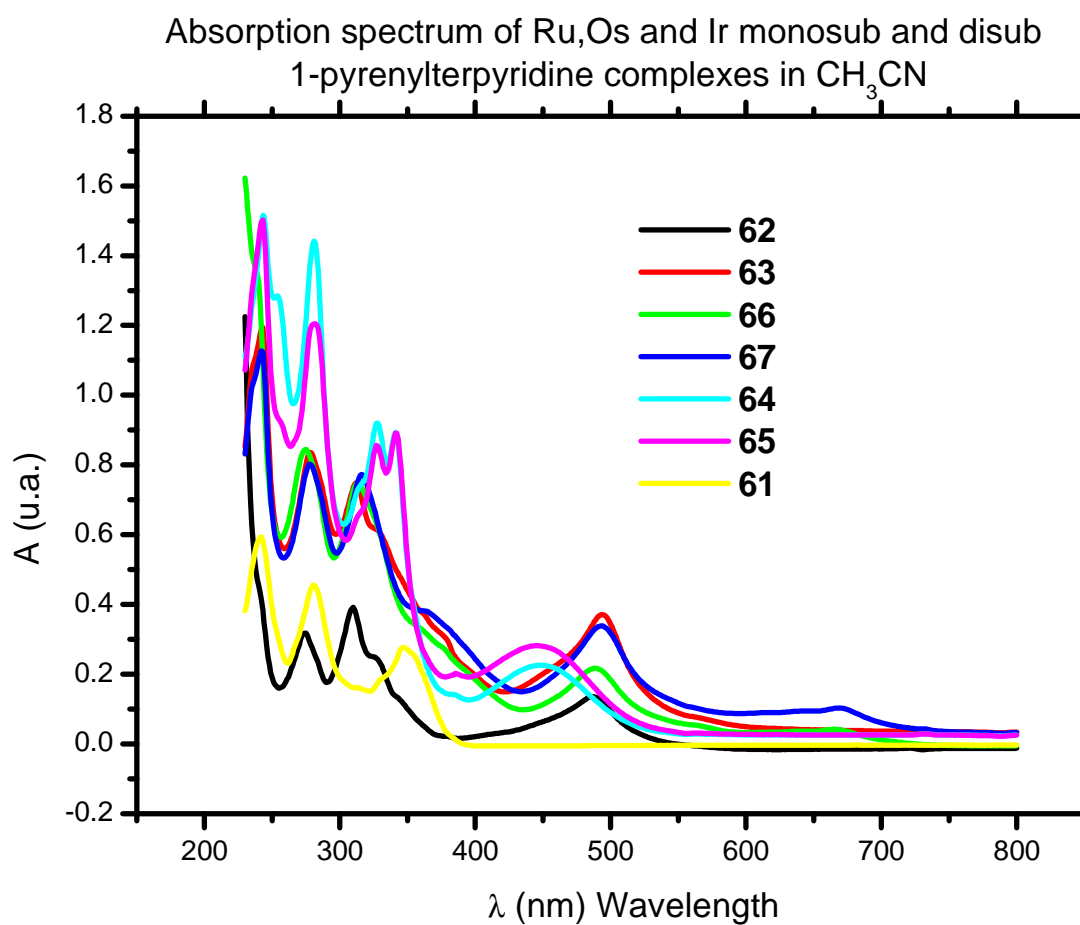


Fig VI-19- Absorption spectra of complex ligand **61** (type) in DCM and complexes **62, 63, 64, 65, 66, 67** in MeCN.

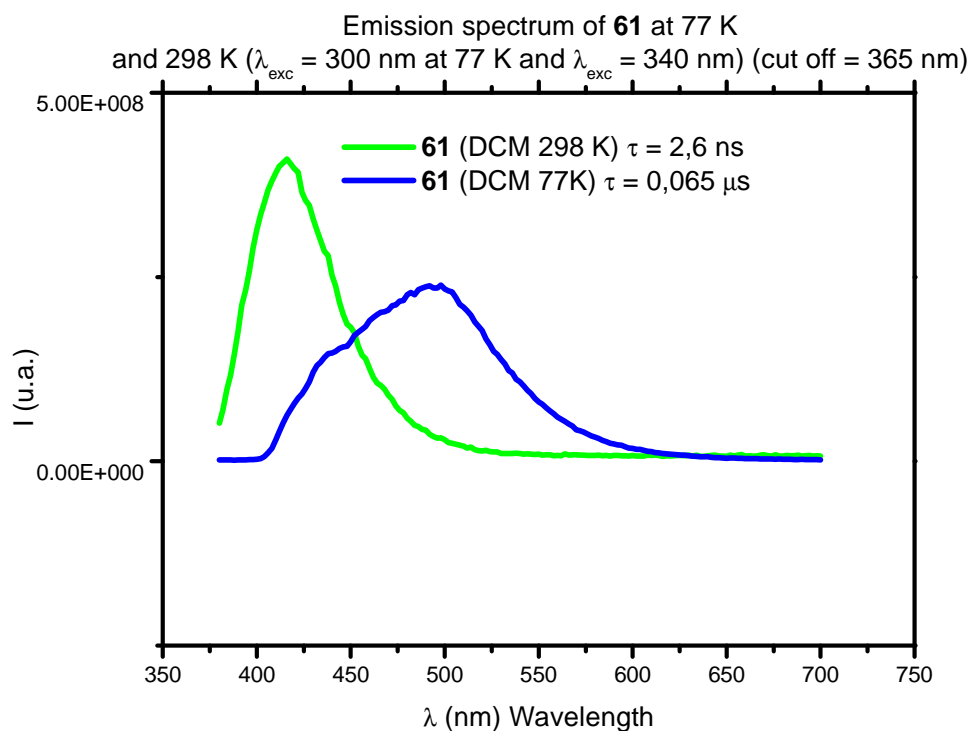


Fig VI-20- Emission spectra of ligand **61** in DCM at 298 K (green) and at 77K (blue).

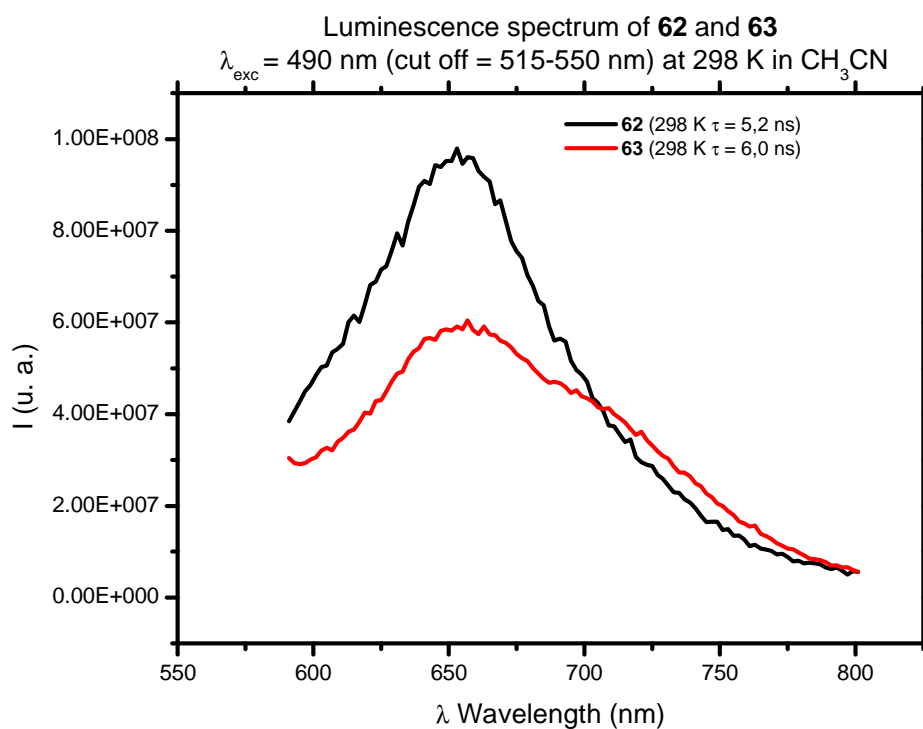


Fig VI-21- Emission spectra of complex **62** and **63** in CH_3CN

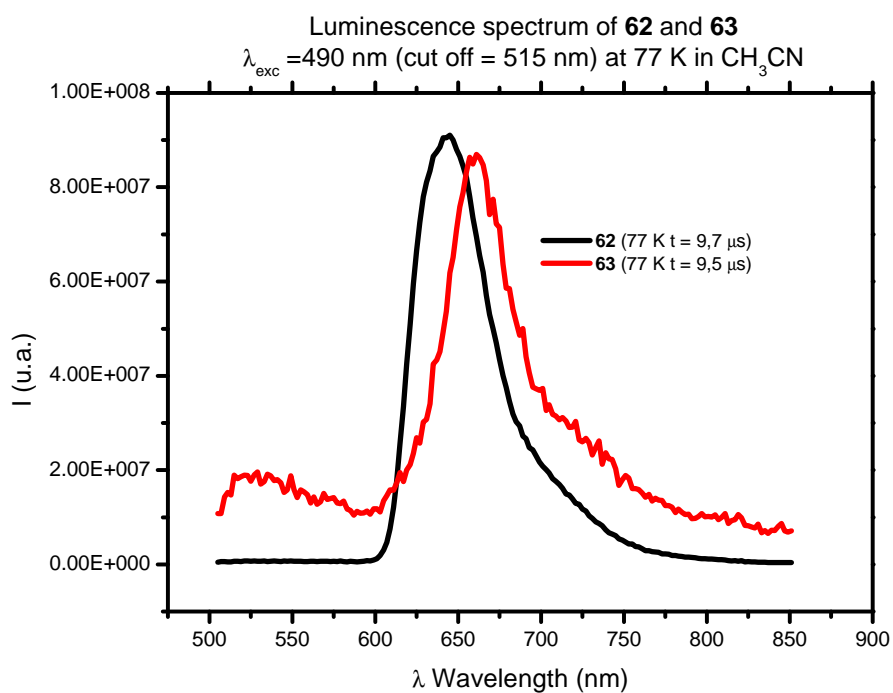


Fig VI-22- Emission spectra of complex **62** and **63** and in CH₃CN at 77 K.

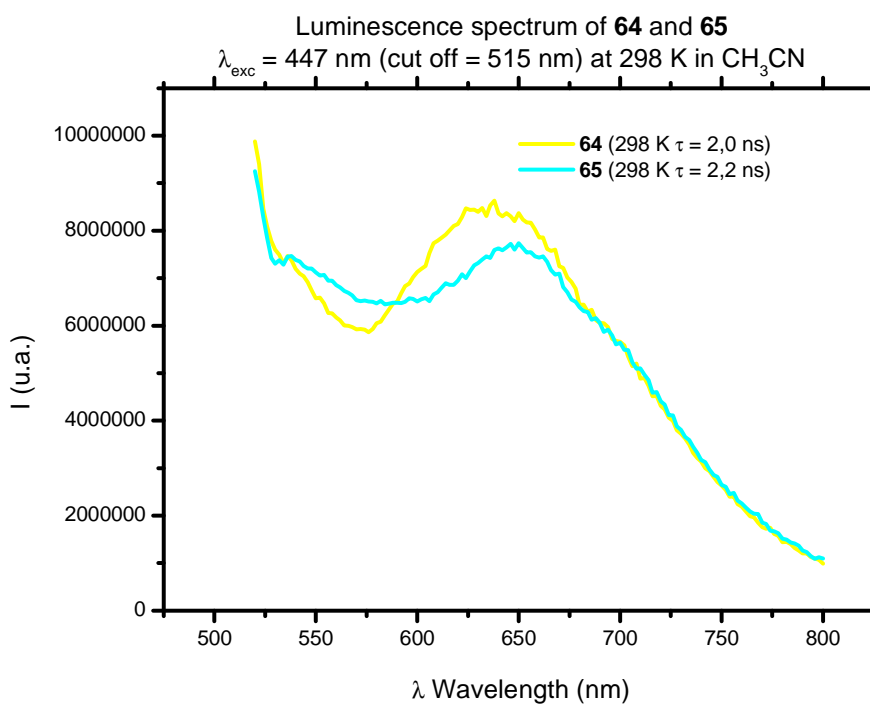


Fig VI- 23- Emission spectra of complex **64** and **65** in CH₃CN at 298 K.

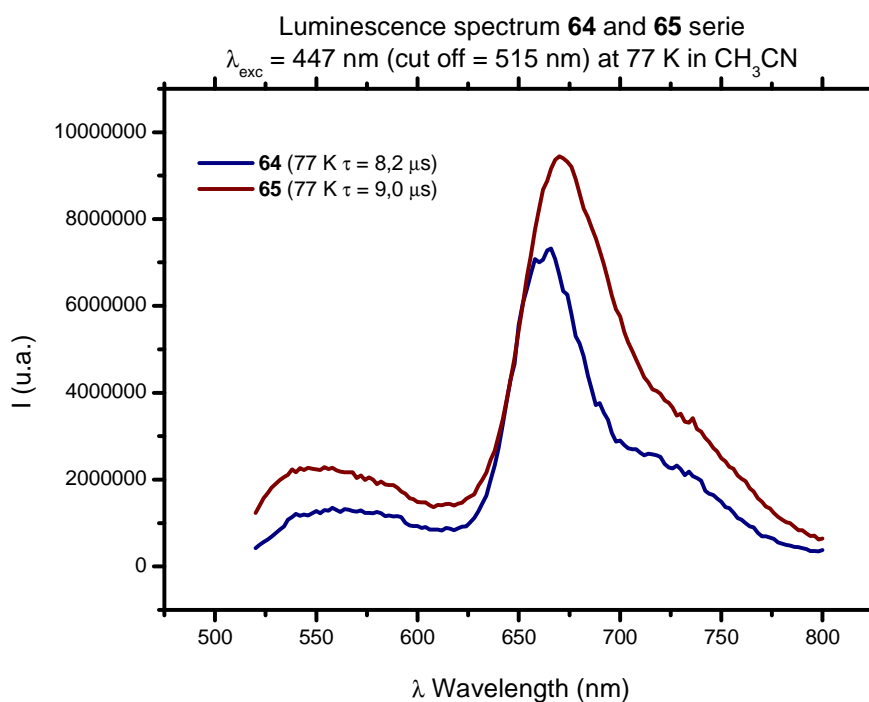


Fig VI-24 Emission spectra of complex **64** and **65** in CH_3CN at 77 K.

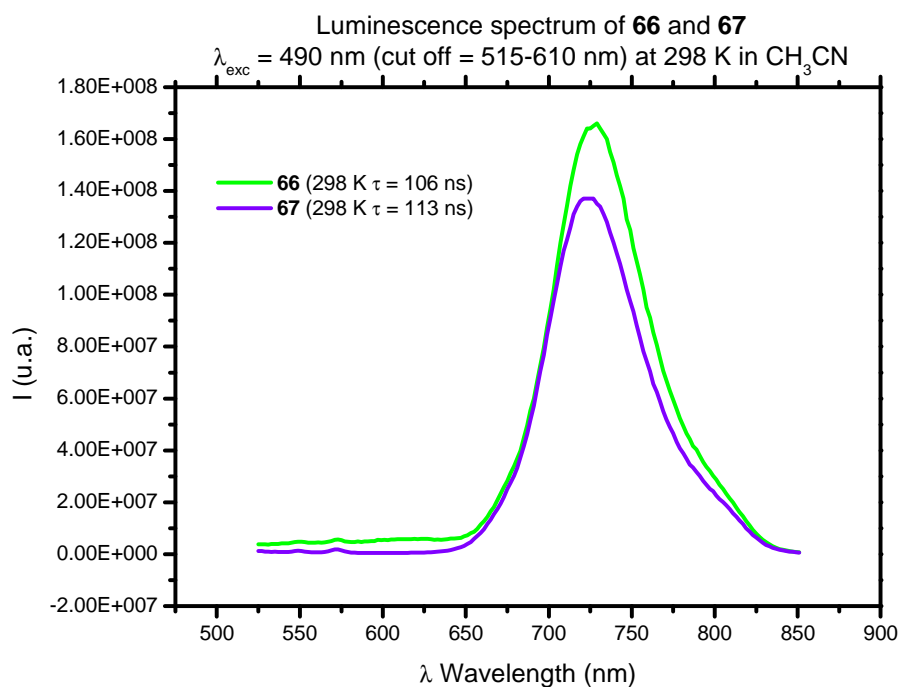


Fig VI-25 Emission spectra of complex **66** and **67** in CH_3CN at 298 K.

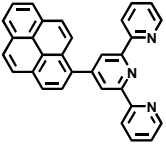
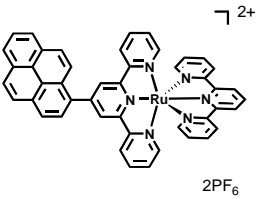
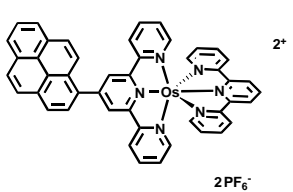
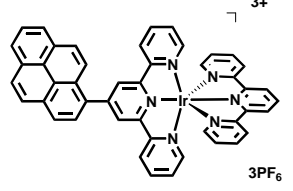
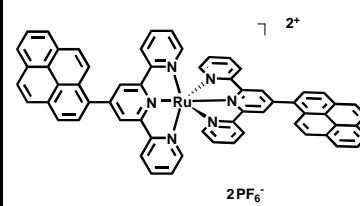
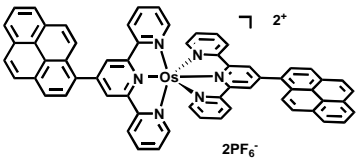
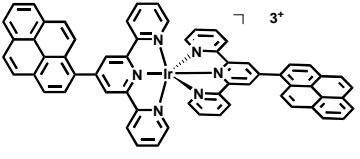
Formula	Name solvent	Absorption		Emission 298 K air equilibrated			Emission 77 K air equilibrated	
		λ_{\max} (nm)	$\epsilon(\text{M}^{-1}\text{cm}^{-1})$	λ_{\max} (nm)	ϕ	τ (ns)	λ_{\max} (nm)	τ (μs)
	61 (DCM)	<u>LC</u> 347 330 275 202	23600 23800 24200 37600	415	1.0	2.6	470	0.065
	62 (CH₃CN)	<u>MLCT</u> 487 <u>LC</u> 308 272 239 232	37600 110000 92200 117000 118500	653	$3.5 \cdot 10^{-5}$	5.2	643	9.7

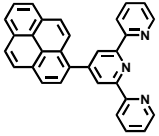
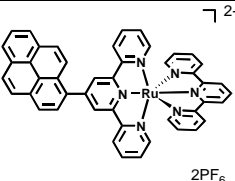
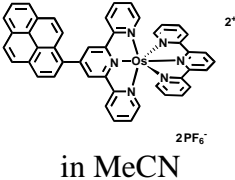
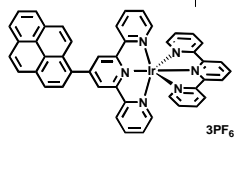
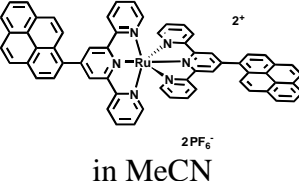
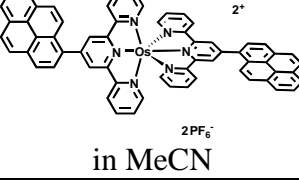
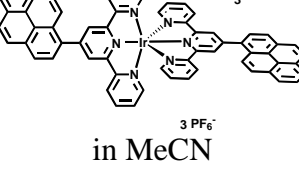
Table VI – Photophysical parameters of luminescence of pyrenyl type compounds.

Formula	Name (solvent)	Absorption		Emission 298 K air equilibrated			Emission 77 K air equilibrated											
		λ_{\max} (nm)	$\epsilon(M^{-1}cm^{-1})$	λ_{\max} (nm)	ϕ	τ (ns)	λ_{\max} (nm)	τ (μs)										
  	63 (CH₃CN)	MLCT 665 489	1200 15900	729	0.017	106 (182)	713	4.5										
	64 (CH₃CN)	LC 308 272 239 232	74000 68000 111000 120500						638	$8.5 \cdot 10^{-4}$	2,0	665	8.2					
	65 (CH₃CN)	MLCT 494	7100											690	$5.8 \cdot 10^{-5}$	6,0	661	9.5
		LC 338 325 278 240	37000 62392 40100 71000															

	<p>66 (CH₃CN)</p>	<p><u>MLCT</u> 668 <u>LC</u> 491 313 275 239</p>	<p>3130 19100 54000 56500 81600</p>	<p>728 0.019 113 732</p>	<p>4.5</p>
	<p>67 (CH₃CN)</p>	<p><u>MLCT</u> 445 <u>LC</u> 328 283 266 226 201</p>	<p>14700 83100 91000 94400 147000 166000</p>	<p>650 3.4 10⁻³ 2,2 671</p>	<p>9.0</p>

Electrochemical investigations

The redox potential of ligand complexes have been measured by cyclovoltammetry and differential pulse method .

<u>Compound</u>	$E_{red}(V)$	$E_{ox}(V)$
 <p>in DCM</p>		-0.613 V, -0.805 V, -0.194 V, -0.632 V, -1.422 V, -1.976 V, -2.324 V
 <p>in MeCN</p>	+1.132 V	-0.644 V, -1.015 V
 <p>in MeCN</p>	+0.529 V +1.711 V	-0.679 V, -1.201 V -0.503 V, -1.399 V, -1.938 V, -2.145 V, -2.603 V
 <p>in MeCN</p>	+1.230 V	-1.026 V, -1.238 V, -1.682 V, -2.286 V, -2.527 V
 <p>in MeCN</p>	+0.655 V	-1.163 V, -1.52 V, -1.777V, -2.366 V, 2.694 V..
 <p>in MeCN</p>	+0.856 V +1.712 V	-1.077 V, -1.417 V, -1.651 V, -1.807 V, -2.119 V, -2.361 V. -2.678 V.
 <p>in MeCN</p>	+0.947 V	-1.078 V, -1.188 V, -1.561 V, -1.954 V, -2.508 V

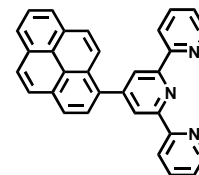
Conclusion:

The 1-pyrenyl substituted terpy complexes have very interesting properties due to the presence of pyrene substituent which could play an electron reservoir role in the complexes when they are excited at the MLCT level. The second possible property was to form excimeric dimers with the different complexes, and forming non-rigid bridged dyad at excited state. However the desired excited state of the pyrene substituent was not reached according to the lifetimes and quantum yields obtained and the electron-reservoir equilibrium was observed after excitation at the MLCT max absorbance only for the complexes **64** and **65** in MeCN.

Experimental Section

Synthesis of 61.

2-Acetylpyridine (2.03 g, 16.8 mmol) was added dropwise to a solution of *t*-BuOK (4.0 g) in dry THF (50 ml). This was stirred at room temperature for 30 min to result in a creamy yellow suspension, before 1-pyrenecarboxaldehyde (2.0 g, 8.7 mmol) in THF (30 ml) were added.

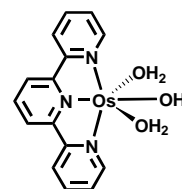


Immediately, the solution turned a bright clear orange to red. It was left stirring for 17 hours at room temperature. A suspension of NH₄OAc (15 g) in EtOH/AcOH (2:1 v/v 200 ml) was added to the reaction mixture. The mixture was heated to reflux for 24 hours and the reaction mixture is cooled and distilled water is added a yellow precipitate of **61** is obtained after filtration over büchner filter. (m= 1,28 g, Yield = 34 %).

Experimental datas : Formula :C₃₁H₁₉N₃. **NMR** ¹H (400 MHz) in CD₃CN : 9.34 (2H, s) **H**_{3'}, 8.77 (d, 1H) **H**_{pyr}, 8.61 (d, 2H, *J* = 8.1 Hz) **H**₃, 8.55-8.44 (m, 5H) **H**_{pyr} 8.25 (s, 1H) **H**_{pyr}, 8.29-7.89 (m, 9H) **H**_{pyr}, 7.97 (t, 2H, *J* = 7.75 Hz) **H**₄, 7.47 (d, 2H, *J*= 4.75 Hz) **H**₆, 7.47 (m, 2H) **H**₅. **FAB-MS**: *m/z* [*M*⁺]: 433. **IR** (ν cm⁻¹): 3035 (w), 2358.8 (w), 1583.4 (w), 1396.4 (w), 840.9 (s). **UV Absorption** λ_{max} : 344, 289 nm **Emission** λ_{max} : 424 nm.

Synthesis of [Os(tpy)(H₂O)₃][PF₆]₂.

2,2':6',2''-Terpyridine (0.21 g, 0.91 mmol) and (NH₄)₂[OsCl₆] (0.40 g, 0.91 mmol) were suspended in 60 ml of a water and MeOH mixture (1:4), and the mixture heated to reflux during 4 hours. After cooling the precipitate was filtered and washed with a small amount of cold MeOH and dried (71 mg). Half of the reaction solvent is removed

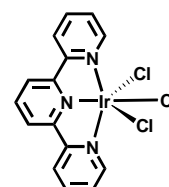


under reduced pressure and an additional 20 mg of solid from this solution (273 mg Yield : 51 %), black solid. The product was used in the second step without characterisation and purification. [Os(tpy)Cl₃] (0.20 g, 0.38 mmol) and AgNO₃ (98 mg, 0.38 mmol) were refluxed in water (150 ml) for 3 days. The solvent was reduced in volume to 70 % and the resulting dark solution stirred into a saturated solution of NH₄PF₆ in water (50 ml). After 15 min the

precipitate was collected by filtration and treated with diluted 1 M NH₃ in an ultrasonic bath for 2 h to remove AgCl. The product was isolated by filtration, washed with water and EtOH and dried under vacuum (100 mg, Yield : 34 %). C₁₅H₁₇N₃O₃OsP₂F₁₂, black powder.

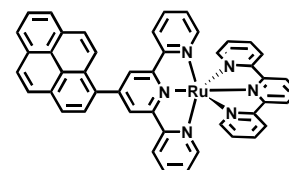
Synthesis of [Ir(tpy)Cl₃].

88.0 mg (0.377 mmol) of 2,2':6',2''-terpyridine and 120 mg (0.402 mmol) of IrCl₃·H₂O were suspended in 10 ml of ethylene glycol, and degassed by bubbling with N₂ through the solution for 10 min. This suspension was heated to 160°C for 15 min in the dark. A red precipitate formed was filtered off, washed with EtOH, water and ether. Yield : 160 mg (80 %).



Synthesis of **62**.

[Ru(tpy)Cl₃] (200 mg, 0.76 mmol) and of **61** (659 mg, 0.76 mmol) are dissolved in EtOH (10 ml) 10 drops of NEM are added then the mixture is held at reflux for four hours. After reaction, the mixture is treated with a saturated aqueous solution

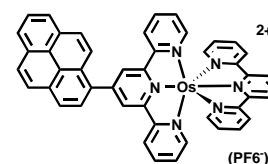


of NH₄PF₆ and the precipitate removed and dissolved in acetonitrile and chromatographed over silica with Asol as eluent. A brown dark solid is obtained after reprecipitation from methanol (m = 684 mg, Yield = 85 %).

Experimental datas : ¹H NMR in CD₃CN (δ ppm) at 500 MHz : 9.07 (s, 2H) **H**^{3,A}, 8.82 (d, 2H, J = 8 Hz) **H**^{3B}, 8.68 (d, 1H, J = 9.5 Hz) **H**^{3A}, 8.57 (d, 6H, J = 8Hz) **H**^{3B}, 8.50-8.33 (m, 9H) **H**^{Pyr}, 8.19 (t, 1H, J₁ = 7.5 Hz) **H**^{4,A}, 7.96 (t, 2H, J₁ = 8 Hz) **H**^{6B}, 7.91 (t, 2H, J = 8 Hz) **H**^{6A}, 7.61 (d, 2H, J = 5.4 Hz) **H**^{4B}, 7.41 (d, 2H, J = 5.3 Hz) **H**^{4A}, 7.26 (ddd, 2H, J₁ = 6.6 Hz) **H**^{5B}, 7.19 (ddd, 2H, J₁ = 6.7 Hz) **H**^{5A}. ¹³C NMR in CD₃CN at (MHz): 208.8, 159.2, 159.1, 156.4, 156.2, 153.64, 153.57, 149.7, 139.2, 139.1, 136.9, 134.3, 133.2, 132.5, 131.9, 129.9, 129.8, 129.6, 129.0, 128.5, 127.9, 127.2, 126.8, 126.32, 126.30, 125.8, 125.6, 125.5, 125.4, 125.36, 124.8. **ES-MS** : [M⁺-(PF₆⁻)] 914.9, [M⁺-2(PF₆⁻)] 830.1, 384.1. **IR** (ν cm⁻¹): 3072.4 (w), 2358.8 (w), 1600.8 (w), 1448.4 (w), 1244.0 (w), 995.2 (w), 833.2 (s). **UV** (MeCN) *Absorption* λ_{max} : 487 nm *Emission* λ_{max} : 653 nm.

Synthesis of **63**.

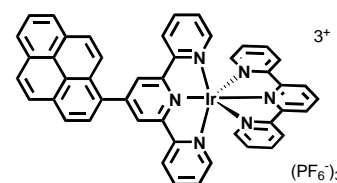
[Os(tpy)(H₂O)₃]Cl₃ (240 mg, 0.41 mmol) and of **61** (178 mg, 0.41 mmol) are dissolved in diethyleneglycol (10 ml) heated under microwave at 600 W during 5 min, after cooling the reaction mixture is precipitate with NH₄PF₆ to give a brown precipitate. The brown slurry is filtered over celite and the brown-red complex is extracted after dissolution with CH₃CN. The filtrate is evaporated to dryness and then washed with acetonitrile and purified with a silica column using Asol as eluant. We obtained a nice brown complex after reprecipitation with NH₄PF₆ in methanol. (m = 260 mg, Yield = 80 %).



Experimental Datas : ¹H NMR in CDCl₃ (δ ppm) : ¹H NMR in CD₃CN (δ ppm) at 500 MHz : 9.11 (s, 2H) **H**^{3,A}, 8.86 (d, 2H, J = 7.8 Hz) **H**^{3,B}, 8.68 (d, 6H, J = 9.5 Hz) **H**^{3,B}, 8.59-8.35 (m, 9H) **H**^{Pyr}, 8.22 (t, 1H, J = 8.5 Hz) **H**^{4,B}, 7.85 (t, 2H, J₁ = 7.75 Hz) **H**^{6,B}, 7.80 (t, 2H, J = 7.75 Hz) **H**^{6,A}, 7.51 (d, 2H, J = 6.75 Hz) **H**^{4,B}, 7.33 (d, 2H, J = 6.75 Hz) **H**^{4,A}, 7.23 (t, 2H, J₁ = 5.75 Hz) **H**^{5,B}, 7.15 (t, 2H, J = 5.75 Hz) **H**^{5,A}. **ES-MS** : 920.1, 429.7. **IR** (ν cm⁻¹): 2360 (w), 1421 (s), 821 (s).

Synthesis of **64**.

[Ir(tpy)Cl₃] (200 mg, 0.67 mmol) and (580 mg, 1.34 mmol) of **61** are dissolved in EtOH (10 ml) are added then the mixture is carry at reflux for four hours. After reaction the mixture is treated with an saturated aqueous solution of NH₄PF₆ and the precipitate removed and dissolved in acetonitrile and chromatographed over silica with Asol as eluent , a brown dark solid is obtained after reprecipitation in methanol (m = 685 mg, Yield = 85 %).

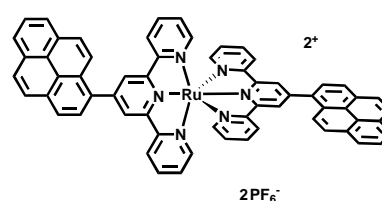


Experimental data: ¹H NMR at 500 MHz (CD₃CN) : ¹H NMR in CD₃CN (δ ppm) at 500 MHz : 9.17 (s, 2H) **H**^{3,A}, 8.89 (d, 2H, J = 8.5 Hz) **H**^{3,B}, 8.79 (t, 1H, J = 9.5 Hz) **H**^{4,B}, 8.68 (d, 6H, J = 9 Hz) **H**^{3,B}, 8.63-8.35 (m, 9H) **H**^{Pyr}., 8.24 (t, 2H, J₁ = 7.25 Hz) **H**^{6,B}, 8.19 (t, 2H, J = 7 Hz) **H**^{6,A}, 7.80 (d, 2H, J = Hz) **H**^{4,B}, 7.64 (d, 2H, J = 6 Hz) **H**^{4,A}, 7.57 (t, 2H, J₁ = Hz) **H**^{5,B},

7.49 (t, 2H, $J = 5.75$ Hz) \mathbf{H}^{5A} . ^{13}C NMR (CD_3CN): 157.9, 156.8, 154.8, 154.4, 153.6, 153.5, 143.7, 142.9, 142.8, 133.05, 131.4, 130.8, 129.8, 129.6, 129.5, 128.1, 128.0, 127.5, 127.4, 127.3, 127.1, 126.7, 126.6, 126.2, 125.3, 124.8. **ES-MS** : 1294.1($[\text{M}^+]$), 1149.1($[\text{M}^+(\text{PF}_6^-)]$), 1004.1($[\text{M}^+(2\text{PF}_6^-)]$), 857.2 ($[\text{M}^+(3\text{PF}_6^-)]$). **IR** (v cm^{-1}): 3375.2 (w), 2360.7 (w), 1608.5 (s), 1477 (s), 1247 (w), 1031.9 (s). 833 (s). **Elementar-Analysis:** $\text{C}_{46}\text{H}_{30}\text{N}_6\text{IrP}_3\text{F}_{18}$: (% *calculated*) C : 42.16 % (42.65), H : 2.32 % (2.52), N : 6.91 % (6.50).

Synthesis of **65**.

61 (200 mg, 0.46 mmol) and $\text{RuCl}_3 \cdot 3\text{H}_2\text{O}$ (60 mg, 22.9 mmol) are dissolved in diethlenglycol (10 ml) and heated under microwave at 600 W during 5 min. After cooling the reaction mixture is precipitated with NH_4PF_6 salt. A brown precipitate appears, the brown

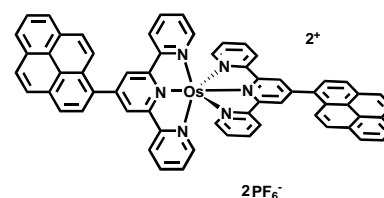


slurry is filtered over celite and the brown-red complex is extracted with CH_3CN and purified with a silica column using Asol as eluant. We obtained a nice brown complex after reprecipitation with NH_4PF_6 in methanol. (m = 260 mg Yield =80 %)

Experimental datas: NMR ^1H (δ ppm): NMR ^1H at 400 MHz in CD_3CN : 9.20 (s, 4H) $\mathbf{H}^{3'}$, 8.77 (d, 2H, $J = 9.2$ Hz) \mathbf{H}^3 , 8.60 (d, 2H, $J_1 = 8$ Hz) \mathbf{H}^3 , 8.70-8.21 (m, 9H) \mathbf{H}^{pyr} , 8.30 (t, 4H, $J = 7.6$ Hz) \mathbf{H}^4 , 7.56 (td, 4H, $J_1 = 7.8$ Hz $J_2 = 2$ Hz) \mathbf{H}^6 , 7.23 (d, 4H, $J_1 = 5.2$ Hz), 7.23 (d, 4H, $J_1 = 7$ Hz) \mathbf{H}^5 . **ES-MS**: 1113.2, 967.2, 460.1. **IR** (v cm^{-1}): 3080.1 (w), 2360.7 (m), 1607 (m), 1454 (m), 1365 (s), 833.2 (s).

Synthesis of **66**.

61 (200 mg, 0.46 mmol) and (112 mg, 0.23 mmol) of K_2OsCl_6 are dissolved in diethylene glycol (10 ml) heated under microwave at 600 W during 5 min. After cooling the reaction mixture is precipitated with NH_4PF_6 . The

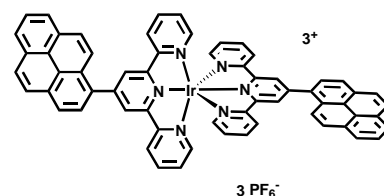


brown slurry is filtered over celite and the brown-black complex extracted with CH_3CN of the celite, the filtrate is removed of his solvent and the solid is washed with acetonitrile and purified with a silica column using Asol as eluant. We obtained a nice black complex after reprecipitation with NH_4PF_6 in methanol. (m = 260 mg Yield =80 %).

Experimental datas NMR ^1H at 400 MHz in CD_3CN : 9.13 (s, 4H) H^3 , 8.77 (d, 2H, $J = 9.2$ Hz) H^3 , 8.50 (d, 2H, $J_1 = 8$ Hz) H^3 , 8.60-8.21 (m, 9H) H^{pyr} , 7.83 (t, 4H, $J = 7.2$ Hz) H^4 , 7.56 (d, 4H, $J = 5.6$ Hz) H^6 , 7.23 (t, 4H, $J_1 = 6$ Hz) H^5 . ^{13}C NMR (at MHz): 161.0, 158.5, 156.8, 155.9, 153.8, 148.8, 138.8, 138.41, 132.3, 131.8, 130.0, 129.9, 129.7, 129.6, 128.7, 128.3, 127.8, 127.2, 126.7, 126.1, 125.7, 125.3, 125.0. **ES-MS** : $[\text{M}^+(\text{PF}_6^-)]$ 1203.1, $[\text{M}^+-2(\text{PF}_6^-)]$ 1058.2, 529.1. **IR** (ν cm^{-1}): 2360.7 (w), 1635.5 (w), 1328.9 (s), 1039 (w), 829 (s). **UV** in CH_3CN Absorption λ_{max} : 668, 491 nm Emission λ_{max} : 728 nm.

Synthesis of 67.

61 (200 mg, 0.46 mmol) of and IrCl_3 , H_2O (69 mg, 0.23 mmol) are dissolved of diethleneglycol (10 ml) (protected from light) and heated under microwave at 600 W during 5 min. After cooling the reaction mixture is precipitated with NH_4PF_6 salt to give a brown precipitate. The brown



slurry is filtered over celite and the intense orange complex is extracted with CH_3CN and purified with a silica column using Asol as eluant. We obtained a nice orange complex after reprecipitation with NH_4PF_6 in methanol. (m = 125 mg Yield = 40 %).

Experimental datas : ^1H NMR in CD_3CN (δ ppm) at 400 MHz: : 9.32 (2H, s) H_3 , 8.51 (d, 2H, $J = 8.1$ Hz) H_3 , 8.51 (d, 1H) H_{pyr} , 8.49-8.34 (m, 5H) H_{pyr} 8.25 (s, 1H) H_{pyr} , 8.29-7.89 (m, 9H) H_{pyr} , 7.97 (t, 2H, $J = 7.75$ Hz) H_4 , 7.47 (d, 2H, $J = 4.75$ Hz) H_6 , 7.51 (m, 2H) H_5 . **ES-MS**: 1349.4 ($[\text{M}^+]$), 1204.2 ($[\text{M}^+(\text{PF}_6^-)]$), 1059.3 ($[\text{M}^+-2(\text{PF}_6^-)]$). **IR** (ν cm^{-1}): 3070 (w), 1602.8 (w), 1450.3 (s), 1307.7 (w), 1251.7 (w), 1049 (w), 926 (w).

References:

- [1]. Schlicke, B., Belser, P., De Cola, L., Sabbioni, E., Balzani, V., *J. Am. Chem. Soc.* **1999**, *121*, 4207.
- [2]. Armaroli, N., Barigelletti, F., Constable, E. C., Encinas, S., Figgmeier, E., Flamigni, L., Housecroft, C. E., Schofield E. R., Vos, J. G., *Chem. Commun.* **1999**, 869.
- [3]. Encinas, S., Flamigni, L., Barigelletti, F., Constable, E. C., Housecroft, C. E., Schofield, E. R., Figgemeier, E., Fenske, D., Neuburger, J. G., Vos, M., Zehnder, M., *Chem. Eur. J.* **2002**, *8*, 137.
- [4]. Turro, N. J., *Modern Molecular Photochemistry*, University Science Book, **1991**.
- [5]. Krass, H., Plummer, E. A., Haider, J. M., Barker, P. R., Alcock, N. W., Pikramenou, Z., Hannon, M. J., Kurth, D. G., *Angew. Chem. Int. Ed.* **2001**, *40*, 3862.

Chapter VII : Synthesis of narrow band gap spacers using non-classical π -electrons ring systems.

I. Introduction.

The design of photo- and redox-active systems with potential application as photocatalysts for solar energy conversion has been identified as a research imperative for the 21st Century [1]. One of the commonest design strategies for potential photocatalytic systems builds upon the incorporation of redox- and photoactive transition metal complexes into modular homo- or heterogeneous assemblies. Particular interest has centered upon the use of complexes incorporating oligopyridine metal-binding domains, as these possess favourable kinetic and thermodynamic stabilities, useful redox and photophysical properties, are easily synthesised and may be structurally varied to allow a library of modular units to be constructed. Our interests have centred upon a modular approach based upon $\{M(\text{tpy})_2\}$ (tpy= 2,2':6',2''-terpyridine) metallotectons and we have demonstrated that pendant or bridging aromatic units may be used to control energy and electron transfer processes between in such systems [2-13].

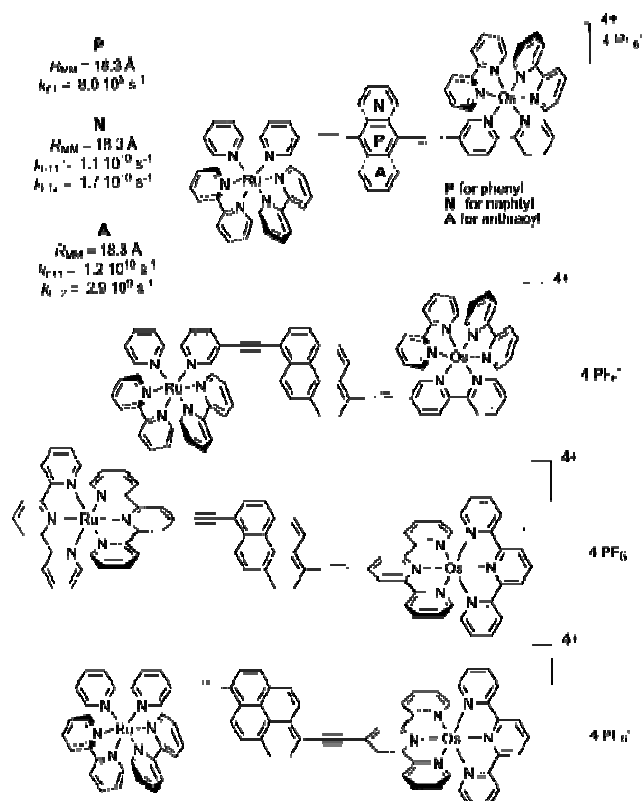


Fig VII-1- Example of alkyne-aromatic bridging systems in some photoactive polypyridine Ru/Os dyads.

II. Organic π -conjugated systems.

Organic π -conjugated oligomers and polymers constitute a class of semiconducting materials useful in device applications ranging from light-emitting diodes^[14,15], photovoltaic cells^[16,17], field-effect transistors^[18,19], to non-linear optics^[20,21]. Reducing and tuning energy gaps between the highest occupied molecular orbital (HOMO) and the lowest unoccupied molecular orbital (LUMO) of such π -conjugated species plays a crucial role in optimizing the performance of electronic and optical devices based on active organic components^[22].

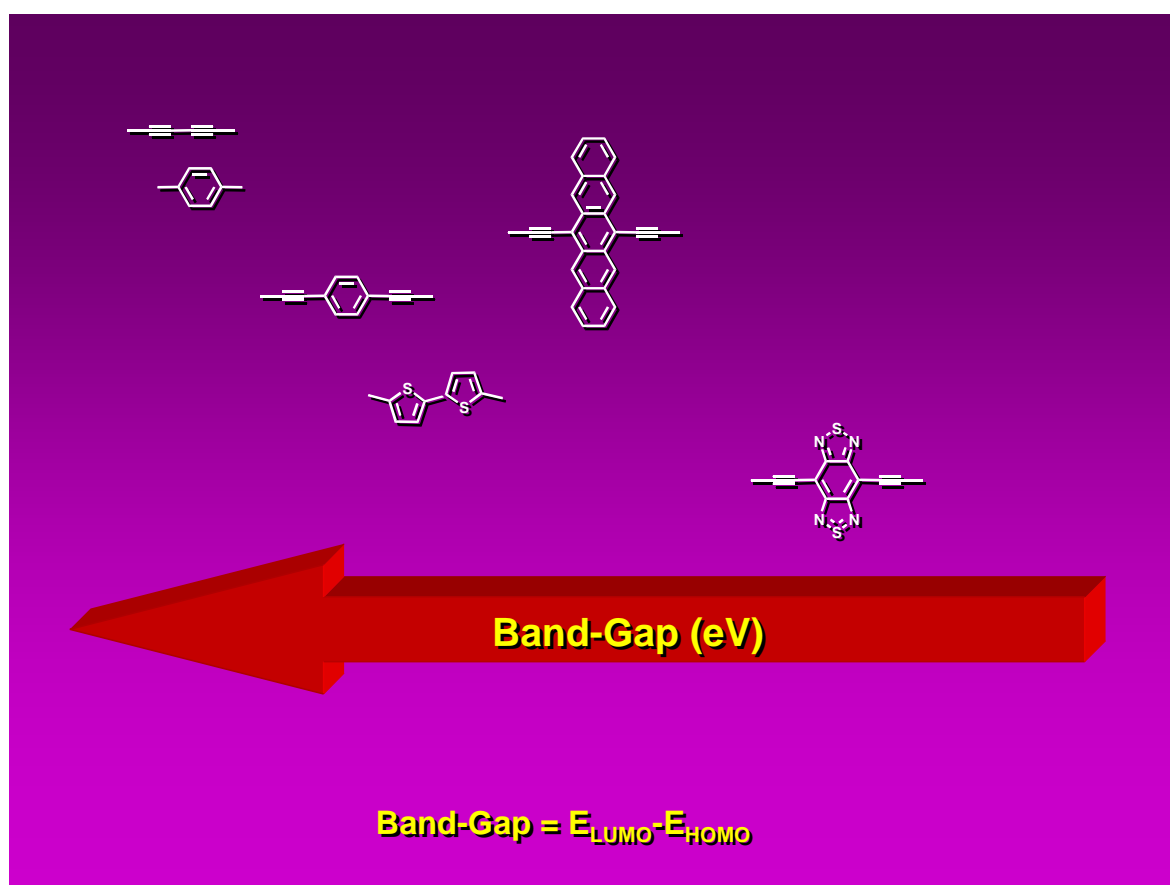


Fig VII-2- Schematic classification of π -bonded spacers function of the energy of the band-gap.

In order to decrease the band gap energy difference between the HOMO and the LUMO non classical π -conjugated systems have been used in porphyrinic systems. In the *Fig VII-3* two

different π -conjugated systems and their HOMO and LUMO energy levels have been calculated with the AM1 method for the aromatic compounds without heteroatom and the PM3 method for heteroatomic spacer. The orbital configuration of the conjugated form of the oligothiophene shows two energy level at respectively -8.65 eV and -1.38 eV for respectively the HOMO and the LUMO, the band is the difference between the HOMO and the LUMO energy level when the band gap is low the conduction through the molecule is high, we need less energy to reach the LUMO which correspond to the conduction energy level when the π -electrons are delocalised along the molecule. The (Fig-VII-2) describe the band-gap electronic repartition for different nature of H-Bond -conjugated systems like oligothiophenic system and diethynylphenyl system (Fig-VII-2b).

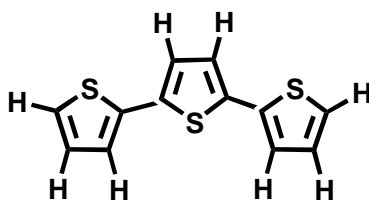
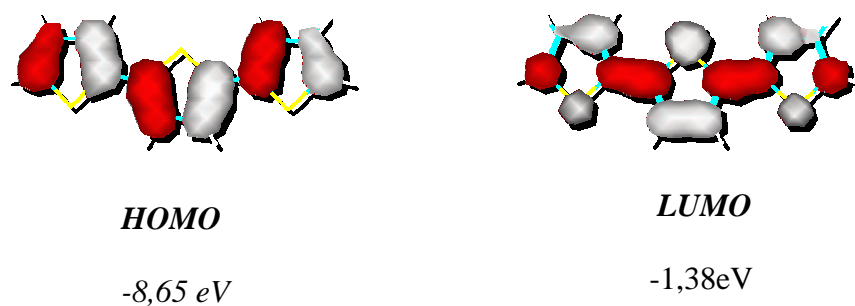
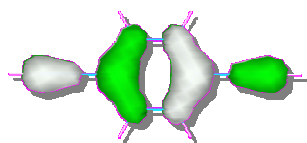


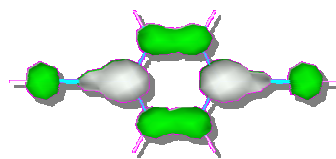
Fig VII-2b-PM3 calculations for a oligothiophenyl and diethynylbenzene unit.





HOMO

E= -9,07 eV



LUMO

E= -0,41 eV

The AM1 and PM3 calculations concerning the phenyl-diacetylene unit show that the gap between the two energy levels is equal to -8,66 eV.

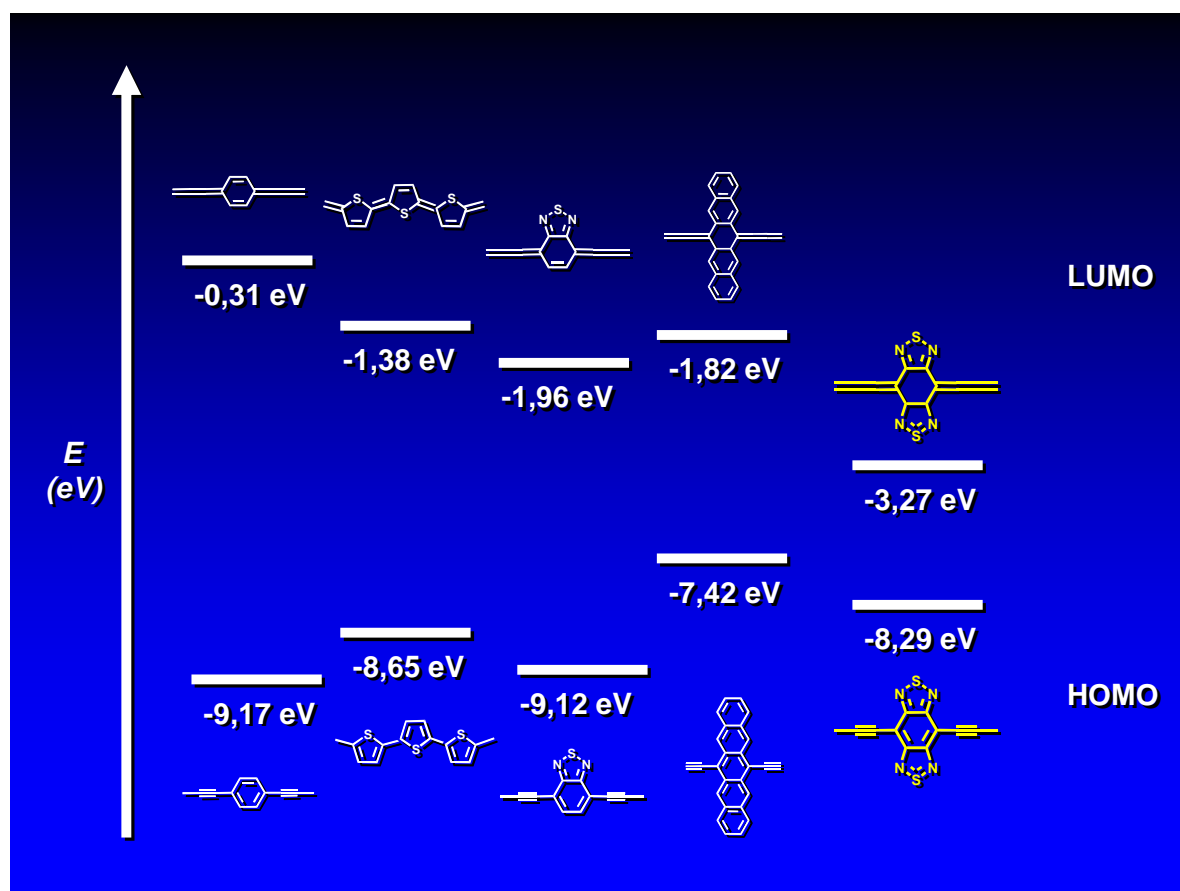
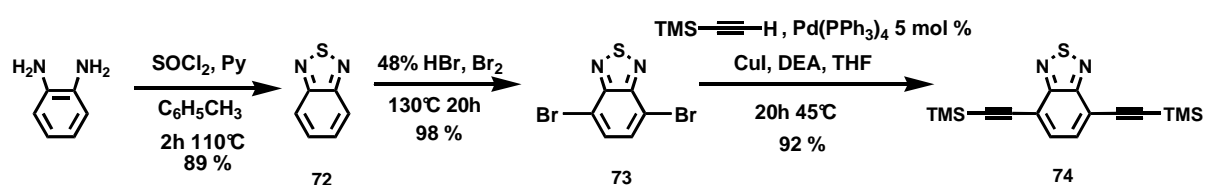


Fig VII-3- Schematic diagram of HOMO-LUMO energy level of several π -conjugated spacers, energy in (eV) after computational calculation

The PM3 calculation of energy levels of the HOMO-LUMO band gap shows that such latter decreases when we have a non-classical π electron ring system.

III-Synthesis of 4,7-diethynyltrimethylsilyl-benzo[c][1,2,5]thiadiazole **74**.

The synthesis of compound **74** is according to the procedure of Susumu^[23] (*Fig VII-4*) starting with 1,2-phenylenediamine which reacts with thionyl chloride in toluene in presence of pyridine. After neutralisation of the reaction, the product **72**^[24] is recrystallised from CHCl₃. The second step reaction is a bromination with Br₂ in 48% HBr solution at 130 °C during 20 hours to give compound **73**^[25]. The compound **74** was obtained after a Sonogashira-Hagihara coupling with TMSA in presence of CuI, DEA and Pd(PPh₃)₄ catalyst in THF^[23].



*Fig VII-4- Synthesis of compound **74**.*

The crystal structure of compound **72**^[24], **73** and **74** were elucidated by X-rays, the data collection is developed in Annex part (cf compounds **72**, **73**, **74**).

Crystal structure of **72**.

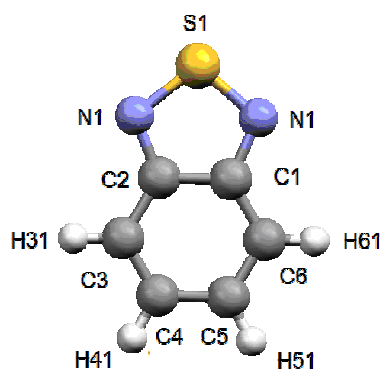


*Fig VII-5- Representation of the crystal structure of compound **72**.*

Distance parameters.

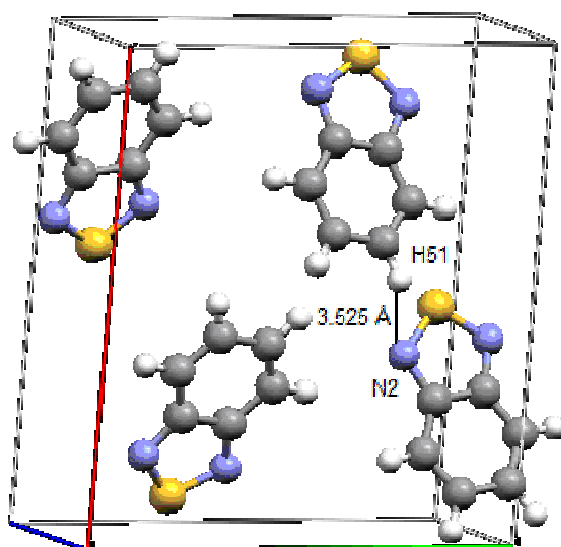


Fig VII-6- Structure of compound **72** in its packed form (distances in Å).

Crystal structure of **73**.

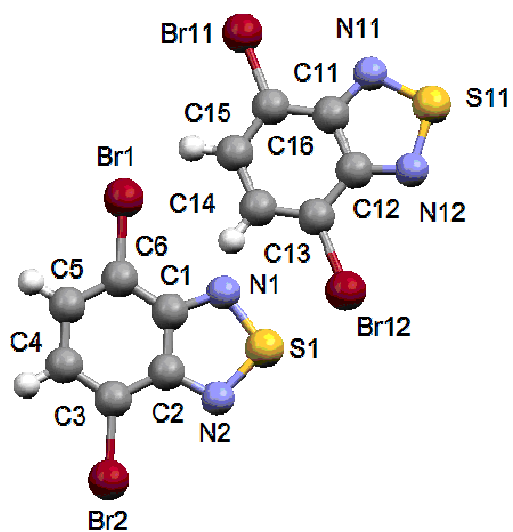


Fig VII-7- Representation of the crystal structure of the compound **73**.

H-Bond table of **73**.

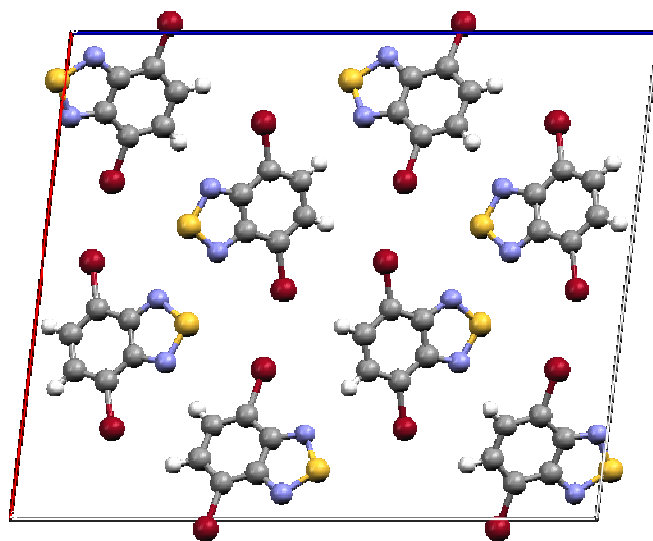


Fig VII-8- Structure of compound **73** in its packed form (distances in Å).

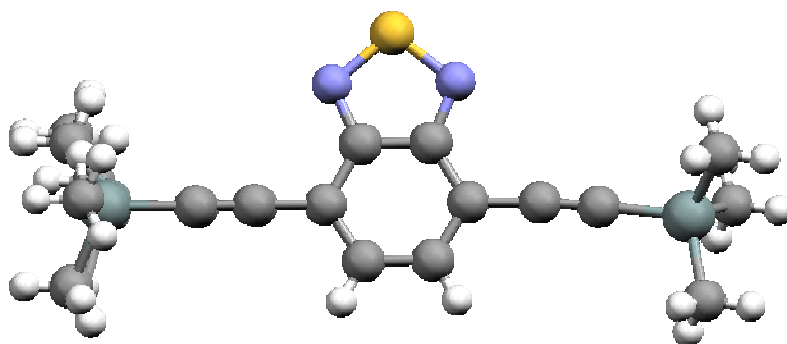


Fig VII-9- Representation of the crystal structure of the compound **74**.

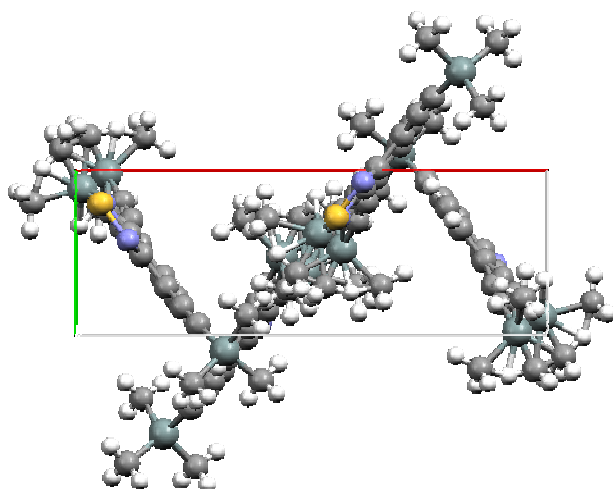


Fig VII-10- Structure of compound **74** in its packed form (distances in Å).

Synthesis of compound 75.

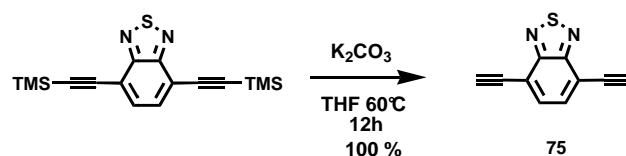


Fig VII-11- Synthesis of compound **75** by deprotection

The deprotection with K_2CO_3 of the compound **74** was not efficient. The method of Negishi^[26] should be an interesting synthetic way. This coupling consists of the reaction of compound **73** with the organozinc reagent formed in-situ by the transmetallation of ethynylmagnesium bromide with $ZnCl_2$ in presence of $[Ni(PPh_3)_2Cl_2]$ catalyst in THF (Fig VII-12). This method has been investigated but gave unfortunately none of the desired product.

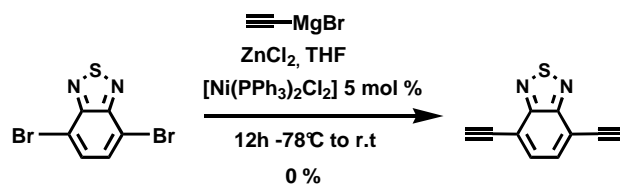


Fig VII-12- Attempted synthesis of compound **75** by Negishi coupling.

*Synthesis of tpy derivative **76** via Sonogashira-Hagihara coupling.*

The bridged tpy ligand could be formed by Sonogashira-Hagihara cross coupling between the 4-bromo tpy derivate and the spacer **74**. This coupling has been performed in presence of $[\text{Pd}(\text{PPh}_3)_4]$ as catalyst, CuI as co-catalyst, K_2CO_3 , TEA in THF/MeOH solvent. The reaction

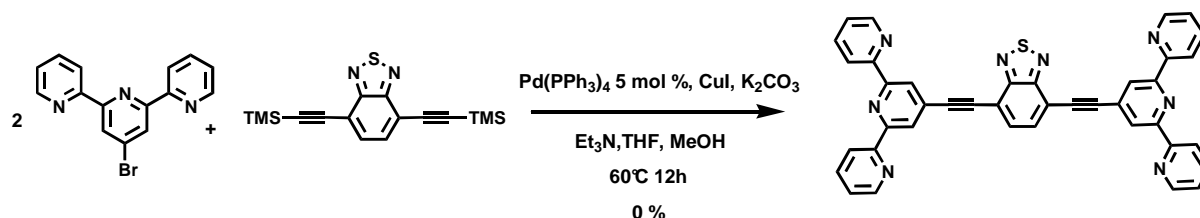


Fig VII-11- Attempted synthesis of ligand **76**.

mixture was heated over 12h at 60°C. However after reaction and purification, the coupling result was not the desired compound **76**.

Synthetic perspective.

The dinuclear species should be obtained by direct coupling on the spacer of two bromo tpy Ru (II) complexes using the Sonogashira-Hagihara coupling with $\text{Pd}(\text{PPh}_3)_4$ as catalyst in THF/MeOH/TEA solvent (Fig VII-12).

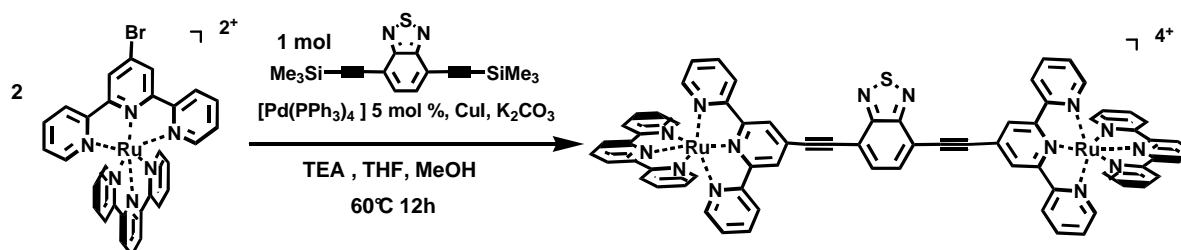


Fig VII-12- Synthesis of compound **77**.

IV-Synthesis of 6,13- pentacene derivates.

The 6,13- pentacene derivatives can be used as spacer for the same reasons explained in I. Therefore, the synthesis of 6,13-diethynylpentacene is developed.

Synthesis of 6,13-diethynylpentacene.

We required 6,13-bis(ethynyl)pentacene, to introduce it as spacer between two {M(tpy)₂} units, and used minor variations on the literature procedure to prepare 6,13-bis[(triisopropylsilyl)ethynyl]pentacene^[22]. Pentacene-6,13-dione **78** was prepared as a yellow solid from the reaction of cyclopentane-1,4-dione^[27] with 1,2-benzenedicarboxaldehyde in ethanolic KOH in 95 % yield . Reaction of **78** with TIPSCCLi in THF gave a green solid comprising the desired diol, **79** and a highly fluorescent ($\lambda_{em} = 434 \text{ nm}$) product, characterised as 13-hydroxy-13-[(triisopropylsilyl)ethynyl]pentacene-6(13H)-one **80**. We have subsequently optimized the yield of orange **80** by reaction of **78** with one equivalent of TIPSCCLi.

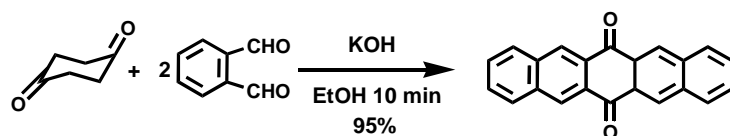


Fig VII-13- Synthesis of **78**.

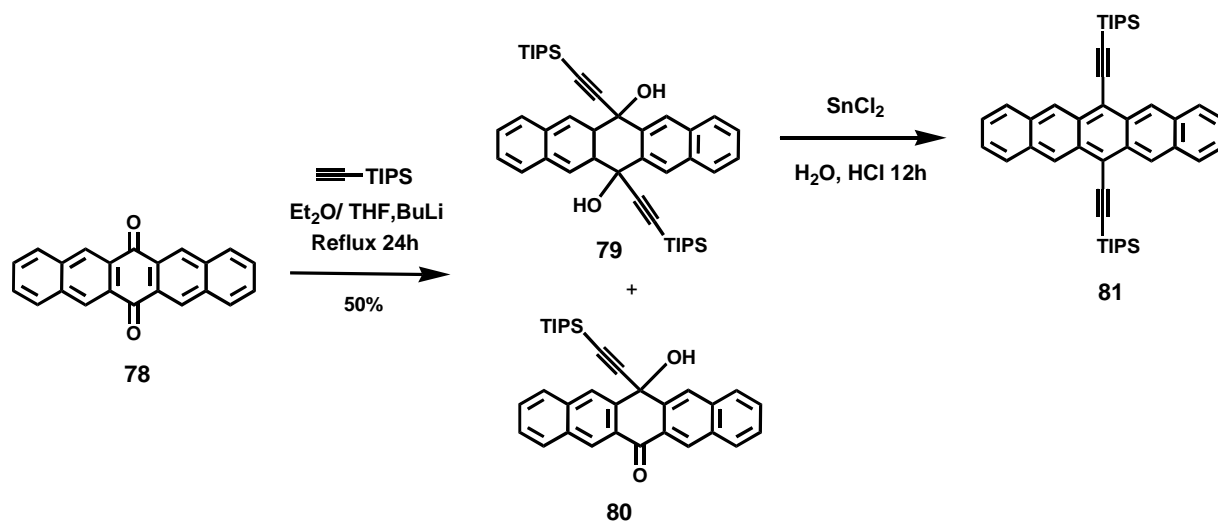


Fig VII-14-Synthesis of **80**.

We have determined the solid state crystal structure of the compound **80**^[30]. Fig VII-14 shows the structure of a molecule of **80** together with numbering scheme adopted. As expected on the basis of hydrogen bonding (see later) and the non-aromatic ring structure, the carbonyl CO bond in 1 is slightly longer (C(23)-O(2), 1.238(3) Å) than that in the quinone (1.215 Å)^[28]. Within the pentacene system, the aromatic rings exhibit typical delocalised C-C bond distances in the range 1.358(4) to 1.424(3) Å similar to those of the aromatic rings in other pentacenes and 6,13-dihydropentacenes. In the central ring, the C-C bonds to the carbonyl group are little longer (1.476(3), 1.474(3) Å) similar to those of the aromatic rings in other pentacenes and 6,13-dihydropentacenes. In the central ring, the C-C bonds to the carbonyl group are a little longer (1.476(3), 1.474(3) Å) and similar in length to those in pentacene-6,13-dione (1.483 Å)^[28]. The formally single C-C bonds to C12 in the central ring show distances of 1.528(3) and 1.535(3) Å which are similar to, if slightly longer than, those in 6,13-dihydropentacene (1.475, 1.524 Å)^[29]. In contrast to 6,13-dihydropentacene where the least squares planes through the “naphthalene” units intersect at the sp³ carbon C12 from the least squares plane of the aromatic rings being only 0.160 Å.

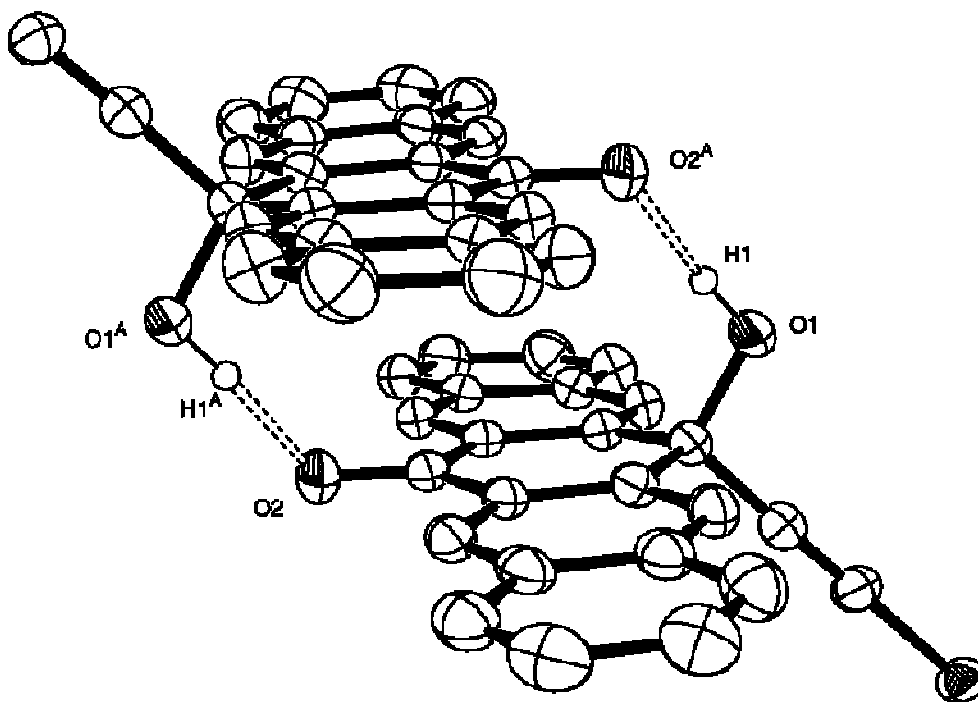


Fig VII-15- The dimeric assembly of two molecules of **80** in the crystal structure^[30].

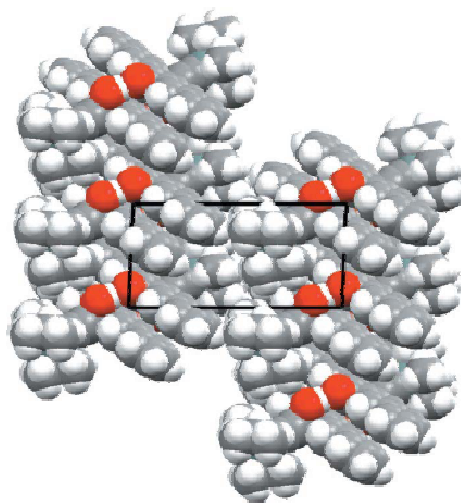


Fig VII-16-Space filling representation of packed crystal structure of **80** down the b axis, showing the packing of the dimers into columns, between which lie the trisopropyl-silyl groups^[30].

V Conclusion.

The compound **75** has been synthesized as spacer for a potential rod like dinuclear species containing two $\{M(tpy)_2\}$ units. The coupling via the Sonogashira-Hagihara reaction of bromo ligand **25** with the compound **75** to obtain the ligand **76** has unfortunately not been successful. Nevertheless a second hypothetical synthetic way should be investigated, such consists on the direct coupling of two moles of bromo complex **36** on the diethylenic protected spacer **74** via the Sonogashira-Hagihara coupling. The second narrow band-gap p-conjugated spacer **81** is really interesting, because such latter did not contain an heteroatom susceptible to influence the coordination with transition metals. Such compounds have to be investigated in the future because their properties of decrease of the HOMO-LUMO band gap is essential to perform very interesting rod-like polynuclear diad.

VI. Experimental section.

Synthesis of 72^[24].

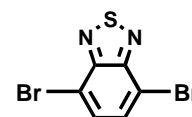
1,2-diaminobenzene (10.0 g, 92.5 mmol) and pyridine (10 ml) are dissolved in toluene (100 ml) then thionyl chloride (25 ml) is added slowly dropwise to the solution at room temperature. The reaction mixture was heated at reflux for 2 hours. After reaction the mixture is neutralised with water and after separation of the organic phase, the water layer is washed three times with 30 ml of chloroform. The collected organic fractions are then evaporated and purified on a SiO₂/CHCl₃ to obtain pure 3,1,2-benzothiadiazole (m = 11.2 g, Yield = 89 %).



Experimental data **NMR** ¹H: 8.00 (dd, 2H, *J*₁ = 9.75 Hz, *J*₂ = 2.25 Hz) **H4**, 7.58 (dd, 2H, *J*₁ = 9.25 Hz, *J*₂ = 2.5 Hz) **H5**. **NMR** ¹³C : 155.1 **C3**, 129.6 **C4**, 121,9 **C5**. **ES-MS**: 136 [M⁺], 109 **Mass-Analysis** (% *calculated*) Formula: C₆H₄N₂S: C 53,00% (52,92%), H 2,86% (2,96%), N 20,40% (20,50%) **IR** (ν cm⁻¹): 3051 (w), 2918 (w), 2358 (w), 1517 (s), 1477 (s), 1130 (s), 846 (w) **M. P.**: 42.5-44.5 °C.

Synthesis of 73^[25].

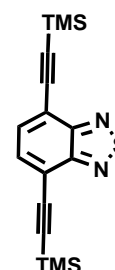
72 (16.1 g, 0.118 mol) was dissolved in concentrated HBr (100 ml) then Br₂ (100ml) was dropwise added to the reaction mixture and the solution heated to reflux during 20 hours at approx. 130°C. After reaction, the mixture is cooled to room temperature and extracted with CHCl₃, the excess of HBr neutralized with triethylamine, and the solution evaporated under vacuum and the residue recrystallized from chloroform. 4,6-Dibromo-3,1,2-benzothiadiazole is obtained after filtration over Büchner filter (m = 34.0 g, Yield 98%, white needles).



Experimental datas **NMR** ¹H (*δ* in ppm): 7,76 (s, 2H) **H5-H6**, ¹³C **NMR** (*δ* in ppm): 207.4 , 132.8, 114,2 **ES-MS**: 293.8 [M⁺], 214,9, 134, **IR** (ν cm⁻¹): 3095 (w), 1626 (w), 1475 (s), 1308 (s), 1182 (s), 933 (s). **Mass-Analysis** (% *calculated*) Formula: C₆H₂N₂Br₂S: C 23,69% (24,52%), H 1,06% (0,69%), N 9,50% (9,53%) **M. P.**: 128-130°C.

Synthesis of **74**^[23].

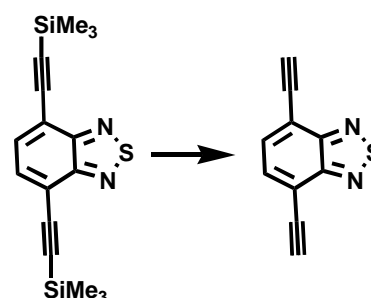
73 (4.0 g, 13.6 mmol), CuI (0.11 mg, 0.58 mmol) DEA (10 ml), [Pd(PPh₃)₄] (650 mg, 1.76 mmol) and TMSA (21 ml, 27.2 mmol) are dissolved in THF (50 ml) under argon atmosphere. The reaction mixture is maintained at 45°C during 20 hours, after which the solvent is removed under vacuum and the residue purified over silica with hexane : chloroform 1:1 as eluant. The product **73** was obtained after evaporation of the collected fraction as nice yellowish crystals. (m = 4.1g, Yield = 92%)



Experimental datas : NMR ¹H (δ ppm) : 7.69 (s, 2H) **H⁵-H₆**, 0.31 (s, 18H) -Si-(CH₃)₃. NMR ¹³C (δ ppm): 154.6, 133.5, 104.0, 100.4 **ES-MS** : 328.1 [M⁺], 313.1. **Mass-Analysis** (% calculated) Formula: C₁₂H₂₀N₂SSi₂: C 58,48% (58,49%), H 6,13% (6,18 %), N 8,42 % (8,53%) **IR** (ν cm⁻¹): 2957 (w), 2150.4 (w), 1488 (w), 1247 (s), 1026 (s), 835 (s) **M. P.**: > 400 °C.

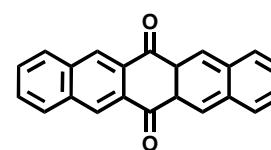
Attempted synthesis of **75**.

74 (4.0 g, 12.2 mmol) was dissolved with K₂CO₃ (820 mg, 5.9 mmol) in MeOH (20 ml). The reaction mixture is quenched with water and extracted 3 times with 20 ml of chloroform. The collected organic fractions are evaporated in vacuum and the product **74** was obtained after thin layer chromatography.



Synthesis of pentacen-6,13-dione **78**^[27].

1,4-cyclopentanedione (5.0 g, 44.6 mmol) and 1,2-dicarbadehydebenzene (12.0 g, 89.2 mmol) are dissolved in ethanol (50 ml) potassium hydroxide solution then of a (2M, 20 ml) is added to reactional mixture. The reaction mixture is stirred

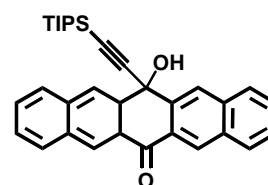


at room temperature during 10 min, a yellow suspension appears this is filtered off with a büchner filter, the yellow solid is then recolcted and washed with methanol.(m = 13.0 g, Yield = 95%)

Experimental section $^1\text{H NMR}$ in CDCl_3 (δ ppm) : 8.97 (s, 4H) , 8.14 (dd, 4H, $J_1 = 4.7$ Hz, $J_2 = 3.25$ Hz), 7.73 (dd, 4H, $J_1 = 6.1$ Hz, $J_2 = 3.5$ Hz) $^{13}\text{C NMR}$ in CDCl_3 (δ ppm) : 132.5, 127.9, 127.8. **FAB-MS** : 308.1 [M^+], 280.1, 252.1. **IR** (ν cm^{-1}): 3049 (w), 1673 (s), 1280 (s), 1189 (w), 986 (w), **M.P.** : .

13-hydroxy-13-[(triisopropylsilyl)-ethynyl]pentacen-6(13H)-one **79**.

Pentacene-6,13-dione (5.00 g, 16.2 mmol), was dissolved in freshly distilled diethyl ether (50 ml) and the solution added to a mixture of triisopropylsilylacetylene (6.00 mL, 4.88 g, 26.7 mmol) and n-BuLi (5 mL, 1.6 M in THF, 8 mmol) in THF (10 mL). After

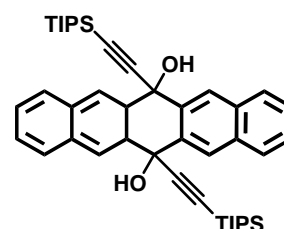


stirring at room temperature under nitrogen for 24 h the solvent was removed in vacuo and the residue purified by chromatography over silica (hexanes- CHCl_3 1:1) to give 13-hydroxy-13-((triisopropylsilyl)ethynyl)pentacen-6(13H)-one as a green solid (5.50 g, 69.2 %) together with some 6,13-bis((triisopropylsilyl)ethynyl)pentacene (1.26 g, 11.7%).

Experimental section: $^1\text{H NMR}$ in CDCl_3 (δ ppm) 250 MHz: 8.81 (s, 2H) $\text{H}^{\text{P}5,7}$, 8.72 (s, 2H) $\text{HP}^{12,14}$, 8.03 (d, 2H, $J = 8.2$ Hz) $\text{HP}^{4,8}$, 7.92 (d, 2H, $J = 8.2$ Hz) $\text{HP}^{1,11}$, 7.62 (d, 2H, $J = 8.2$, 6.8, $J = 1.3$ Hz) $\text{HP}^{2,10}$, 1.78 (m, 3H) H^{TIPS} , 1.15 (m, 18H) H^{TIPS} . $^{13}\text{C NMR}$ in CDCl_3 (δ ppm): 206.9, 138.8, 135.6, 132.8, 129.7, 129.6, 128.9, 128.6, 128.2, 127.3, 127.2, 108.2, 90.0, 68.6, 18.6, 11.2. **ES-MS** : (m/z) 490, **M. P.** : $> 400^\circ\text{C}$.

13-hydroxy-13-[(triisopropylsilyl)-ethynyl]pentacen-6(13H)-one **80**.

The synthesis of **77** gives as major product the disubstitued compound and a minor part of monosubstitued compound. The fractions recolcted by the crystallisation of the monosubstitued compound are analysed by X-rays diffraction



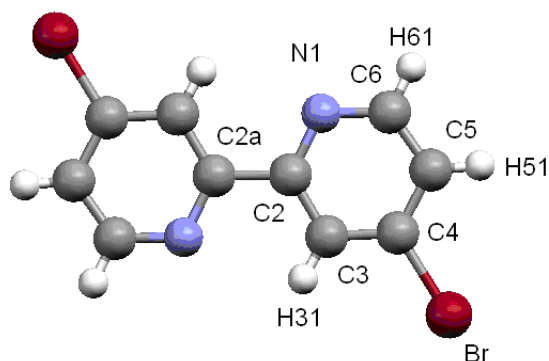
Experimental section: ^1H NMR in CDCl_3 (δ ppm) 250 MHz: 8.88 (s, 4H) $\text{H}^{\text{P } 5,7,12,14}$, 7.93 (m, 4H) $\text{HP}^{1,4, 8,11}$, 7.59 (m, 4H) $\text{HP}^{2,3,9,10}$, 1.62 (s, 6H) H^{TIPS} , 1.20 (m, 36H) H^{TIPS} . ^{13}C NMR in CDCl_3 (δ ppm): 207.4, 136.0, 133.2, 130.2, 130.0, 129.3, 129.1, 128.7, 127.8 . **ES-MS** : (m/z) 655.5 [M^+]. **Mass analysis** (calculated %) $\text{C}_{44}\text{H}_{55}\text{O}_2\text{Si}_2$: C % 77.25 (78.63 %), H % 8.59 (8.25 %) **M. P.** : $> 400^\circ\text{C}$.

References

- [1] Eisenberg, R., Nocera, D. G., *Inorg. Chem.* **2005**, *44*, 6799.
- [2] Constable, E. C., Smith, D. R., *Supramol. Chem.* **1994**, *4*, 5.
- [3] Constable, E. C., Smith, D. R., *Tetrahedron* **1996**, *52*, 935.
- [4] Albano, G., Balzani, V., Constable, E. C., Maestri, M., Smith, D. R., *Inorg. Chim. Acta* **1998**, *277*, 225.
- [5] Hjelm, J., Constable, E. C., Figgemeier, E., Hagfeldt, A., Handel, R., Housecroft, C. E., Mukhtar, E., Schofield, E. R., *Chem. Commun.* **2002**, 284.
- [6] Hjelm, J., Handel, R., Hagfeldt, A., Constable, E. C., Housecroft, C. E., Forster, R. J., *J. Phys. Chem. B* **2003**, *107*, 10431.
- [7] Constable, E. C., Handel, R., Housecroft, C. E., Neuburger, M., Schofield, E., Zehnder, M., *Polyhedron* **2004**, *23*, 135.
- [8] Figgemeier, E., Aranyos, V., Constable, E. C., Handel, R. W., Housecroft, C. E., Risinger, C., Hagfeldt, A., Mukhtar, E., *Inorg. Chem. Commun.* **2003**, *7*, 117.
- [9] Encinas, S., Flamigni, L., Barigelletti, F., Constable, E. C., Housecroft, C. E., Schofield, E., Figgemeier, E., Fenske, D., Neuburger, M., Vos, J. G., Zehnder, M. *Chem. Eur. J.* **2002**, *8*, 137.
- [10] Armaroli, N., Barigelletti, F., Constable, E. C., Encinas, S., Figgemeier, E., Flamigni, L., Housecroft, C. E., Schofield, E. R., Vos, J. G., *Chem. Commun.* **1999**, 869.
- [11] Hjelm, J., Handel, R. W., Hagfeldt, A., Constable, E. C., Housecroft, C. E., Forster, R. J., *Electrochem. Commun.* **2004**, *6*, 193.
- [12] Hjelm, J., Handel, R. W., Hagfeldt, A., Constable, E. C., Housecroft, C. E., Forster, R. J. *Inorg. Chem.* **2005**, *44*, 1073.
- [13] Constable, E. C., Figgemeier, E., Housecroft, C. E., Olsson, J., Zimmermann, Y. C., *Dalton Trans.* **2004**, 1918.
- [14] Segura, J. L., *Acta. Polym.* **1998**, *49*, 319.
- [15] Mitschke, U., Bäuerle, P., *J. Mater. Chem.* **2000**, *10*, 1471.
- [16] Yu, G., Gao, J., Hummelen, J. C., Wudl, F., Heeger, A., *Science* **1995**, *270*, 1789.
- [17] Brabec, C. J., Sariciftci, N. S., Hummelen, J. C., *Adv. Func. Mater.* **2001**, *11*, 15.
- [18] Katz, H. E., *J. Mater. Chem.* **1997**, *7*, 369.
- [19] Katz, H. E., Bao, Z., Gilat, S. L. *Acc. Chem. Res.* **2001**, *34*, 359.
- [20] Nalwa, H. S., *Adv. Mater.* **1993**, *5*, 341.

- [21] Tikwinski, R. R., Gubler, U., Martin, R. E., Diederich, F., Bosshard, C., Günter, P., *J. Phys. Chem. B* **1998**, *102*, 4451.
- [22]. Anthony, J. E., Eaton, D. L., Parkin, S. R., *J. Am. Chem. Soc.* **2001**, *123*, 9482.
- [23]. Susumu, K., Duncan, T. V., Therien, M. J., *J. Am. Chem. Soc.* **2005**, *127*, 5186.
- [24]. Weinstock, L. M., Davis, P., Handelsman, B., Tull, R., *J. Org. Chem.* **1967**, *32*, 2823.
- [25]. Pilgram, K., Zupan, M., Skiles, R. J., *J. Heterocycl. Chem.* **1970**, *7*, 629.
- [26]. Negishi, E., Anastasia, L., *Chem. Rev.*, **2003**, *103*, 1979.
- [27]. Reid, W., Anthöfer, F., *Angew. Chem.* **1953**, *65*, 601.
- [28]. Dzyabchenko, A. V., Zavodnik, V. E., Bel'skii, V. K., *Acta Crystallogr., Sect. B: Struct. Crystallog. Cryst. Chem.* **1979**, *35*, 2250.
- [29]. Mattheus, C. C., Baas, J., Meetsma, A., de Boer, J. L., Kloc, C., Siegrist, T., Palstra, T.T.M. *Acta Crystallogr. Sect. E: Struct. Rep. Online* **2002**, *58*, o1229.
- [30]. Boudebous, A., Constable, E. C., Housecroft, C. E., Neuburger, M., Schaffner, S., *Acta. Cryst.* **2006**, *C62*, o243.

Annexe: Crystallographic data, data collection and refinement parameters of compound 4.



Empirical formula	C ₁₀ H ₆ Br ₂ N ₂
Formula weight	313.98 g mol ⁻¹
Temperature	173 K
Wavelength	0.71073 Å
Crystal system	Monoclinic
Space group	P21/n
a	3.93630(10) Å
b	15.7981(3) Å
c	7.87180(10) Å
β	93.6905(12)°
Volume, Z	488.50(2) Å ³ , 2
Density (calculated)	2.135 Mg m ⁻³
Absorption coefficient	8.253 mm ⁻¹
F (000)	300
Crystal size	0.13 x 0.25 x 0.26 mm
θ range for data collection	2.6, 27.9 °
Index ranges	-5 < h < 5 ; -20 < k < 20 ; -10 < l < 10
Reflection collected	4603
Independent reflections	1166
Data/restraints/parameters	1012
R, wR2, S	0.0266, 0.0317, 1.10
Largest diff. peak and hole	-0.33 e 0.49 Å ⁻³

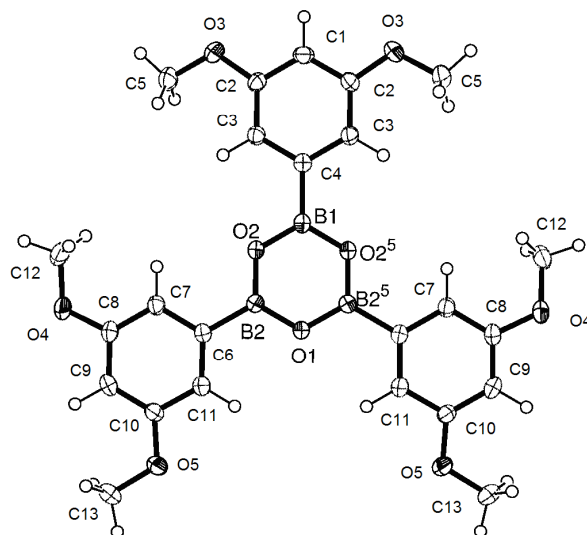
Table - Bond Distances (Angstrom)

Bond	l (Å)	Bond	l (Å)
Br1-C4	1.8912(16)	C4-C5	1.387(2)
N1-C2	1.346(2)	C5-C6	1.387(2)
N1-C6	1.340(2)	C3-H31	0.9600
C2-C3	1.398(2)	C5-H51	0.9600
C2-C2_a	1.490(2)	C6-H61	0.9700
C3-C4	1.385(2)		

Table - Bond Angles (Degrees)

Atoms	Angle (°)	Atoms	Angle (°)
C2-N1-C6	117.15(14)	C4-C5-C6	117.09(15)
N1-C2-C3	123.10(14)	N1-C6-C5	124.43(15)
N1-C2-C2_a	116.95(14)	C2-C3-H31	120.00
C2_a-C2-C3	119.95(13)	C4-C3-H31	122.00
C2-C3-C4	117.74(14)	C4-C5-H51	123.00
Br1-C4-C3	119.08(11)	C6-C5-H51	120.00
Br1-C4-C5	120.44(11)	N1-C6-H61	116.00
C3-C4-C5	120.48(15)	C5-C6-H61	119.00

Annexe: Crystallographic data, data collection and refinement parameters for 9.



Empirical formula	$C_{24} H_{27} B_3 O_9$
Formula weight	491.91 g mol ⁻¹
Temperature	173 K
Wavelength	0.71073 Å
Crystal system	Monoclinic
Space group	$C2/c$
a	17.5959(3) Å
b	14.4656(3) Å
c	12.5459(2) Å
β	129.1179(8)°
Volume, Z	2477.58(8) Å ³ , 4
Density (calculated)	1.319 Mg m ⁻³
Absorption coefficient	0.098 mm ⁻¹
F (000)	1032
Crystal size	0.08 x 0.10 x 0.29 mm
θ range for data collection	2.1, 27.9 °
Index ranges	-23: 23 ; -19: 19 ; -16: 16
Reflection collected	2950
Independent reflections	1724
Data/restraints/parameters	165
Final R indices [$I > 3\sigma I$]	1724
R, wR2, S	0.0394, 0.0902, 1.16
Largest diff. hole and peak	-0.25, 0.22 e Å ⁻³

Table 2 – Interatomic bonds length parameters datas in Å of compound **9**.

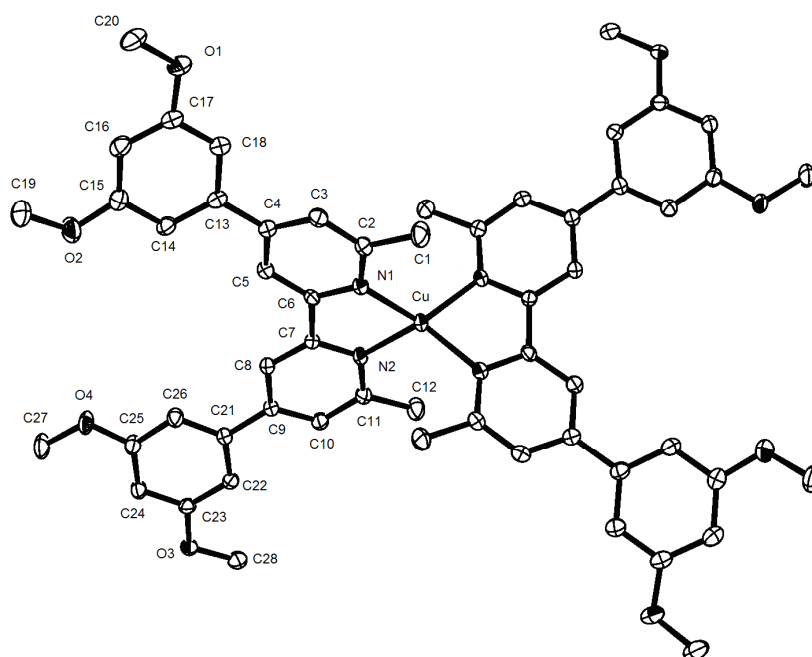
Bond	l (Å)	Bond	l (Å)
O1-B2	1.382(2)	C7-C8	1.388(3)
O1-B2_a	1.382(2)	C8-C9	1.396(2)
O2-B1	1.3785(18)	C9-C10	1.381(3)
O2-B2	1.377(2)	C10-C11	1.399(3)
O3-C2	1.366(3)	C1-H11	1.0000
O3-C5	1.428(3)	C3-H31	1.0000
O4-C8	1.372(3)	C5-H51	1.0000
O4-C12	1.430(2)	C5-H52	1.0000
O5-C10	1.3698(19)	C5-H53	1.0000
O5-C13	1.427(3)	C7-H71	1.0000
C1-C2	1.389(2)	C9-H91	1.0000
C1-C2_a	1.389(2)	C11-H111	1.0000
C2-C3	1.391(2)	C12-H121	1.0000
C3-C4	1.399(2)	C12-H122	1.0000
C4-B1	1.552(3)	C12-H123	1.0000
C6-C7	1.406(3)	C13-H131	1.0000
C6-C11	1.390(2)	C13-H132	1.0000
C6-B2	1.553(3)	C13-H133	1.0000

Table 3- Bond Angles (Degrees)

Atoms	Angle (°)	Atoms	Angle (°)
B2-O1-B2_a	120.55(15)	C4-C3-H31	120.00
B1-O2-B2	120.44(17)	O3-C5-H52	109.00
C2-O3-C5	116.97(14)	O3-C5-H53	109.00
C8-O4-C12	116.64(17)	O3-C5-H51	109.00
C10-O5-C13	117.36(17)	H52-C5-H53	109.00
C2-C1-C2_a	120.51(19)	H51-C5-H53	109.00
O3-C2-C1	115.65(15)	H51-C5-H52	109.00
O3-C2-C3	124.39(18)	C8-C7-H71	120.00
C1-C2-C3	119.97(19)	C6-C7-H71	120.00
C2-C3-C4	119.83(19)	C8-C9-H91	120.00
C3-C4-B1	120.06(11)	C10-C9-H91	120.00
C3-C4-C3_a	119.89(18)	C6-C11-H111	120.00
C3_a-C4-B1	120.06(11)	C10-C11-H111	120.00
C7-C6-C11	119.38(19)	O4-C12-H122	109.00
C7-C6-B2	119.78(15)	O4-C12-H123	109.00
C11-C6-B2	120.83(18)	O4-C12-H121	109.00
C6-C7-C8	119.77(15)	H121-C12-H123	109.00
O4-C8-C7	124.09(16)	H122-C12-H123	109.00
O4-C8-C9	115.25(18)	H121-C12-H122	109.00
C7-C8-C9	120.65(19)	H131-C13-H132	109.00
C8-C9-C10	119.54(19)	H131-C13-H133	109.00

O5-C10-C9	124.26(19)	H132-C13-H133	110.00
O5-C10-C11	115.31(18)	O5-C13-H131	109.00
C9-C10-C11	120.42(15)	O5-C13-H132	109.00
C6-C11-C10	120.23(19)	O5-C13-H133	109.00
C2_a-C1-H11	120.00	O2_a-B1-C4	120.13(10)
C2-C1-H11	120.00	O2-B1-O2_a	119.75(19)
C2-C3-H31	120.00	O2-B1-C4	120.13(10)
O2-B2-C6	120.19(18)	O1-B2-O2	119.39(18)
O1-B2-C6	120.41(14)		

Annexe: Crystallographic data, data collection and refinement parameters for 59.



Empirical formula	$C_{56} H_{56} Cu N_4 O_8 N_4 F_{12} P_2$
Formula weight	1162.64 g mol ⁻¹
Temperature	173 K
Wavelength	0.71073 Å
Crystal system	Orthorhombic
Space group	C2221
a	8.14880(10) Å
b	29.8383(3) Å
c	22.1765(2) Å
α	°
β	°
γ	°
Volume, Z	5392.14(10) Å ³ , 4
Density (calculated)	1.432 Mg m ⁻³
Absorption coefficient	0.516 mm ⁻¹
F (000)	2416
Crystal size	0.15 x 0.16 x 0.23 mm
θ range for data collection	1.6, 28.7 °
Index ranges	-11<h<11, -40<k<40, -29<l<29
Reflection collected	6964
Independent reflections	5500
Data/restraints/parameters	365
Final R indices [$I > 2\sigma I$]	5500
R indices (all data, 5500 ref.)	0.0266, 0.0317, 1.10
Largest diff. peak and hole	-0.49, 0.52 e Å ⁻³

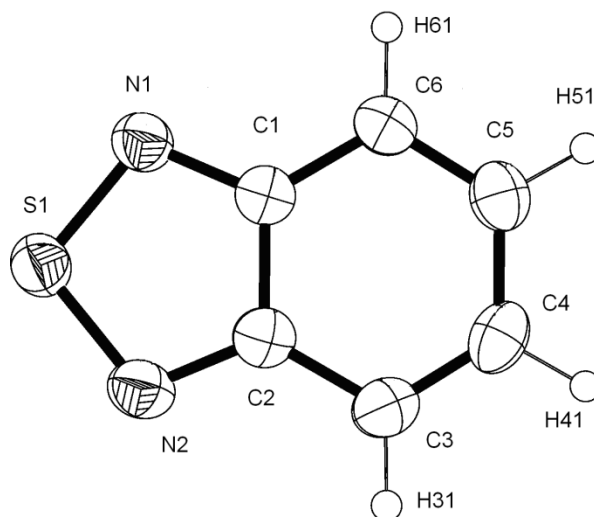
Bond	l (Å)	Bond	l (Å)
Cu1-N1	2.0102(12)	C5-C6	1.387(2)
Cu1-N2	2.0218(13)	C6-C7	1.489(2)
Cu1-N1_b	2.0102(12)	C7-C8	1.390(2)
Cu1-N2_b	2.0218(13)	C8-C9	1.396(2)
P2-F1	1.5931(15)	C9-C21	1.484(2)
P2-F2	1.5840(16)	C9-C10	1.395(2)
P2-F3	1.5964(14)	C10-C11	1.386(2)
P2-F1_a	1.5931(15)	C11-C12	1.498(2)
P2-F2_a	1.5840(16)	C13-C14	1.388(2)
P2-F3_a	1.5964(14)	C13-C18	1.407(2)
O1-C15	1.363(2)	C14-C15	1.393(2)
O1-C19	1.420(2)	C15-C16	1.385(2)
O2-C17	1.3657(19)	C16-C17	1.400(2)
O2-C20	1.438(2)	C17-C18	1.388(2)
O3-C27	1.424(2)	C21-C22	1.396(2)
O3-C23	1.370(2)	C21-C26	1.392(2)
O4-C25	1.362(2)	C22-C23	1.390(2)
O4-C28	1.427(3)	C23-C24	1.393(3)
N1-C6	1.3548(19)	C24-C25	1.393(2)
N1-C2	1.347(2)	C25-C26	1.397(2)
N2-C11	1.349(2)	C1-H12	0.9600
N2-C7	1.3553(19)	C1-H13	0.9600
N3-C30	1.100(7)	C1-H11	0.9600
C1-C2	1.498(2)	C3-H31	0.9600
C2-C3	1.395(2)	C5-H51	0.9600
C3-C4	1.394(2)	C8-H81	0.9600
C4-C13	1.491(2)	C10-H101	0.9600
C4-C5	1.401(2)	C12-H123	0.9600
C12-H121	0.9600	C24-H241	0.9600
C12-H122	0.9600	C26-H261	0.9600
C14-H141	0.9600	C27-H273	0.9600
C16-H161	0.9600	C27-H272	0.9600
C18-H181	0.9600	C27-H271	0.9600
C19-H192	0.9600	C28-H281	0.9600
C19-H193	0.9600	C28-H282	0.9600
C19-H191	0.9600	C28-H283	0.9600
C20-H202	0.9600	C29-C30	1.465(8)
C20-H201	0.9600	C29-H293	0.9600
C20-H203	0.9600	C29-H291	0.9600
C22-H221	0.9600	C29-H292	0.9600

Atoms	Angle (°)	Atoms	Angle (°)
N1-Cu1-N2	81.78(5)	Cu1-N2-C7	113.63(10)
N1-Cu1-N1_b	133.01(5)	Cu1-N2-C11	127.44(10)

N1-Cu1-N2_b	118.33(5)	C7-N2-C11	118.25(13)
N1_b-Cu1-N2	118.33(5)	N1-C2-C3	121.46(14)
N2-Cu1-N2_b	130.84(6)	N1-C2-C1	117.22(14)
N1_b-Cu1-N2_b	81.78(5)	C1-C2-C3	121.32(15)
F1_a-P2-F2	89.47(8)	C2-C3-C4	120.69(14)
F2-P2-F2_a	91.60(8)	C3-C4-C5	116.84(14)
F2-P2-F3_a	90.39(8)	C3-C4-C13	121.64(13)
F1_a-P2-F3	89.29(8)	C5-C4-C13	121.52(13)
F2_a-P2-F3	90.39(8)	C4-C5-C6	120.14(13)
F3-P2-F3_a	178.65(10)	N1-C6-C5	122.02(13)
F1_a-P2-F2_a	178.89(8)	N1-C6-C7	115.19(13)
F1_a-P2-F3_a	89.75(8)	C5-C6-C7	122.73(13)
F2_a-P2-F3_a	90.55(8)	N2-C7-C6	114.39(13)
F1-P2-F3_a	89.29(8)	N2-C7-C8	122.45(14)
F2-P2-F3	90.55(8)	C6-C7-C8	123.14(13)
F1-P2-F1_a	89.46(8)	C7-C8-C9	119.46(14)
F1-P2-F2	178.89(8)	C8-C9-C10	117.53(14)
F1-P2-F3	89.75(8)	C8-C9-C21	122.03(13)
F1-P2-F2_a	89.47(8)	C10-C9-C21	120.37(14)
C15-O1-C19	117.99(14)	C9-C10-C11	120.33(14)
C17-O2-C20	117.19(12)	N2-C11-C10	121.97(14)
C23-O3-C27	117.75(15)	N2-C11-C12	116.71(14)
C25-O4-C28	118.33(14)	C10-C11-C12	121.32(15)
C2 -N1-C6	118.79(12)	C4-C13-C18	120.02(13)
Cu1-N1-C6	113.77(10)	C4-C13-C14	120.39(13)
Cu1-N1-C2	126.56(10)	C14-C13-C18	119.59(14)
C13-C14-C15	120.37(14)	C2-C3-H31	120.00
O1-C15-C14	115.33(14)	C4-C5-H51	120.00
O1-C15-C16	123.83(14)	C6-C5-H51	120.00
C14-C15-C16	120.84(14)	C7-C8-H81	120.00
C15-C16-C17	118.46(14)	C9-C8-H81	120.00
C16-C17-C18	121.55(14)	C11-C10-H101	120.00
O2-C17-C16	114.49(13)	C9-C10-H101	120.00
O2-C17-C18	123.95(14)	H121-C12-H123	109.00
C13-C18 -C17	119.09(14)	H121-C12-H122	109.00
C9-C21-C22	120.80(14)	C11-C12-H121	110.00
C9-C21-C26	119.60(13)	C11-C12-H122	110.00
C22-C21-C26	119.46(14)	C11-C12-H123	110.00
C21-C22-C23	119.80(16)	H122-C12-H123	109.00
O3-C23-C22	115.09(16)	C13-C14-H141	120.00
O3-C23-C24	123.61(15)	C15-C14-H141	120.00
C22-C23-C24	121.30(15)	C15-C16-H161	121.00
C23-C24-C25	118.59(15)	C17-C16-H161	121.00
O4-C25-C24	124.29(15)	C13-C18-H181	120.00
O4-C25-C26	115.07(14)	C17-C18-H181	120.00
C24-C25-C26	120.64(16)	O1-C19-H191	110.00
C21-C26-C25	120.19(14)	O1-C19-H192	109.00

C2-C1-H11	109.00	O1-C19-H193	110.00
C2-C1-H12	109.00	H191-C19-H192	109.00
H11-C1-H12	109.00	H191-C19-H193	109.00
H11-C1-H13	109.00	H192-C19-H193	110.00
C2-C1-H13	109.00	O2-C20-H201	109.00
H12-C1-H13	110.00	O2-C20-H202	109.00
C4-C3-H31	120.00	H201-C20-H203	109.00
O2-C20-H203	109.00	O4-C28-H281	109.00
H201-C20-H202	109.00	O4-C28-H282	109.00
H202 -C20-H203	110.00	O4-C28-H283	109.00
C23-C22-H221	120.00	H281-C28-H282	110.00
C21-C22-H221	120.00	H281-C28-H283	110.00
C23-C24-H241	121.00	H282-C28-H283	109.00
C25-C24-H241	121.00	N3-C30-C29	165.5(4)
C25-C26-H261	120.00	N3-C30-C29_c	165.5(3)
C21-C26-H261	120.00	C29-C30-C29_c	28.9(5)
H272-C27-H273	109.00	C30-C29-H291	110.00
O3-C27-H271	109.00	C30-C29-H292	110.00
O3-C27-H272	109.00	C30-C29-H293	109.00
O3-C27-H273	109.00	H291-C29-H292	110.00
H271-C27-H272	109.00	H291-C29-H293	109.00
H271-C27-H273	109.00	H292-C29-H293	109.00

Annexe: Crystallographic data of **72**, data collection and refinement parameters.

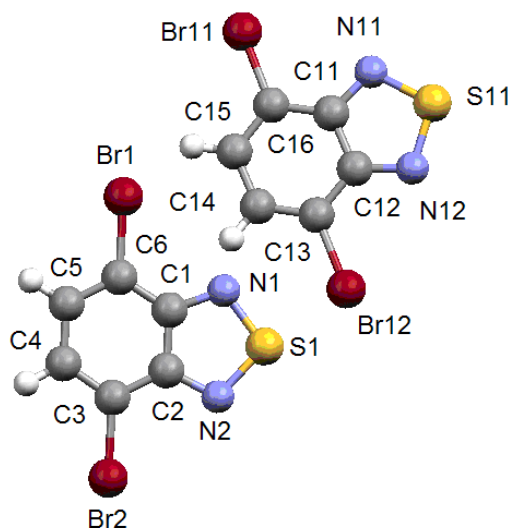


Empirical formula	C ₆ H ₄ N ₂ S
Formula weight	136.18 g mol ⁻¹
Temperature	173 K
Wavelength	0.71073 Å
Crystal system	Orthorhombic
Space group	Pna21
a	12.5766(10) Å
b	12.1433(11) Å
c	3.8280(3) Å
Volume, Z	584.62(8) Å ³ , 4
Density (calculated)	1.547 Mg m ⁻³
Absorption coefficient	0.440 mm ⁻¹
F (000)	280
Crystal size	0.12 x 0.12 x 0.34 mm
θ range for data collection	3.2, 30.0 °
Index ranges	-17<h<17 ; -17<k<17 ; -5<l<5
Reflection collected	6377
Independent reflections	1707
Data/restraints/parameters	83
Final R indices [I > 2σI]	1041
R indices (all data, 6100 ref.)	0.0339, 0.0458, 1.03
Largest diff. peak and hole	-0.28, 0.24 e Å ⁻³

Bond	l (Å)	Bond	l (Å)
S1-N1	1.611(2)	C3 -C4	1.348(4)
S1-N2	1.613(2)	C4 -C5	1.424(3)
N1-C1	1.349(3)	C5 -C6	1.361(4)
N2 -C2	1.348(3)	C3 -H31	1.0000
C1-C2	1.440(3)	C4 -H41	1.0000
C1-C6	1.405(3)	C5 -H51	1.0000
C2-C3	1.419(4)	C6-H61	1.0000

Atoms	Angle (°)	Atoms	Angle (°)
N1-S1-N2	101.25(11)	C4 -C5-C6	121.0(2)
S1-N1-C1	106.59(16)	C1-C6-C5	118.5(2)
S1-N2-C2	106.24(17)	C2-C3-H31	120.00
N1-C1-C2	112.7(2)	C4-C3-H31	121.00
N1-C1-C6	126.8(2)	C3-C4-H41	119.00
C2-C1-C6	120.5(2)	C5-C4-H41	119.00
N2-C2-C1	113.2(2)	C4-C5-H51	120.00
N2-C2-C3	127.5(2)	C6 -C5-H51	119.00
C1-C2-C3	119.3(2)	C1-C6-H61	121.00
C2 -C3-C4	118.4(2)	C5-C6 -H61	121.00
C3-C4-C5	122.3(2)		

Annexe: Crystallographic data of **73**, data collection and refinement parameters



Empirical formula	C ₆ H ₂ Br ₂ N ₂ S
Formula weight	293.97 g mol ⁻¹
Temperature	173 K
Wavelength	0.71073 Å
Crystal system	Monoclinic
Space group	P21/c
a	18.3494(4) Å
b	3.90220(10) Å
c	22.0454(5) Å
α	90°
β	97.2268(14)°
γ	90°
Volume, Z	1565.98(6) Å ³ , 8
Density (calculated)	2.494 mg m ⁻³
Absorption coefficient	10.545 mm ⁻¹
F (000)	1104
Crystal size	0.04 x 0.06 x 0.51 mm
θ range for data collection	3.1, 27.4°
Index ranges	-23<h<23, -4<k<5, -28<l<28
Reflection collected	24503
R, R _w , S	0.0713, 0.0598, 0.99
Largest diff. peak and hole	-1.36, 1.51 e Å ⁻³

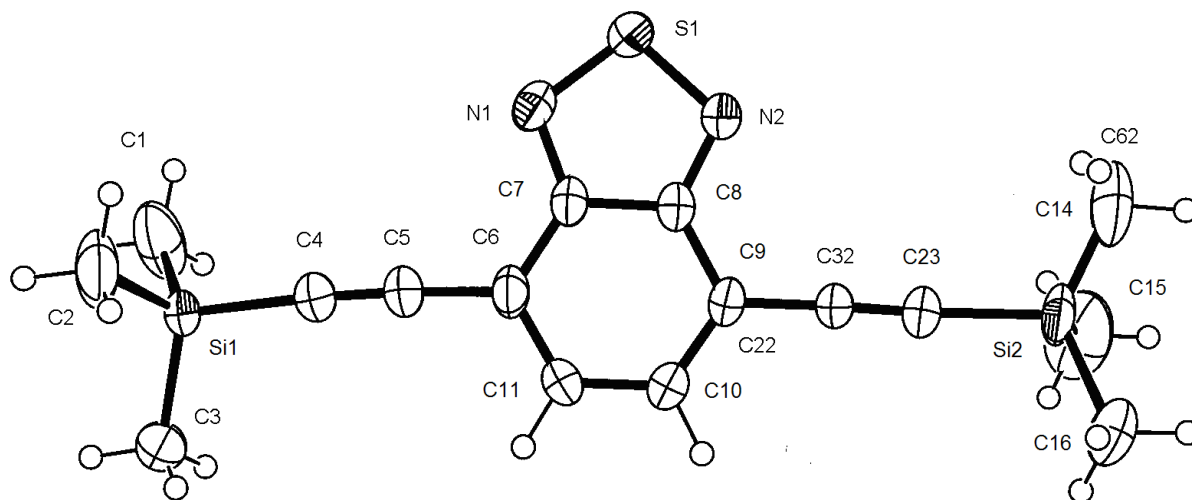
Annexe- Table - Bond Distances (Angstrom)

Bond	l (Å)	Bond	l (Å)
C1-C6	1.418(7)	C15-H151	1.0000
Br1 -C6	1.890(6)	C2-C3	1.399(7)
Br2-C3	1.891(6)	C3-C4	1.385(8)
Br11-C16	1.891(6)	C4-C5	1.403(8)
Br12-C13	1.886(5)	C5-C6	1.393(7)
S1-N2	1.612(4)	C4-H41	1.0100
S1-N1	1.613(5)	C5-H51	1.0000
S11-N11	1.612(4)	C11-C12	1.433(8)
S11-N12	1.622(5)	C11-C16	1.419(7)
N1-C1	1.348(7)	C12-C13	1.415(6)
N2-C2	1.348(6)	C13-C14	1.395(8)
N11-C11	1.344(6)	C14-C15	1.411(8)
N12-C12	1.344(7)	C15-C16	1.387(8)
C1-C2	1.415(8)	C14-H141	1.0100

Table S6 - Bond Angles (Degrees)

Atoms	Angle (°)	Atoms	Angle (°)
N1-S1-N2	100.8(3)	C5-C4-H41	119.00
N11-S11-N12	101.1(2)	C4-C5-H51	122.00
S1-N1-C1	105.9(4)	C6-C5-H51	117.00
S1-N2-C2	106.6(3)	N11-C11-C12	112.6(4)
S11-N11-C11	106.7(3)	N11-C11-C16	128.9(5)
S11-N12-C12	105.6(4)	C12-C11-C16	118.5(4)
N1-C1-C2	114.0(4)	N12-C12-C11	114.0(4)
N1-C1-C6	126.2(5)	N12-C12-C13	125.5(5)
C2 -C1-C6	119.8(5)	C11-C12-C13	120.4(4)
C1-C2-C3	120.1(4)	Br12-C13-C12	118.8(4)
N2-C2-C1	112.8(4)	Br12-C13-C14	121.3(4)
N2-C2-C3	127.1(5)	C12-C13-C14	119.9(5)
Br2-C3-C4	119.7(4)	C13-C14-C15	119.6(6)
Br2-C3-C2	120.2(4)	C14-C15-C16	121.6(6)
C2-C3-C4	120.1(5)	Br11-C16-C11	119.6(4)
C3-C4-C5	120.0(5)	Br11-C16-C15	120.4(4)
C4-C5-C6	121.3(5)	C11-C16-C15	120.0(5)
C1-C6-C5	118.7(5)	C13-C14-H141	119.00
Br1-C6-C1	119.9(4)	C15-C14-H141	121.00
Br1-C6-C5	121.5(4)	C14-C15-H151	119.00
C3-C4-H41	121.00	C16-C15-H151	119.00

Annexe: Crystallographic data of compound **74**, data collection and refinement parameters.



Empirical formula	$C_{16}H_{20}N_2S Si_2$
Formula weight	328.59 g mol ⁻¹
Temperature	173K
Wavelength	0.71073Å
Crystal system	Monoclinic
Space group	P21/n
a	17.6305(3) Å
b	5.74260(10)Å
c	20.0975(3)Å
β	112.0158(10)°
Volume, Z	1886.40(6) Å ³ , 4
Density (calculated)	1.157 Mg m ⁻³
Absorption coefficient	0.294 mm ⁻¹
F (000)	696
Crystal size	0.13 x 0.18 x 0.28 mm
θ range for data collection	1.3, 27.9 °
Index ranges	-23: 23 ; -7: 7 ; -26: 26
Reflection collected	4504
Independent reflections	2671
Data/restraints/parameters	245
R, wR2, S	0.0394, 0.0608, 1.03
Largest diff. peak and hole	-0.26, 0.30 e Å ⁻³

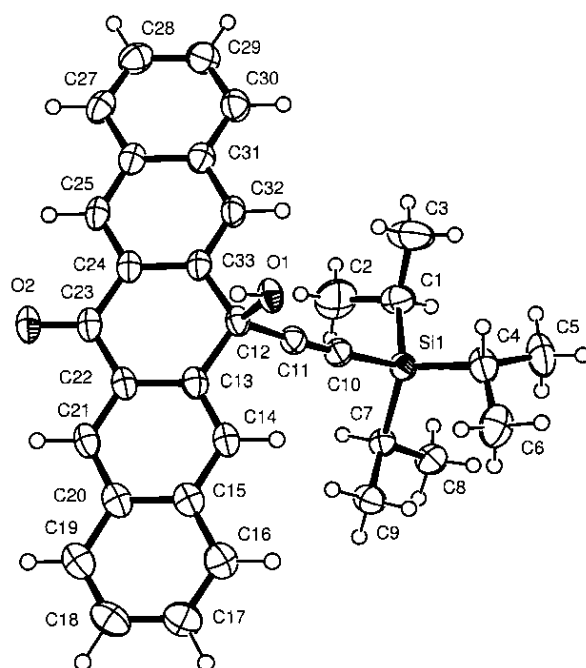
Bond	l (Å)	Bond	l (Å)
S1-N1	1.611(2)	C1-H13	0.9600
S1-N2	1.617(2)	C2-H21	0.9600
Si1-C1	1.839(4)	C2-H22	0.9600
Si1-C2	1.847(4)	C2-H23	0.9600
Si1-C3	1.834(4)	C3-H31	0.9600
Si1-C4	1.839(3)	C3-H32	0.9600
Si2-C13	1.842(6)	C3-H33	0.9600
Si2-C14	1.850(8)	C10-H101	0.9600
Si2-C15	1.855(5)	C11-H111	0.9600
Si2-C16	1.867(15)	C14-H141	0.9600
Si20-C26	1.862(16)	C14-H142	0.9600
Si20-C25	1.836(8)	C14-H143	0.9600
Si20-C23	1.846(11)	C15-H151	0.9600
Si20-C24	1.838(8)	C15-H152	0.9600
N1-C7	1.345(3)	C15-H153	0.9600
N2-C8	1.348(3)	C16-H161	0.9600
C4-C5	1.204(4)	C16-H162	0.9600
C5-C6	1.443(4)	C16-H163	0.9600
C6-C7	1.425(3)	C24-H241	0.9600
C6-C11	1.377(4)	C24-H242	0.9600
C7-C8	1.427(3)	C24-H243	0.9600
C8-C9	1.429(3)	C25-H251	0.9600
C9-C12	1.468(13)	C25-H252	0.9600
C9-C22	1.40(2)	C25-H253	0.9600
C9-C10	1.373(4)	C26-H261	0.9600
C10-C11	1.411(4)	C26-H262	0.9600
C1-H11	0.9600	C26-H263	0.9600
C1-H12	0.9600		

Table – Bond Angles (°)

Atoms	Angle (°)	Atoms	Angle (°)
N1-S1-N2	101.22(11)	N1-C7-C8	113.0(2)
C1-Si1-C2	109.84(17)	C7-C8-C9	121.1(2)
C1-Si1-C3	111.53(19)	N2-C8-C9	125.3(2)
C1-Si1-C4	108.66(16)	N2-C8-C7	113.68(19)
C2-Si1-C3	108.97(17)	C8-C9-C22	119.2(9)
C2-Si1-C4	110.32(15)	C8-C9-C10	116.8(2)
C3-Si1-C4	107.50(14)	C8-C9-C12	121.2(5)
C13-Si2-C14	107.6(3)	C10-C9-C12	121.7(5)
C13-Si2-C15	108.7(3)	C10-C9-C22	122.9(9)
C13-Si2-C16	108.4(5)	C9-C10-C11	122.3(2)
C14-Si2-C15	110.1(3)	C6-C11-C10	122.5(3)
C14-Si2-C16	110.6(6)	Si1-C1-H11	109.00
C15-Si2-C16	111.3(5)	Si1-C1-H12	109.00
C23-Si20-C26	109.5(8)	Si1-C1-H13	109.00

C24-Si20-C25	112.0(7)	H11-C1-H12	109.00
C24-Si20-C26	109.9(10)	H11-C1-H13	109.00
C25-Si20-C26	110.6(8)	H12-C1-H13	110.00
C23-Si20-C24	108.7(7)	Si1-C2-H21	109.00
C23-Si20-C25	106.0(4)	Si1-C2-H22	109.00
S1-N1-C7	106.38(16)	Si1-C2-H23	109.00
S1-N2-C8	105.71(16)	H21-C2-H22	109.00
Si1-C4-C5	175.5(2)	H21-C2-H23	110.00
C4-C5-C6	175.4(3)	H22-C2-H23	109.00
C5-C6 -C7	122.1(2)	Si1-C3-H31	109.00
C7-C6-C11	117.1(2)	Si1-C3-H32	109.00
C5-C6-C11	120.7(2)	Si1-C3-H33	109.00
N1-C7-C6	126.7(2)	H31-C3-H32	109.00
C6-C7-C8	120.3(2)	H31-C3-H33	110.00
H32-C3-H33	109.00	H161-C16-H163	110.00
C9-C10-H101	119.00	H162-C16-H163	110.00
C11-C10-H101	119.00	Si20-C24-H241	109.00
C6-C11-H111	119.00	Si20-C24 -H242	109.00
C10 -C11-H111	119.00	Si20-C24 -H243	110.00
Si2-C14-H141	109.00	H241-C24 -H242	109.00
Si2-C14 -H142	109.00	H241-C24 -H243	109.00
Si2-C14-H143	109.00	H242-C24 -H243	110.00
H141-C14-H142	109.00	Si20-C25-H251	110.00
H141-C14-H143	110.00	Si20-C25-H252	109.00
H142-C14-H143	110.00	Si20-C25-H253	109.00
Si2-C15-H151	109.00	H251-C25-H252	110.00
Si2-C15-H152	109.00	H251-C25-H253	109.00
Si2-C15-H153	110.00	H252-C25-H253	109.00
H151-C15-H152	109.00	Si20-C26-H261	109.00
H151-C15-H153	110.00	Si20-C26-H262	109.00
H152-C15-H153	109.00	Si20-C26-H263	110.00
Si2-C16-H161	109.00	H261-C26-H262	109.00
Si2-C16-H162	109.00	H261-C26-H263	109.00
Si2-C16-H163	109.00	H262-C26-H263	110.00
H161-C16-H162	110.00		

Annexe: Crystallographic data, data collection and refinement parameters for **80**.



Empirical formula	$C_{33}H_{34}O_2Si$
Formula weight	$490.72 \text{ g mol}^{-1}$
Temperature	173 K
Wavelength	0.71073 \AA
Crystal system	Triclinic
Space group	$P - 1$
a	$8.8875(3) \text{ \AA}$
b	$8.9910(3) \text{ \AA}$
c	$17.6023(7) \text{ \AA}$
α	$90.406(2)^\circ$
β	$92.223(2)^\circ$
γ	$105.032(2)^\circ$
Volume, Z	$1357.19(9) \text{ \AA}^3, 2$
Density (calculated)	1.201 Mg m^{-3}
Absorption coefficient	0.114 mm^{-1}
F (000)	524
Crystal size	$0.02 \times 0.34 \times 0.40 \text{ mm}$
θ range for data collection	$2.32 - 27.47^\circ$
Index ranges	$-11 < h < 11, -11 < k < 11, -22 < l < 22$
Reflection collected	11207
Independent reflections	6138
Data/restraints/parameters	3673/2/329
Final R indices [$I > 3\sigma I$]	$R1 = 0.0868, wR2 = 0.0968$
R indices (all data, 6100 ref.)	$R1 = 0.465, wR2 = 0.0643$
Largest diff. peak and hole	$0.30, -0.22 \text{ e \AA}^{-3}$

Annexe- Table - Bond Distances (Angstrom)

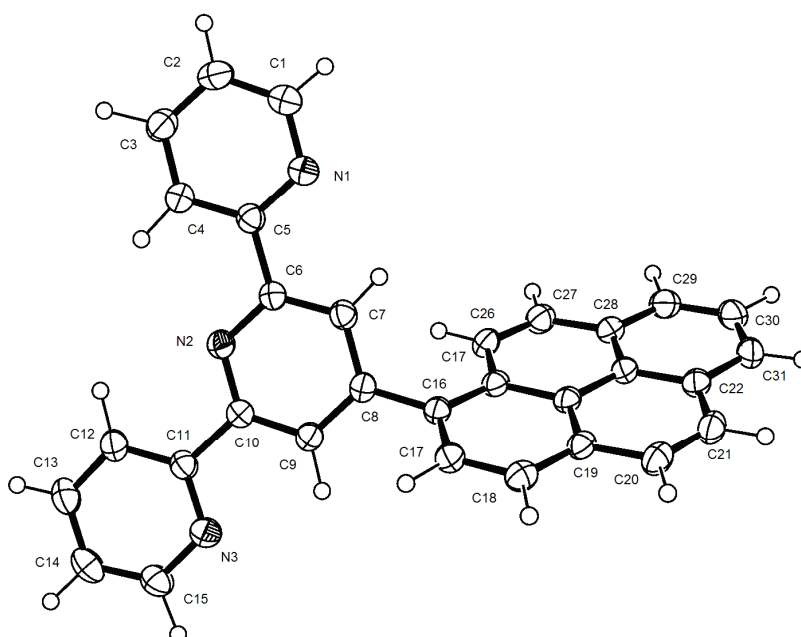
Bond	l (Å)	Bond	l (Å)
Si1-C1	1.883(3)	C22-C23	1.476(4)
Si1-C4	1.880(3)	C23-C24	1.474(4)
Si1-C7	1.880(3)	C24-C25	1.384(4)
Si1-C10	1.837(3)	C24-C33	1.420(4)
O1-C12	1.439(3)	C25-C26	1.405(4)
O2-C23	1.238(3)	C26-C27	1.423(4)
O1-H1	0.946(19)	C26-C31	1.426(4)
C27-C28	1.358(4)	C28-C29	1.412(4)
C29-C30	1.362(4)	C30-C31	1.414(4)
C31-C32	1.418(4)	C32-C33	1.368(4)
C10-C11	1.207(4)	C11-C12	1.487(4)
C12-C13	1.528(4)	C12-C33	1.534(4)
C13-C14	1.376(4)	C13-C22	1.423(4)
C14-C15	1.415(4)	C15-C20	1.420(4)
C15-C16	1.421(4)	C16-C17	1.370(4)
C17-C18	1.404(4)	C18-C19	1.360(4)
C19-C20	1.421(4)	C20-C21	1.409(4)
C21-C22	1.379(4)		

Table - Bond Angles (Degrees).

Atoms	Angle (°)	Atoms	Angle (°)
C1-Si1-C4	110.51(12)	C14-C15-C16	122.0(2)
C1-Si1-C7	110.66(12)	C16-C15-C20	118.8(2)
C1-Si1-C10	105.88(12)	C14-C15-C20	119.2(2)
C4-Si1-C7	115.40(12)	C15-C16-C17	120.1(2)
C4-Si1-C10	107.86(12)	C16-C17-C18	120.8(2)
C7-Si1-C10	105.94(12)	C17-C18-C19	120.7(3)
C12-O1-H1	108.6(16)	C18-C19-C20	120.2(2)
C15-C20-C21	118.4(2)	C19-C20-C21	118.7(2)
C15-C20-C19	119.4(2)	C20-C21-C22	121.7(2)
C13-C22-C21	119.9(2)	C13-C22-C23	121.3(2)
C21-C22-C23	118.8(2)	O2-C23-C24	120.2(2)
C22-C23-C24	118.7(2)	C26-C31-C32	122.2(2)
Si1-C10-C11	176.3(2)	O2-C23-C22	121.2(2)
C10-C11-C12	177.1(3)	C23-C24-C33	121.2(2)
O1-C12-C13	109.83(19)	C25-C24-C33	119.8(2)
O1-C12-C33	109.3(2)	C23-C24-C25	119.0(2)
C11-C12-C13	110.2(2)	C24-C25-C26	122.5(2)
C11-C12-C33	108.5(2)	C25-C26-C31	121.7(2)
C13-C12-C33	114.1(2)	C27-C26-C31	118.5(2)
O1-C12-C11	104.5(2)	C25-C26-C27	119.0(2)
C12-C13-C14	118.7(2)	C26-C27-C28	122.5(2)
C14-C13-C22	119.2(2)	C27-C28-C29	120.6(3)

Atoms	Angle (°)	Atoms	Angle (°)
C12-C13-C22	122.1(2)	C28-C29-C30	120.3(3)
C13-C14-C15	121.6(2)	C29-C30-C31	120.8(3)
C30-C31-C32	122.7(2)	C26-C31-C30	120.7(3)
C31-C32-C33	122.0(2)	C12-C33-C32	118.7(2)
C24-C33-C32	119.3(2)	C12-C33-C24	118.5(2)

Annexe: Crystallographic data, data collection and refinement parameters for 61.



Empirical formula	C ₃₁ H ₁₉ N ₃
Formula weight	433.51 g mol ⁻¹
Temperature	173 K
Wavelength	0.71073 Å
Crystal system	Triclinic
Space group	P-1
a	8.9944(5) Å
b	9.9000(5) Å
c	13.2388(7) Å
α	78.592(3)°
β	89.650(2)°
γ	67.208(3)°
Volume, Z	1062.08(10) Å ³ , 2
Density (calculated)	1.355 Mg m ⁻³
Absorption coefficient	0.080 mm ⁻¹
F (000)	452
Crystal size	0.10 x 0.10 x 0.10 mm
θ range for data collection	3.0, 28.7 °
Index ranges	-12<h<12 ; -13<k<13 ; -17<l<17
Reflection collected	3274
Independent reflections	2719
Data/restraints/parameters	308
Final R indices [I > 2σI]	3274
R, wR2, S	0.0563, 0.0879, 0.92
Largest diff. peak and hole	-0.22, 0.24 e Å ⁻³

Table – Interatomic bonds length parameters datas in Å of compound **61**.

Bond	l (Å)	Bond	l (Å)
N1-C1	1.340(2)	C1-H1	1.0000
N1-C5	1.347(2)	C2 -H2	1.0000
N2-C6	1.348(2)	C3-H3	0.9900
N2-C10	1.345(2)	C4-H4	1.0000
N3-C11	1.343(2)	C7-H7	0.9900
N3-C15	1.341(3)	C9-H9	1.0000
C1-C2	1.375(3)	C12-H12	1.0000
C2-C3	1.380(3)	C13-H13	0.9900
C3-C4	1.383(3)	C14-H14	0.9900
C4-C5	1.392(3)	C15-H15	1.0000
C5-C6	1.489(3)	C17-H17	1.0100
C6-C7	1.393(3)	C18-H18	1.0100
C7-C8	1.384(3)	C20-H20	1.0100
C8-C9	1.394(3)	C21-H21	1.0100
C8-C16	1.486(3)	C26-H26	1.0100
C9-C10	1.390(3)	C27-H27	1.0100
C10-C11	1.490(3)	C29-H29	1.0100
C11-C12	1.392(3)	C30-H30	1.0100
C12-C13	1.384(3)	C31-H31	1.0100
C13-C14	1.374(3)		
C14 -C15	1.375(4)		
C16-C17	1.398(3)		
C16-C25	1.410(3)		
C17-C18	1.381(3)		
C18-C19	1.397(3)		
C19-C20	1.439(3)		
C19-C24	1.423(3)		
C20-C21	1.344(3)		
C21-C22	1.435(3)		
C22-C23	1.422(3)		
C22-C31	1.403(3)		
C23-C24	1.427(3)		
C23-C28	1.416(3)		
C24-C25	1.424(3)		
C25-C26	1.438(3)		
C26-C27	1.355(3)		
C27-C28	1.431(3)		
C28-C29	1.397(3)		
C29-C30	1.382(4)		
C30 -C31	1.386(3)		

Table- Angle in degrees of compound **61**.

Atoms	Angle (°)	Atoms	Angle (°)
C1-N1-C5	117.40(17)	C8-C16-C17	118.53(16)
C6-N2-C10	117.41(17)	C8-C16-C25	122.26(17)
C11-N3-C15	117.50(18)	C17-C16-C25	119.11(18)
N1-C1-C2	123.98(18)	C16-C17-C18	121.84(18)
C1-C2-C3	118.33(18)	C17-C18-C19	120.55(18)
C2-C3-C4	119.05(18)	C18-C19-C20	122.52(18)
C3-C4-C5	119.05(17)	C18-C19-C24	118.91(17)
N1-C5-C4	122.18(17)	C20-C19-C24	118.57(17)
N1-C5-C6	115.35(17)	C19-C20-C21	121.45(18)
C4-C5-C6	122.47(17)	C20-C21-C22	121.47(18)
N2-C6-C5	117.15(17)	C21-C22-C23	118.69(17)
N2-C6-C7	122.69(17)	C21-C22-C31	122.47(18)
C5-C6-C7	120.16(16)	C23-C22-C31	118.85(17)
C6-C7-C8	119.91(17)	C22-C23-C24	119.92(17)
C7-C8-C9	117.32(17)	C22-C23-C28	120.00(17)
C7-C8-C16	121.67(17)	C24-C23-C28	120.08(17)
C9-C8-C16	120.72(16)	C19-C24-C23	119.85(17)
C8-C9-C10	119.78(17)	C19-C24-C25	120.14(16)
N2-C10-C9	122.80(17)	C23-C24-C25	120.00(17)
N2-C10-C11	117.12(17)	C16-C25-C24	119.26(17)
C9-C10-C11	120.08(16)	C16-C25-C26	122.55(17)
N3-C11-C10	116.03(17)	C24-C25-C26	118.18(16)
N3-C11-C12	122.16(17)	C25-C26-C27	121.49(18)
C10-C11-C12	121.79(16)	C26-C27-C28	121.29(18)
C11-C12-C13	118.94(17)	C23-C28-C27	118.80(17)
C12-C13-C14	119.12(19)	C23-C28-C29	118.87(19)
C13-C14-C15	118.46(19)	C27-C28-C29	122.34(19)
N3-C15-C14	123.81(19)	C28-C29-C30	121.2(2)
C29-C30-C31	120.42(19)	N3-C15-H15	115.00
C22-C31-C30	120.67(19)	C14-C15-H15	121.00
N1-C1-H1	115.00	C16-C17-H17	119.00
C2-C1-H1	121.00	C18-C17-H17	119.00
C1-C2-H2	122.00	C17-C18-H18	121.00
C3-C2-H2	120.00	C19-C18-H18	119.00
C2-C3-H3	121.00	C19-C20-H20	118.00
C4-C3-H3	120.00	C21-C20-H20	121.00
C3-C4-H4	122.00	C20-C21-H21	121.00
C5-C4-H4	119.00	C22-C21-H21	117.00
C6-C7-H7	120.00	C25-C26-H26	120.00
C8-C7-H7	121.00	C27-C26-H26	119.00
C8-C9-H9	121.00	C26-C27-H27	120.00
C10-C9-H9	119.00	C28-C27-H27	119.00
C11-C12-H12	118.00	C28-C29-H29	118.00

C13-C12-H12	123.00	C30-C29-H29	121.00
C12-C13-H13	120.00	C29-C30-H30	119.00
C14-C13-H13	121.00	C31-C30-H30	120.00
C13-C14-H14	121.00	C22-C31-H31	118.00
C15-C14-H14	120.00	C30-C31-H31	121.00

